ELECTROPHYSIOLOGICAL CHARACTERIZATION OF A MOUSE DEFICIENT FOR OLIGOPHRENIN1: A MOUSE MODEL OF X-LINKED MENTAL RETARDATION

By

PIERRE-PHILIPPE SAINTOT

A thesis submitted to
The University of Birmingham
For the degree of
DOCTOR OF PHILOSOPHY

Department of Neurophysiology
The Medical School
The University of Birmingham
May 2010

UNIVERSITY OF BIRMINGHAM

University of Birmingham Research Archive

e-theses repository

This unpublished thesis/dissertation is copyright of the author and/or third parties. The intellectual property rights of the author or third parties in respect of this work are as defined by The Copyright Designs and Patents Act 1988 or as modified by any successor legislation.

Any use made of information contained in this thesis/dissertation must be in accordance with that legislation and must be properly acknowledged. Further distribution or reproduction in any format is prohibited without the permission of the copyright holder.

ABSTRACT

Mental retardation is the most common brain disease. One of the first genes identified in X-linked mental retardation (XLMR) was the OPHN-1 gene. Mutation of this gene has been described in patients with moderate to severe cognitive impairments.

MR is characterized by reduced cognitive function with or without other clinical features, thus providing a direct approach to study the neurobiology of cognition and pathogenesis of MR. I propose in this thesis to clarify the underlying mechanisms responsible for the learning impairments.

My first approach was to investigate the functioning of a neuronal population using extracellular recording of fast oscillations which are thought to underlie higher cognitive performance. I showed that *Ophn-1* null mice displayed weaker gamma oscillations. Thereafter, Investigation of the synaptic properties of CA3 pyramidal neurons using the patch-clamp technique has been undertaken. I have shown reduced inputs of excitatory and inhibitory neurotransmission to CA3 pyramidal neurons accompanied with reduced frequency dependent facilitation of the inhibitory neurotransmission at 33Hz. Finally, a reduction in readily releasable pool size in inhibitory synapses of CA3 area was unravelled. This defect explained the reduction of frequency of sIPSCs and consequently the reduction in gamma oscillations power in *Ophn-1*$^{-/y}$ slices.

Pierre-Philippe Saintot declares that:

I am the sole author of this thesis. The work presented here is original work, completed by me during the period of registration as a postgraduate student candidate. The exception to this statement relates to the frequency dependent facilitation, Paired pulse stimulation and readily releasable pool experiments in CA3 neurons, which were completed in collaboration with my supervisor, Dr A.D. Powell. Dr. Powell completed about 25% of these experiments.

Table of contents

Chapter 1: GENERAL INTRODUCTION 1

1.1 Mental retardation 1
1.1.1 Definition of mental retardation **2**
1.1.2 Incidence and aetiology of mental retardation **4**
1.2 X-Linked Mental Retardation 5
1.2.1 Definition of X-linked mental retardation **5**
1.2.2 Incidence and aetiology of X-linked mental retardation **6**
1.2.3 Categorization of X-linked mental retardation **7**
1.2.4 Deficits observed in X-linked mental retardation. **9**
1.2.5 Involvement of RhoGTPases pathways in XLMR. **9**
1.3 Oligophrenin1 protein and the syndrome of oligophrenin1 deficiency 11
1.3.1 Oligophrenin1: from past to present **11**
1.3.2 Clinical features **12**
1.3.3 Physiology of oligophrenin1 protein **17**
1.3.4 Characterization of the *Ophn-1*$^{-/y}$ mice **21**
1.4 RhoGTPases family 24
1.4.1 Role of the small RhoGTPases **24**
1.4.2 Mechanisms of activation **26**
1.4.3 RhoGTPase and dendritic structures in neurons **27**
1.5 Hippocampal gamma rhythms and higher cognitive function 29
1.5.1 Hippocampal network morphology **30**
1.5.2 Neurotransmission and mechanisms underlying gamma oscillations **32**
1.5.3 Role of the hippcampal gamma rhythm in memory processes **36**
1.6 Working hypothesis 39
1.7 Outline of the thesis 40

Chapter 2: MATERIALS AND METHODS **41**

2.1 Experimental animals **41**
2.2 Mouse identification **43**
2.2.1 DNA digestion protocol **43**
2.2.2. Polymerase Chain Reaction (PCR) assay **44**
2.3 *In Vitro* slices preparation **46**
2.4 Electrophysiology **48**
2.4.1 Extracellular Field Recording **48**
2.4.2 Whole cell recordings **62**
2.5 Statistical analysis **73**

Chapter 3: INVESTIGATION OF HIPPOCAMPAL GAMMA OSCILLATIONS **74**

3.1. AIM **74**
3.2. Induction of gamma oscillations *in vitro* **75**
3.3. Development of gamma oscillations *in vitro* **78**
3.4 Pharmacological investigation of KA-induced gamma oscillations **80**
3.4.1 KA-induced gamma oscillations were abolished by the application of bicuculline. **80**
3.4.2 KA-induced gamma oscillations were inhibited by NBQX. **82**
3.4.3 KA depolarized and increased the spontaneous firing of *Ophn-1*$^{+/y}$ CA3 pyramidal neurons **84**
3.5 Effect of the loss of oligophrenin1 on the KA-induced gamma oscillations **85**
3.5.1 *Ophn-1*$^{-/y}$ mice slices displayed a reduced strength of KA induced gamma oscillations at relatively low bath temperature (30 ºC) **85**
3.5.2 Rhythmicity of gamma oscillations in *Ophn-1*$^{-/y}$ slices **91**

3.5.3 *Ophn-1*$^{-/y}$ mice slices displayed no difference in synchronization along the Ammon horn **95**

3.5.4 *Ophn-1*$^{-/y}$ mice slices displayed a higher frequency of KA induced gamma oscillations at higher bath temperature (32°C) **98**

3.6 Effect of Y27632 on KA-induced gamma oscillations 100

3.7 Effect of the loss of oligophrenin1 on spontaneous gamma oscillations 102

3.8 SUMMARY 103

Chapter 4: MECHANISMS UNDERLYING THE LOSS OF POWER IN KA-INDUCED GAMMA OSCILLATIONS IN *Ophn-1*$^{-/y}$ SLICES 105

4.1 AIM 105

4.2 Electrophysiological characterization of field potential in CA3 area 106

4.2.1 Single pulse stimulation of afferents to CA3 neuronal population **106**

4.2.2 Reduction of paired pulse facilitation in *Ophn-1*$^{-/y}$ slices. **112**

4.3 Electrophysiological characterization of CA3 pyramidal neurons. 116

4.3.1 Distinction between pyramidal neurons and interneurons **116**

4.3.2 Intrinsic neuronal properties were unaltered in *Ophn-1*$^{-/y}$ CA3 pyramidal neurons **119**

4.3.3 Excitatory postsynaptic currents of CA3 pyramidal neurons **121**

4.3.4 Inhibitory postsynaptic currents of CA3 pyramidal neurons **124**

4.4 SUMMARY 142

Chapter 5 ELECTROPHYSIOLOGICAL CHARACTERIZATION OF CA1 HIPPOCAMPAL AREA 143

5.1. AIM 143

5.2 Single stimulation field potential in the CA1b area 144
5.2.1 Biology of evoked postsynaptic potentials in CA1 area. **144**
5.2.2 Single evoked response in CA1 area **146**
5.3 Synaptic responses to paired pulse stimulation were unaltered in *Ophn-1*$^{-/y}$ slices. 149
5.4 Currents characterization of CA1 pyramidal neurons 155
5.4.1 CA1 Intrinsic neuronal properties **155**
5.4.2 Excitatory postsynaptic currents of CA1 pyramidal neurons. **162**
5.4.3 Inhibitory postsynaptic currents of CA1 pyramidal neurons. **172**
5.5 DISCUSSION 180
5.5.1 *Ophn-1*$^{-/y}$ slices displayed a reduced PSP. **180**
5.5.2 Paired-pulse facilitation was unaltered in *Ophn-1*$^{-/y}$ slices **181**
5.5.3 *Ophn-1*$^{-/y}$ CA1 pyramidal neurons displayed a reduced eEPSC **182**
5.5.4 Neither sEPSCs amplitude nor the frequency were affected *Ophn-1*$^{-/y}$ CA1 pyramidal neurons **184**
5.5.5. Paired pulse stimulation on eEPSC was unchanged in *Ophn-1*$^{-/y}$ pyramidal neurons. **185**
5.5.6 The potentiation of the eEPSC induced by frequency dependant facilitation in *Ophn-1*$^{-/y}$ CA1 pyramidal neurons was unaffected **186**
5.5.7 Deficits were specific to excitatory neurotransmission in CA1 **186**
5.5.8 Spontaneous inhibitory postsynaptic current were unaffected in *Ophn-1*$^{-/y}$ CA1 pyramidal neurons. **189**
5.5.9 No change in intrinsic properties of neurons of *Ophn-1*$^{-/y}$ CA1 neurons **188**
5.5.10 Speculation and design of futures experiments **188**
5.5.11 Conclusion on CA1 **191**

Chapter 6 GENERAL DISCUSSION 193

6.1 Relevance of the *Ophn-1*$^{-/y}$ mice as a model of X-linked mental retardation 193

6.2 ***Ophn-1*$^{-/y}$ slices displayed reduced KA-induced gamma oscillations compared to *Ophn-1*$^{+/y}$ slices** **194**

6.3 **Hippocampal neuronal network properties.** **202**

6.4 **The excitatory and inhibitory neurotransmission in CA3 pyramidal neurons were altered in *Ophn-1*$^{-/y}$ mice.** **204**

6.5 **Readily releasable pool size was reduced in *Ophn-1*$^{-/y}$ CA3 pyramidal neurons.** **211**

6.6 **Putative mechanism of action of oligophrenin1** **215**

6.7 **CONCLUSION** **217**

List of references **223**

List of tables

Table 1.1 Synopsis of various clinical studies reported to date **15**

Table 1.2 Cellular functions of small GTPases proteins. **25**

Table 1.3 Recapitulation of the roles of gamma oscillations **38**

Table 4.1: Values for action potentials characteristics and membrane resistance. **121**

Table 4.2 The kinetics of excitatory postsynaptic currents were unaffected in *Ophn-1*$^{-/y}$ CA3 pyramidal neurons **123**

Table 4.3 The kinetics of inhibitory currents were unaltered in *Ophn-1*$^{-/y}$ CA3 pyramidal neurons. **129**

Table 5.1 The kinetics of excitatory postsynaptic currents were unaltered in *Ophn-1*$^{-/y}$ CA1 pyramidal neurons. **167**

Table 5.2 The kinetics of inhibitory postsynaptic currents were unaltered in *Ophn-1*$^{-/y}$ CA1 pyramidal neurons. **179**

List of illustrations

Figure 1.1	Table of classification of mental retardation degree.	**3**
Figure 1.2	Schematic of an X-chromosome	**8**
Figure 1.3	Rho-linked mental retardation proteins and effectors pathways.	**11**
Figure 1.4	Oligophrenin1 deficiency	**16**
Figure 1.5	Oligophrenin1 expression.	**18**
Figure 1.6	Schematic representation of the oligophrenin1 protein (91Kd).	**19**
Figure 1.7	RhoGTPases cycle.	**21**
Figure 1.8	Mechanisms of activation of RhoGTPase	**27**
Figure 1.9	Different spines's shapes	**28**
Figure 1.10	Hippocampal structure	**31**
Figure 1.11	Mechanism of gamma oscillations	**34**
Figure 2.1	Schematic representation of the constitutive inactivation of OPHN-1 gene.	**42**
Figure 2.2	Transmission and detection of *Ophn-1*$^{-/y}$	**46**
Figure 2.3	Evoked field experiments in CA1 area.	**51**
Figure 2.4	Evoked field experiments in CA3 area.	**52**
Figure 2.5	Schematic representation of the experimental protocol	**54**
Figure 2.6	Measuring the power spectrum	**58**
Figure 2.7	Example of coherence analysis.	**59**

Figure 2.8 Assessment of gamma oscillations rhythmicity **61**

Figure 2.9 Measurement of the intrinsic neuronal properties. **65**

Figure 2.10 Measurement of multiple repetitive ePSCs. **69**

Figure 2.11 Evaluation of series resistance. **72**

Figure 3.1 Development of KA-induced gamma oscillations. **77**

Figure 3.2 Frequency and power development in *Ophn-1*$^{+/y}$ slices. **78**

Figure 3.3: Waterfall representation of KA-induced gamma oscillations development along the time. **79**

Figure 3.4 Sensitivity of the gamma oscillations to the $GABA_A$ receptors antagonist bicuculline (10 μM) **81**.

Figure 3.5 Seizures-like events induced by the application of bicuculline **82**

Figure 3.6 Sensitivity of the KA-induced gamma oscillations to the AMPA/KA antagonists NBQX. **83**

Figure 3.7 KA-induced depolarisation in *Ophn-1*$^{+/y}$ CA3 pyramidal neurons. **85**

Figure 3.8 Characteristic traces showing the raw gamma oscillations recordings. **87**

Figure 3.9 *Ophn-1*$^{-/y}$ mice displayed reduced gamma oscillations. **89**

Figure 3.10 Averaged gamma waveform presented a similar shape **90**

Figure 3.11 Autocorrelation of gamma oscillations at 60 min **92**

Figure 3.12 Normalisation of the power of the *Ophn-1*$^{-/y}$ according to *Ophn-1*$^{+/y}$ power **93**

Figure 3.13 Events autocorrelogram of gamma oscillations in *Ophn-1*$^{-/y}$ slices **94**

Figure 3.14 *Ophn-1*$^{-/y}$ gamma oscillations displayed no difference in coherence. **97**

Figure 3.15 *Ophn-1*$^{-/y}$ mice displayed reduced gamma oscillation power at 32.3°C. **98**

Figure 3.16 Percentage of reduction and increase of frequency at 30ºC and 32ºC **99**

Figure 3.17 Effect of Y27632 (10 μM) in KA-induced gamma oscillations. **101**

Figure 3.18 Spontaneous gamma oscillations were unchanged between genotypes **103**

Figure 4.1 Single pulse stimulation of the mossy fibres pathway. **109**

Figure 4.2 Sensitivity of the responses to ionotropic glutamatergic receptors blockers. **111**

Figure 4.3 Altered paired pulse facilitation on PSP in *Ophn-1*$^{-/y}$ slices. **114**

Figure 4.4 Altered paired pulse facilitation on PS in *Ophn-1*$^{-/y}$ slices. **115**

Figure 4.5 Interneurons and pyramidal neurons displayed different firing pattern upon voltage step of 200 pA. **117**

Figure 4.6 Interneurons and pyramidal neurons had significant different action potentials half width duration and fAHP, allowing clear discrimination in *Ophn-1*$^{-/y}$ mice. **119**

Figure 4.7 CA3 pyramidal neurons intrinsic properties. **120**

Figure 4.8 Spontaneous EPSCs were recorded from CA3 pyramidal neurons **122**

Figure 4.9 Spontaneous EPSCs of *Ophn-1*$^{-/y}$ CA3 pyramidal neurons were less frequent compared to *Ophn-1*$^{+/y}$. **123**

Figure 4.10 Altered eIPSCs in *Ophn-1*$^{-/y}$ CA3 pyramidal neurons. **126**

Figure 4.11 Inhibitory neurotransmission onto CA3 pyramidal neurons is reduced in *Ophn-1*$^{-/y}$ neurons. **128**

Figure 4.12 sIPSCs were of similar amplitude, but less frequent in *Ophn-1*$^{-/y}$ CA3 pyramidal neurons. **128**

Figure 4.13 TTX resistant IPSCs are unaltered in *Ophn-1*$^{-/y}$ CA3 pyramidal neurons. **131**

Figure 4.14 Histogram of sIPSCs and mIPSCs frequencies. **132**

Figure 4.15 Paired pulse stimulation of eIPSCs was altered in *Ophn-1*$^{-/y}$. **135**

Figure 4.16 Responses to repetitive stimulation at 33Hz were reduced in *Ophn-1*$^{-/y}$ neurons. **138**

Figure 4.17 *Ophn-1*$^{-/y}$ CA3 interneurons displayed a smaller readily releasable pool size. **141**

Figure 5.1 fPSP and PS recorded in CA1 area of *Ophn-1*$^{+/y}$ slices. **145**

Figure 5.2 Sensitivity of the synaptic responses to NBQX and D-APV. **145**

Figure 5.3 Synaptic transmission was reduced in *Ophn-1*$^{-/y}$ CA1 neurons. **147**

Figure 5.4 *Ophn-1* null mice displayed no difference in paired-pulse stimulation. **151**

Figure 5.5 *Ophn-1*$^{-/y}$ displayed no difference in paired-pulse stimulation on PS. **154**

Figure 5.6 Intrinsic neuronal properties were unaltered in *Ophn-1*$^{-/y}$ CA1 pyramidal neurons. **156**

Figure 5.7 *Ophn-1*$^{-/y}$ CA1 pyramidal neurons displayed no difference in sAHP. **159**

Figure 5.8 mAHP unchanged in *Ophn-1*$^{-/y}$ CA1 pyramidal neurons. **161**

Figure 5.9 Evoked EPSCs were reduced in *Ophn-1*$^{-/y}$ CA1 pyramidal neurons. **163**

Figure 5.10 Spontaneous EPSCs recorded from CA1 pyramidal neurons. **165**

Figure 5.11 Spontaneous EPSCs showed similar amplitude and frequency by genotype. **165**

Figure 5.12 Evoked EPSCs paired-pulse stimulation was unaltered in CA1 pyramidal neurons. **169**

Figure 5.13 Frequency facilitation of eEPSC was unaltered in *Ophn-1*$^{-/y}$ CA1 pyramidal neurons. **171**

Figure 5.14 Input-output relationship of eIPSCs was unaltered in *Ophn-1*$^{-/y}$ CA1 pyramidal neurons held at 0 mV. **173**

Figure 5.15 Input-output relationship of eIPSCs is unaffected in *Ophn-1*$^{-/y}$ CA1 PN held at -70mV. **174**

Figure 5.16 I/V relationship of eIPSCs recorded from CA1 pyramidal neurons in presence of NBQX and D-APV **176**

Figure 5.17 Representative spontaneous IPSCs recordings **177**

Figure 5.18 Spontaneous IPSCs mean amplitude and mean frequency were unaltered in *Ophn-1*$^{-/y}$ CA1 pyramidal neurons. **178**

Figure 5.19 Summary of the results obtained in CA1 area. **190**

Figure 5.20 Schematic of a CA3/CA1 or CA1/CA1 PN synapse. **191**

Figure 6.1 Synaptic defects observed in CA3 neuronal networks in *Ophn-1*$^{-/y}$ mice. **207**

Figure 6.2 Schematic of a GABAergic synapses. **215**

Figure 6.3 Schematic of a presynaptic terminal **217**

Figure 6.4 Schematic representation of the hippocampal neuronal circuitry. **219**

Figure 6.5 Schematic representation of different neuronal populations of the hippocampal pathways. **221**

List of Abbreviations

AC	Associational commissural pathway
aCSF	Artificial cerebrospinal fluid
AHP	Afterhyperpolarisation
AMPA	α-amino-3-hydroxy-5-methyl-4-isoxasole-propionic acid
ANOVA	Univariate analysis of variance
AP	Action potential
ARHGEF6	A rho guanine nucleotide exchange factor 6
ATP	Adenosine-5'-triphosphate
ATPA	2-amino-3-(5-*tert*-butyl-3-hydroxy-4-isoxazolyl)propionic acid
BAR	Bin, Amphiphysin , RSV
Bp	Base pair
CA1	Cornu ammonis 1
CA3	Cornu ammonis 1
Cdc42	Cell division cycle 42 protein
D-APV	(2*R*)-amino-5-phosphonovaleric acid
DG	Dentate gyrus
DHPG	(S)-3,5-dihydroxyphenylglycine
Dia	Diaphanous-related formins
DNA	Deoxyribonucleic acid
EAA	Excitatory amino acid
EC	Enthorhinal cortex
EEG	electroencephalography
eEPSC	Evoked excitatory postsynaptic current
EGTA	Ethylene glycol tetraacetic acid
eIPSCs	Evoked inhibitory postsynaptic current
EPSP	Excitatory postsynaptic potential
ES	Embryonic stem
FMRP	Fragile-X Mental Retardation Protein
GAP	GTPases activating protein
GDI	GDP dissociation inhibitor
GDP	Guanosine diphosphate
GEF	Guanine nucleotide exchange factor
GTP	Guanosine-5'-triphosphate
HEPES	4-(2-hydroxyethyl)-1-piperazineethanesulfonic acid
IQ	Intellectual Quotient
IN	Interneuron
IPSC	Inhibitory postsynaptic current
IPSP	Inhibitory postsynaptic potential
KA	Kainic Acid
KAR	KA receptor
KO	Knockout (*Ophn-1*$^{-/y}$)
LD	Learning disabilities
LIMK	Lin-11, Isl-1 and Mec-3 kinase
mAHP	Medium afterhyperpolarisation

MeCP2	Methyl-CpG binding protein 2
MEGAP	Mental disorder-associated GAP protein
MF	Mossy fibres
mGluR	Metabotropic glutamatergic receptor
mIPSC	Miniatures inhibitory postsynaptic current
MLCK	Myosin light chain kinase
MR	Mental retardation
MWM	Morris water maze test
NBQX	2,3-dihydroxy-6-nitro-7-sulfamoyl-benzo[f]quinoxaline-2,3-dione
NMDA	N-methyl-d-aspartate
P1	Pulse 1
P2	Pulse 2
PAK	p21-activated kinase
PAK3	p21-activating kinase-3
PCR	Polymerase chain reaction
PH	Plekstrin Homology
Pi	Inorganic phosphate
PN	Pyramidal neuron
PP	Perforant pathway
PPF	Paired-pulse facilitation
PSD95	Postsynaptic density protein 95
PSP	Postsynaptic potential
PS	Population spike
Rac1	Ras related C3 botulinium toxin substrate 1
RhoA	Ras homologous member
RhoGAP	RhoGTPase Activating Protein
RMP	Resting membrane potential
RNA	Ribonucleic acid
ROCK	Rho-kinase
RRP	Readily releasable pool
RT PCR	Reverse transcriptase-polymerase chain reaction
s.	Stratum
sAHP	Slow afterhyperpolarisation
Sb	Subiculum
SC	Schaffer collaterals pathway
sEPSC	Spontaneous excitatory postsynaptic current
SH3	Src homology 3
sIPSC	Spontaneous inhibitory postsynaptic current
STDP	Spike timing-dependent plasticity
TTX	Tetrodotoxin
WCR	Whole cell recording
WT	Wild type *(Ophn-1*$^{+/y}$
XLMR	X-linked mental retardation

Chapter 1: GENERAL INTRODUCTION

1.1 Mental retardation

In the UK, the term “mental retardation” has been replaced by “learning disabilities” (LD) largely due to the acquisition of negative connotations. 1.2 million People have a mild to moderate LD and 210 000 have a severe LD (from www.mencap.org.uk). Moreover 200 babies are born with a learning disability every week in Great Britain (from www.who.int). Disparate nomenclatures are used worldwide to describe this handicap, such as learning difficulties, intellectual disabilities and mental impairment for example. A learning disability affects the ability of people to learn, communicate or perform daily tasks. In this report the term mental retardation will be kept for clarity, as it is acceptable in a scientific context.

The diagnosis criteria are set according the International Classification of Disease-10 (ICD-10th revision) coordinated by the World Health Organization. In USA, DSM IV (Diagnostic and Statistical Manual of mental disorder) classification was largely used until recently. According to this classification, the category “mental handicap” exceeds all other categories. Hence, in Europe, this category accounts for ~8% of the overall health care expenses (Ropers and Hamel, 2005). Mental retardation remains a major challenge for modern medicine. In particular, the cost in the UK is 3 billion pounds per year. Many problems persist in spite of numerous recent political and social efforts, including an increased financial support to the patients and the carers.

Tony Blair optimistically said "People with learning disability can lead full and rewarding lives as many already do" (quote from *Valuing people, a new strategy for learning disability for the 21st century, department of health*). However, mentally retarded individuals are still considered to have a low level of economic productivity and are often seen as a burden to society. Especially in developing countries where beliefs and customs lead to the affected child, being regarded as a curse. This is mainly because the child will fail to participate to the economic support of the family and will also be seen as a heavy burden for the family concerned, as extra care and family resources will be required.

1.1.1 Definition of mental retardation

Mental retardation is a complex disorder; therefore a simple definition is difficult to give. Many organisations have given comprehensive definitions of mental retardation; according to the *American Association on Mental Retardation* recently rebranded in June 2006 as the *American Association on Intellectual and Developmental Disabilities* (AAIDD)

"Mental retardation is a disability characterized by significant limitations both in intellectual functioning and in adaptive behaviour as expressed in conceptual, social, and practical adaptive skills. The disability originates before age 18" (from www.aamr.org)

Adaptive behaviours generally refer to the skills needed to live independently, for instance communication and social skills.

It is accepted that people who have a score between 70 and 50 are considered as mildly retarded, whereas people with an IQ of less than 50 are severely retarded (fig. 1.1 A.). The cognitive abilities can be measured according the Intellectual Quotient (IQ) scaling. The IQ of the population is normally distributed around the average (fig. 1.1 B.). The intelligence can be defined as the capacity to understand complex ideas, to adapt efficiently to the environment, to think rationally and abstractly to solve problems. In addition cognitive abilities can be reflected by the practical sense, initiative and self critical capacity.

A.

Mental retardation	IQ range	Mental age (years old)
Borderline	70-85	
Mild	55-69	8 to 11
Moderate	40-54	5 to 8
Severe	25-39	3 to 5
Profound	<25	<3

B.

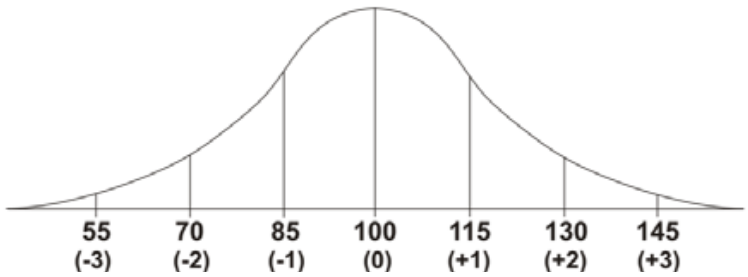

Figure 1.1: (A.) Table of classification of mental retardation degree. **(B.)** IQ bell curve, Standard deviations are in parentheses. (From a Ph.D. thesis entitled: “Molecular genetics of nonspecific X-linked mental retardation” by Helena Geertje Ijntema, 2001)

1.1.2 Incidence and aetiology of mental retardation

The prevalence of mental retardation is difficult to measure; however it was estimated as being between 1 and 3% of the population. This estimate was derived from the bell curve showing IQ. As it follows a normal distribution, it is possible to estimate the extremes (fig. 1.1 B.) (McLaren and Bryson, 1987, Chelly and Mandel, 2001). It is interesting to note that the IQ of males is largely represented on the two tails of the IQ Bell curve, showing that they have a higher degree of variability in IQ value. The IQ of females, on the other hand, tends to be closer to the mean (Hedges and Nowell, 1995). This is now explained by the discovery of X-linked genes highly related to cognition. As males possess are only hemizygous X chromosome, this makes males more susceptible to genetic polymorphic variations. Due to the random X inactivation in females, it is more likely to select suitable alleles.

The causes of mental retardation are multiple. They can be due environmental factors such as foetal alcohol exposure, infection, malnutrition or anoxia during infanthood. Additionally genetics factors such as triplication of chromosome 21 leading to the Down's syndrome or a single mutation on the X chromosome can result in mental retardation. This study is concerned with a single mutation on the X chromosome.

Typing "mental retardation" in the Online Mendelian Inheritance in Man (OMIM) (www.ncbi.nlm.nih.gov/sites/entrez?db=omim) database gives 1446 entries (September 2007), whereas "X-linked mental retardation" gives 399 entries. This means that 28% of all entries deals with X-linked mental retardation (Zechner et al., 2001). It is known that only 4 % of all genes are present on the X chromosome

(Venter et al., 2001). There is an 8 fold higher incidence of mental retardation related to the X chromosome rather than other chromosomes. This has been explained by the fact that a large number of the genes which shape our nervous system are located in the X chromosome.

1.2 X-Linked Mental Retardation

1.2.1 Definition of X-linked mental retardation

In 1938, Penrose made an early observation of a higher prevalence of mental retardation in males[1]. This discrepancy was first explained by the fact that females were kept at home (Raymond, 2006). This explanation was later discarded after the finding of the presence of many mutations on the X-chromosome which result in mental retardations (Renieri et al., 2005). Thus, it is now evident, that many mental retardations are linked to mutations of the X genes and that these mutations account for the excess of learning disabilities in males.

X-linked mental retardation (XLMR) represents a large part of the overall classification of mental retardation. Since the late 90s, XLMR has been subject to extensive effort in gene sequencing of families affected by mental retardation. This has been due, in part, to the establishment of the European XLMR consortium, which has encouraged collaboration between teams in clinical and molecular biology which has led to the establishment of a large genetic database of families affected by X-linked mental

[1] penrose L.S. (1938) A clinical and genetic study of 1280 cases of mental defects.

retardation (www.euromrx.com). They were responsible of the discovery of 20 genes responsible for non syndromic forms and for 25 syndromic forms of XLMR, notably thanks to the powerful positional cloning strategies techniques (Raymond, 2006). The complete sequencing of the X chromosome published in March 2005, confirmed that an important number of its genes encode for proteins essential to brain function (Ross et al., 2005).

1.2.2 Incidence and aetiology of X-linked mental retardation

Amongst single gene mutations causing mental retardation, the most frequent one is the fragile X syndrome, affecting about 1 in 4000 live births. The fragile X syndrome is due to the repetition of the CGG triplet inside the FMR1 gene, which normally encodes for the Fragile X Mental Retardation Protein (FMRP). FMRP is involved in RNA transport (Verkerk et al., 1991). Fragile X syndrome accounts for 20 to 25% of XLMR cases. The second most frequent mutation in a single gene in the X chromosome is the mutation of the MECP2 gene which normally encodes for Methyl-CpG binding protein 2 (MeCP2). A defect in MECP2 gene is responsible for the RETT syndrome (Chahrour and Zoghbi, 2007).

1.2.3 Categorization of X-linked mental retardation

Historically, XLMR has been divided into two categories: *i)* **non syndromic** XLMR where affected patients do not have any distinctive clinical features apart from the cognitive impairment and *ii)* **syndromic** XLMR where the individuals affected have in addition to the intrinsic mental retardation, visible anatomic or metabolic characteristics of the disease (e.g.: strabismus). Syndromic XLMR is further classified by categories according to similar features e.g. cerebellar hypoplasia. This classification is still matter of debate since some XLMR genes are classified in the two categories, for instance ARX, MECP2, FMR1, DCX and GDI. Mutations in these genes lead to syndromic XLMR in some case and non syndromic XLMR in other cases.

Although this classification is not ideal, it is still in use and is acknowledged by the majority. Most of XLMR related genes were discovered through the identification of a X chromosome rearrangement in patient. The cloning of the breakpoint then led to identification of the genes (blue box fig. 1.2); whilst others were discovered by mutational screening (green box).

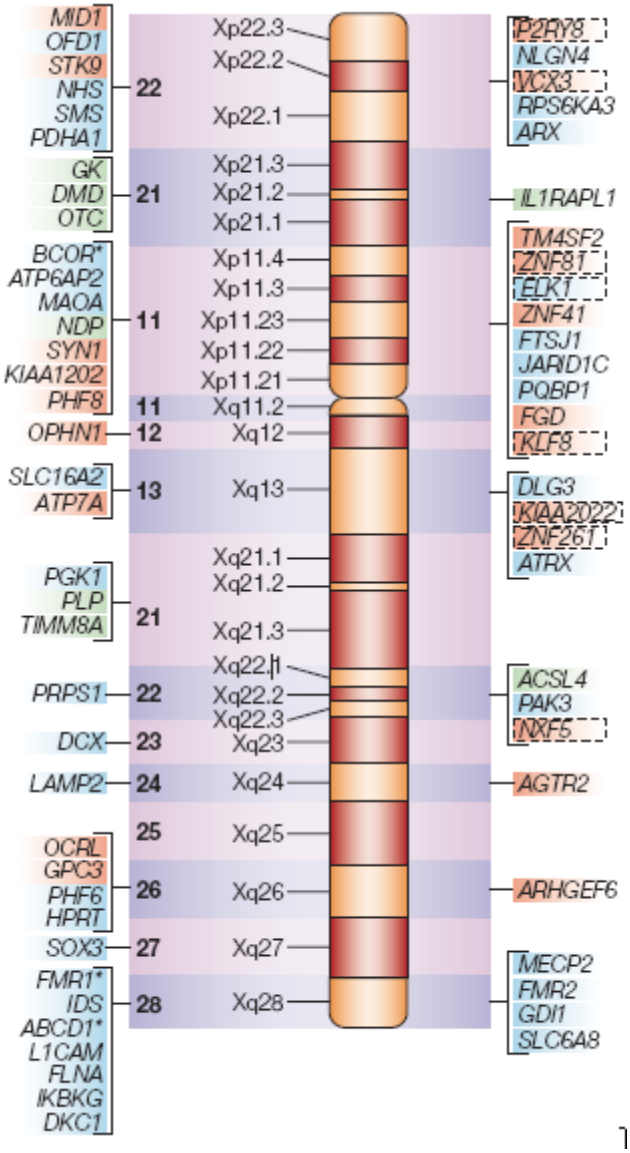

Figure 1.2: Schematic of an X-chromosome illustrating the genes implicated in syndromic and non syndromic XLMR (left and right side respectively). Blue and red colours represent XLMR identified by studying balanced X-chromosome rearrangement, such as OPHN1. Green colour represents XLMR identified by mutation screening. (Ropers and Hamel, 2005).

1.2.4 Deficits observed in X-linked mental retardation.

About three decades ago seminal studies from Huttenlocher et al (1970) and Purpura et al (1974) reported an alteration of the structure in the dendrite and the dendritic spines in MR with a shift to either absent or abnormally long and thin ones in affected individuals (Purpura, 1974, Purpura, 1979). The dendritic structures were extensively studied thereafter in XLMR model as reviewed by (Kaufmann and Moser, 2000). The neuroanatomical examination of XLMR in mouse models revealed several morphological abnormalities such as dendritic spines malformations, notably for fragile X syndrome (Grossman et al., 2006b) and in down's syndrome (Kaufmann and Moser, 2000). Spine dysgenesis certainly induces alteration in the synaptic transmission which may lead to deficits in intellectual performance. The alteration in spine structure which accompanies XLMR could have a significant impact on mental function.

Dendritic morphology is tightly controlled by actin cytoskeleton rearrangement. Several XLMR genes were found to be regulators of effectors of RhoGTPases, which regulate the actin rearrangement.

1.2.5 Involvement of RhoGTPases pathways in XLMR.

Several XLMR genes were found to be involved in signal transduction through the small RhoGTPases protein. Oligophrenin1, in addition to four other proteins encoded by genes known to be involved in XLMR are members of the RhoGTPases signalling

pathway, either as regulators (αPIX or cool2, , oligophrenin-1) or as downstream effectors (PAK3 (p21-activating kinase-3.), FMRP).

In addition, mutations in a X-chromosome gene, termed Rab GDP-dissociation inhibitors (GDI), have been found to lead also to XLMR (D'Adamo et al., 1998).

Figure 1.3 shows the signaling pathways which involve the small RhoGTPases protein leading to cytoskeleton rearrangements. Two major typical signaling pathways for oligophrenin1 has been studied: *i)* RhoA activates Rho-kinase (ROCK), which in turn activates the myosin light chain (MLC) protein by phosphorylating it, leading to actomyosin contractility phenomenon (Maekawa et al., 1999). *ii)* Another signaling pathway is as follow: after activation of Rho-kinase, the latter will phosporylate/activate a protein named LIMK (which also responsible for MR when mutated (Meng et al., 2002), once activated LIMK in turn phosphorylates the Cofilin, inactivating it. Cofilin is an actin depolymerization factor, therefore inactivation leads to actin polymeristation. The protein effector Diaphanous-related formins (Dia) has also been shown to be activated by RhoAGTPase (Li and Higgs, 2003).

Another GAP protein, MEGAP, coded by a gene located on the chromosome 3; mutation in this gene lead to severe MR (Endris et al., 2002). FMRP (O'Donnell and Warren, 2002) and PAK3 (Allen et al., 1998) proteins are effectors of Rac and Cdc42 and are also involved when they are lacking in XLMR (fig. 1.3).

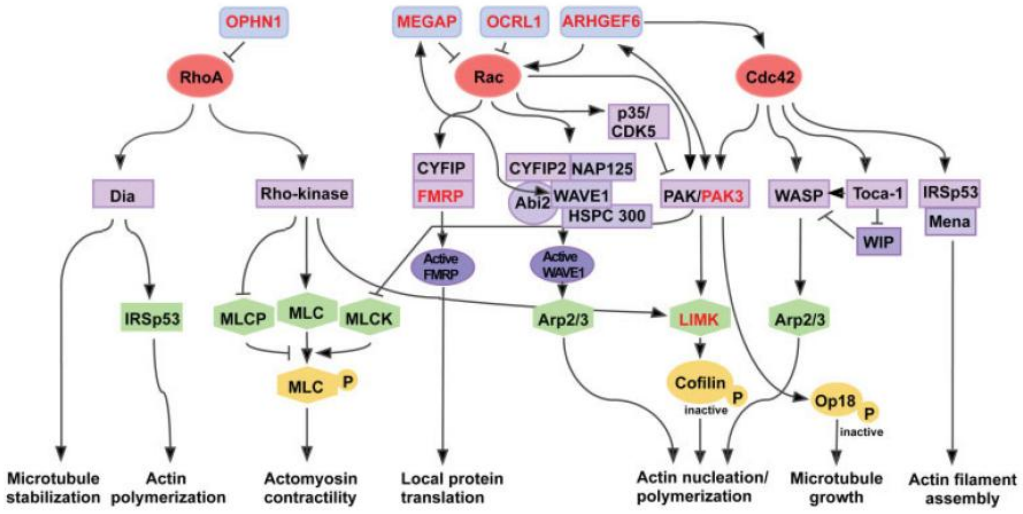

Figure 1.3: Rho-linked mental retardation proteins and effectors pathways. Red colour illustrates proteins inducing MR when lacking (From (Newey et al., 2005)). Important abbreviations: MEGAP, Mental disorder-associated GAP protein; ARHGEF6 (or αPIX or Cool-2), a Rho guanine nucleotide exchange factor 6; PAK, p21-activated kinases; LIMK, Lin-11, Isl-1 and Mec-3 kinase; MLCK, myosin light chain kinase; Dia, Diaphanous-related formins.

1.3 Oligophrenin1 protein and the syndrome of oligophrenin1 deficiency.

1.3.1 Oligophrenin1: from past to present

Bienvenu et al (1997) reported a case of X-breakpoint balanced translocation (X;12) in a female affected with a mild mental retardation (family MRX60). By cloning the breakpoint, Billuart et al (1998) identified a single base pair deletion in a gene named

OPHN1 (MIM 300127), which contains 25 exons spanning the breakpoint in Xq12 and encodes for a protein named oligophrenin1 (Molecular mass ~ 91 kDa). They therefore concluded that loss of function of this gene is responsible for X-linked non specific mental retardation, assuming, that the mutation leads to the non expression of oligophrenin1 in the brain. It is actually not possible to prove this assumption, due to the lack of access to human brain materials. Although RT PCR analysis of RNA in lymphoblastoid cell from the patient revealed that the mutation resulted in an almost undetectable level of oligophrenin1 transcript (Chabrol et al., 2005).

Clinical studies have identified multiple mutations in the OPHN1 sequence of different families (see table 1). Briefly the pathophysiologies of the disease observed are cerebellar hypoplasia, ventriculomegaly, hydrocephaly, epilepsy, hypogenitalism, and strabismus (Chelly, 2000). Initially classified as a non syndromic XLMR, a closer re-examination of the clinical phenotype in families affected as well as the discovery of new families, suggested a syndromic form of XLMR (Bergmann et al., 2003, Chabrol et al., 2005). This was mainly concluded from the observation, that affected patients were associated with permanent cerebellum hypoplasia, which constitutes a clear distinctive clinical feature.

1.3.2 Clinical features

Many mutations in the sequence of OPHN1 have been observed in several distinct families over the past 10 years since the discovery of OPHN1 gene. The first studies presented a chromosomal rearrangement mutations in a mild mentally retarded

female (MRX60) and a 1 base pair deletion in her affected children (Bienvenu et al., 1997, Billuart et al., 1998, Tentler et al., 1999). Later on additional mutations located on the OPHN1 sequence were discovered (Tentler et al., 1999, Bergmann et al., 2003, Philip et al., 2003, Zanni et al., 2005, des Portes et al., 2004). All patients with mutations in OPHN1 gene showed similar learning disabilities symptoms, ranging from moderate to severe mental retardation. Furthermore, a trend towards milder MR was observed for females heterozygote and a trend to more severe MR was observed for the males hemizygote.

The clinical features defining the oligophrenin1 deficiency as a syndromic XLMR are the followings: Cerebellar hypoplasia notably of the vermis was observed for all the individuals affected (Tentler et al., 1999, Philip et al., 2003, Bergmann et al., 2003, Chabrol et al., 2005, Zanni et al., 2005, Menten et al., 2007, des Portes et al., 2004). Cerebellar hypoplasia is probably responsible of the developmental delay such as the late walking in the infants, although an ataxia was observed in only one case (Bergmann et al., 2003). The OPHN-1 gene has been suggested to play a role in the development of the cerebellum (Bergmann et al., 2003;Philip et al., 2003;Tentler et al., 1999). The cerebellum hypoplasia is interesting, because it is found in other MR as well, indicating that the cerebellum could be involved in cognitive function (Riva and Giorgi, 2000). A variable degree of cerebral ventricles enlargement, including the laterals and the 4th ventricles, are observed amongst all male patients mutated but only sometimes in females. A third major clinical feature is the development of epileptic seizures at early stage of the development in approximately 50 % of the families, such as early onset complex partial seizures (des Portes et al., 2004) and

myoclonic astatic (Bergmann et al., 2003)). In addition to these main features several adjunct features are observed such as strabismus, hypogenitalism, specific facial appearance or a tall stature. Table 1 summarizes the results of different clinical studies with families affected by oligophrenin1 deficiency reported to date. These clinical features characterize the “oligophrenin syndrome”.

Reference	Family details	OPHN1 mutations	Clinical Features
Bienvenu, T (1998)	1 female	Breakpoint translocation Xq12	mild MR
Billuart, P. (1998)	MRX 60, 4 males	1-bp deletion 1578	MR only (then reassessed by des portes)
Billuart, P. (2000)	screening of 164 patients	found 3 polymorphisms	determination of gene structure study
Tentler, D. (1999)	two sisters of Finnish descent	microdeletion of 1.1Mb	psychomotor retardation,enlarged cerebral ventricles, cerebellar hypoplasia, seizures, ataxia
Philip, N. (2003)	2 families	1578del, 1385ins; 8-bp duplication in exon 9	moderate MR, cerebellar hypoplasia
Bergmann, C. (2003)	1 family, 5 brothers	genomic deletion of exon 19(17.6-kb deletion)	moderate to severe MR, myoclonic-astatic epilepsy, ataxia, strabismus and hypogenitalism, enlargement of the lateral ventricles
Des portes, V. (2004)	2 families, 1female and 4 males (MRX60)		moderate to severe MR, ventricles enlargment strabismus, early onset complex partial seizures, vermian dysgenesis
Chabrol, B. (2005)	3 families (1 new and 2 families from Philip et al)	2-bp deletion, oligophrenin truncated	moderate to severe MR, seizures, strabismus, cerebellar hypoplasia, ventricles enlargment,specific facial appearance
Zanni, G. (2005)	4 families, 14 males	two nonsense mutations,deletion of exons 16 to 1, splice site mutation	Moderate to severe MR, strabismus, ataxia, moderate dilatation of lateral ventricles, hypoplasia of the cerebellum, epilepsy.
Menten, B. (2007)	1 female	balanced chromosomal rearrangement	Mild MR, epilepsy,strabismus, ventricles enlargment, cerebellar hypoplasia, Dysmorphic facial features, tall stature
(Bedeschi et al., 2008)	1 male	Duplication including OPHN1 gene	Severe MR, ventricular dilatation, cerebellar hypoplasia, microcephaly, distinct facial appearance
(Madrigal et al., 2008)	1 family, 4 males	deletion spanning exons 21 and 22	MR, cerebellar hypoplasia and ventriculomegaly

Table 1.1: Synopsis of various clinical studies reported to date

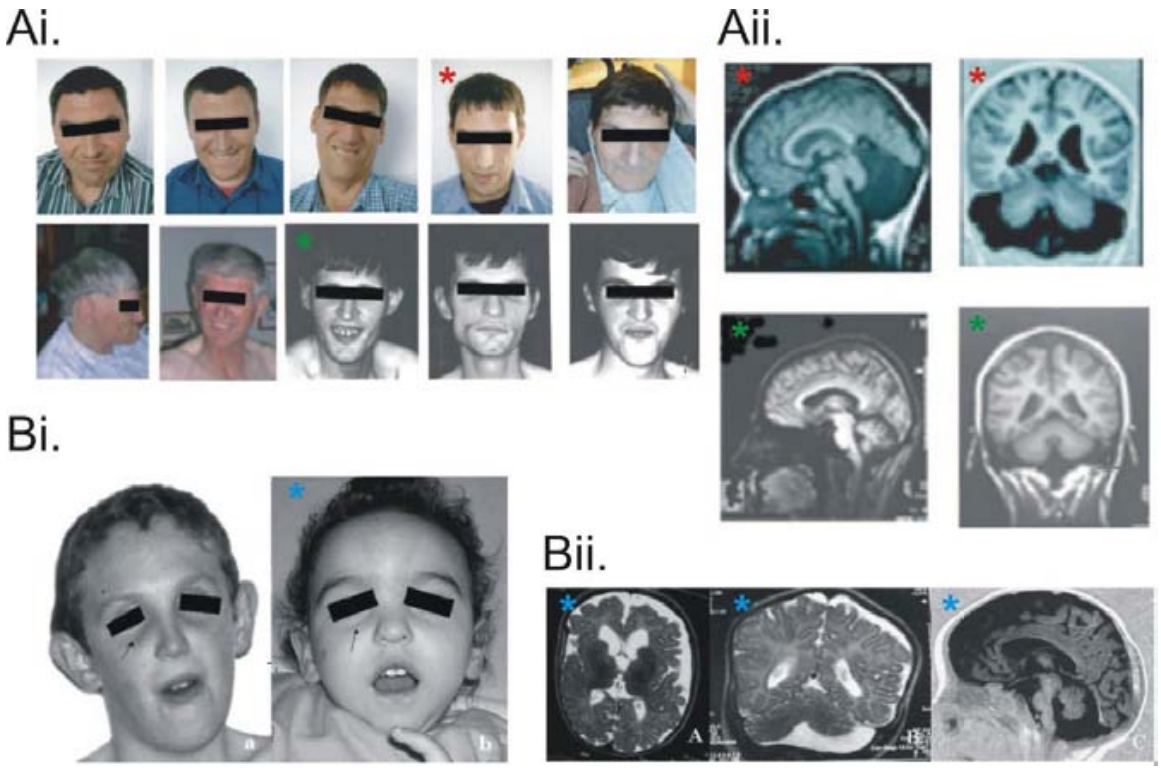

Figure 1.4: Oligophrenin1 deficiency (Ai). Facebook of 3 distinct families affected by oligophrenin1 deficiency showing facial dysmorphy features associated with brain magnetic resonance imaging (MRI) **(Aii.)**.Picture of patients * and * showing ventricles enlargement and cerebellar hypoplasia (illustrations taken from (Zanni et al., 2005)) **(Bi.)** Pictures of two affected males. **(Bii.)** Brain MRI corresponding to the patient *. (illustrations taken from (Chabrol et al., 2005)).

Unfortunately, to date no curative therapy is available, only educational efforts are made to enhance the cognitive performance of patients (Ramakers, 2002).

1.3.3 Physiology of oligophrenin1 protein

Oligophrenin1 expression

Oligophrenin1 (802 AA) present its highest expression in brain during early development. Later at the adult state, it is enriched in the hippocampus, the olfactory bulb and the cerebellum (Billuart et al, 1998). Oligophrenin1 is highly expressed during the development of the brain and is localised in neurons where it directly interacts with actin, notably at the tip of the growing neurite (Fauchereau et al., 2003). Oligophrenin1 is expressed in both the pre and post synaptic compartments (Billuart et al., 1998, Govek et al., 2004). Additionally, outside the brain it has been shown to be expressed in the enteric nervous system, where it could have an important role in colorectal tumor development (Xiao et al., 2003). Additionally, oligophrenin1 is further expressed in neurons as well as in glial cells, and it is noteworthy to consider that oligophrenin1 have been shown to be overexpressed in glial tumour cells (Ljubimova et al., 2001). Oligophrenin1 has been found to interact with postsynaptic protein HOMER, which regulates glutamatergic metabotropic receptors (Sala et al., 2003, Govek et al., 2004).

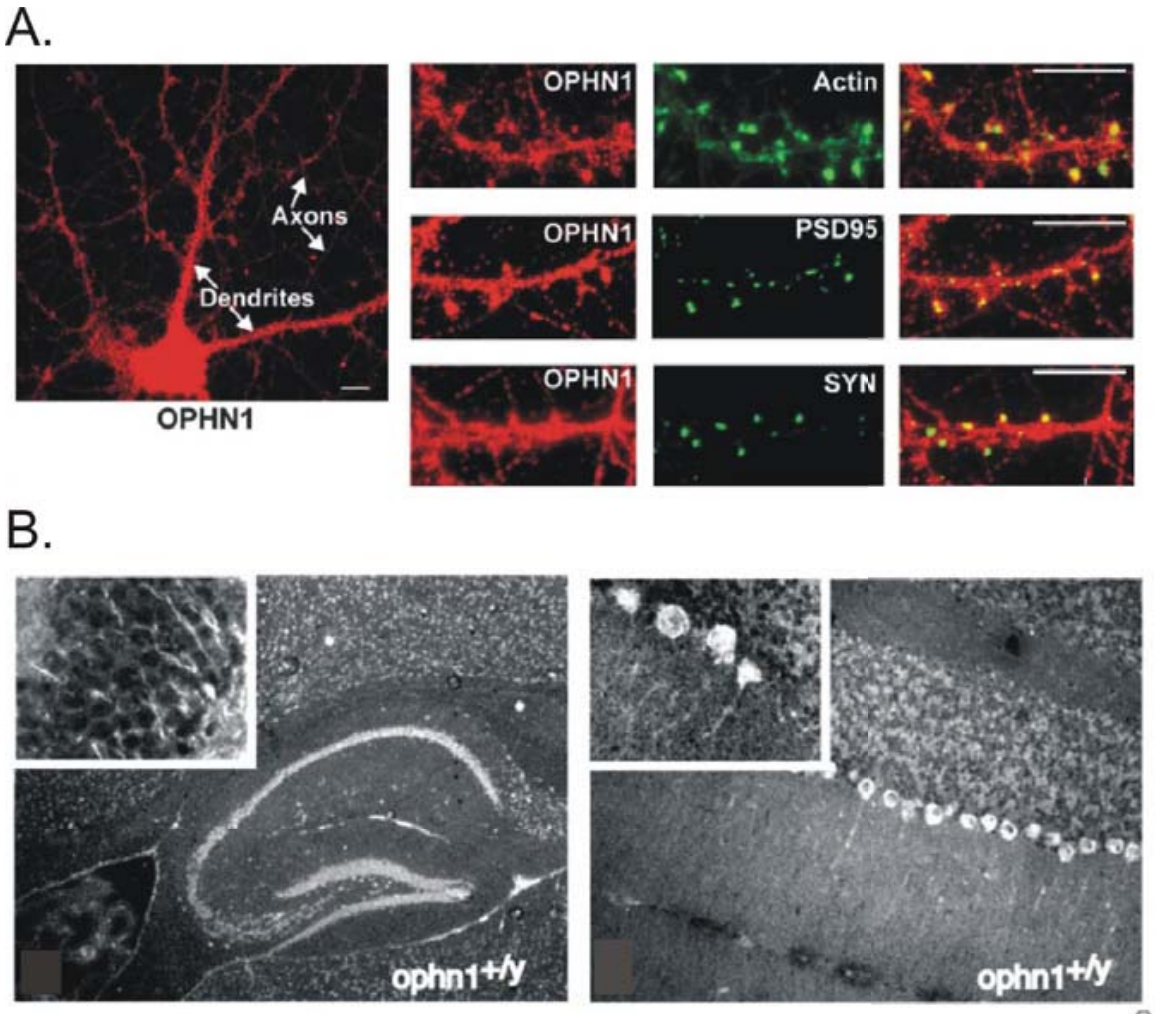

Figure 1.5: Oligophrenin1 expression. **(A.)** Oligophrenin1 is present throughout the neurons and notably coimmunostain with actin, PSD95 and synaptophysin, revealing its presence in pre and postsynaptic compartments closely linked with actin (immunostaining from Govek et al (2004)). **(B.)** Immunolocalization of *Ophn-1* transcript in mouse brain slice in the hippocampus and the cerebellum (left and right panel respectively) (illustrations taken from (Khelfaoui et al, 2007)).

Figure 1.5 B demonstrates that oligophrenin1 transcripts are ubiquitously spread in the soma and dendritic processes.

Oligophrenin1 binding domains

Oligophrenin1 contains a central RhoGTPase Activating Protein domain (RhoGAP). Oligophrenin1 also possesses an N-terminal BAR (Bin, Amphiphysin , RSV) domain which function is to bind to curved membrane and a Plekstrin Homology (PH) domain which interacts with phosphoinositides, which, in doing so, confers specificity to membrane binding (Peter et al., 2004). At its C-terminal is present a prolin rich domain which binds to Src homology 3 domain (SH3 domain) of proteins, such as amphiphysin, endophilin (P. Billuart, personal communication) (Figure 1.6).

Figure 1.6: Schematic representation of the oligophrenin1 protein (91Kd). Numbers signify nucleotides.

Oligophrenin1: its function and its regulation

Oligophrenin1 protein belongs to the GAP family of proteins which are estimated to comprise 140 members (Symons and Settleman, 2000). Oligophrenin1 protein contains a central GAP domains constituted of 140 AA, with an F-actin binding domain, which negatively regulates RhoGTPases by increasing the intrinsic catalytic properties of the RhoGTPase itself (Fauchereau et al., 2003). The GAP domain possesses an “arginine finger” which penetrates into the catalytic sites of the small G

protein acting as a switch, increasing the hydrolysis rate up to 10000 times (Gamblin and Smerdon, 1998).

Oligophrenin1 has been shown to interact with at least 3 RhoGTPases which are amongst the most extensively studied RhoGTPases: i.e. the Ras homologous member A protein (RhoA), the Ras related C3 botulinium toxin substrate 1 (Rac1) and Cell division cycle 42 protein (Cdc42). Oligophrenin1 reduces the GTPase activity of these proteins without any specificity (Billuart et al., 1998, Govek et al., 2004). Briefly, these RhoGTPases act as a molecular switch which transduces signals from extracellular stimuli to a variety of intracellular functions. (fig. 1.7 & table 2 for function) (Luo, 2000, Schmitz et al., 2000, Newey et al., 2005). Lack of oligophrenin1 protein thus leads to a constitutive activation or an abnormally high degree of activation of these RhoGTPases itself and consequently in an activation of its downstream effectors (P. Billuart, personal communication). It is supposed that other GAP proteins could carry out the function of oligophrenin1, such rich1 and rich2 which share some similarities with oligophrenin1, depending of their location. Using chimeric oligophrenin1 protein, Fauchereau et al (2003) determined the mechanism of oligophrenin1 regulation. The authors showed that oligophrenin1 was able to inhibit itself through the interaction with its N-terminal. The precise mechanism is yet to be uncovered.

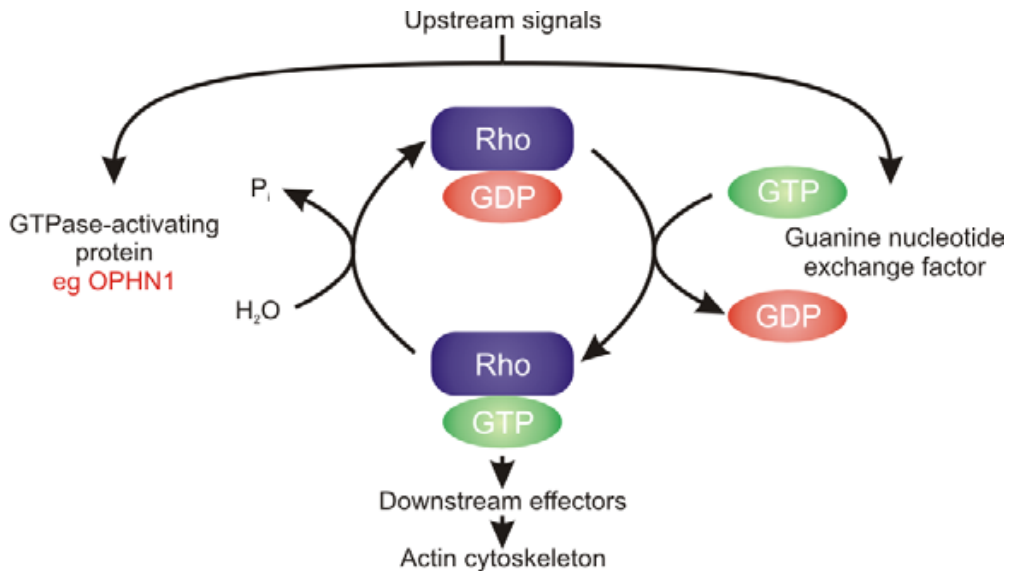

Figure 1.7: RhoGTPases cycle. Abb. Rho: Ras homology; GTP: Guanosine-5'-triphosphate; GDP: Guanosine-5'-diphosphate; Pi: inorganic phosphate. Explanations are contained in the text.

1.3.4 Characterization of the *Ophn-1*$^{-/y}$ mice

The phenotypic characterization of the oligophrenin1 knocked out mouse by Khelfaoui et al (2007) revealed that enlargement of lateral ventricles seen in affected individuals was replicated in the mouse model, whereas the cerebellum was anatomically normal in *Ophn-1*$^{-/y}$ mouse.

Behavioural phenotype of *Ophn-1*$^{-/y}$ mouse

Ophn-1$^{-/y}$ mice and their wild-type littermates have been submitted to a thorough series of behavioural tests, performed by Khelfaoui et al (2007). These tests aimed to

assess exploratory related behaviour, as well as anxiety, social and cognitive-related behaviours. Exploratory behaviours were evaluated by tests, such as locomotor activity test and Y-maze test, which assessed the locomotion and the rearing. In addition, the Open-field test, the light-dark box test, the elevated O-maze test were performed to assess anxiety-related behaviour. The social interaction behaviours were assessed by the resident intruder test and social memory test. The cognitive-related behaviours were evaluated with the Morris water maze test (MWM) and the paw preference test.

The main behaviour observed was a deficit in spatial memory in *Ophn-1*$^{-/y}$ mice, which correspond to a deficit in learning in the MWM. Additionally *Ophn-1*$^{-/y}$ mice showed disturbed social behaviour associated with novelty driven hyperactivity. Deficits in lateralization have also been revealed by the paw preference test. (Khelfaoui et al., 2007).

Ultrastructural phenotype of *Ophn-1*$^{-/y}$ mice

Govek and colleagues compared the spine morphology, by knocking down oligophrenin1 expression with two different approaches: RNA interference and antisense approaches in hippocampal organotypic slices. This study revealed a significant reduction of the length of the dendritic spines in CA1 pyramidal cell. The mechanism underlying this reduction is through RhoAGTPase and subsequently Rho kinase (ROCK) signalling (Govek et al., 2004). As they have shown that Y27632, which is an inhibitor of ROCK protein, rescued the deficit in spines morphology. It is

well established that these dendritic specialisations play an important role in synaptic integration and noteworthy that, spine dysgenesis is observed in other MR (Boda et al., 2004, Grossman et al., 2006a).

Deficit in dendritic spines was also observed by Khelfaoui et al (2007). They showed a reduction in length of the dendritic spines at the basal side and a reduction of the density of these in the apical side of *Ophn-1*$^{-/y}$ cultured CA1 pyramidal neurons. Furthermore, they demonstrated that the number of filopodia was increased in *Ophn1*$^{-/y}$ CA1 hippocampal neurons. Quantification of the number of CA1 neurons and excitatory synapses were unaltered by the loss of oligophrenin1 (Khelfaoui et al., 2007). Taken together, this data revealed that more synapses were formed directly onto the dendritic shafts. These results indicate that the maturition process of the dendritic spines is impaired by the loss of oligophrenin1 protein.

Electrophysiological characterization of *Ophn-1*$^{-/y}$ mice

Electrophysiologically, long-term potentiation and mGluR dependent long-term depression induced by (S)-3,5-dihydroxyphenylglycine (DHPG), were normal in the hippocampal slices (CA1), whilst paired pulse facilitation has been shown to be reduced in *Ophn-1*$^{-/y}$ slices (Khelfaoui et al., 2007). This suggested that the presynaptic release of neurotransmitters is somehow affected in *Ophn-1*$^{-/y}$ mouse.

1.4 RhoGTPases family.

The following part introduces the RhoGTPases family protein which is important to understand the functional implication of the loss of oligophrenin1.

Approximatively one percent of the human genome encodes proteins related to members of Rho family of GTPases. The Rho family of GTPases constitutes a distinct family amongst the superfamily of Ras-small GTPases. Members of this family couple extracellular signalling events to a change in intracellular function. The Rho family includes at least fifteen members, amongst them the Rho subfamily (A, B, C), the Rac subfamily (1, 2, 3) and Cdc42 protein, to mention the most important ones (Jaffe and Hall, 2005). RhoGTPases act as a molecular switch between an inactive state (bound to GDP) and an active state (bound to GTP) and provide a link between membrane receptors and intracellular signalling pathways (fig. 1.8). The activity of these proteins is determined by the ratio of their GTP/GDP bound form. The diverse cellular functions of RhoGTPases are summarized in table 2.

1.4.1 Role of the small RhoGTPases

The major role of RhoGTPases is the regulation of the actin cytoskeleton. Consequently, RhoGTPases play an important role wherever filamentous actin is involved in a cellular process. It is noteworthy that RhoGTPases were extensively studied in fibroblast cultured cells where they have been shown to hold a prominent role in cellular biology processes, such as cell polarisation, microtubules dynamics.

Additionally, RhoGTPases are demonstrated to play an important role in neuronal development where they interfere at every step of the development of the neurons (Govek et al., 2005). It is also well established, that these RhoGTPases are involved in tumor genesis.

RhoGTPases cellular functions	**References**
Regulation of actin polymerisation	(Hall, 1998)
Neurite outgrowth	(Govek et al., 2005)
Differentiation	(Govek et al., 2005)
Axon guidance and pathfindings	(Govek et al., 2005)
Dendritic spine formation and maintenance	(Govek et al., 2005)
Synapse formation	(Govek et al., 2005)
Exocytosis	(Gasman et al., 2003)
Tumourigenesis	(Schmitz et al., 2000)
Cell migration and invasion	(Schmitz et al., 2000)
Cell division	(Narumiya and Yasuda, 2006)
Cell morphogenesis	(Narumiya and Yasuda, 2006)
Cell movement	(Jaffe and Hall, 2005)
Cell polarity	(Etienne-Manneville and Hall, 2002)
Microtubules dynamics	(Etienne-Manneville and Hall, 2002)
Activation of factors transcription	(Etienne-Manneville and Hall, 2002)
Gene transcription	(Etienne-Manneville and Hall, 2002)

Table 1.2: Cellular functions of small GTPases proteins.

Taken together, these studies have shed light on the important function of RhoGTPases signalling in the regulation of the actin cytoskeleton. The actin cytoskeleton, in turn, controls different aspects of the neuronal development, from cell division to the formations of mature synapses, comprising maintaining the stability of the synapses and the remodelling of them.

1.4.2 Mechanisms of activation

A typical signalling pathway including the activation of RhoGTPases is as follow: activation of a receptor kinase by an extracellular signal lead to the recruitment of guanine nucleotide exchange factors (GEFs) to the plasma membrane, concomitantly the small G protein is translocated to the membrane, mainly controlled by the action of GDP dissociation inhibitors (GDIs), which itself is controlled by cytoskeletal proteins. This recruitment further triggers activation of Rho which then interacts with downstream effectors. RhoGTPases contain endogenous GTPase activity, which is enhanced by GTPase activating proteins (GAPs). As oligophrenin1 is an important member of this family of GAP proteins, it functions to return the RhoGTPases to their inactive state. Consequently inactivating mutations in oligophrenin1 result in a constitutively activated Rho protein (Govek et al., 2005).

To summarize, RhoGTPase are thus finely controlled by the concerted action of the regulatory proteins, such as GAP, GEF and GDI (fig 1.8)

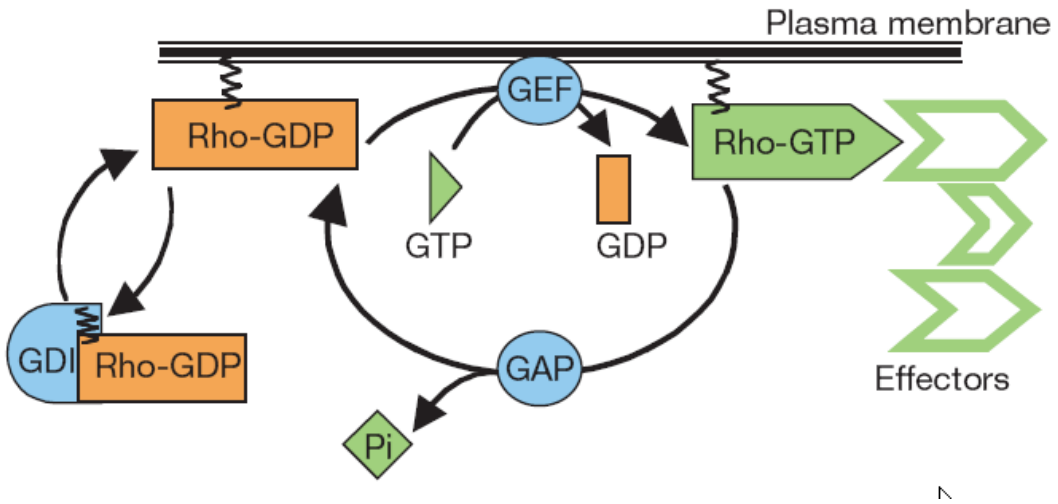

Figure 1.8: Mechanisms of activation of RhoGTPase (Illustration taken from (Etienne-Manneville and Hall, 2002)). Explanations are contained in the text.

1.4.3 RhoGTPase and dendritic structures in neurons

Dendritic spines were discovered more than a century ago, and described by Ramon y Cajal. Dendritic spines have many functions; increasing the dendritic surface area, making synaptic connections tight and furthermore they are critical for the development of synaptic connections. They further are involved in the compartmentalisation of the post synaptic element, and as they impede Ca^{2+} elevations in the dendrite; they may therefore play a role in neuroprotection of the neuron (Segal, 1995) (fig.1.9).

Recently, progress in time lapse imaging showed the rapid motility of dendritic spines controlled by Rho-induced rearrangement of the actin cytoskeleton (Yuste and Bonhoeffer, 2004). As RhoGTPases have a fundamental role in neuronal

development (Govek et al., 2005). Its involvement in the signalling and the morphology of the neuron makes RhoGTPases key player in neuronal development.

Several studies revealed an important antagonistic role of RhoA and Rac1 in regulating the cytoskeleton in neuronal growth cone. Rac1 tends to promote actin polymerization and Rho tends to promote neurite retraction. Similar studies in cultured hippocampal neurons have shown that the overexpression of a constitutely active RhoA led to convert a mature neuron (highly ramified and spiny neuron) into a primitive neurons (less ramified and aspiny neuron) (Tashiro et al., 2000, Nakayama et al., 2000). This agrees with the findings of Govek et al (2004), who described the reduction of the dendritic spines length via an overactivation of the RhoA pathway and subsequently ROCK signalling pathway which regulates actomyosin contractility in dendritic spines.

In conclusion, in this model oligophrenin1 would normally repress the RhoA signalling pathway in order to maintain the length of the dendritic spines. Absence of oligophrenin1, then lead increase of the ROCK activity, a cascade of events, finally resulting in a decrease of spine length via actomyosin contraction.

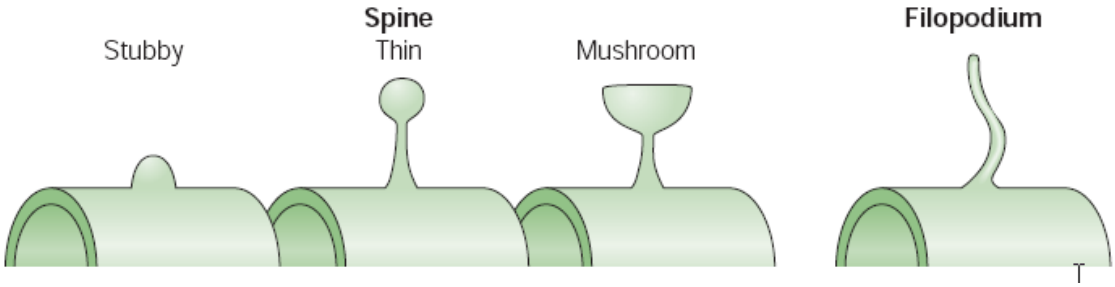

Figure 1.9: Different spines's shapes (Illustration taken from (Yuste and Bonhoeffer, 2004)

In summary, the spine morphology is regulated by the reorganization of the actin cytoskeleton. An additional role of the actin is that, as it is a contractile molecule that binds to a family of adaptor and linking molecule, to connect those to the postsynaptic density (PSD) and receptors.

A valuable approach to determine the synaptic connectivity is to examine the neuronal population synchronisation, so called oscillations, in the brain particularly those generated in the hippocampus.

1.5 Hippocampal gamma rhythms and higher cognitive function

The brain exhibits a variety of network population synchronisation between different areas which can be recorded by electroencephalography (EEG) in humans. These oscillations are recognized to be key factors of sensory processing. They have been extensively studied and are divided according their relative frequency.

The sensory binding concept has been introduced by the work of Gray and Singer who demonstrated the involvement of oscillations in visual and auditory processing (Gray et al., 1990, Gray et al., 1989, Gray and Singer, 1989). Their theory is that, these synchronous oscillations can link together features of sensory stimuli, by synchronising neuronal populations between distant areas of the brain.

Additionally gamma oscillations have been associated with the binding of discontiguous objects (Gruber et al., 2002). Synchronous oscillatory activity has been seen in hippocampus in dentate gyrus and CA3 regions, *in vivo*, in rat during exploratory behaviour. This was accompanied with gamma oscillations nested in theta

oscillations (Bragin et al., 1995). Additionally, synchronous population activity in the gamma band is thought to be correlated with intense mental activity and cognitive function (Lutz et al., 2004).

1.5.1 Hippocampal network morphology.

The hippocampus remains the most studied brain area due its readily identifiable structures. The hippocampus is organised in a laminar fashion comprising several layers, with the stratum pyramidale containing the cell body of bipolar pyramidal neurons, the apical dendrites project into the stratum oriens, whilst the basal dendrites project into the stratum radiatum layer. The trisynaptic pathway in the hippocampus is known to be a uni-directional network, with a main input from the enthorhinal cortex (EC) which connects with the dentate gyrus (DG) and CA3 via the perforant pathway (PP). An additional input for the CA3 region is the mossy fibres which originate in the dentate gyrus. The output of CA3 neurons is to the CA1 neurons via the Schaffer collateral (SC) and to the contralateral CA1 via the associational commissural pathway (AC). The perforant pathway also inputs to CA1 with outputs to the subiculum. The subiculum itself has outputs to the entorhinal cortex ensuring interconnectivity of the hippocampus (see fig 1.10 B.).

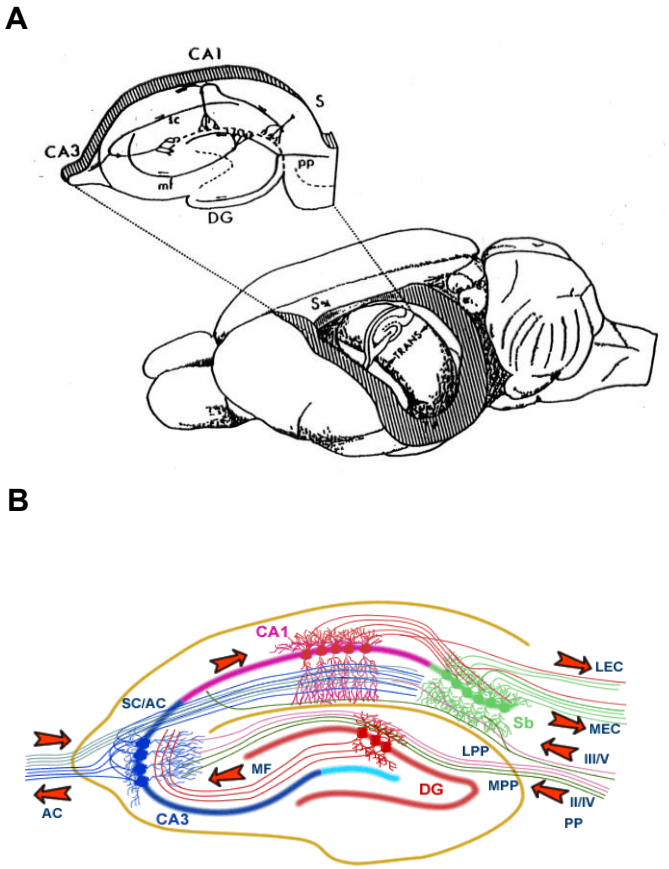

Figure 1.10: The hippocampal structure (A.) localisation of the hippocampus *in situ* in rat. **(B.)** Schematic representation of the hippocampal neuronal network. Abbr. :PP: perforant pathway (M: medial; L: lateral), DG: dentate gyrus, MF: mossy fibres, SC: Schaffer collaterals pathways, AC: associational commissural pathway, Sb: subiculum, EC: enthorhinal cortex (M: medial; L: lateral). (Figure taken from http://www.bristol.ac.uk/Depts/Synaptic/info/pathway/hippocampal.htm)

1.5.2 Neurotransmission and mechanisms underlying gamma oscillations.

The majority of the excitatory synapses are glutamatergic. The fast excitatory effect of glutamate is via the N-methyl-d-aspartate (NMDA) receptor and α-amino-3-hydroxy-5-methyl-4-isoxasole-propionic acid (AMPA)/Kainate, which are non-selective cation channel receptors and are termed ionotropic glutamatergic receptors. The inhibitory neurotransmission is exerted by the ionotropric $GABA_A$ receptors which are permeant to chloride anion. The activation of $GABA_A$ receptor by GABA leads classically to membrane hyperpolarisation, although shunting inhibition and membrane depolarisation have been reported in some circumstances, and are thought to be important in gamma oscillations (Vida et al., 2006). On the one hand, the excitatory synapses in the hippocampus are formed by principal neurons termed pyramidal neurons. On the other hand, inhibitory synapses are formed by a variety of interneurons which are widespread throughout the hippocampus.

Gamma oscillations involve the interplay of both pyramidal cells and interneurons, nobably from the basket cells type. Several studies from in vitro slices shows gamma oscillations involve an alternating sink-source pair of currents in the somatic and apical dendritic regions of CA3 (Hajos et al., 2004, Csicsvari et al., 2003). This denotes that gamma oscillations involve an intense synaptic interplay between neuronal populations.

One putative mechanism of KA induced gamma oscillations is described below, although additional mechanisms has been proposed (McBain and Fisahn, 2001). KA acts on the KA receptors, notably on inhibitory interneurons and principal neurons to a

lesser extent, leading to an overall tonic excitation of interneurons (Fisahn, 2005). The network of inhibitory neurons tonically excited would entrain each other into a rhythmic firing through their mutual inhibitory connections. This could act as a clock, determining when pyramidal cells can fire (see fig 1.11B). The pyramidal cells firing produce recurrent excitatory postsynaptic potentials (EPSPs) in the nearby pyramidal cells, however, are shortened by the disynaptic inhibitory postsynaptic potentials (IPSPs) allowing another cycle to begin (Fisahn et al., 1998, Mann et al., 2005). Additionally, the electrical coupling between pyramidal cells axons and between interneuron dendrites was reported to be important for the genesis of KA-induced gamma oscillations (Traub et al., 2003), and furthermore to their modulation in power (Hormuzdi et al., 2001). Gamma oscillations are finely tuned by the network of interneurons through $GABA_A$ergic neurotransmission. Application of barbiturates, modulate allosterically the $GABA_A$ receptors, have been shown to slow down the frequency of gamma oscillations (Jefferys et al., 1996).

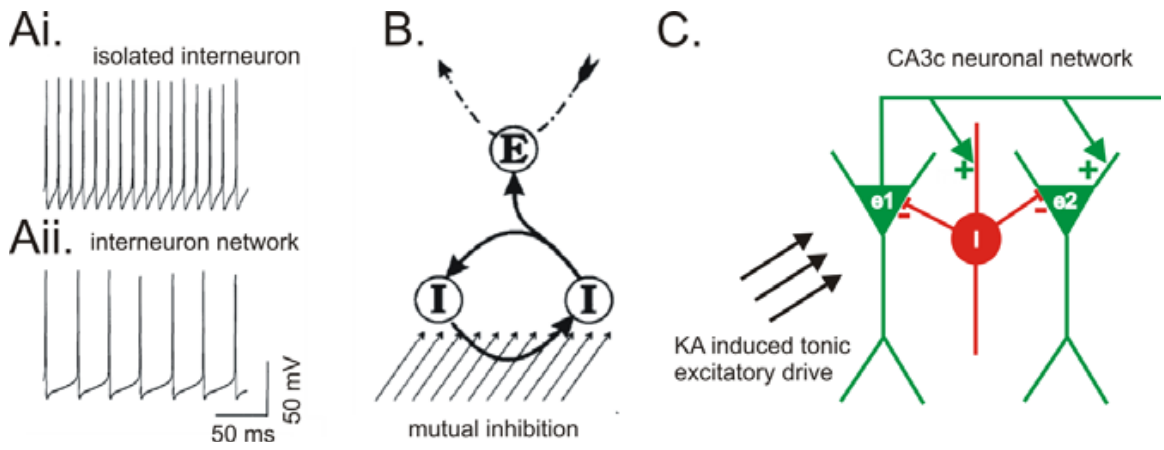

Figure 1.11: Mechanism of gamma oscillations (A.) computer modeling showing that an isolated interneuron would fire at a higher frequency than when the interneuron is included into an interneuron network where it fire at about 33 Hz (http://www.neuroscience.bham.ac.uk/neurophysiology/research/brainwaves/ing.htm.) **(B.)** Model where tonically excited (arrows) inhibitory neurons (I) are interconnected via $GABA_A$ergic synapses, controlling the pyramidal cell (E) to fire action potentials in each cycle of the oscillations (figure modified from Jefferys et al, with permission). **(C.)** CA3c neuronal network involved in gamma oscillations, (+) indicates excitatory synapses and (-) indicates inhibitory synapses.

Involvement of the KA receptors in KA-induced gamma oscillations

The distribution of KA receptors (KAR), either in presynaptic or postsynaptic localization and its presence on principal cells and interneurons, suggest that KA receptors fulfil a variety of roles in the hippocampal network. The application of KA induces a slow intracellular current in CA3 pyramidal neurons (Vignes and

Collingridge, 1997). Several studies have investigated the involvement of these glutamatergic currents in gamma oscillations.

Fisahn et al (2004) have investigated particularly the different subunits of KAR involvement in gamma oscillations. They found that the KAR containing GluR6 subunit which is mainly located on the somatodendritic region of pyramidal neurons and interneurons, are responsible for the generation of gamma oscillations, whilst KAR containing GluR5 subunit seems to prevent gamma oscillations, when located on the axons of the interneurons. The authors further pointed to the importance of KAR containing GluR6 in the control of the slow and medium afterhyperpolarisation (s/mAHP) in CA1 interneurons (Fisahn et al., 2005). Another study, extended this result to CA1 pyramidal neurons, showing that KA inhibit the sAHP through the GluR6 subunit, increase the neuronal excitability and consequently, allowing gamma oscillations genesis (Melyan et al., 2002). Previous studies suggested that application of the 2-amino-3-(5-*tert*-butyl-3-hydroxy-4-isoxazolyl) propionic acid (ATPA), which is a selective agonist of GluR5 induces an inward current which results in the firing of interneurons CA1 area. These inhibitory currents are responsible for a tonic GABAergic inhibition (Cossart et al., 1998). The same authors analysed interneuron-interneuron synapses in CA1 (Cossart et al., 2001). They confirmed that the activation of the KAR containing GluR5 which are present on GABAergic presynaptic terminals, induced an increase in the frequency of the miniatures IPSCs without a change in their amplitude. Therefore, this demonstrates that KA increases the mutual inhibition in CA1 area. In summary, KA increases the efficiency of the inhibitory neurotransmission between interneurons and induces a slow depolarisation of CA3

pyramidal neurons (Vignes and Collingridge, 1997). KAR containing GluR5 subunits are controlling the release of GABA, i.e. set the inhibitory tone. KAR containing GluR6 are providing the necessary depolarisation of pyramidal neurons and interneurons.

In summary, interneurons in CA3, which are synaptically and electrotonically connected, induces a rhythmic activity under the tonic excitation induced by KA. This rhythmic activity of interneurons has for function to synchronize principal cells firing.

The principal functions allocated to gamma oscillations are *i)* a role in awakeness, as it is shown that general anaesthesia inhibit gamma oscillations (Faulkner et al., 1998); *ii)* sensory processing and *iii)* memory formation. The latter is described in the following section

1.5.3 Role of the hippocampal gamma rhythm in memory processes

The concomitant activation of the mossy fibres and the CA3 neurons in the gamma frequency would induce long-term potentiation at the recurrent synapse in CA3 (Lisman, 1999). The gamma frequency range would be the most suited to induce memory processes compared to slower and faster frequencies (Buszsaki, 2006).Gamma oscillations are satisfying the Hebbian principles of learning, which state that activity must occur at the same time in the pre- and postsynaptic cells in order for the synaptic potentiation to occur.

Once the CA3 neurons population is synchronized by KA, it may induce a form of plasticity which is called spike timing-dependent plasticity (STDP). The STDP would play an important role in the processing and storage of information in neural circuits

(Dan and Poo, 2006). Gamma oscillations synchronize pre and postsynaptic activity so that they induce LTP in the neural circuitry. It is important to note that the CA3 pyramidal neurons recurrent network is thought to be the place where the information is stored in the hippocampus. Therefore the potentiation of those synapses induced by gamma oscillations would be the mechanisms by which the informations are stored (Lisman, 1999). It is now well described by several *in vivo* studies that episodic memory formation is associated with synchronous neuronal activity in the gamma frequency range (Montgomery and Buzsaki, 2007). In *In vivo* EEG studies in human, it can be observed an increase mainly of the gamma oscillations during the formation of new episodic memories (Gruber et al., 2002, Sederberg et al., 2003). The fact that gamma oscillations could underlie the working memory in the hippocampus has become well established by the work of Basar-Eroglu et al. (2007), assessing working memory via several tests in schizophrenic patients. Additionaly, gamma oscillations have been associated with selective attention (Jensen et al., 2007). The diverse roles of gamma oscillations are summarized in table 3. Gamma oscillations is related to memory task performance (Montgomery and Buzsaki, 2007)

role of gamma oscillations	References
Loss of power during anesthesia	(Faulkner et al., 1998)
Mental practice	(Lutz et al., 2004)
Working memory	(Jensen and Lisman, 2005)
Episodic memory	(Montgomery and Buzsaki, 2007)
Sensory binding	(Engel et al., 2001, Montgomery and Buzsaki, 2007)
Object representation	(Tallon-Baudry and Bertrand, 1999)
Perceptual learning task	(Gruber et al., 2002)
selective attention	(Jensen et al., 2007)

Table 1.3: Recapitulation of the roles of gamma oscillations

1.6 Working hypothesis

This study aimed to examine the neuronal phenotype of OPHN1 knockout mice. As patients with mutations in the OPHN1 gene (and hence no oligophrenin1) display mental retardation, it may be predicted that *Ophn-1*$^{-/y}$ mice may provide a good model of mental retardation. To that end, the aim of this study was to examine the ability of *Ophn-1*$^{-/y}$ mice to generate kainate-induced gamma oscillations, which are predicted to underlie higher cognitive function.

1.7 Outline of the thesis

The first chapter addresses the electrophysiological characterisation of the hippocampus of *Ophn-1*$^{-/y}$ mice using extracellular recordings. As synchronous neuronal activity is thought to underlie higher cognitive function, KA-induced gamma oscillations were studied in the CA3 region of the hippocampus. In the second chapter, I investigated the inhibitory and excitatory neurotransmission which input to CA3 pyramidal neurons and are highly involved in gamma oscillations, using whole cell recordings techniques. The mechanisms underlying the loss of gamma power in *Ophn-1*$^{-/y}$ mice was established. A third chapter was dedicated to an electrophysiological investigation of a deficit in excitatory neurotransmission in *Ophn-1*$^{-/y}$ CA1 pyramidal neurons

Chapter 2: MATERIALS AND METHODS

2.1 Experimental animals

Ophn-1 mutant mice were generated by homologous recombination. This consisted of inserting a hygromycin resistant gene cassette flanked with Lox P sites into the coding sequence of the exon 9, the deletion of the sequence was catalyzed by the CRE recombinase between LoxP sites (fig. 2.1 A.). The inserted 100 bp of junk DNA into the open reading frame of the exon 9 contained led to a premature STOP codon (frameshift mutation) after the BAR domain and in front of the PH and GAP domains. The suitable embryonic stem (ES) cells were selected and implanted in female breeders. The mice were cross-bred for at least 8 F1 generations in order to obtain a stable colony of *Ophn-1*$^{-/y}$ mice. The mice were developed by Dr. Pierre Billuart and colleagues (Khelfaoui et al., 2007).

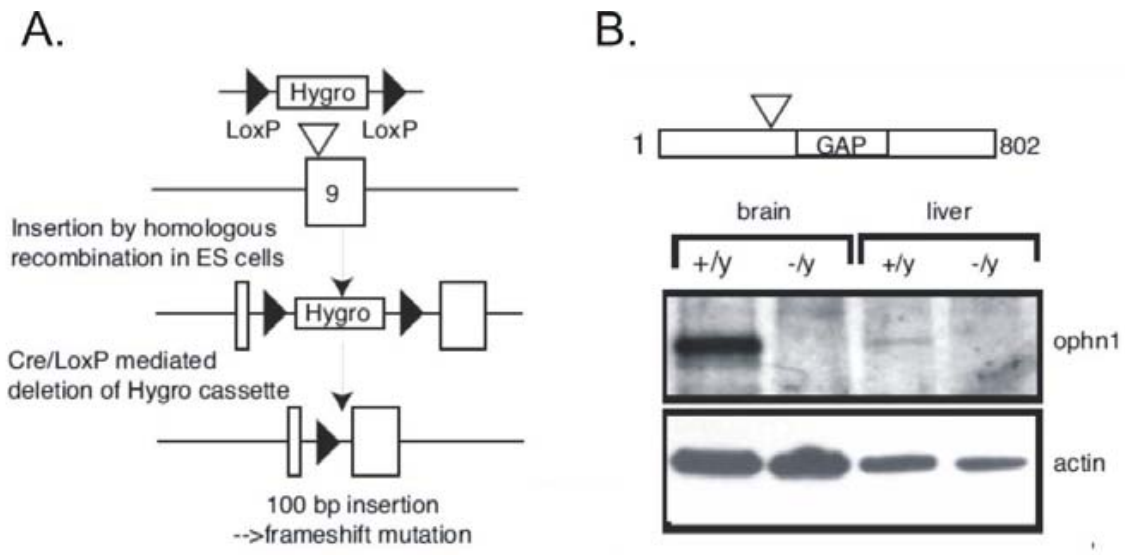

Figure 2.1: Schematic representation of the constitutive inactivation of OPHN-1 gene. (A.) Strategy of the constitutive inactivation of the OPHN-1 gene (explanation contained in the text) **(B)** Western blot of brain and liver from *Ophn-1*$^{+/y}$ and *Ophn-1*$^{-/y}$ mice with antibodies recognizing both ends of oligophrenin1 protein (Both figures are courtesy from Dr P. Billuart, Institut Cochin, Paris, France)

Figure 2.1B shows the western blot of brain and liver extracts for both genotypes. It can be noted that neither the full length nor truncated forms of oligophrenin1 protein were detected in adult *Ophn-1*$^{-/y}$ mice.

A colony of *Ophn-1* mice was generated by breeding C57bl6 wild type (WT) male mice with heterozygote (*Ophn-1*$^{+/-}$) female mice. As the OPHN1 gene resides on the X-chromosome, male mice were either *Ophn-1*$^{+/y}$ (WT) or *Ophn-1*$^{-/y}$ (KO), in an approximately 50:50 ratio (fig. 2.2 A.). Mice were bred in the Biomedical Services

Unit, University of Birmingham, according to the Animals (Scientific Procedures) Act (1986).

All mice were adult (20-30 g, 3-8 weeks) when used for experiments, which were carried out according to the UK Animals (Scientific Procedures) Act (1986) and care was taken to minimize the number of animals and their suffering. Experiments were performed blind to the genotype of the animal. Genotyping of the experimental animals was performed at weaning and also after analysis of the experimental results. Genotyping was performed using polymerase chain reaction (PCR) assay (see below).

2.2 Mouse identification

2.2.1 DNA digestion protocol

DNA was obtained from either an ear notch or a 5 mm piece of tail. Ear tissue was taken when the animals were weaned; mice were exposed to isoflurane (4% maintain at 2%) prior to tissue sampling. Tail tissue (5mm) was taken post-mortem. Tissue was digested in 0.5 ml of lysate buffer plus 0.1 mg/ml of proteinase K at 55°C overnight. Lysate buffer comprised 100 mM Tris (pH 8.5), 5 mM EDTA, 0.2% SDS and 200 mM NaCl.

2.2.2. Polymerase Chain Reaction assay

DNA purification

Following tissue digestion, vials were vortexed and centrifuged at 16 g for 5 minutes in order to remove the hair (Centrifuge 5415D, Eppendorf UK limited, Cambridge, UK). The resulting supernatant was gently mixed with equal volumes of isopropanol, and then the DNA was allowed to precipitate. After DNA precipitation samples were centrifuged at 16 g for 30 minutes. The supernatant was then removed and the DNA pellet was carefully washed with ethanol (70% v/v) to remove contaminants from the DNA sample which strongly inhibit the *taq* polymerase. The ethanol was removed and the pellet was allowed to dry for ~ 15 minutes prior to re-suspension in 50 μl of sterile, distilled water either in the fridge overnight or for 10 minutes in a water bath at 50°C.

PCR mix preparation

In order to optimize the process of genotyping, PCR was performed using commercial PCR kits (reddyMix PCR Master Mix, ABgene, Epson, Surrey, UK). This mix contained all essential PCR components (water, buffer, dNTPs and *taq* DNA polymerase). The solution for the PCR reaction contained, 1 μl each of the forward primer (gcc cat gtt gtg adc aga gaa atc), 1 μl each of the reverse primer (gga agc tag agg atg acc ctg), 1μl of sample DNA and 17μl of master mix.

PCR conditions

The PCR reaction was performed in a thermal cycler (Mastercycler gradient, Eppendorf UK limited, Cambridge, UK) in the presence of 1.5mM $MgCl_2$. The initial denaturation was done at 94 °C for 3 minutes followed by 35 cycles of PCR. Each cycle comprised: 30 s of denaturation at 94 °C, 30 s of annealing at 55 °C and 30 s of elongation at 72 °C.

PCR results visualization and interpretation

As the mastermix already contained the loading buffer, 10 μl of the PCR products were directly loaded and ran in a 2%n agarose gel at 130 V for an hour (Figure 2.2B.). As *Ophn-1*$^{-/y}$ mice were generated by insertion of 100 base pairs of junk DNA (see section 2.1), *Ophn-1*$^{-/y}$ mice were identified by the presence of a larger DNA fragment which allowed differentiation between genotypes.

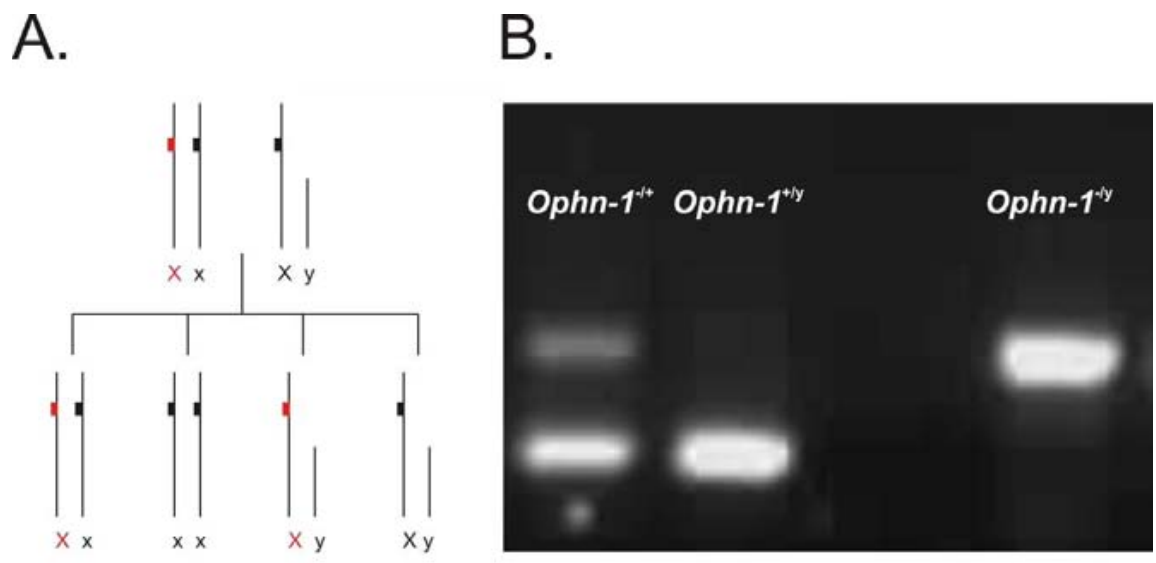

Figure 2.2: Transmission and detection of *Ophn-1*$^{-/y}$ (A.) Genetic transmission of oligophrenin1 deficiency. **(B.)** Photograph taken from an agarose gel, showing the PCR products resulting from the genotyping. Each line represents different PCR products corresponding to one mouse; *Ophn-1*$^{+/-}$ is the pattern for female heterozygote; *Ophn-1*$^{-/y}$ and *Ophn-1*$^{+/y}$ are the pattern for mutated and not mutated males alleles respectively.

2.3 *In Vitro* slices preparation

Randomly selected adult male mice, were anaesthetized by intraperitoneal injection of a ketamine (76 mg/kg)/ medetomidine (1 mg/kg) mixture and then killed by cervical dislocation. After dislocation of the neck, the brain was quickly removed and immersed in ice-cold cutting solution (2ºC) for approximately 1 minute, previously bubbled with carbogen (95% O_2, 5% CO_2) in order to slow down the metabolic rate

and reduce hypoxia-induced damage. The composition of the cutting solution (Sucrose aCSF) was (in mM): 189 sucrose, 26 $NaHCO_3$, 5 $MgCl_2$, 2.5 KCl, 1.2 NaH_2PO_4, 0.1 $CaCl_2$; 10 D-glucose, pH was equilibrated at 7.4 with a 95%-5% O_2/CO_2 gaseous mixture. The use of sucrose aCSF solution brought about many advantages which resulted in enhanced slices quality. The replacement of NaCl by sucrose means that less Chloride is available for the slice which reduces cell swelling (Aghajanian and Rasmussen, 1989). Additionally, the reduced concentration in Na^+ attenuated cells spike firing. It is noteworthy that the cutting solution also contained a low concentration of Ca^{2+} which further attenuated neurotransmitters release.

It is important to note that for the CA3 neuronal investigations, cardiac perfusion was performed. Animals were intracardiacally perfused, with a needle (gauge 25) with ~ 10 ml of chilled sucrose aCSF (previously gassed with 95%-5% O_2/CO_2) at a flow rate of 2.7 ml per minute, using a syringe pump (Model 341A; Sage Instruments). The liver was punctured using a sterile scalpel (#23 blade) to allow the blood to flow out. The cardiac perfusion was performed by Dr A.D. Powell (University of Birmingham) to comply with the Animals (Scientific Procedures) Act (1986). The rationale of cardiac perfusion performed prior brain removal was to enhance cell survival, notably fragile CA3 neurons. Complete replacement of the circulating blood by sucrose had a strong protective effect on the brain, which allowed CA3 pyramidal neurons to be recorded in this study.

After cooling, the brain was glued onto a support and dissected into separate hemispheres by a cut through the midline. The brain was glued onto the dorsal

surface and cut from ventral surface. The brain was cut either into 400-µm-thick horizontal (extracellular experiments) or 300-µm-thick coronal (CA1 whole cell recording (WCR)) or horizontal slices (CA3 WCR), using an Integraslice (Campden Instruments, Sileby, UK). Cutting was made with a ceramic blade at a speed of 0.1 mm per second. Slices containing the ventral hippocampal structure (typically from when the optic chiasm appeared), were selected and categorised according to their level: from ventral to dorsal (e.g. OC for the slice containing the obvious optic chiasm, D1 for the next more dorsal slice, D2, D3 etc). Slices were transferred into a storage interface chamber (at room temperature) containing aCSF bubbled with a mixture of 95%-5% O_2/CO_2.

2.4 Electrophysiology

2.4.1 Extracellular field recordings

Experimental Protocol:

For extracellular recordings, a first slice was put straight into an interface chamber and allowed to equilibrate for an hour at the interface between aCSF and moist carbogen (300 cm^3/min). Slices were perfused with aCSF at a perfusion rate of ~ 5 ml/min, the temperature was maintained at either 30ºC or 32 ºC (as indicated in text). aCSF contained (in mM): 125 NaCl, 26 $NaHCO_3$,3 KCl, 2 $CaCl_2$, 1.25 NaH_2PO4, 1 $MgCl_2$, and 10 D-glucose, pH was equilibrated at 7.4 with a 95%-5% O_2/CO_2 gaseous mixture. The remaining slices were kept in an interface storage

chamber at room temperature. Slices were visualised with a stereo-microscope (Leica MZ8, Micro Instruments, Long Hanborough, Oxon, UK) mounted above the interface chamber.

Extracellular microelectrodes (tip resistance: 2 to 4 MΩ) were pulled from thick walled borosilicate glass capillaries of 1.2 mm O.D. x 0.69 mm I.D. (Harvard apparatus, Edenbridge, Kent, UK) using a P-97 horizontal micropipette puller (Sutter Instrument Co, Novato, CA, USA) and filled with aCSF. The extracellular microelectrodes were connected to an Axoclamp 2B (Molecular Devices, Sunnyvale, CA). Signals were sampled at 10 kHz using CED 1401 interface (Cambridge Electronic Design [CED], Cambridge, UK)and low-pass filtered at 3 kHz, using a Neurolog NL-125 filter unit (Digitimer, Welwyn Garden City, UK). Additionally, an Humbug 50/60 Hz (Digitimer) was used to remove powerline noise. Either Signal 2 (version 2.16) or Spike 2 (version 5.14) (CED)were used as data acquisition software. Data were then stored onto a computer hard drive for subsequent off-line analysis using either Signal 2 or Spike 2.

***i)* Evoked field potentials in CA1 area.**

Evoked field potentials were recorded from the *Stratum* radiatum and *S*. pyramidale of the CA1 hippocampus. A concentric stainless steel electrode (MCE100x50mm Harvard Apparatus, Edenbridge, UK) was placed onto the Schaffer collateral pathway at the level of CA1c (see fig. 2.3). The Schaffer collateral pathway was stimulated via an isolated stimulator (Model DS2, Digitimer, Welwyn Garden City,

UK). A stimulus response curve was performed in order to determine the voltage which gave the half maximum response (V_{50}), which was used in subsequent experiments.

***ii)* Evoked field potentials in CA3 area.**

Similarly to the CA1 region (see above), evoked field potentials were recorded from extracellular microelectrode impaled in the *S*. pyramidale and S. radiatum of the CA3c area of the hippocampus. A concentric stainless steel electrode was placed in the hilar region to stimulate the mossy fibre pathway. A stimulus response curve was performed. The stimulation of the mossy fibres pathway mimics the activation of the granule cells located in the dentate gyrus which synapse onto CA3 pyramidal cells and interneurons.

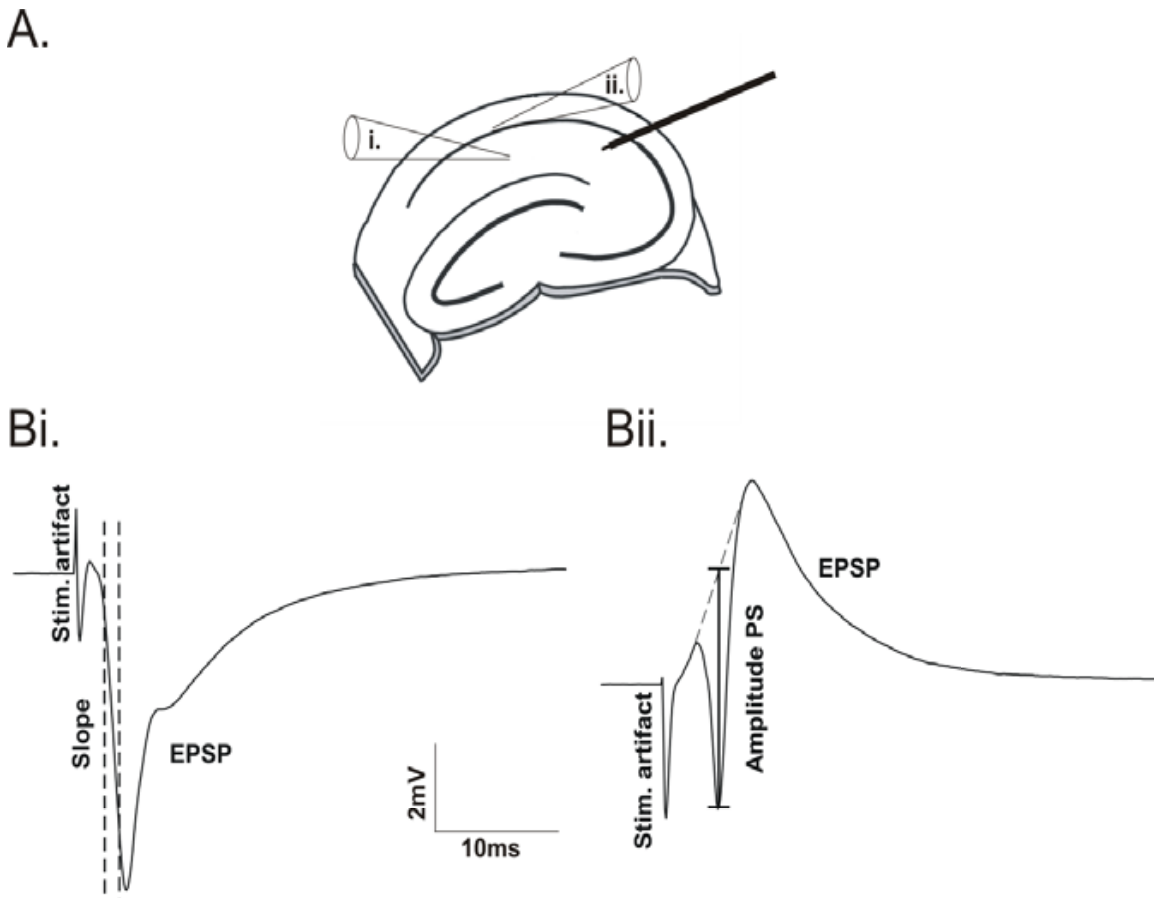

Figure 2.3: Evoked field experiments in CA1 area. (A) Schematic representation of the hippocampus with the position of the microelectrodes **(Bi)** A typical response recorded by the microelectrode placed in the *S.* radiatum (dendritic region), this was the postsynaptic potential (PSP); the measure of the slope yielded an indication of the excitatory synaptic inputs. **(Bii)** A typical response recorded by the microelectrode placed in *S.* pyramidale (soma region) which is termed population spike (PS) and corresponds to synchronous action potentials firing of a population of neurons.

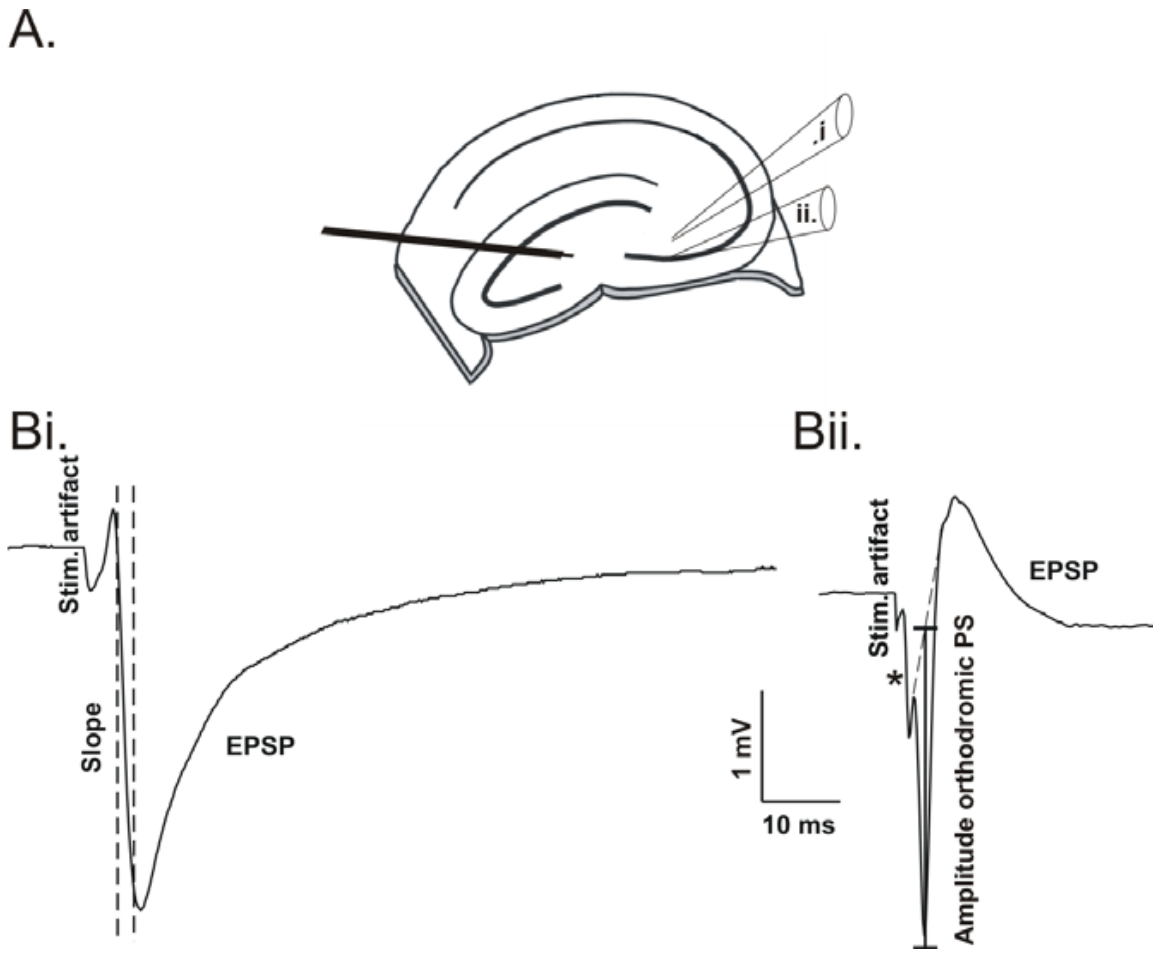

Figure 2.4: Evoked field experiments in CA3 area. (A) Schematic representation of the hippocampus with the respective position of the microelectrodes **(Bi**) Typical response recorded by the microelectrode placed in the *S.* radiatum, this is the postsynaptic potential (PSP) **(Bii)** A typical response recorded by the microelectrode placed in *S.* pyramidale.

Paired-pulse stimulation experiments in CA1 area

Paired-pulse stimulation experiments consisted in two equal intensity stimuli (V_{50}) separated by various time intervals, namely 5, 10, 25, 50, 100, 250 and 500 ms. The

first pulse is usually referred as the conditioning stimulus and the second pulse as the test stimulus which assessed the response of the synapses.

Paired-pulse stimulation experiments in CA3 area

After determination of the V_{50}, paired pulse stimulation of two equal intensity stimuli with inter-pulse intervals 10, 20, 25, 50, 100, 250, 500, 1000 and 1500ms was performed.

Generation of network field oscillations.

After placing the electrodes, baseline activity was recorded for 5 minutes. Subsequent to this gamma oscillations were evoked by addition of 50 nM of Kainic Acid (KA) (Tocris, Bristol, UK) to the circulating aCSF. This concentration is routinely used in this laboratory and is known to produce consistent gamma oscillations (Vreugdenhil and Toescu, 2005). For gamma oscillation studies, extracellular electrodes were placed in stratum pyramidale of CA3c region.

To investigate the synchronization of gamma oscillations within the hippocampal structure, one extracellular microelectrode was left in CA3c and a second electrode was moved randomly in ~200 µm steps along the cell layer of the Ammon horn (fig. 2.5).

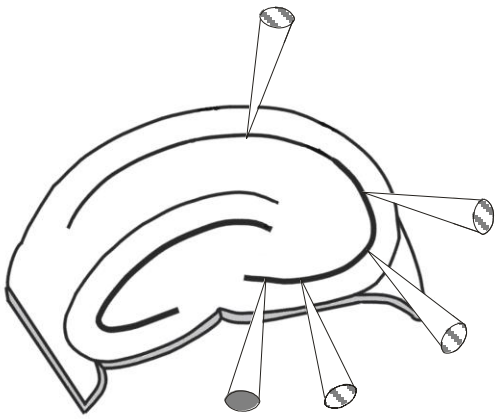

Figure 2.5: Schematic representation of the experimental protocol for the synchronization study. The microelectrode (shaded in grey) was positioned in CA3c, whilst microelectrode 2 (hatching in grey) was moved along the *S.* pyramidale.

Data acquisition and analysis

i) Evoked field potentials analysis

Stimulation of the Schaffer collaterals pathway mimics the activation of CA1 pyramidal neurons by the CA3 pyramidal neurons. Figure 2.3Bi shows the response recorded by the microelectrode placed on the *S.* pyramidale. The population spike is a negative deflection occurring during the postsynaptic potential (PSP) and reflects the net current flowing due to action potential firing. The amplitude was measured by extrapolating a line from the trough of the population spike to the intercept on the PSP (see fig 2.3Bii.). Figure 2.3Bi. shows the population synaptic

potential recorded by the electrode impaled in S. radiatum, the measure of the slope is an indicator of the strength of the synaptic inputs from CA3 through the Schaffer collaterals pathway.

The 10-90% slope of the PSP was taken as a measure of the synaptic activation. Current applied to the axon bundle emerging from the CA3 pyramidal neurons artificially evoked synchronous action potentials in these fibres. This summation of action potentials propagated along the axons to finally induce the release of glutamate at the synaptic cleft. The recording electrodes being placed on the postsynaptic CA1 pyramidal neurons recorded the flow of ions in and out the neurons as a consequence of this synaptic activation. The currents generated by ions flowing in and out the extracellular space were detected by the recording electrodes.

Stimulation of the mossy fibres pathway activated axons from granular cells and consequently CA3 pyramidal neurons. PS was recorded from a microelectrode (microelectrode) placed in CA3c *s.* pyramidale as a negative deflection superimposed to the PSP (fig 2.4 Bi.). It is important to note that in CA3, firstly an antidromic PS was recorded followed by an orthodromic PS. Antidromic PS was the reflection of the direct activation of CA3 pyramidal neurons axon fibres, whilst orthodromic PS was the results of the synaptic activation of CA3 through mossy fibres (fig 2.4 Bii.)

ii) Paired-pulse stimulation analysis

Paired pulse studies were performed using 50% of the maximal PSP slope stimulus intensity. Paired pulse data were expressed as the ratio of either PSP slopes or PS amplitudes of the test pulse over the response of the conditioning pulse (Pulse 2/ Pulse1).

Similar analysis was applied to CA3 paired-pulse stimulation experiments.

iii) Network field oscillations analysis

The power of oscillations was measured by performing fast Fourier transformations over epochs of 100 seconds worth of data. (FFT size: 2048 (1.024s), correspond of the width of peak frequency window). The power spectrum quantified the proportional power of each wavelength within the section of data. The fast Fourier transformation corresponds to the distribution in frequency of the recorded signal. It depicted how a signal was distributed along frequency. The fast Fourier transformation decomposed the signal into cosine wave forms, assigning respective power to each of them. Data were expressed either as peak or summated power values of the gamma frequency band which was considered to be between 20 and 80 Hz. The lower limit of 20 Hz was used as the low superfusing temperature bath solution (~30 °C), in order to alleviate the strong metabolic demand implied in gamma oscillations (Huchzermeyer et al., 2008). The higher limit 80 Hz is classically chosen in this kind of study although some studies used a top frequency range limit

of 60 Hz (Vreugdenhil and Toescu, 2005). Expression of the data as summated power allowed assessing changes across the gamma frequency band (fig. 2.6 grey area).

The normalisation of the power of gamma oscillations was performed by dividing data points by the maximum power.

Gamma waveform average was determined in 5 slices from 5 *Ophn-1*$^{+/y}$ and in 5 slices from 5 *Ophn-1*$^{-/y}$ mice. For each gamma oscillations recordings 5 large gamma cycles (at t=60 min) were averaged. The trough was taken as zero and a normalisation for peak-to-trough amplitude was performed.

To assess the synchronization of gamma oscillations within different areas of the hippocampus through coherence analysis, a Spike 2 script (written by CED) was used. Coherence compared the frequency profile of the power spectra obtained from gamma oscillations. The coherence of two gamma oscillations was the measure of their similarity in frequency domains and ranges from 0 to 1. A coherence value of 1 results from the power at one frequency being identical from both microelectrodes (See fig. 2.7). Figure 2.7 Ai. & Aii. describe gamma oscillations obtained by two different recording microelectrodes. The coherence script performed power spectra for each electrode (Fig 2.7 Bi, Bii) and then compared them, yielding a peak coherence value (Fig 2.7 Biii).

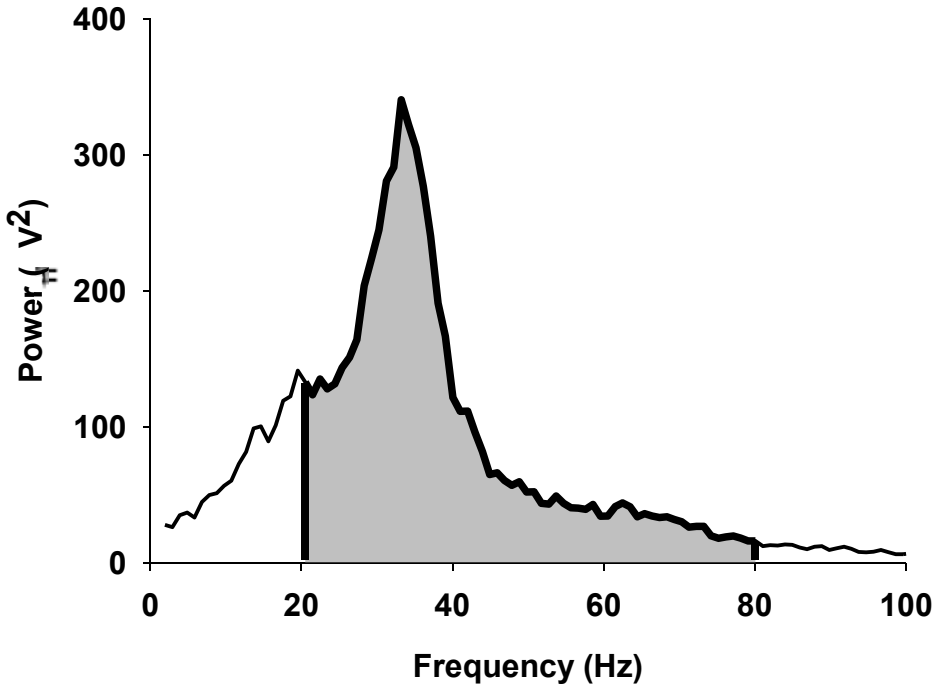

Figure 2.6: Measuring the power spectrum. Peak frequency was taken at the point where the power was the highest (peak power). Summated power corresponds to the area shaded in grey.

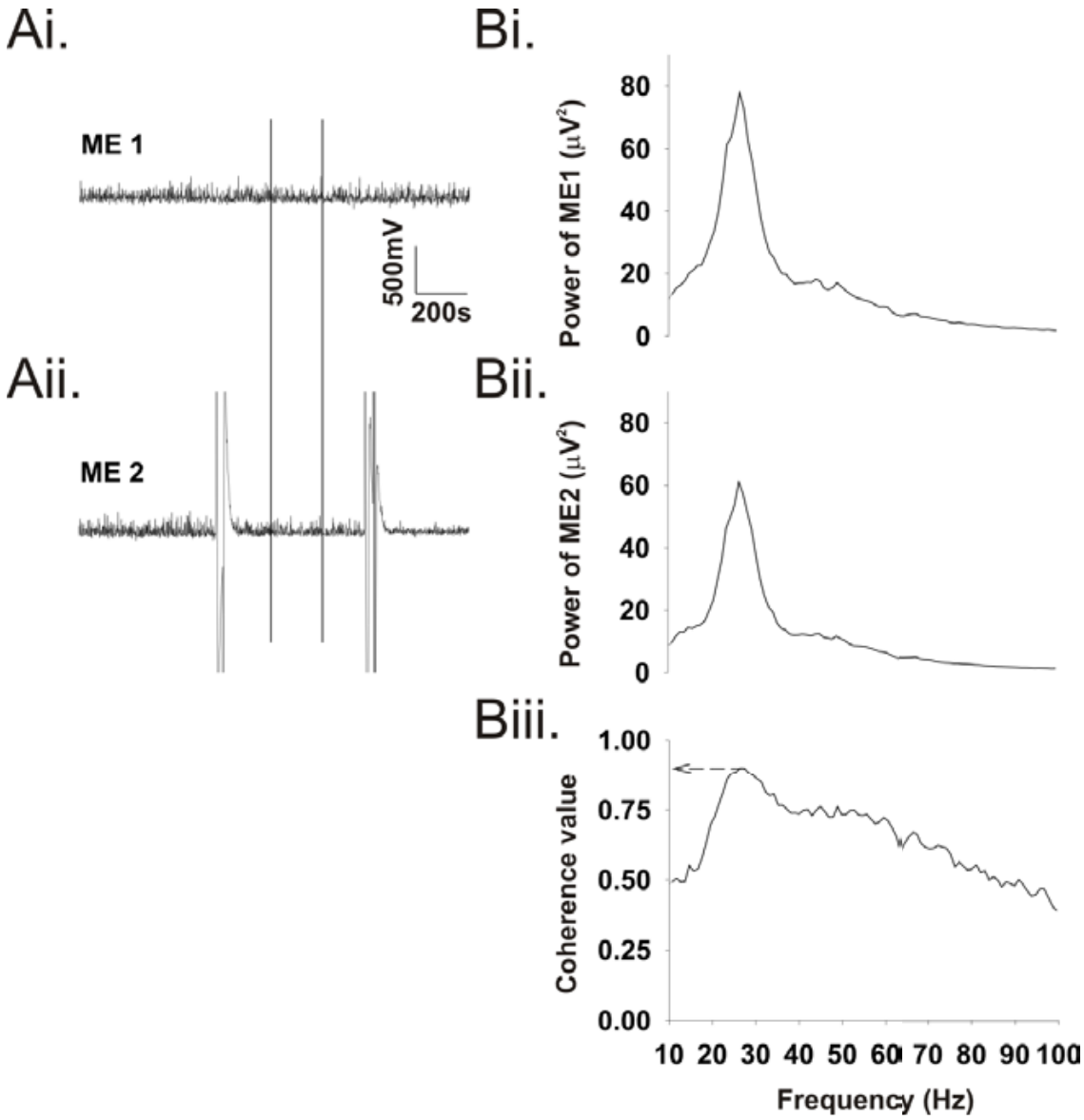

Figure 2.7: Example of coherence analysis. Traces of gamma oscillations for the microelectrode 1 (ME1) impaled in CA3c **(Ai.)** and microelectrode 2 (ME2) impaled CA3c/b **(Aii.)**, and the corresponding power spectra (**Bi.** for ME1) (**Bii.** for ME2). **(Biii.)** The coherence value plotted against the frequency. (The two vertical cursors delineate the data processed by the script)

Rhythmicity of the network field oscillations

Auto-correlation analysis

In order to assess the regularity of the recorded gamma oscillations, I performed autocorrelation analysis which is the cross correlation of the signal with itself. 100 seconds worth of raw taken after 1 hour recording was submitted to the auto-correlation analysis. The second peak value is high in the case of an oscillatory pattern in the signal. Therefore the second peak value was taken as a measure of regularity of gamma oscillations. Figure 2.8 A. illustrates a representative auto-correlogram, the vertical thicker line represented the measure of the secondary peak. This corresponds to the peak in between the trough; the rationale was to cancel out the slow theta component from the signal. On the top panel one can notice that there are very slow underlying oscillations on which the gamma oscillations lie. Those oscillations are about 5Hz. Slower oscillations will not show up as a peak in the autocorrelogram because I measure the time to the next peak which is from a faster rhythm. Therefore the only way to notice that there are slow oscillations is a deviation from 0 in the autocorrelogram. If one observe closely at figure 2.8A and one can notice about half a cycle from that 5 Hz oscillation. In the case that there would be no slow oscillations it would be perfectly at 0.

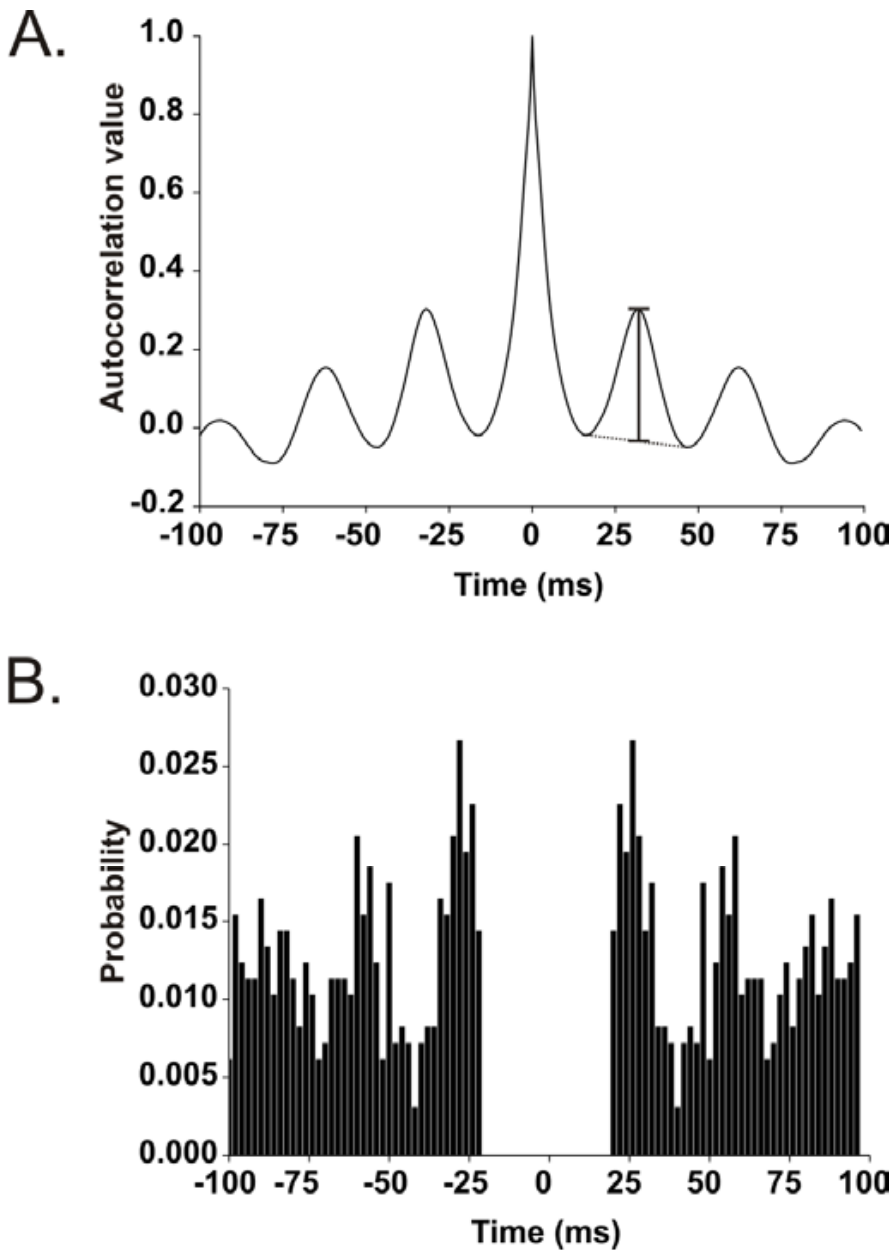

Figure 2.8: Assessment of the rhythmicity of gamma oscillations (A.) Example of an autocorrelogram performed for gamma oscillations recordings at 1h**.** The thicker vertical line indicates the measure of the secondary peak. **(B.)** Example of an event-autocorrelogram performed on an epoch of gamma oscillations recording.

Event-autocorrelation analysis

The trough of each gamma cycle was taken as a reference on a 100 s epoch of gamma oscillations recording. Event-autocorrelation analysis assessed how regular the troughs were separated. In the case of clear rhythmicity, the event-autocorrelogram showed a clear peak which regularly repeated. As the frequency of gamma oscillations were around 30 Hz, the intervals between each trough have been set to be above 20 ms. Furthermore, the bin size had to be less than 20 ms, therefore 2 ms was chosen in order to get a good resolution. Finally, event-autocorrelation was expressed as a probability by dividing the number in each bin with the total numbers of observations.

2.4.2 Whole cell recordings

i) **Experimental protocol**

Slices were transferred to a submerged chamber and continually perfused (5ml/min) with aCSF at either room temperature or 30ºC bubbled with carbogen (for composition refer to aCSF in extracellular field recording). Slices were allowed to equilibrate for 10 minutes in the chamber prior to recording, and changed after ~ 1 hour. Slices were visualized using differential interference contrast optics on an Olympus BX50WI upright microscope.

Whole-cell patch clamp recordings were made from visually identified CA1 pyramidal neurons or CA3 pyramidal neurons. For current clamp recordings the internal solution comprised (in mM): 135 $KMeSO_4$, 8 NaCl, 10 HEPES, 2 Mg-ATP and 0.3 Na-GTP; adjusted to pH 7.3 with KOH (osmolarity ~285 mOsm). The internal solution also contained 200 μM ALEXA 488 to aid visual identification of neurons. Patch electrodes filled with this internal solution had a resistance of ~ 5 MΩ. The resting membrane potential was manually adjusted to -65mV. For voltage clamp recording, several internal solutions were used (stated in the text).

Intrinsic neuronal properties study

An input-output curve was generated by injecting varying amounts of current and counting the resultant number of action potentials. The current injection was 200 ms in duration (see fig.2.9A.). The action potential amplitude was measured from the resting membrane potential (RMP) to the peak of the action potential (fig 2.9B.). The action potential threshold was identified as the start of the upstroke of the action potential (see fig 2.9B. arrow). The “half width” duration of the action potentials was measured as the duration of the action potentials at the half amplitude of the action potential (fig 2.9B).

A commonly investigated phenomenon is the afterhyperpolarisation (AHP) occurring after repetitive action potential firing. To evoke the AHPs, 50 pulses of 3 ms duration

and 0.8 nA of intensity, were applied at a frequency of 5 to 100 Hz for CA1 pyramidal neurons only (fig 2.9C.). This protocol evoked both a medium and a slow AHPs. The medium AHP was measured 300 ms after the last action potentials fired (fig 2.9: first bar figured in the inset). The slow AHP was measured at 1s after cessation of action potentials firing (fig 2.9: see the second bar in the inset). For both the medium AHP and the slow AHP, the amplitude was measured from the resting membrane potential (RMP). Afterhyperpolarisation was also assessed in term of currents. Neurons were held at a potential of -65 mV in voltage clamp mode, then a depolarizing voltage step of 70 mV was given for 300 ms. The measure of I_{AHP} and I_{sAHP} were made at -60mV, the peak of current yielded the medium AHP and a second after yielded the slow AHP (fig. 2.9 D.).

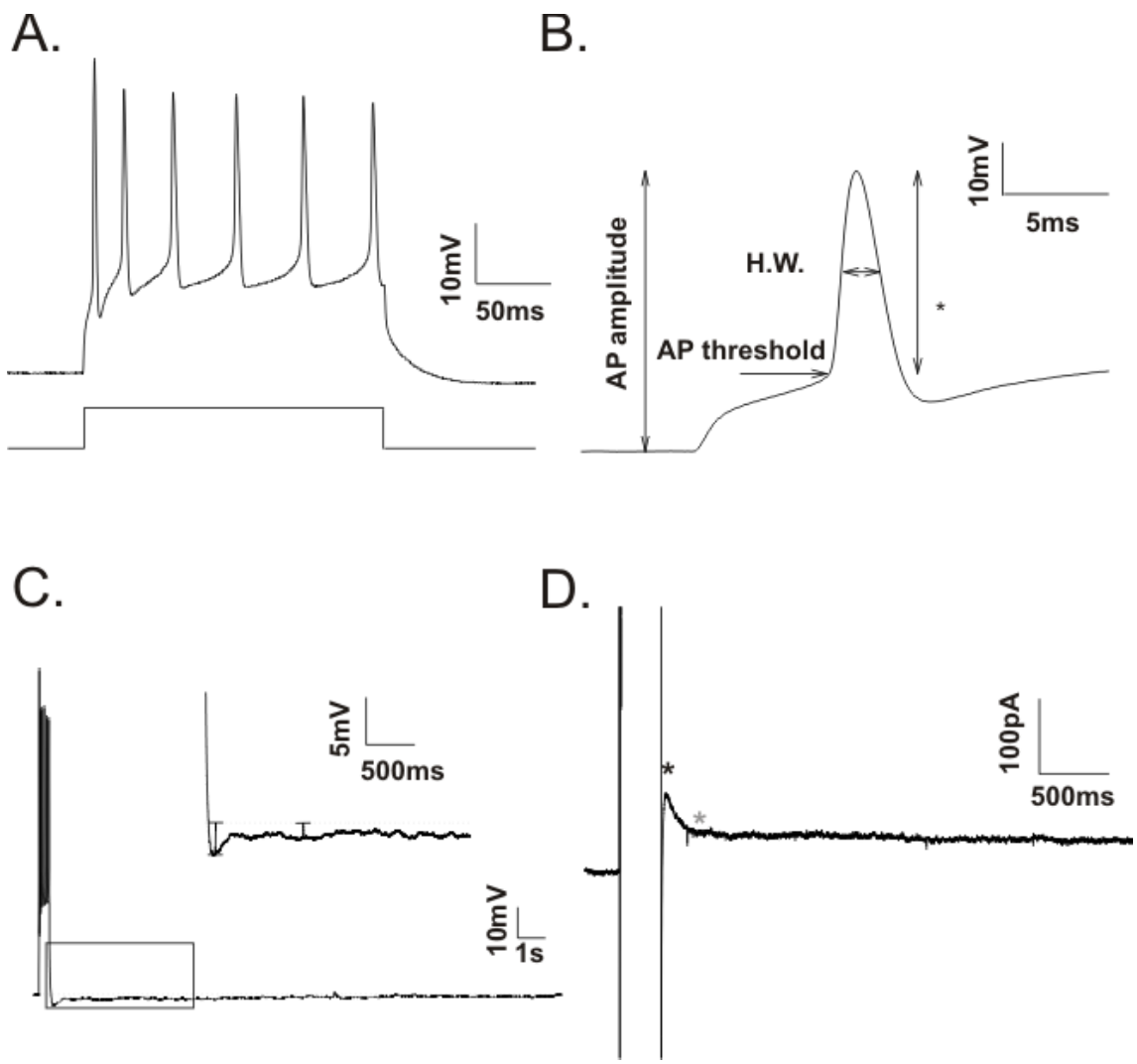

Figure 2.9: Measurement of the intrinsic neuronal properties. (A) Trace of recording of a train of 50 action potentials followed by medium and slow AHP. **(B)** Action potentials fired in response of a step of 200 ms depolarizing current **(C)** sketch of a detailed action potentials. **(D.)** Depolarising step of voltage evoking afterhyperpolarisation currents (I_{AHP} and I_{sAHP})

Synaptic properties study.

Internal solutions contained (in mM): 140 $CsMeSO_4$, 8 NaCl, 10 HEPES, 5 QX-314, 0.5 EGTA, 2 Mg-ATP and 0.3 Na-GTP; adjusted to pH 7.3 with CsOH (osmolarity ~285 mOsm) for the recording of excitatory postsynaptic currents (EPSCs) and 135 $CsCl_2$, 2 $MgCl_2$, 10 HEPES, 5 QX-314, 1 EGTA, 2 Mg-ATP and 0.3 Na-ATP, adjusted to pH 7.3 with CsOH, for inhibitory postsynaptic currents (IPSCs). The main cation K^+ has been replaced by Cs^+ in order to block K^+ related conductances, and improve space clamp, leading to an increase in the membrane resistance.

Both EPSCs and IPSCs were evoked by a stimulation of the Schaffer collaterals pathway or the mossy fibres pathway using a concentric electrode placed ~ 250 µm from the cell recording site. The EPSCs were isolated by holding the membrane potential at the reversal potential for the IPSCs (at 0 mV) (only eIPSC CA1). Spontaneous synaptic events were recorded for ~5 minutes to evaluate basic release properties in the presence of NBQX (20µM) and D-APV (25µM). Similarly the IPSCs were isolated by holding the membrane potential at the reversal potential for the EPSCs (at -70mV) owing to the intracellular solution containing a high concentration of Cl^-. This internal solution displaced the equilibrium potential for the Cl^- to 0 mV, hence when the cell was hold at -70mV the $GABA_A$ergic currents were recorded as negative deflections. The use of this internal solution permitted optimised resolution of the events.

Evoked postsynaptic currents studies

Single stimulation of afferents with a concentric stimulating electrode was used to evoke postsynaptic currents (eEPSCs or eIPSCs) in the patched neurons. Various stimuli intensities were applied. The voltage necessary to evoke the half maximum amplitude response was determined for each experiment to perform subsequent paired pulse stimulation protocol.

Multiple evoked postsynaptic currents studies

Paired pulse stimulation experiments were performed for the IPSC and EPSC components with the following inter-pulse intervals: 10ms, 20ms, 25ms, 50ms, 100ms, 200ms, 500ms, 1000ms and 1500 ms. Digital subtraction of the first evoked postsynaptic currents by an averaged waveform 5 consecutives voltage clamp sweep of a single evoked postsynaptic currents. The digital substraction allowed accurate determination of the amplitude of the second evoked postsynaptic currents to be detected.

Frequency dependent facilitation experiments consisted in a train of ten stimuli of 1 ms duration each at a range of frequencies (10 Hz, 20 Hz, 33 Hz, 50 Hz and 100 Hz).

In some experiments, D-APV, NBQX, bicuculline (Tocris) and TTX (Alomone Labs, Jerusalem, Israel) were applied to the circulating aCSF. D-APV, NBQX and bicuculline were purchased from Tocris (Bristol, UK)

ii) Data acquisition and analysis

The whole-cell recordings were made with an NPI SEC-10L amplifier (Scientifica, Harpenden, UK). Analog signals were acquired and digitized at 10 kHz using a 1401 plus A-D converter (Cambridge Electronic Design, Cambridge, UK). The data were low pass filtered at 2 kHz by a Neurolog NL-125 filter unit (Digitimer, Welwyn Garden City, UK) and then stored onto a computer hard drive. Signal 2 software (CED) was used for data acquisition and analysis.

The evoked postsynaptic currents were quantified by their absolute amplitude. Individual stimulus response curve was fitted with a Boltzmann function (y=A2+ (A1-A2)/ (1+exp ((x-x0/dx)).

Paired pulse stimulation experiments

Ratio between the second amplitude responses over the first amplitude response was performed.

Frequency dependent facilitation experiments

A train of stimuli of equal intensity (10 pulses) was applied to the Schaffer collaterals or the mossy fibres pathways. Each evoked postsynaptic currents was ratioed to the first one, yielding the strength of the facilitation or depression.

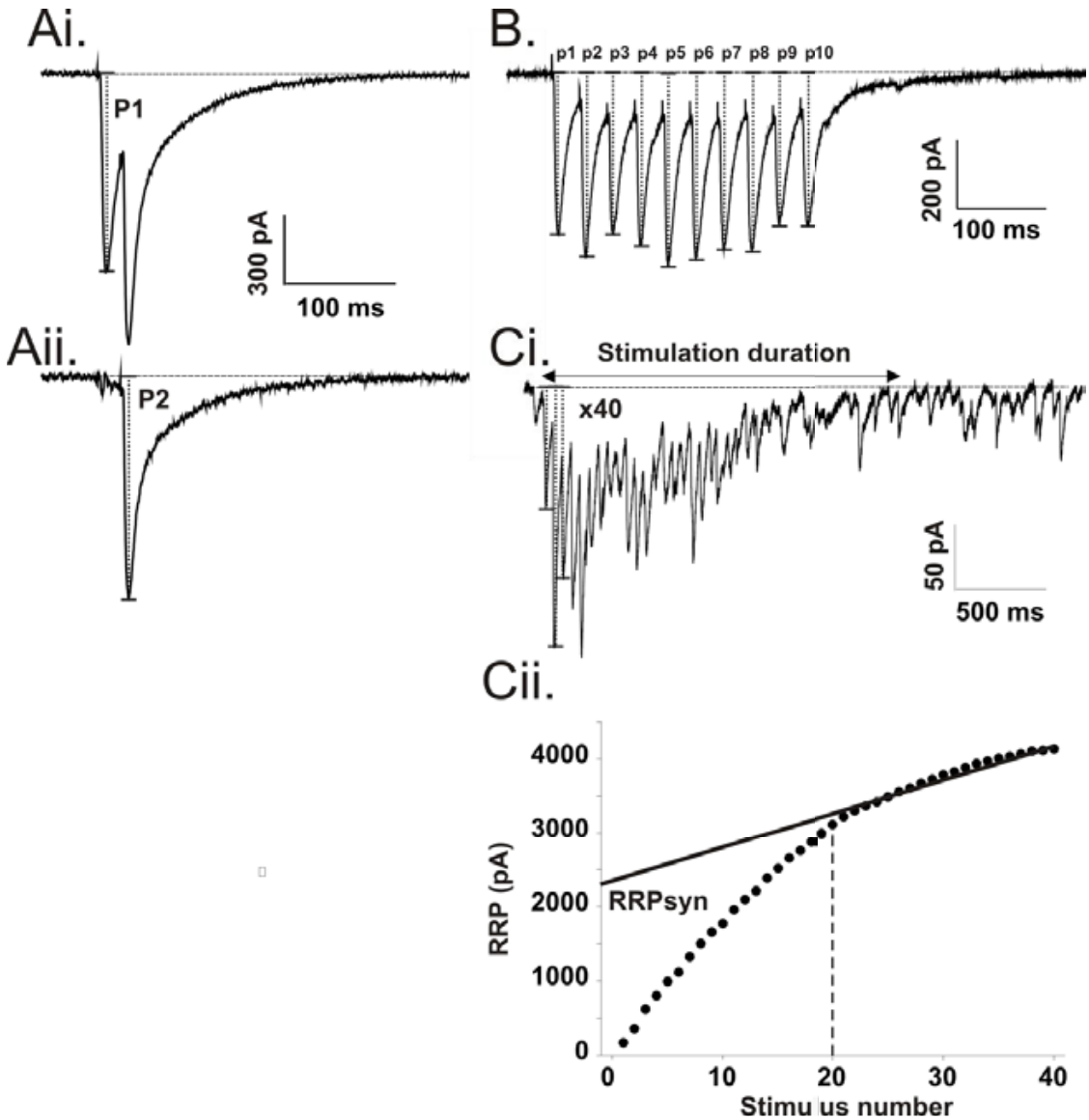

Figure 2.10: Measurement of multiple repetitive evoked postsynaptic currents. Double evoked postsynaptic currents separated by 20 ms **(Ai.)** and trace showing the subtraction of first evoked postsynaptic currents **(Aii.)**. Evoked postsynaptic currents evoked by a train of 10 stimuli at 33H **(B.)** and to 40 stimuli at 20 Hz **(Ci.)** Each evoked postsynaptic currents peak were added up and plotted in the cumulative plot where the RRP was extrapolated from **(Cii.)**. NB:Vertical dotted lines show the absolute measure taken.

Spontaneous synaptic events have been analyzed with minianalysis software (Synaptosoft, Decatur,GA)). Diverse measures were taken in consideration such as the median inter-event intervals, the median amplitude and the kinetics which were the 10-90% rise time and the decay time (τ). A 5 fold residual noise amplitude was used to set the threshold for detecting the events. In order to test the validity of this automatic spontaneous postsynaptic currents analysis, files have been visually checked for quality control purposes. No differences have been revealed between the two ways of analysis. For the inter-event intervals, the percentage of difference was 9.93 ±1.59%, n=4 for *Ophn-1*$^{+/y}$ and was 7.34 ±2.62%, n=4 for *Ophn-1*$^{-/y}$ (p=0.43). For the median amplitude: *Ophn-1*$^{+/y}$ 5.14 ±0.88%, n=4; *Ophn-1*$^{-/y}$ 9.61 ±3.25%, n=4, p=0.23)

Cumulative amplitude analysis

This analysis aimed to evaluate the size of the readily releasable pool size (RRP_{syn}). The RRP_{syn} size was delineated by adding up peak postsynaptic currents amplitudes evoked by 40 repetitive stimuli at 20 Hz (fig. 2.10 Ci.). Stimulation intensity chosen should evoke the smallest eIPSC in order to activate as few synapses possible. It typically induced a depression, termed steady-state phase, limited by the recycling rate of synaptic vesicles. The fit with a linear regression of the cumulative plot of 20 last data points was performed and extrapolated to time 0. The intercept with the y-axis yielded the RRP_{syn}. The total number of synaptic vesicles (N) ready for release was obtained by dividing the RRP_{syn} by the mean amplitude of the miniature postsynaptic currents.

Quality control

Cells patched were accepted for subsequent analysis if 1) the resting membrane potential was more hyperpolarized than -60 mV, 2) in current clamp mode, the RMP was manually adjusted to -65mV with less than 60 pA holding current, 3) the series resistance remained stable throughout the experiment and was about 10 MΩ, a variation of more than 20% led to cell recording exclusion, 4) the membrane resistance remained stable from the beginning to the end of the recording, calculated according the ohm law R=V/I.

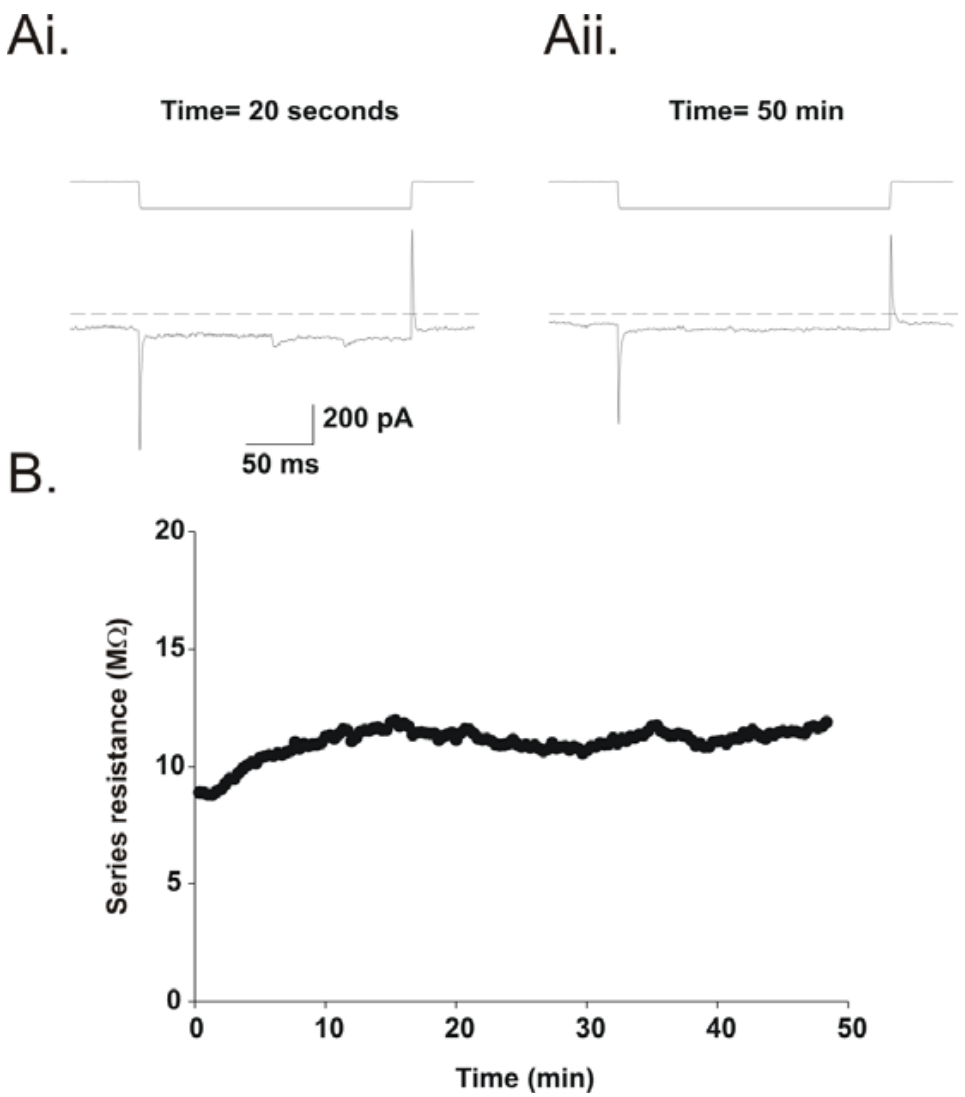

Figure 2.11: Evaluation of series resistance. Hyperpolarizing steps (5 mV, 200 ms) were applied before each current trace (upper panel). Series resistance was calculated from the instantaneous current according to Ohms law. Lower panel shows series resistance recorded over the time course of an experiment.

2.5 Statistical analysis

Data were tested for normality with Shapiro-Wilk test. When normal distribution was established, unpaired student *t*-test was then used. Furthermore, univariate analysis of variance (ANOVA) was also used (SPSS v.15, SSPS inc., Chigaco, USA). Bonferroni correction has also been performed in some instance.

In this study, most statistics shown are from student *t*-test, unless otherwise tested. Significance was taken for a p value less than 0.05.

If distribution was not normal, then Mann-Whitney Rank Sum Test was performed

Chapter 3: INVESTIGATION OF HIPPOCAMPAL GAMMA OSCILLATIONS

3.1. AIM

Previous studies have shown deficits in the morphology of dendritic spines (Govek et al., 2004) and of the synaptic activity in CA1 hippocampus in *Ophn-1*$^{-/y}$ neurons (Khelfaoui et al., 2007). However, these deficits in *Ophn-1*$^{-/y}$ mice do not adequately explain the cognitive impairment observed in *Ophn-1*$^{-/y}$ mouse (Khelfaoui et al., 2007). In the following, I investigated the locus of the cognitive impairment and which effects are exerted on synaptic activity by the lack of Oligophrenin1. I firstly assessed the properties of the hippocampal network activity using extracellular field potentials recordings. The glutamatergic receptor agonist, Kainic Acid (KA), was used to induce neuronal synchronisation of hippocampal neurons, a phenomenon termed gamma oscillations. The function of the hippocampal trisynaptic network was investigated in *Ophn-1*$^{-/y}$ ventral horizontal slices. Typical features of these gamma oscillations were investigated, namely the sensitivity to diverse pharmacological agents. It could be argued that the assessment of the cortical gamma oscillations would have been more relevant in studying higher cognitive processes in mice. However, preliminary investigations on cortical gamma oscillations found that it was difficult to reliably record stable gamma oscillations. Therefore, hippocampal gamma oscillations were chosen as these were able to be recorded reliably, and are

well characterised (Bartos et al., 2007) and hence permit accurate comparison between genotypes.

3.2 Induction of gamma oscillations *in vitro*

The effect of lack of oligophrenin1 expression on neuronal population activity and synchrony was investigated through gamma oscillations in the gamma band frequency. They were induced by addition of 50 nM KA to the circulating artificial cerebrospinal fluid (aCSF). Previous studies in the laboratory have demonstrated that this concentration was sufficient to induce sub-maximal gamma oscillations (Vreugdenhil and Jefferys, personal communication) and does not evoke bursting activity which is often observed with higher concentrations of KA (Ben-Ari and Cossart, 2000). 50 nM KA was chosen as the preferred method to evoke gamma oscillations as it is below the threshold of neurotoxicity for KA, which has been shown to occur at micromolar levels (Sperk, 1994). Neuronal population synaptic activity was recorded from an extracellular electrode placed on the pyramidal cells layer of the CA3c area of ventral hippocampal horizontal slices. In the majority of the experiments, no neuronal population synchronisation was observed before the application of KA, however some slices (1 out of 3 slices in average) showed small spontaneous gamma oscillations even in absence of KA (see fig 3.6; baseline gamma). The origin of these baseline oscillations remains unknown; however it may reflect an endogenous gamma rhythm (Pietersen et al., 2009). The application of 50 nM of KA transformed irregular and small oscillations into a larger rhythmic and

synchronous neuronal activity. This synchronisation of the neuronal population synaptic activity proceeded after a short lag period (see fig 3.1A), presumably reflecting the time for KA to diffuse into the slice and act on the kainate receptors. The neuronal synchrony increased in power until the end of the experiment at 80 minutes (see fig. 3.1). Analysis of the gamma oscillations showed that the dominant frequency occurred within the gamma range (29 $\pm$1.4 Hz at t=40 min; n=13) and remained constant throughout the duration of the experiment (Figures 3.1, 3.2 and 3.3).

At this concentration KA is neither toxic nor epileptogenic (Fisahn, 2005, Vreugdenhil and Toescu, 2005). Several studies have investigated the effects of KA on neurons which may explain the generation of gamma oscillations. KA increases the glutamate release at mossy fibres terminals (Ben-Ari and Cossart, 2000, Schmitz et al., 2001). Underlying this observation may be a feedback at the synapse between granule cells and CA3 pyramidal cells. In addition, inhibition of the Ca^{2+} activated K^{+} current underlying the slow afterhyperpolarisation by KA, may produce increased neuronal excitability (Fisahn et al., 2005, Melyan et al., 2002). An increase of the release of GABA at the synapse between CA1 interneurons has also been suggested (Cossart et al., 2001). If this phenomenon exists in the CA3 area, it may play a key role in the genesis of gamma oscillations.

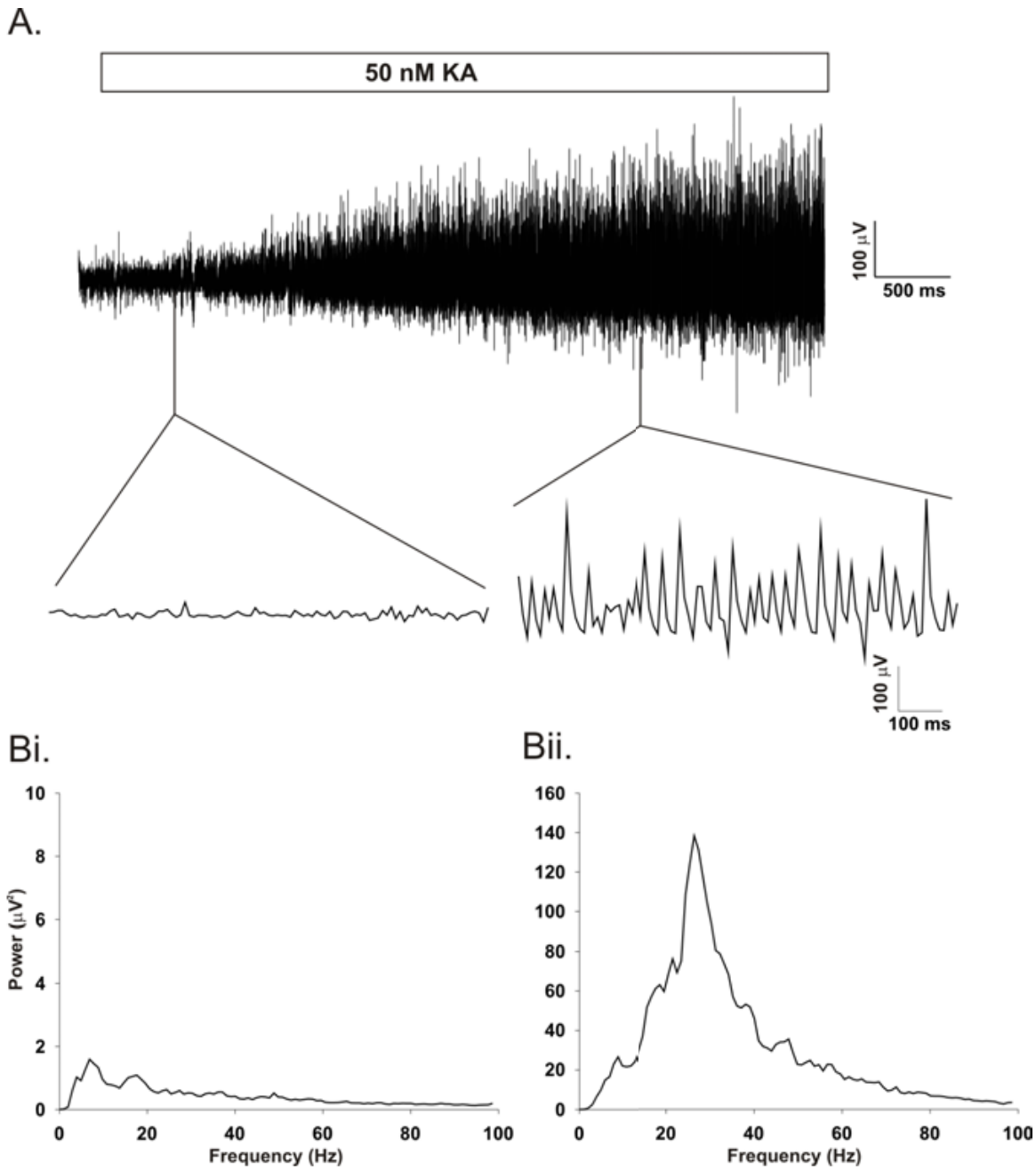

Figure 3.1: Development of KA-induced gamma oscillations. (A) Application of 50 nM KA induced neuronal synchrony in the gamma frequency range recorded from stratum pyramidale in a typical Ophn-1$^{+/y}$ slice. The power of these oscillations increased over time. *Inset* Expanded time for t= 5 min (left) and t = 80 min (right). Power spectra obtained at t = 5 min **(Bi.)** and t = 80 min **(Bii.).**

3.3 Development of gamma oscillations *in vitro*.

The frequency of gamma oscillations was determined by the frequency of firing of the interneurons 50 nM KA was chosen as the preferred method to evoke gamma oscillations as it is below the threshold of neurotoxicity for KA, which has been shown to occur at micromolar levels (Jefferys et al., 1996, Whittington et al., 1995). It is known that KA-induced gamma oscillations are, by nature, irregular oscillations owing to the fact that the length of the cycle is correlated to the amplitude of the population synaptic potentials (Vreugdenhil and Toescu, 2005). The peak frequency did rise between the 20th and the 40th minutes after KA application. In the second part of the recording the peak frequency remained stable, around 30 Hz, due to the low temperature bath used. Nevertheless, the strength of the gamma oscillations increased steadily throughout the recording (Figures 3.2B and 3.3)..

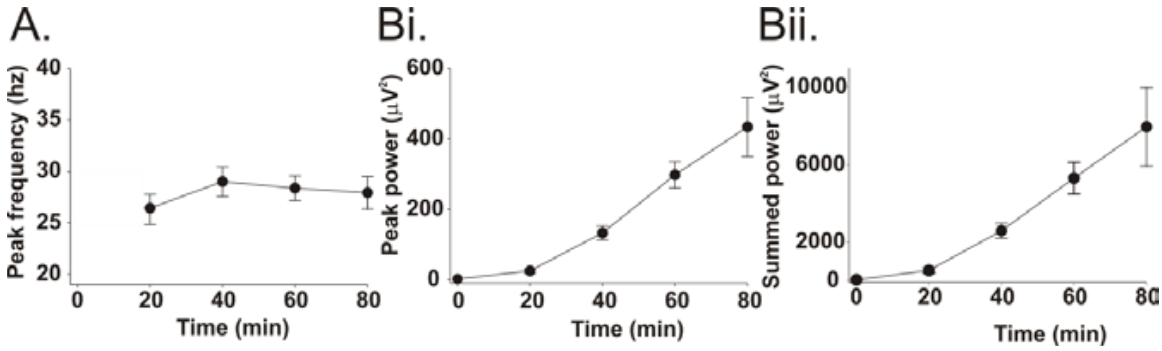

Figure 3.2: Frequency and power development in *Ophn-1*$^{+/y}$ slices. (A.) Plot of the dominant frequency over a time period of 80 minutes. Peak **(Bi.)** and summated power **(Bii.)** over a time period of 80 minutes. (n=8 slices from 6 animals)

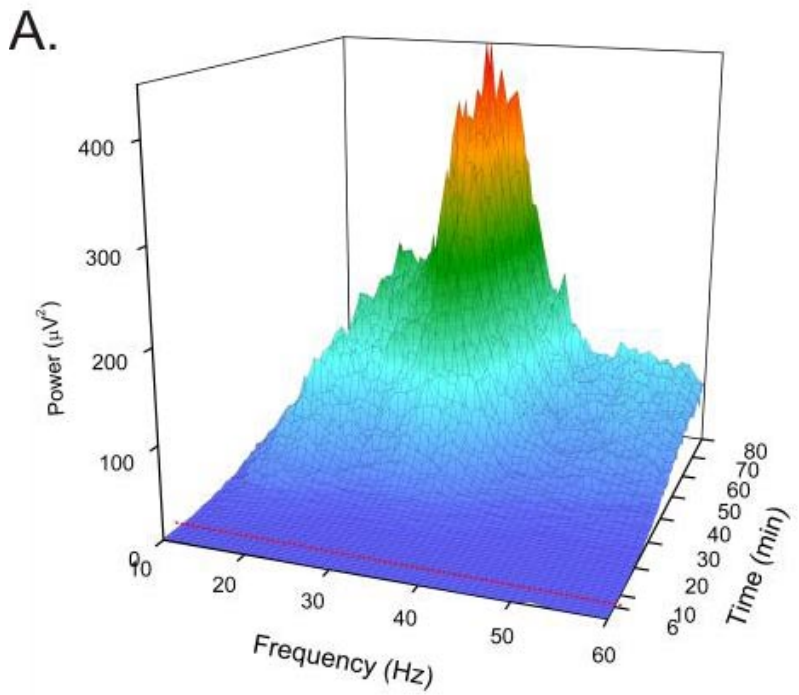

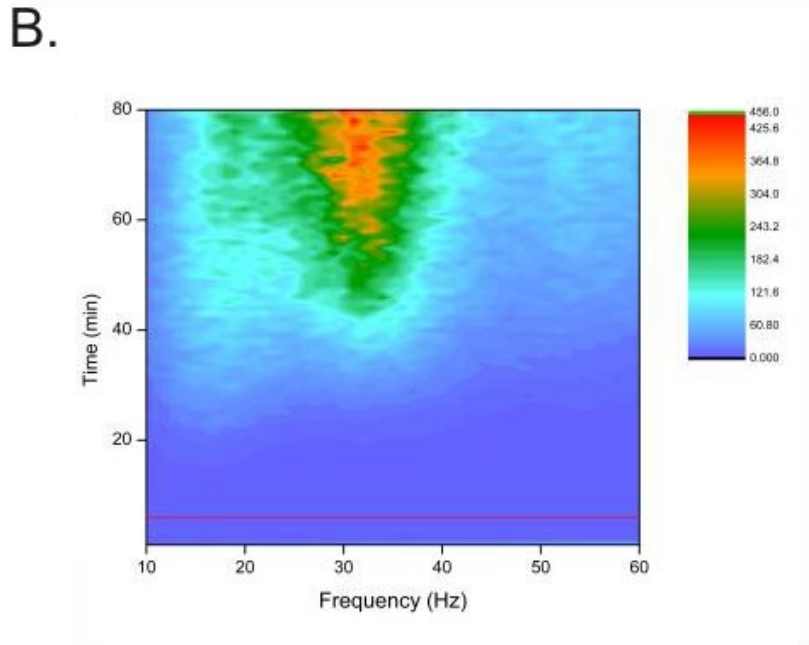

Figure 3.3: (A.) Waterfall representation of KA-induced gamma oscillations development along the time. **(B.)** Spectrogram showing that the dominant frequency of KA induced gamma oscillations remained stable throughout the recording. The red line denotes the time at which KA (50nM) was added.

Figure 3.3 illustrates that that KA induced gamma oscillations show a single dominant frequency that remained stable throughout the whole time course of the experiment.

3.4 Pharmacological and electrophysiological investigation of KA-induced gamma oscillations

3.4.1 KA-induced gamma oscillations were abolished by the application of bicuculline.

To verify that KA-induced gamma oscillations were indeed due to the actions of inhibitory interneurons (Fisahn, 2005), the competitive $GABA_A$ receptor antagonist, bicuculline (10μM), was applied in addition to the KA. Figure 3.4 revealed that gamma oscillations were abolished by bicuculline application, as previously described by Fisahn et al (2005). In addition to this inhibition of gamma oscillations, bicuculline induced recurrent seizure-like events in the slice, after its continued application, as shown in figure 3.5 Ai. & Aii.

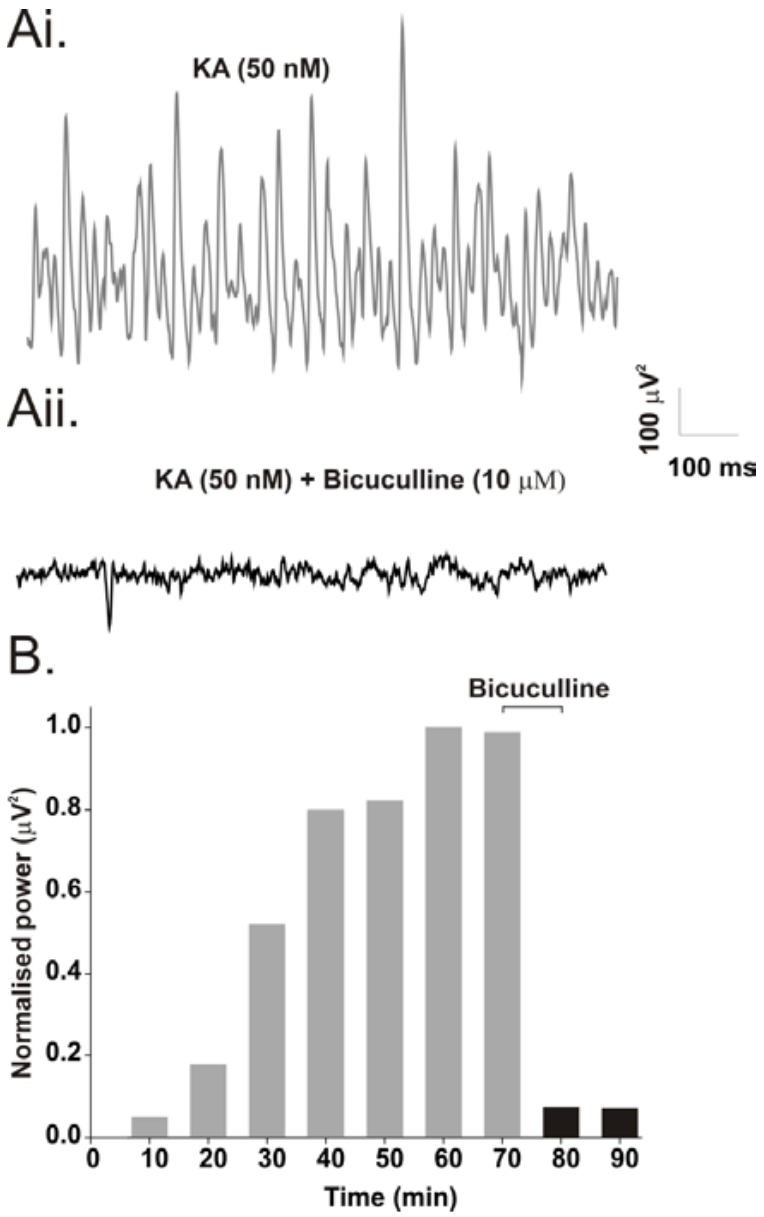

Figure 3.4: Sensitivity of the gamma oscillations to the $GABA_A$ receptors antagonist bicuculline (10 μM). (Ai.) Representative trace of the KA (50 nM) induced gamma oscillations. **(Aii.)** Trace of recordings after application of bicuculline. **(B.)** Histogram of development of the gamma strength normalised over time (grey bars display the normalised gamma power before bicuculline treatment (dark bars)

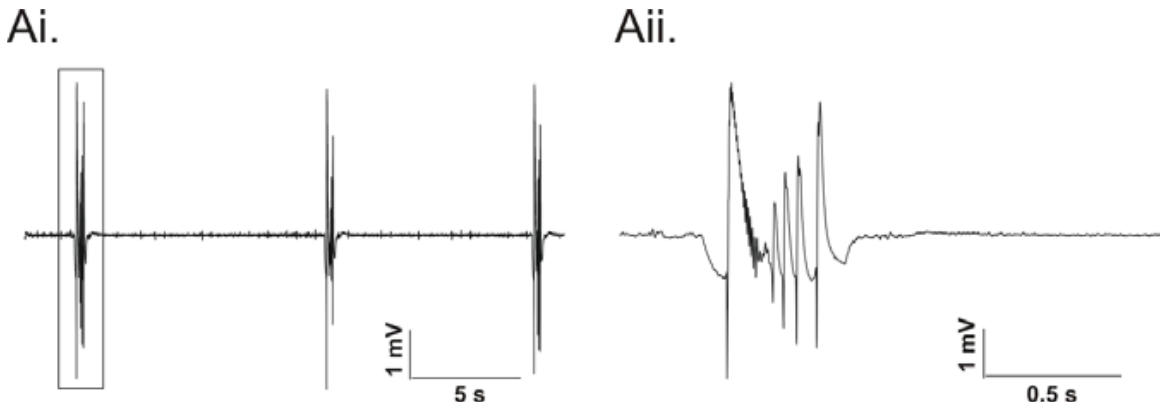

Figure 3.5: Seizures-like events induced by the application of bicuculline (Ai.). (Aii.) Magnification of a single seizure.

3.4.2 KA-induced gamma oscillations were abolished by NBQX.

To confirm that the activation of KA receptors accounted for the gamma oscillations observed, the non-NMDA receptor antagonist, 2,3-dihydroxy-6-nitro-7-sulfamoyl-benzo[f]quinoxaline-2,3-dione (NBQX, 20 μM) was applied once the gamma oscillations were established (fig 3.5 Ai.). As a result of NBQX addition a quick decline in the power of the KA-induced gamma oscillations was observed (Fig 3.5 Aiii. & B.).

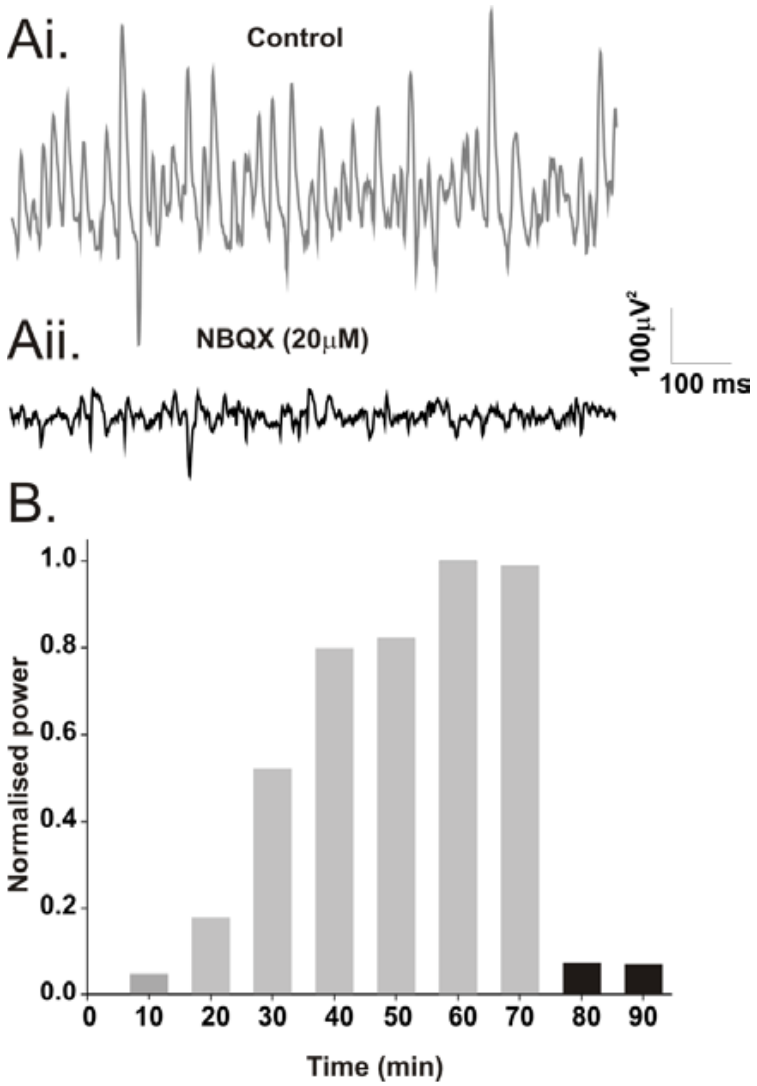

Figure 3.6: Sensitivity of the KA-induced gamma oscillations to the AMPA/KA antagonists NBQX. Representative traces of the KA-induced gamma oscillations before **(Ai)** and after **(Aii)** NBQX application **(B.)** Development of the gamma strength normalised to the maximum power over time.

To summarize, KA induced gamma oscillations were sensitive to bicuculline and NBQX. This is in agreement with previous studies (Fisahn, 2005) and a precondition for the following studies on *Ophn-1*$^{-/y}$ mice

3.4.3 KA depolarized and increased the spontaneous firing of *Ophn-1*$^{+/y}$ CA3 pyramidal neurons

To confirm the idea that KA-induced gamma oscillations relied on the activation of inward depolarizing currents in CA3 neurons. I monitored the variation of membrane potential of CA3 pyramidal neurons upon KA (200 nM) application in whole cell recordings (current clamp mode) as well as assessing the frequency of firing.

Figure 3.7 A. shows that bath application of KA (200 nM) onto the bath superfusate depolarised the membrane potential. It can be supposed that this depolarisation is due to the activation of inward currents. This depolarisation (11.45 ± 4.65 mV @ 20 min, fig 3.7 A.), led to an increase of spontaneous firing of *Ophn-1*$^{+/y}$ CA3 pyramidal neurons (2.20 ±1.47 Hz at 20 min., fig. 3.7 B.). This finding confirmed results from previous study (Fisahn et al., 2004). The frequency of firing is low and confirmed the idea that CA3 pyramidal neurons do not fire at every gamma cycle, but every ≈ 10 cycles, unlike the perisomatic interneurons. In effect, the interneurons fire at the frequency of the gamma oscillations (26.3 ±3.7 Hz, n=3, data not shown).

Mechanistically, KA induced inward currents which are generated specifically by KA receptors containing the subunit GluR6, as it has been shown that GluR6$^{-/-}$ CA3 neurons do not show depolarisation under KA treatment (Fisahn et al., 2004). This study has confirmed the key role of the subunit GluR6 in the genesis of gamma oscillations.

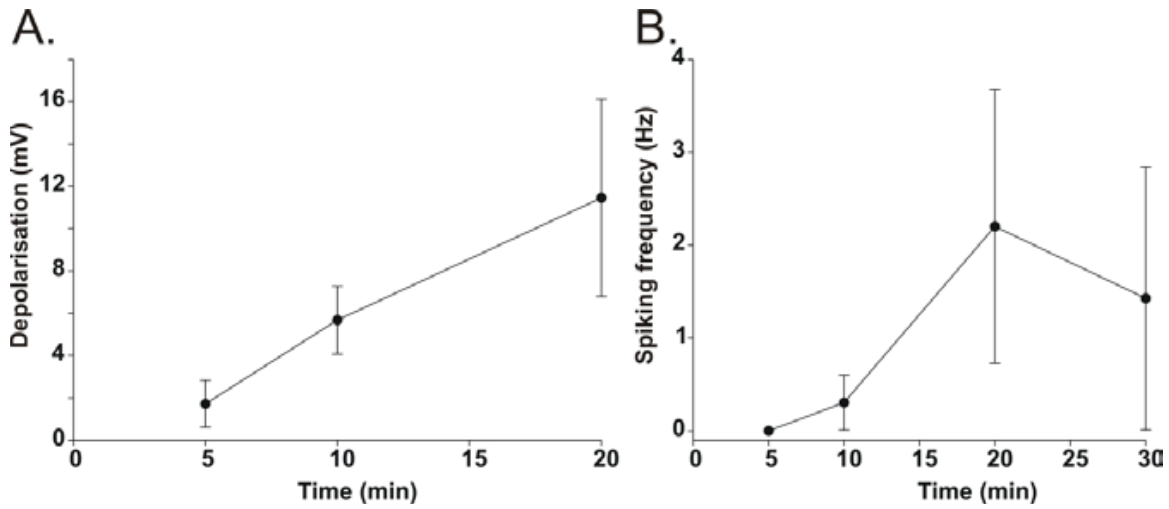

Figure 3.7: KA-induced depolarisation in *Ophn-1*$^{+/y}$ CA3 pyramidal neurons. (A.) Histogram of the depolarisation the membrane potential plotted against the time (n=5) **(B.)** Spontaneous firing frequency plotted against the time (n=5).

These data confirmed that gamma oscillations recorded in this study present similar feature to those observed in previous study.

3.5 Effect of the loss of oligophrenin1 on the KA-induced gamma oscillations

3.5.1 *Ophn-1*$^{-/y}$ mice slices displayed a reduced strength of KA-induced gamma oscillations at relatively low bath temperature (30 ºC)

The rationale for the following study was the fact, that patients with XLMR showed abnormal cortical brain activities in electroencephalography (EEG) (Cantagrel et al.,

2004, Wittwer et al., 1996). Furthermore, Grice and co-workers (2001) demonstrated an altered oscillatory activity in brain, especially an altered gamma oscillations, possibly related to visual binding in autism and in the William syndrome which are accompanied by learning disability. Moreover, Khelfaoui et al (2007) demonstrated a deficit in spatial memory assessed by the Morris water maze in *Ophn-1*$^{-/y}$ mice. *In vivo* electrophysiological studies on the hippocampal neuronal network phenomenon have shown that oscillations in the range of theta and gamma can be observed concomitantly to exploratory behaviour in rat (Bragin et al., 1995, Csicsvari et al., 2003). Interestingly, the spatial memory is thought to take place in a specific brain structure named the hippocampus. It is known that although some *Ophn-1*$^{-/y}$ mice display lateral ventricles enlargement, the hippocampal structure of these mice is anatomically unaltered compared to the *Ophn-1*$^{+/y}$ mice (Khelfaoui et al., 2007). To study the biological defects underlying this deficit in spatial memory, I performed electrophysiological recordings of neuronal population synchronization. Furthermore, oscillations in the gamma range are thought to underlie memory formation in the hippocampus, notably the spatial memory formation (Axmacher et al., 2006).

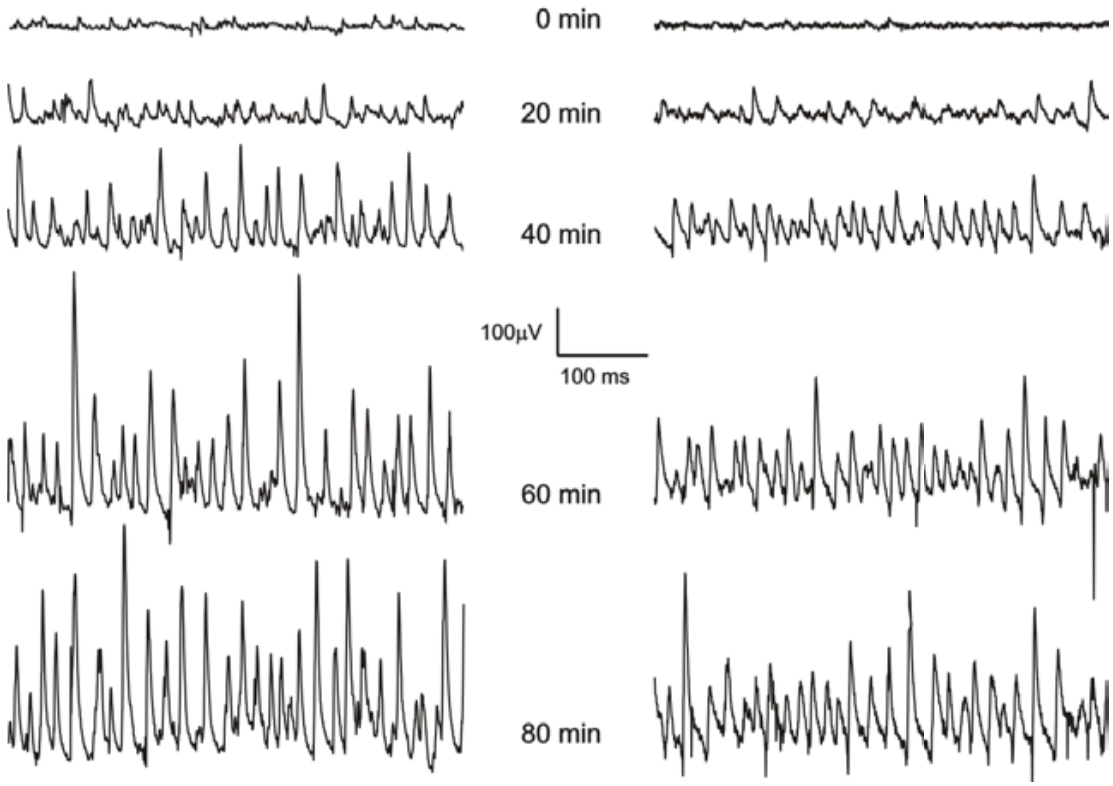

Figure 3.8: Characteristic traces showing the raw gamma oscillations recordings. (0 min) Baseline activity (t=0min) of epochs of data without KA. **(20 min)**, **(40 min)**, **(60 min)** and **(80 min)** show the development of the gamma oscillations analysed every 20 minutes for *Ophn-1*$^{+/y}$ and *Ophn-1*$^{-/y}$ slices (left and right panels respectively).

The development of the neuronal population synchronization over time in *Ophn-1*$^{+/y}$ and *Ophn-1*$^{-/y}$ slices is illustrated in figure 3.8. After the period of baseline activity recording (0 min), which showed little or no synchrony, 50 nM KA was applied and induced synchronization of neuronal population within 20 min. The strength of these

oscillations increased in power over time until the end of the experiment (t=80 min). Figure 3.8 shows an apparent reduction in the size of the rhythmic field potentials. Interestingly, KA-induced oscillations from *Ophn-1*$^{-/y}$ were significantly lower than from *Ophn-1*$^{+/y}$ throughout the experiment. At 60 minutes after KA application, the peak power in *Ophn-1*$^{-/y}$ was reduced by approximately 50% compared to *Ophn-1*$^{+/y}$ slices (*Ophn-1*$^{+/y}$: 297.4 ±37.3 μV^2, n=9; *Ophn-1*$^{-/y}$; 148.5 ±31.5 μV^2, n=8, p=0.008 (t-test), fig 3.9 Bi.). Moreover, the univariate analysis of variance test (ANOVA) revealed that the peak power (fig. 3.9 Bi.) as well as the summated power (fig. 3.9 Bii.) were significantly reduced (p=0.002 and 0.023 respectively) in *Ophn-1*$^{-/y}$ slices across the whole time course of the experiments. However there were no significant differences in the peak frequency between *Ophn-1*$^{+/y}$ and *Ophn-1*$^{-/y}$ at any time point (fig. 3.9A.). It is noteworthy that the power was still increasing at time 80, and that the plateau was reached at longer time intervals (not shown).

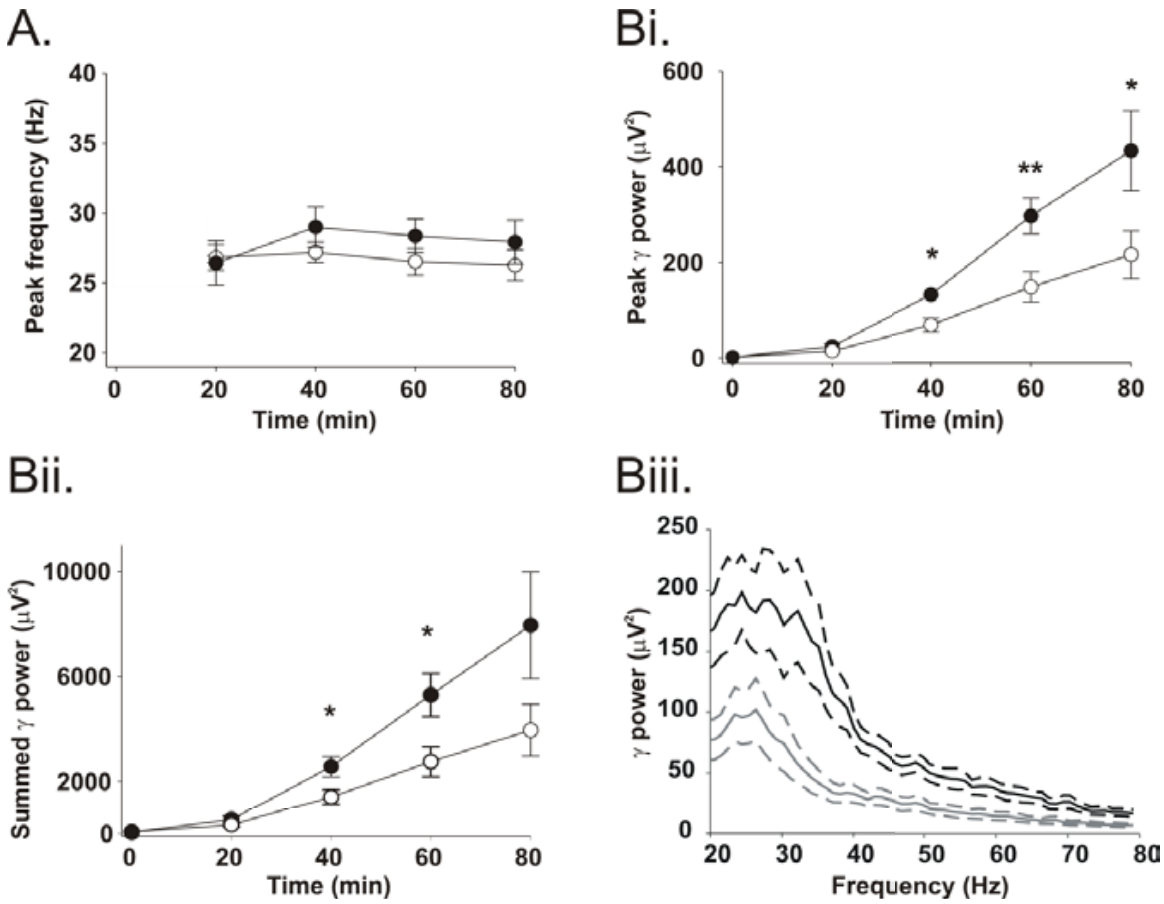

Figure 3.9: *Ophn-1*$^{-/y}$ mice displayed reduced gamma oscillations. (A.) Peak frequency *vs.* time did not differ significantly between *Ophn-1*$^{+/y}$ (filled symbols) and *Ophn-1*$^{-/y}$ (open symbols). Peak power **(Bi.)** and summated power **(Bii.)** of gamma oscillations. (filled symbols) *Ophn-1*$^{-/y}$, n=9 and ((open symbols) *Ophn-1*$^{+/y}$, n=8) (p=0.002 and 0.023 (ANOVA). **(Biii.)** Power spectrum averaged at 60 min of recording, dashed lines indicated S.E.M.. Recording were made at 30.1± 0.2°C.

In summary, comparison of the strength of gamma oscillations revealed a significant reduction in *Ophn-1*$^{-/y}$ slices whereas the dominant frequency of these oscillations remained similar. A similar loss of gamma power without a change in frequency

have been previously observed in ageing (Vreugdenhil and Toescu, 2005, Basar-Eroglu et al., 2007), Alzheimer disease (Uhlhaas and Singer, 2006) and in hypoxia (Fano et al., 2007). However, it is the first time that a deficit of this kind was demonstrated in a mouse model of X-linked mental retardation.

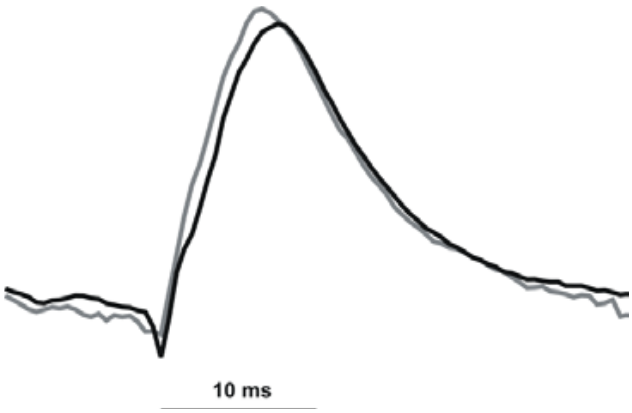

Figure 3.10: Averaged gamma waveform presented a similar shape, *Ophn-1*$^{+/y}$ (dark line) and *Ophn-1*$^{-/y}$ (grey line), normalisation was made from peak to trough.

In the figure 3.10, the trace of the averaged gamma waveform for each genotype showed a matching overlay. The average gamma waveform showed that although an overall reduction in gamma oscillations power in *Ophn-1*$^{-/y}$ slices, the neuronal circuitry necessary to generate gamma oscillations was still present in *Ophn-1*$^{-/y}$ slices. The gamma cycle represents a variation of field potentials which is mainly constituted by the inhibitory neurotransmission (IPSP) exerted by the perisomatic interneurons onto CA3 pyramidal neurons. In effect, it is well characterised that the perisomatic interneurons (basket cells) fire at every gamma cycle (Jefferys et al., 1996). Therefore, the peak of the gamma waves is mainly constituted by IPSPs,

whilst EPSPs weakly contribute to the gamma cycles owing to the low frequency of firing of CA3 pyramidal neurons during gamma oscillations (Traub et al., 1997) (see section 3.4.3). Thus, the overlay of these averaged gamma cycle waveform further confirmed that in spite of the significant loss of power in *Ophn-1*$^{-/y}$ slices, the neuronal network responsible for the genesis of gamma oscillations was still preserved in these slices.

Several different reasons might explain this loss of gamma power in *Ophn-1*$^{-/y}$. Weaker gamma power could be due to a smaller neuronal CA3 network, less neurons or less synapses. Furthermore, an impaired rhythmicity of gamma oscillations in *Ophn-1*$^{-/y}$ slices could be a reason, and one would also expect that irregular oscillations would be smudged out by the power spectrum. To address the latter possibility, I evaluated the rhythmicity of gamma oscillations in *Ophn-1*$^{-/y}$ slices.

3.5.2 Rhythmicity of gamma oscillations in *Ophn-1*$^{-/y}$ slices

The concept of rhythmicity of gamma rhythms usually encloses a main factor which is the predictability of gamma oscillations over time. In other words, how regular the gamma oscillations are over time.

In order to assess the rhythmicity, I first performed an autocorrelation spectrogram at a time where the gamma oscillations were well established namely at 60 min. I then analysed the value of the secondary peak (see methods # 2.4.1), which indicated the regularity of the gamma cycles. A significant decrease of this secondary peak was found in *Ophn-1*$^{-/y}$ slices compared to the secondary peak in *Ophn-1*$^{+/y}$ slices

(0.20 ±0.03, n=12; 0.29 ±0.03, n=14, respectively, p=0.04 (t-test), fig. 3.11 B.). This result suggested a deficit in gamma oscillations rhythmicity in *Ophn-1*$^{-/y}$ slices. This loss of regularity of the gamma oscillations in *Ophn-1*$^{-/y}$ slices could explain the reduction in gamma power observed. The underlying mechanism could be that the firing of the baskets cells was not in perfect synchrony. Hence, the IPSCs generated are more widespread in time, resulting in wider and smaller field potentials (IPSPs). I concluded from these experiments that the power of gamma oscillations in *Ophn-1*$^{-/y}$ slices could be smudged out by the deficit in gamma oscillations rhythmicity.

Figure 3.11: Auto-correlation of gamma oscillations at 60 min. Typical auto-correlogram for *Ophn-1*$^{+/y}$ **(Ai.)** and *Ophn-1*$^{-/y}$ **(Aii.)** **(B.)** Histogram depicting the amplitude of the secondary peak. (*Ophn-1*$^{+/y}$, n=14 and *Ophn-1*$^{-/y}$, n=12, p= 0.04, power of statistic = 0.427<0.8).

Nevertheless, statistical power analysis was performed on this result; it turned out to be 0.427 which was under the desired 0.8. This result is underpowered, therefore further investigations of the rhythmicity were undertaken.

Power spectral analysis can give an indication on the regularity of the oscillations. Oscillations are considered regular when a clear and narrow peak is observed, as opposed to irregular who have a broader peak. Figure 3.12 shows the normalised averaged power spectra in *Ophn-1*$^{-/y}$ compared to *Ophn-1*$^{+/y}$ at 60 min. It can observed that the power spectrum for *Ophn-1*$^{-/y}$ presented a narrower peak which denotes that gamma oscillations were more regular in *Ophn-1*$^{-/y}$ compared to *Ophn-1*$^{+/y}$ slices. This latter result was in contradiction with the previous one.

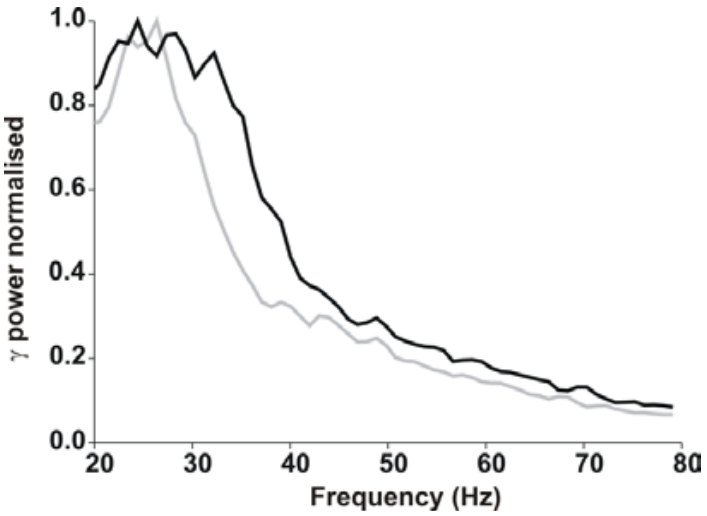

Figure 3.12: Normalisation of the averaged power spectrum from the Ophn-1$^{-/y}$ in reference of *Ophn-1*$^{+/y}$ averaged power spectrum. (Grey and dark line respectively).

To further investigate this discrepancy, I used the events autocorrelation analysis to measure the regularity of the gamma oscillations cycles. The trough was taken as references. This analysis assessed the regularity of the intervals between the

troughs. If the troughs were separated regularly a regular pattern would be expected.

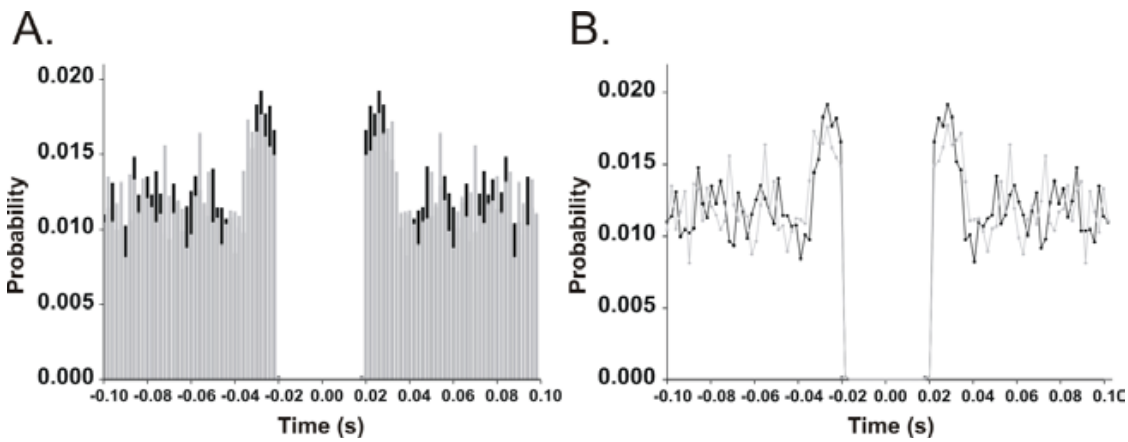

Figure 3.13: Events auto-correlogram of gamma oscillations in *Ophn-1*$^{-/y}$ slices

(A.) Histogram of "events auto-correlogram" for *Ophn-1*$^{+/y}$ (n=6) and *Ophn-1*$^{-/y}$ (n=7) gamma oscillations (black and grey bars respectively). (**B.)** Plot of "events autocorrelogram" for *Ophn-1*$^{+/y}$ and *Ophn-1*$^{-/y}$ gamma oscillations (black and grey lines respectively)

Figure 3.13 shows that no clear pattern appeared in the histogram plot, revealing similar rhythmicity by genotype. This would suggest that the loss of power was not due to a lack of rhythmicity of oscillations in *Ophn-1*$^{-/y}$. Alternatively, the loss of power could result from the fact that less currents were flowing at each cycle (see chapter 4). No clear conclusion could be drawn for this study of the rhythmicity of gamma oscillations in *Ophn-1*$^{-/y}$ slices; it may be possible that the loss of regularity observed with the auto-correlogram study was a false positive result, as the power of statistic revealed that the statistic was underpowered.

3.5.3 *Ophn-1*$^{-/y}$ mice slices displayed no difference in synchronization along the Ammon horn.

In the following, I will deal with the question how gamma oscillations are propagated within the hippocampal formation. It is well described that *in vivo* hippocampal gamma oscillations are generated in CA3 area and are propagated to CA1 through the Schaffer collaterals which excite directly CA1 interneurons (Bragin et al., 1995). As it is assumed that higher cognitive function are mediated by the communication of different cerebral areas through oscillations, a phenomenon generally referred as the “binding” (Engel et al., 2001, Gray et al., 1989, Bragin et al., 1995). The synchronisation of gamma oscillations within the hippocampus was therefore investigated. To that end, gamma oscillations were recorded at various locations along the Ammon horn of the hippocampus, such as on CA3c, CA3b, CA3a and CA1 areas and they were compared with a fixed recording of CA3c gamma oscillations. Figure 3.14 A. depicts typical gamma oscillations obtained in CA3c and CA1 (grey and white square respectively). An analysis of coherence was used (See methods # 2.4.1.2 fig. 2.7). The coherence value was determined and compared between the different genotype as well as between different hippocampal areas. The strength of coherence of gamma oscillations decreased with the distance from CA3c area in *Ophn-1*$^{+/y}$ as well as in *Ophn-1*$^{-/y}$ (67.4% and 65% of reduction from CA3c to CA1 respectively). However, *Ophn-1*$^{-/y}$ gamma oscillations showed the same the degree of synchronisation as *Ophn-1*$^{+/y}$ (For CA1: 0.29 ±0.09, n=8; 0.37 ±0.09, n=7

respectively, p=0.93,) (For CA3b: 0.74 ±0.06; 0.65 ±0.06 respectively, p=0.79, fig 3.14 Bii.).

This result suggested that gamma oscillations in *Ophn-1*$^{-/y}$ slices propagated normally within the hippocampus.

In this section, I have shown a significant loss of power in *Ophn-1*$^{-/y}$ slices which cannot be explained by a loss of rhythmicity of gamma oscillations. However, an indication of a loss of rhythmicity was revealed by the autocorrelation study, whilst the overlay of the averaged power spectrum plot would suggest the opposite. These discrepancies have been clarified with the events autocorrelation analysis. From this analysis, I concluded that gamma oscillations were as regular in *Ophn-1*$^{-/y}$ as in *Ophn-1*$^{+/y}$ slices. Furthermore, the propagation of gamma oscillations amongst the ammon horn was not altered in *Ophn-1*$^{-/y}$ slices, as revealed by synchronisation of gamma oscillations experiments.

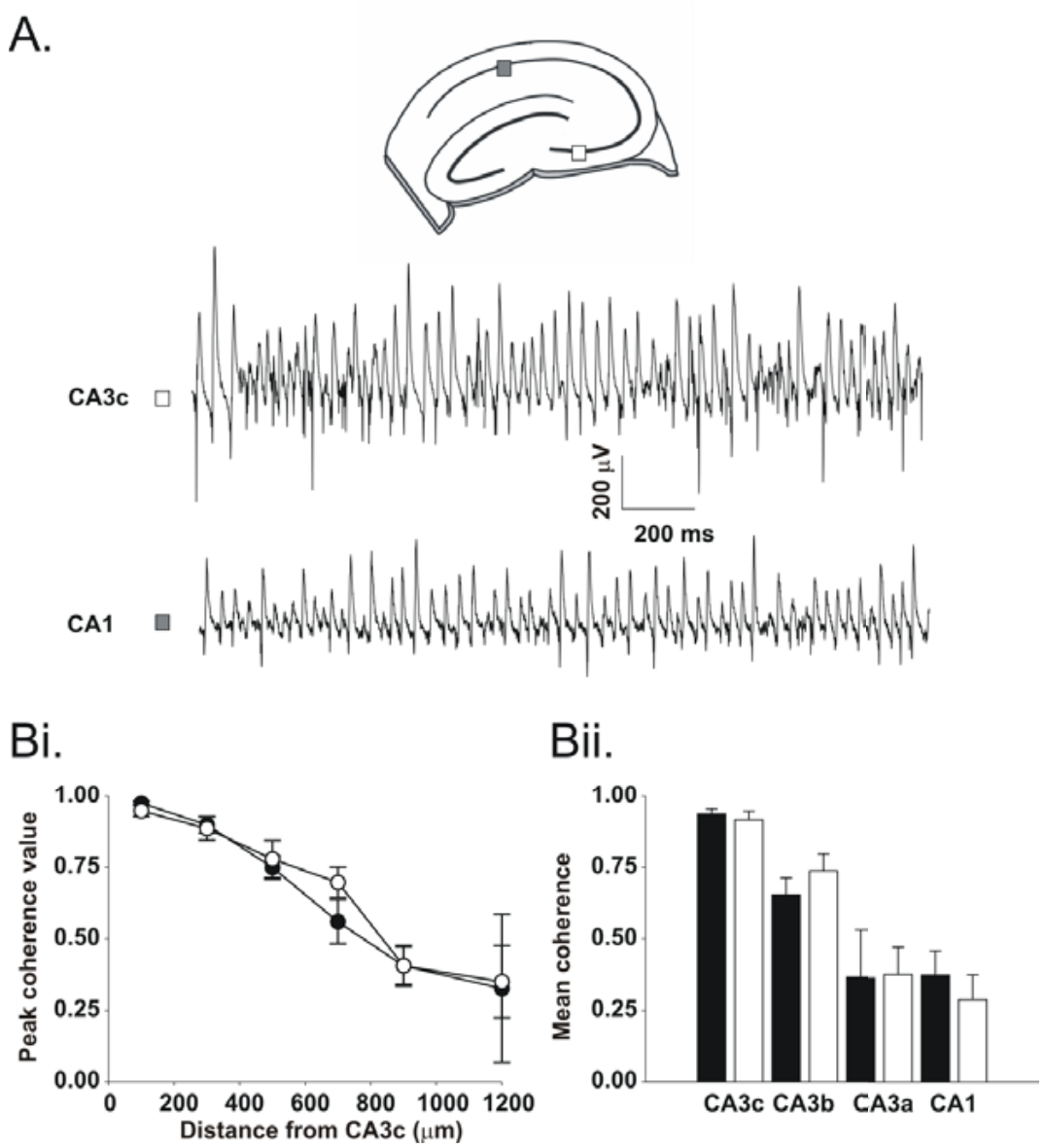

Figure 3.14: *Ophn-1*$^{-/y}$ gamma oscillations displayed no difference in synchronisation. (A.) Typical gamma oscillations evoked by 50 nM KA recorded at the same time in two different hippocampal areas, (open square) represents the localization of one electrode in CA3c stratum pyramidale and the other in CA1 stratum pyramidale (filled square) **(Bi.)** plot showing the mean peak coherence value decreasing according the distance from CA3c. **(Bii.)** Histogram of the mean coherence value with reference to the hippocampal areas (Ophn-1$^{+/y}$ black chart n= 7 and Ophn-1$^{-/y}$ white chart n=8, $p > 0.05$ (t-test) for every area).

3.5.4 *Ophn-1*$^{-/y}$ mice slices displayed a higher frequency of KA-induced gamma oscillations at higher bath temperature (32°C)

The dominant frequency of the gamma oscillations exhibits a steep dependence to the bath temperature (Dickinson et al., 2003). By raising the bath temperature from 30 ºC to 32 ºC, a significant increase of the mean dominant frequency of the gamma oscillations accompanied by a strong increase in gamma power was observed (fig. 3.15). Nonetheless, the reduction in power in *Ophn-1*$^{-/y}$ slices was less clear. Nevertheless, a significant difference was observed in summated power at the time point 60 min. (*Ophn-1*$^{+/y}$: 12820 ± 3540 μV^2 and *Ophn-1*$^{-/y}$: 5370 ± 939 μV^2 with student's t- test p value of 0.0398, fig 3.15.).

Analysis using ANOVA did not reveal a significant difference for either peak or summated power (p=0.748 and p=0.806, respectively).

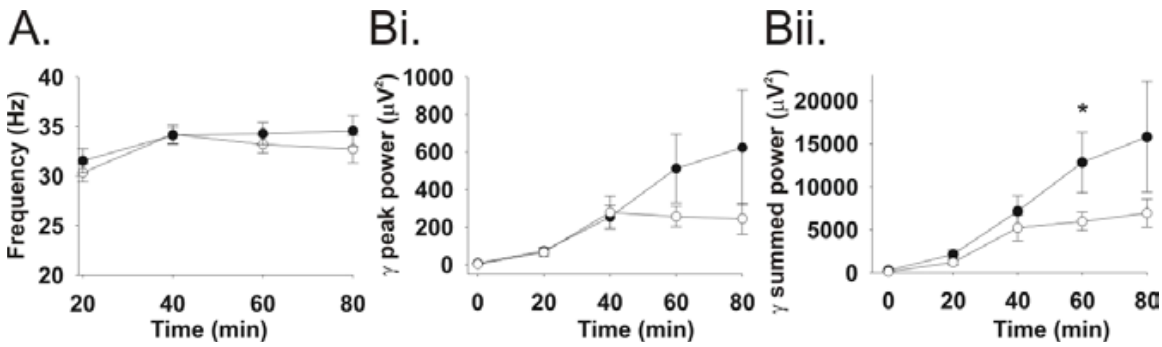

Figure 3.15: *Ophn-1*$^{-/y}$ mice displayed reduced gamma oscillation power at 32.3°C. Peak frequency *vs.* time was similar between *Ophn-1*$^{+/y}$ (filled symbols) and *Ophn-1*$^{-/y}$ (open symbols). Peak power **(Bi.)** and summated power **(Bii.)** of gamma oscillations. (open symbols) *Ophn-1*$^{-/y}$ (n=19); (filled symbols) *Ophn-1*$^{+/y}$ (n=16) (p=0.748 for Bi and p=0.806 for Bii).

Figure 3.16 A. recapitulates the percentage of reduction in gamma oscillations power, the plot revealed similar reduction at 30 or 32 ºC.

The dominant frequency at 32 ºC was significantly higher than the dominant frequency at 30 ºC at any time points for both genotypes (60 min.: 34.27 ±1.12 Hz; 28.39 ±1.20 Hz respectively, p=0.0014 (t-test).

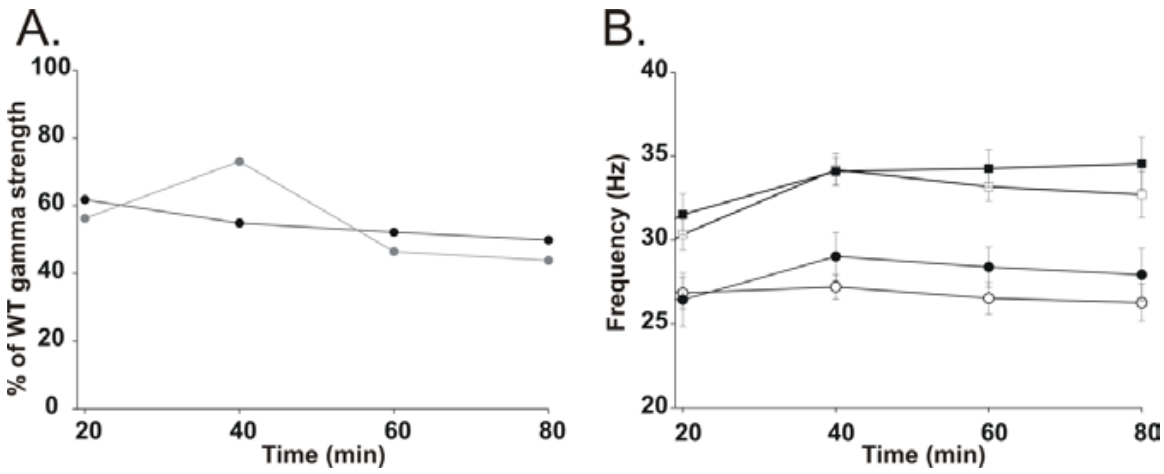

Figure 3.16: Percentage of reduction of gamma oscillations and increase of frequency at 30ºC and 32ºC (A.) Plot of the percentage of the gamma power reduction in *Ophn-1*$^{-/y}$ at 30 ºC (black symbols) and 32 ºC (grey symbols). **(B.)** Representation of the variation of the peak frequency *vs.* the time at 30ºC and 32ºC. (filled circles) WT (30.1°C) (n=8); (open circles) KO (30°C) (n=9); (filled squares) WT (32.3°C) (n=19) (open squares) and KO (32°C) (n=16) ($p<0.05$ for every time point).

In the following experiment, pharmacological tools were used to attempt to restore the deficit of KA-induced gamma oscillations observed in *Ophn-1*$^{-/y}$ slices.

3.6 Effect of Y27632 on KA-induced gamma oscillations

In the following, I tried to rescue the loss of power in *Ophn-1*$^{-/y}$ using the small molecule Y27632. It is known, that the loss oligophrenin1 induces an over-activation of the small Rho proteins. Therefore, in an attempt to rescue the loss of power phenotype for *Ophn-1*$^{-/y}$ slices, Y27632 (10 μM) was applied in a pre-treatment and concomitantly to the KA throughout the recordings. A concentration of 10 μM was chosen as it was thought to be effective from previous studies (Govek et al., 2004). In effect Govek et al (2004) have shown that 10 μM was effective in rescuing the deficit in spine's length, by putatively inhibiting RhoA protein. Additionally, study from the laboratory also shown effectiveness of this concentration (Powell et al, 2009 submitted). The application of Y27632 antagonised the action of a protein called Rho-kinase (or ROCK) which is a member of a signalling pathway downstream to RhoA. RhoA is one of the small GTPase protein inhibited by oligophrenin1. Thus, it was expected to counterbalance the over-activation of RhoA (Govek et al., 2005) induced by the lack of oligophrenin1 (Ishizaki et al., 2000). Furthermore, Y27632 has been previously shown to rescue the shrinkage of the dendritic spines in *Ophn-1*$^{-/y}$ CA1 pyramidal neurons and this result has shed in light the key role played by ROCK in the intracellular signalling of oligophrenin1 (Govek et al., 2004). Figure 3.17 shows an apparent reduction of the gamma power which was not however significant in *Ophn-1*$^{-/y}$ and *Ophn-1*$^{+/y}$ (B. and A. respectively). At t=60min: *Ophn-1*$^{-/y}$ /KA: 4170 ±1104 μV^2 (n=7); *Ophn-1*$^{-/y}$ /KA+Y27632: 1273 ±197 μV^2 (n=5), p=0.26 (t-

test), fig. 3.15 B. and; *Ophn-1*$^{+/y}$ /KA: 6077 ±2911 μV^2 (n=5); *Ophn-1*$^{+/y}$ /KA+Y27632: 2858 ±1360 μV^2 (n=6), p=0.32 (t-test), fig 3.15 A. Additionally, univariate analysis of variance (ANOVA) was performed. In Ophn-1$^{+/y}$ conditions, Y-27632 had no effect on the power of KA-induced gamma oscillations (p=0.121). Similar negative result was observed in the Ophn-1$^{-/y}$ conditions (p=0.075).

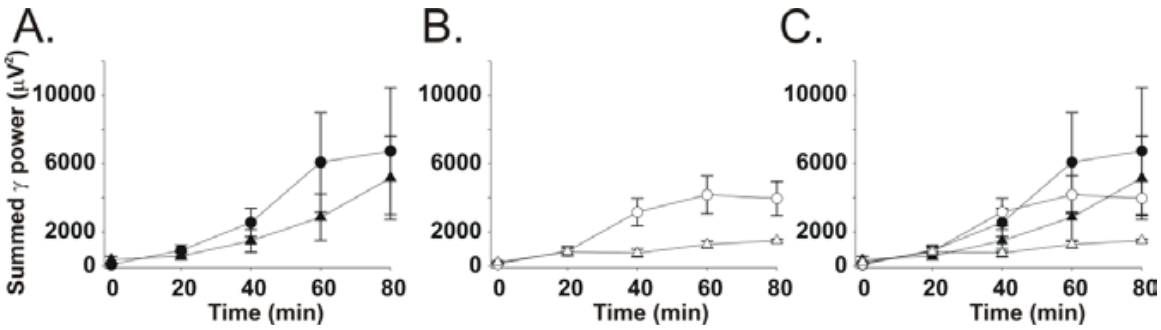

Figure 3.17: Effect of Y27632 (10 μM) in KA-induced gamma oscillations. (Bath temperature: 32ºC). **(A)** ***S***ummated gamma power of KA-induced gamma oscillations in *Ophn-1*$^{+/y}$: KA only (filled circle) (n=5) and KA+Y27632 (filled triangle) (n=6) (ANOVA p=0.121). **(B)** Effect of pretreatment of Y27632 on KA induced gamma oscillations in *Ophn-1*$^{-/y}$: KA only (open circle)(n=7) and KA+Y27632 (open triangle)(n=5) (ANOVA p=0.075) **(C.)** Gathered data

This result indicated that Y27632 had no effect on the power of KA-induced gamma oscillations in wild-type and knock out conditions. It is however possible that the concentration of Y27632 was too low. A study from Nakayama et al (2000) has used a concentration of 100μM to reach efficiency.

3.7 Effect of the loss of oligophrenin1 on spontaneous gamma oscillations

In addition to the characterization of KA-induced gamma oscillations, I investigated spontaneous gamma oscillations when they visually occurred. This small neuronal population synchronisation was recorded without any pharmacological agents applied. Spontaneous gamma oscillations occurred with an average of 1 out of 3 slices and can be quantified. It usually concerned the electrophysiological recordings which follow the cutting of the slices. The origin of the small spontaneous gamma oscillations remains to be elucidated (Pietersen et al., 2009)

Figure 3.18 Ai. & Aii. depict representative traces of spontaneous gamma oscillations observed in *Ophn-1*$^{+/y}$ and *Ophn-1*$^{-/y}$ slices respectively. *Ophn-1*$^{-/y}$ showed similar dominant frequency to *Ophn-1*$^{+/y}$ slices (30.14 ±1.45 Hz, n=7; 31.55 ±1.48 Hz, n=7, respectively, p=0.51, fig 3.18 Bi.). Similarly, the peak and summated power in *Ophn-1*$^{-/y}$ were not significantly different than in *Ophn-1*$^{+/y}$ (11.67 ±2.98 μV^2; 12.60 ±3.28 μV^2, respectively, p=0.84 fig 3.18 Bii.; 173.94 ±44.41μV^2; 169.47 ±39.11 μV^2 respectively, p=0.94, fig. 3.18 Biii.)

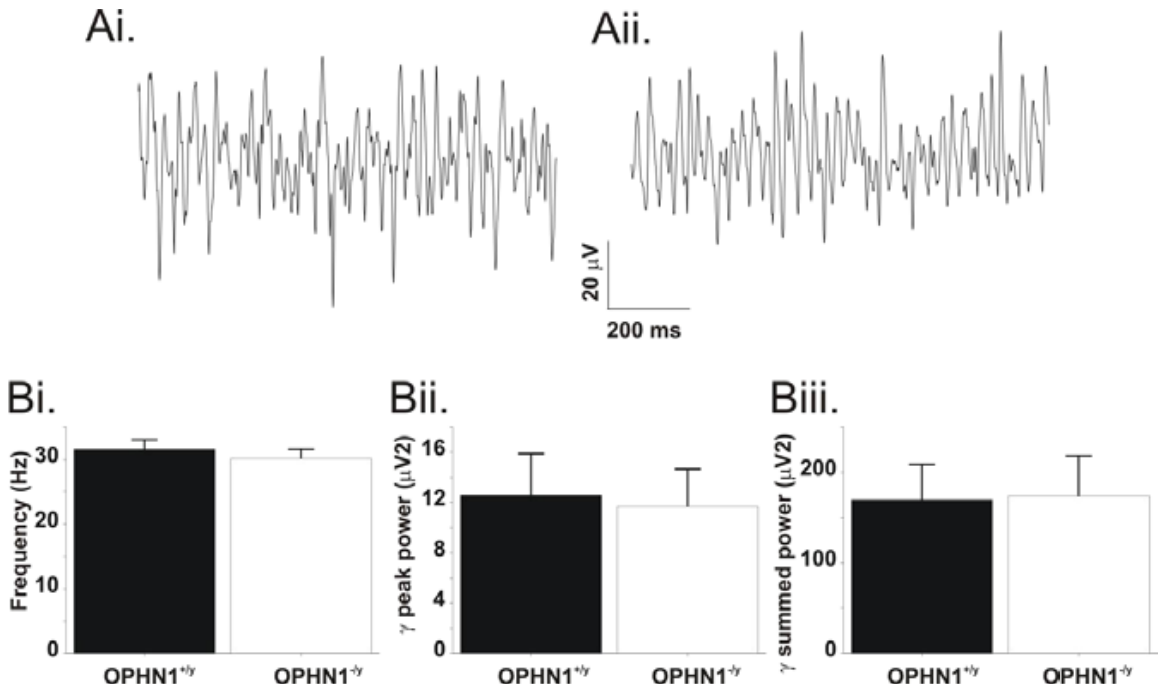

Figure 3.18: Spontaneous gamma oscillations were unchanged between genotypes (Bath temperature: 32ºC). Typical traces showing spontaneous gamma oscillations in *Ophn-1*$^{+/y}$ **(Ai)** and *Ophn-1*$^{-/y}$ slices **(Aii)**. **(Bi)** Histogram of the peak frequency (p=0.51). **(Bii)** Histogram of the peak power (p=0.84). **(Biii)** Histogram of the summated power (p=0.94) (*Ophn-1*$^{+/y}$ n=7 and *Ophn-1*$^{-/y}$ n=7).

3.8 SUMMARY

To summarize on extracellular recording experiments of gamma oscillations, I have shown:

i) a significant loss of power in KA-driven gamma oscillations was observed.

ii) that the rhythmicity of gamma oscillations in *Ophn-1*$^{-/y}$ slices appeared normal.

iii) that the synchronization of gamma oscillations in *Ophn-1*$^{-/y}$ slices within the hippocampal structure was normal.

iv) that the loss of gamma oscillations power in *Ophn-1*$^{-/y}$ slices failed to be rescued by the small molecule Y27632.

v) that the spontaneous gamma oscillations in *Ophn-1*$^{-/y}$ slices were unaltered.

Chapter 4: MECHANISMS UNDERLYING THE LOSS OF POWER IN KA-INDUCED GAMMA OSCILLATIONS IN *Ophn-1*$^{-/y}$ SLICES

4.1 AIMS

The lack of oligophrenin1 protein in humans leads to learning disabilities (Billuart et al., 1998). A mouse model of oligophrenin1 deficiency has shown impairments in learning, particularly spatial memory (Khelfaoui et al., 2007). Structural deficits such as alterations in shape and density of the dendritic spines have also been observed (Khelfaoui et al., 2007, Govek et al., 2004). Whether these structural deficits can explain the functional deficits in this mouse model remains unanswered?

In this chapter, I investigated deficits in CA3 hippocampal area. To that end, I used two distinct and complementary electrophysiological techniques, namely the measurement of neuronal population field potentials using extracellular recordings and single cell recordings. As gamma oscillations are generated by coherent synaptic activity between various interneurons and CA3 pyramidal neurons (Bartos et al., 2007); I proposed to investigate the synaptic deficits which underlie the reduced KA-induced gamma oscillations previously observed in CA3 area in *Ophn-1*$^{-/y}$ slices (see chapter 3). This interplay between neurons involves both excitatory and inhibitory currents which can be dissected and quantified in *Ophn-1*$^{-/y}$ CA3 pyramidal neurons. Deficits in either excitatory or inhibitory neurotransmission could explain the reduced gamma oscillations strength.

First, I assessed the field potentials generated by a population of neurons using extracellular recording. Second, I performed patch clamp studies to distinguish changes in either excitatory or inhibitory neurotransmission in *Ophn-1*$^{-/y}$ CA3 pyramidal neurons. The excitatory and inhibitory postsynaptic currents observed were the result of the synaptic activity occurring within the complex CA3 neuronal network.

4.2 Electrophysiological characterization of field potentials in CA3 area

4.2.1 Single pulse stimulation of afferents to CA3 neuronal population

Field postsynaptic potentials and population spikes quantification

It has been shown previously that *Ophn-1*$^{-/y}$ mice show deficits in synaptic processes, notably a reduction in the paired-pulse facilitation in the CA1 area (Khelfaoui et al., 2007). Alteration in synaptic function may provide evidence to explain the altered gamma oscillations. To examine the CA3 area, field potentials recordings were performed using electrodes placed in CA3c; electrodes were placed on the stratum pyramidale (somatic area of the pyramidal neurons) and on the stratum radiatum (apical dendritic arborization). The extracellular recording electrodes recorded the potential generated by the electrical activity of neurons located at the vicinity of the electrodes.

On the stratum pyramidale source field potentials were recorded after orthodromic electrical stimulation. The stimulating electrode was placed in the middle of hilus to stimulate the mossy fibre pathway. Potentials were recorded as a positive deflection, owing to currents generated at the apical dendrites and flowing down the dendritic arborisation to finally exit at the somatic level (source). On the top of this source potentials, a population spike (PS) occurred for high stimulus intensities, which corresponded to a large entry of Na^+ ions via the opening of voltage gated sodium channels as action potentials fired in the pyramidal cells (fig 4.1 Ci. & Cii.). On the stratum radiatum, field postsynaptic potentials (PSP) were recorded as a negative deflection, which corresponded to a large movement of positive ions across postsynaptic glutamatergic receptors inside the neurons, generating sink potentials. This led to the activation of the ionotropic glutamatergic receptors by the release of glutamate from presynaptic afferents (mossy fibres and CA3 pyramidal neurons axons collaterals)(fig 4.1 Ai. & Aii.) (Johnston et al, 1995).

Representative PSP traces are shown for *Ophn-1*$^{+/y}$ and *Ophn-1*$^{-/y}$ slices (fig 4.1 Ai. & Aii. respectively). Figure 4.1B depicts the plot of the input-output relationship of the PSP, the amplitude of PSP increased with the intensity of the stimulus and reached a maximum for stimuli above 25 V. The maximum plateau in *Ophn-1*$^{-/y}$ slices was not significantly different compared to *Ophn-1*$^{+/y}$ slices (1991 ±286 mV.s^{-1}, n=6; 2783 ±337 mV.s^{-1}, n=6, respectively, p=0.10, fig. 4.1B.). This result was close to significance, statistical power analysis was 0.255, well under the desired 0.8 meaning that the statistical test was underpowered. Interestingly, at relatively mild intensity of 12 V, the slope in Ophn-1$^{+/y}$ was significantly steeper than in Ophn-1$^{-/y}$

(1206 ± 292 $mV.s^{-1}$, n=6; 476 ± 73 $mV.s^{-1}$, n=6, respectively, p=0.036, t-test, statistical power: 0.507). It may be possible that at higher stimulus intensities, the stimulus does not only recruit mossy fibres but may also recruit other fibre tracts (such as recurrent collaterals).

Nevertheless, the PSP slope considering the whole range of the stimuli intensity, in *Ophn-1*$^{-/y}$ slices was significantly lower than in *Ophn-1*$^{+/y}$, using univariate analysis of variance (ANOVA p=0.0002). Whilst the half maximal stimulus intensity (V_{50}) was unchanged (15.4 ±1.1V, n=6; 14.4V ±1.7, n=6, respectively, p=0.58). Univariate analysis of variance was also performed over the range 0 to 16V and rendered a value of 0.014. It may be possible that, owing to the relatively large thickness of the stimulating electrode and the high voltage employed, the stimulus may activate additional fibres other than the mossy fibres. Additional experiments are required to resolve this issue, such as testing the specificity of the mossy fibre stimulation in this paradigm. Mossy fibres terminals selectively express group II metabotropic glutamatergic receptors (mGluR) , therefore application of the mGluR agonist DCGIV could be used to confirm selective activation of the mossy fibres (Manzoni and Bockaert, 1995, Yoshino et al., 1996).

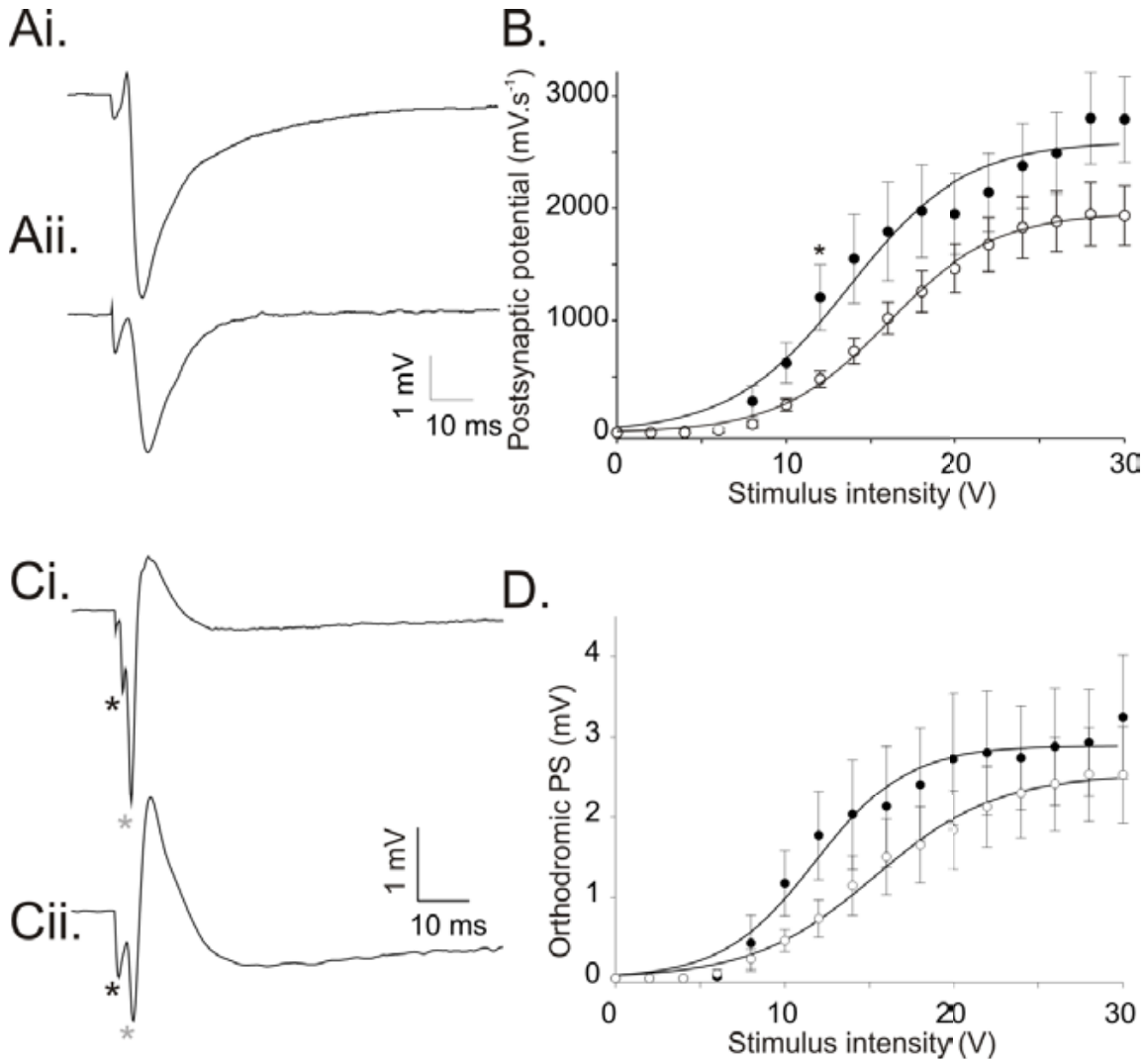

Figure 4.1: Single pulse stimulation of the mossy fibres pathway. Typical PSP recorded on CA3 stratum radiatum in *Ophn-1*$^{+/y}$ slices **(Ai.)** and in *Ophn-1*$^{-/y}$ slices **(Aii.)**. **(B.)** Input-output relationship: PSP values plotted against voltage stimulus intensity (●) *Ophn-1*$^{+/y}$ slices (n=6); (○) *Ophn-1*$^{-/y}$ slices (n=6). **(Ci)** & **(Cii)** Representative orthodromic population spikes (grey star) following an antidromic population spikes (black star) in *Ophn-1*$^{+/y}$ and *Ophn-1*$^{-/y}$ slices respectively **(D)** Input-output relationship: plot of population spike amplitudes vs. voltage (●) *Ophn-1*$^{+/y}$ slices (n=6); (○) *Ophn-1*$^{-/y}$ slices (n=6).

Figure 4.1 Ci and Cii show representative traces of population spikes in *Ophn-1*$^{+/y}$ and *Ophn-1*$^{-/y}$ respectively. Both antidromic and orthodromic population spikes are shown (black and grey * respectively, fig 4.1 Ci.). The antidromic spikes resulted from the direct activation of CA3 pyramidal neurons axons collaterals situated close to the concentric electrode. In contrast, orthodromic spikes which result from the monosynaptic activation of CA3 pyramidal neurons through the mossy fibres pathway showed a slower onset. Paralleling the PSP, the maximum amplitudes of the orthodromic population spikes (obtained from a Boltzmann fit) in *Ophn-1*$^{-/y}$ were unaltered compared to *Ophn-1*$^{+/y}$ (2.69 ±0.65 mV, n=6; 2.67 ±0.54 mV, n=6, respectively, p=0.98, fig 4.1D.). The amplitude of the PS was reduced across the whole stimulus range in *Ophn-1*$^{-/y}$ compared to *Ophn-1*$^{+/y}$ (ANOVA p<0.013).

The reduction in synaptic responses upon a single stimulation indicated a reduction in the synaptic strength between granule neurons and CA3 pyramidal neurons in *Ophn-1*$^{-/y}$ mice.

To determine the nature the postsynaptic potentials, a cocktail of glutamatergic receptor antagonists was added to the aCSF.

Pharmacology of the field postsynaptic potentials.

Both the AMPA/KA receptor antagonist 2,3-dihydroxy-6-nitro-7-sulfamoyl-benzo[f]quinoxaline-2,3-dione (NBQX) (20 μM) (Pitt et al., 2000), and (2*R*)-amino-5-

phosphonovaleric acid (D-APV) (25 μM) (Haberny et al., 2002), were added to the superfusing aCSF. Blocking the fast excitatory neurotransmission significantly reduced the PSP compared to control (aCSF only) (709 ±24 mVs^{-1}; 2022 ± 12$mV.s^{-1}$, respectively, $p<0.0001$ (ANOVA), fig 4.2 A.).

Figure 4.2 B shows traces of PS before and after application of the excitatory amino acid (EAA) blockers. The amplitude of PS after treatment was significantly smaller than before treatment (3.00 ±0.04 mV; 3.97 ±0.05 mV, respectively, $p<0.001$)

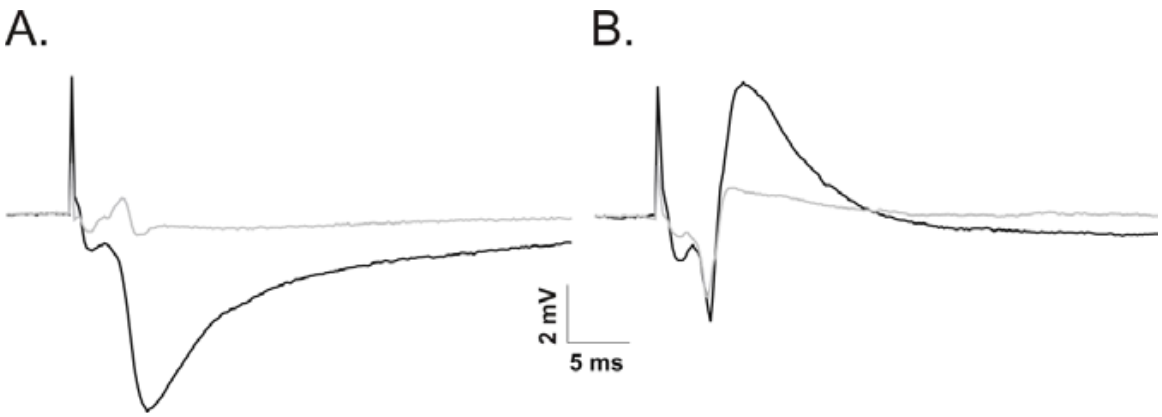

Figure 4.2: Sensitivity of the responses to ionotropic glutamatergic receptors blockers. The panel **(A.)** figures the PSP obtained after treatment with EAA blockers (grey line) as opposed to without drugs condition (black line) recorded from the *s.* radiatum **(B.)** Representative traces of PS before and after drugs application (dark and grey line respectively) recorded from the *s.* Pyramidale.

The PSP and the PS were partially blocked (75% and 25% for PSP and PS respectively) by a cocktail of glutamatergic receptor antagonists. An incomplete blockade of the responses was observed, unlike in CA1 area (see below Chapter 5

section 6.2.2.). A rational explanation could be that unlike CA1 neuronal networks, CA3 networks are extremely complex (Shepherd, 2003). A second explanation could be that the stimulating electrode stimulated directly the axons of CA3 pyramidal neurons, hence the strong antidromic population spikes resistant to EAA blockers (fig. 4.2 grey lines). A final explanation is that the responses could be not only glutamatergic, as other excitatory neurotransmitters, such as Acetylcholine are released onto CA3 pyramidal neurons (Gulledge and Kawaguchi, 2007)

4.2.2 Reduction of paired pulse facilitation in *Ophn-1*$^{-/y}$ slices.

Paired pulse facilitation of field postsynaptic potentials and population spikes

The presence of the oligophrenin1 in the presynaptic compartment (Govek et al., 2004), is suggestive of a presynaptic function, as implied by Khelfaoui (2007). To examine the role of oligophrenin1 in the presynaptic compartment, a paired-pulse protocol was performed (Schulz et al., 1994).

For the paired pulse stimulation experiments, a stimulus which evoked 50 % of the maximal response defined by the input-output relationship (fig 4.1B) was used (*Ophn-1*$^{+/y}$ 14.4 ±1.7 V (n=6); *Ophn-1*$^{-/y}$ 15.4 ±0.45 V (n=6), p=0.58). This stimulation intensity was chosen so that both synaptic facilitation and depression can be detected. The PSPs were evoked by 2 equal stimuli onto the mossy fibres separated by a variable time intervals. The degree of facilitation (or inhibition) was calculated by expressing the PSP slope in response to the 2nd stimulus (test stimulus) as a

function of that obtained for the first stimulus (Conditioning stimulus) (P2/P1). Figure 4.2 Aii & Aii show double PSPs evoked by stimuli separated by 25 ms and 100 ms (left and right panels respectively). In *Ophn-1*$^{+/y}$ slices, a clear facilitation of the second response (test response) is observed (fig 4.2 Ai.). The comparison of P2/P1 between genotypes, revealed that the facilitation in *Ophn-1*$^{-/y}$ was significantly lower than in *Ophn-1*$^{+/y}$ slices for inter-pulse intervals 25, 50, 100, 200, 500, 1000 ms (e.g. 25 ms, 1.40 ±0.14, n=9; 2.03 ±0.20, n=8, respectively, p=0.025; 100 ms, 1.06 ±0.09; 1.57 ±0.10, p=0.002 fig 4.3 B.). Similar results were obtained with inter-pulse interval of 500 ms in which $GABA_B$ neurotransmission occurred (0.87 ±0.03; 1.11 ±0.07, p=0.005). The univariate analysis of variance (ANOVA) rendered a significance value p=0.002 (with bonferroni correction).

Although the PSP measure was most indicative of the effects on synaptic transmission, PS amplitude was also examined to assess the firing of CA3 pyramidal neurons evoked by the synaptic activation (fig 4.4). Figure 4.4 Ai & Aii display typical population spikes traces in *Ophn-1*$^{+/y}$ and *Ophn-1*$^{-/y}$ respectively. Facilitation of the PS in response to the second stimulus was observed for most inter-pulse intervals in *Ophn-1*$^{+/y}$ and *Ophn-1*$^{-/y}$. The P2/P1 ratio in *Ophn-1*$^{-/y}$ was significantly reduced compared to the P2/P1 ratio in *Ophn-1*$^{+/y}$ (50 ms: 1.66 ±0.06, n=8; 2.50 ±0.21, n=9, respectively, p=0.008, fig 4.4 B.). Additionally, for an inter-pulse interval of 10 ms, *Ophn-1*$^{+/y}$ displayed a stronger facilitation than in *Ophn-1*$^{-/y}$ slices (1.75 ±0.18; 0.92 ±0.21, respectively, p=0.03).

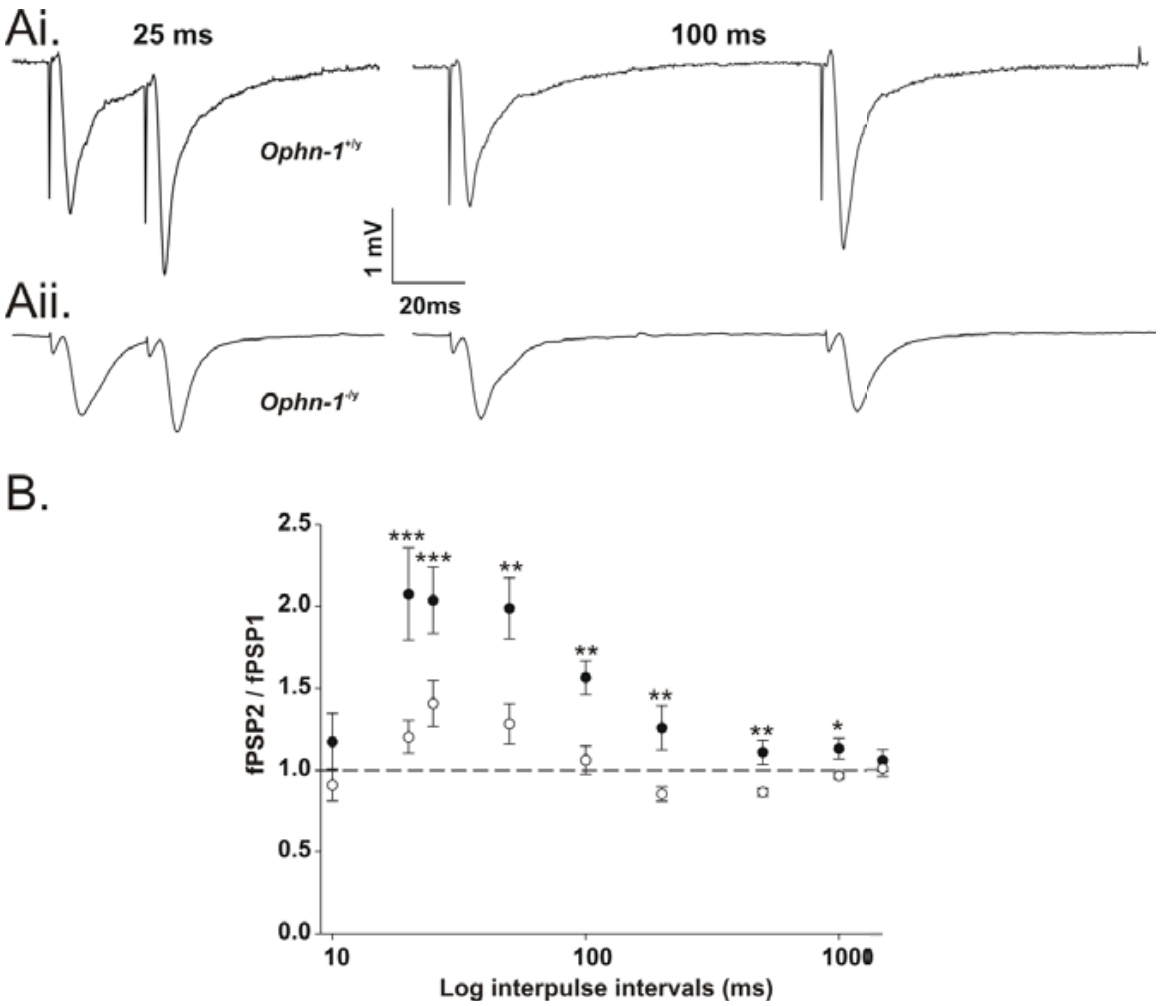

Figure 4.3: Altered paired-pulse facilitation on PSPs in *Ophn-1*$^{-/y}$ slices. Representative double PSP evoked by paired pulse stimulation with inter-pulse intervals 25 ms (left panel) and 100 ms (right panel) for *Ophn-1*$^{+/y}$ **(Ai.)** and in *Ophn-1*$^{-/y}$ slices **(Aii.)** (**B)** PSP paired pulse facilitation ratio for *Ophn-1*$^{+/y}$ (filled symbols) n=8 and in *Ophn-1*$^{-/y}$ (open symbols) n=9. $p<0.05$ (with the Bonferroni correction) for IPI comprised between 20 ms and 1000 ms.

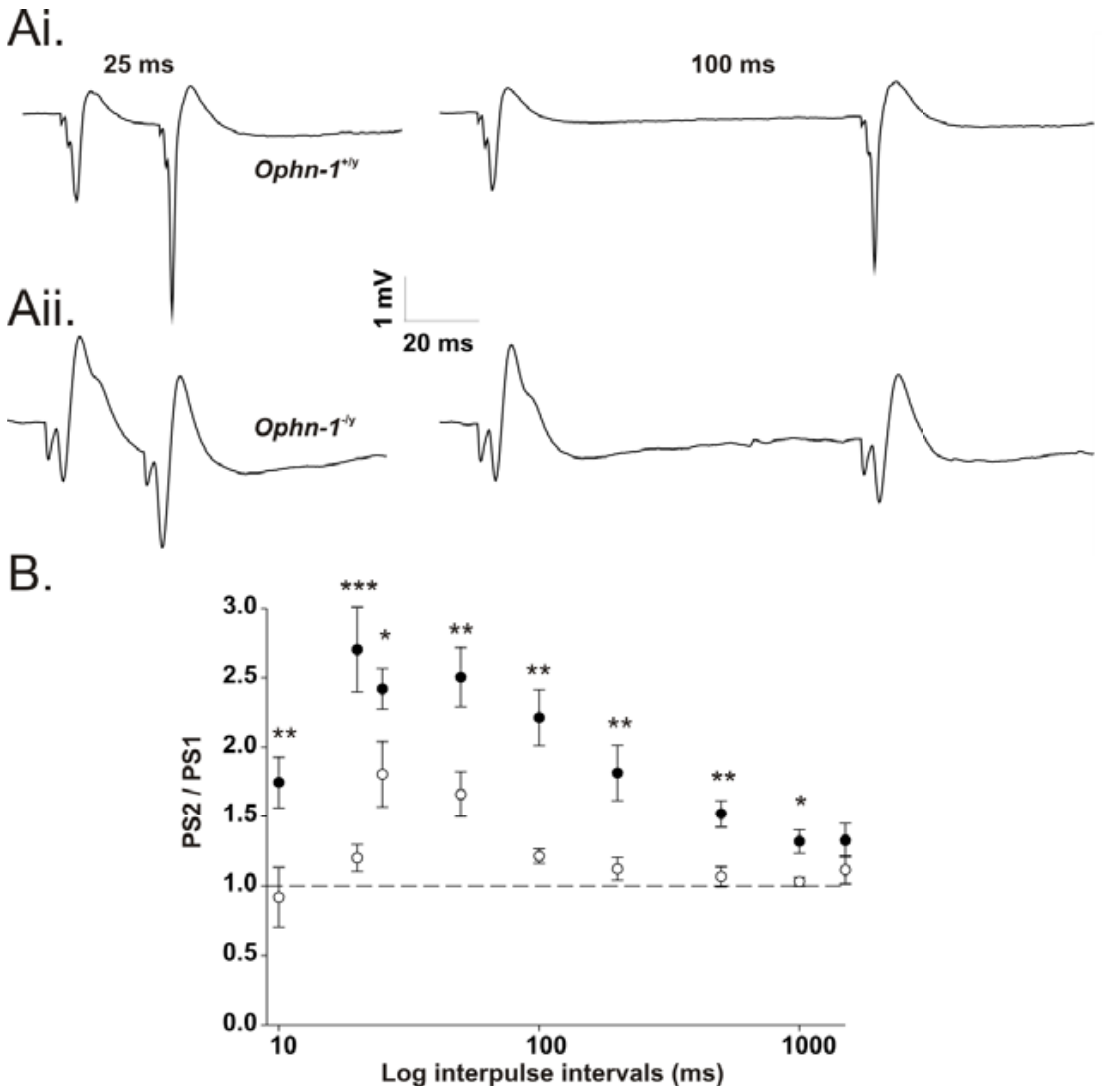

Figure 4.4: Altered paired-pulse facilitation on PS in *Ophn-1*$^{-/y}$ slices. Typical traces showing population spikes for *Ophn-1*$^{+/y}$ **(Ai.)** and *Ophn-1*$^{-/y}$ slices **(Aii.) (B.)** Paired-pulse facilitation on PS in *Ophn-1*$^{-/y}$ (open symbols) (n=8) and in *Ophn-1*$^{+/y}$ (filled symbols) (n=9).(ANOVA, p=0.00015)

The present results on paired-pulse facilitation in CA3 area are in agreement with previous results from Khelfaoui et al (2007), obtained in *Ophn-1*$^{-/y}$ CA1 area. It is

noteworthy that I conducted similar experiments in CA1 and no such differences were observed (see Chapter 5, figure 6.2.2.).

These present results in CA3 suggest that the defects are presynaptic in origin (Schulz et al., 1994, Matilla et al., 1998). To further investigate this observation, synaptic activity at individual CA3 neurons was investigated.

4.3 Electrophysiological characterization of CA3 pyramidal neurons.

4.3.1 Distinction between pyramidal neurons and interneurons

To distinguish between varieties of different neurons present in CA3 stratum pyramidale or juxtaposed to it, it was necessary to characterise the electrophysiological responses to allow distinction between principal neurons and interneurons. Initial, discrimination was based upon by visual appearance. Following successful establishment of a whole-cell recording, additional discrimination was gained by examination of the neuronal firing pattern in response to a 200 ms, 200pA current injection (fig 4.5). Interneurons were characterised by high frequency firing whereas pyramidal neurons possessed lower firing frequencies (fig 4.5 and fig 4.6). Interneurons displayed a mean firing rate of 86.25 ±14.77 Hz (n = 4), whilst putative pyramidal neurons displayed a lower firing frequency of 2.30 ±0.79 Hz (n = 10) ($p<0.0001$) (fig. 4.6 Ai. and Aii.) (Shepherd, 2003, Andersen, 2007).

The final segregation was based upon half width duration of the action potentials (Pyramidal neurons: 1.10 ±0.04 ms (n=10); Interneuron: 0.80 ±0.04 ms (n=4), p<0.001 (t-test) statistical power 0.984) and the value of the fast afterhyperpolarisation (fAHP) ((Pyramidal neurons: 5.57 ±0.76 mV (n=10); Interneuron: 15.45 ±2.13 mV (n=4), p=0.004 (Mann-Whitney Rank Sum Test)) (fig. 4.6 Bi. and Cii. respectively).

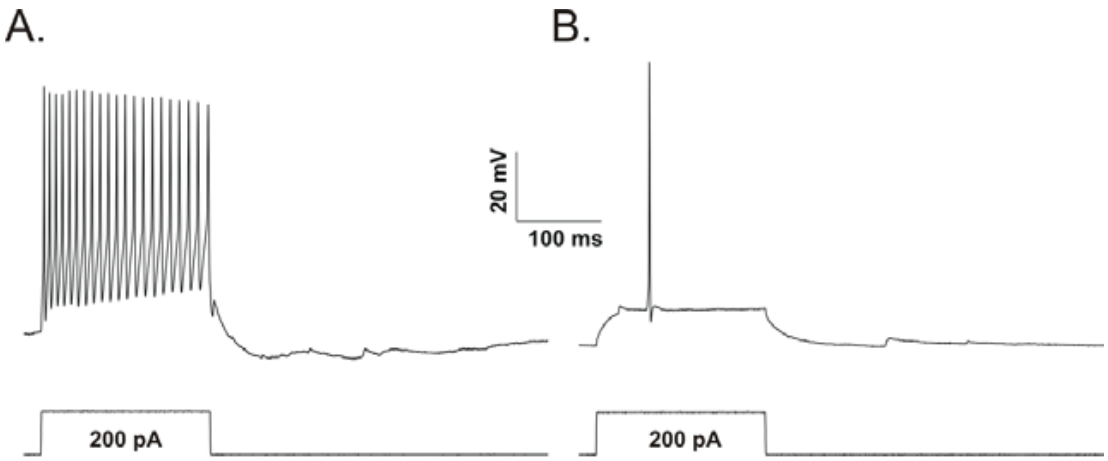

Figure 4.5: Interneurons and pyramidal neurons displayed different firing pattern upon current injection of 200 pA. (A.) Typical high frequency firing pattern recorded from putative interneuron whilst putative pyramidal neurons displayed a slower a firing pattern **(B.).**

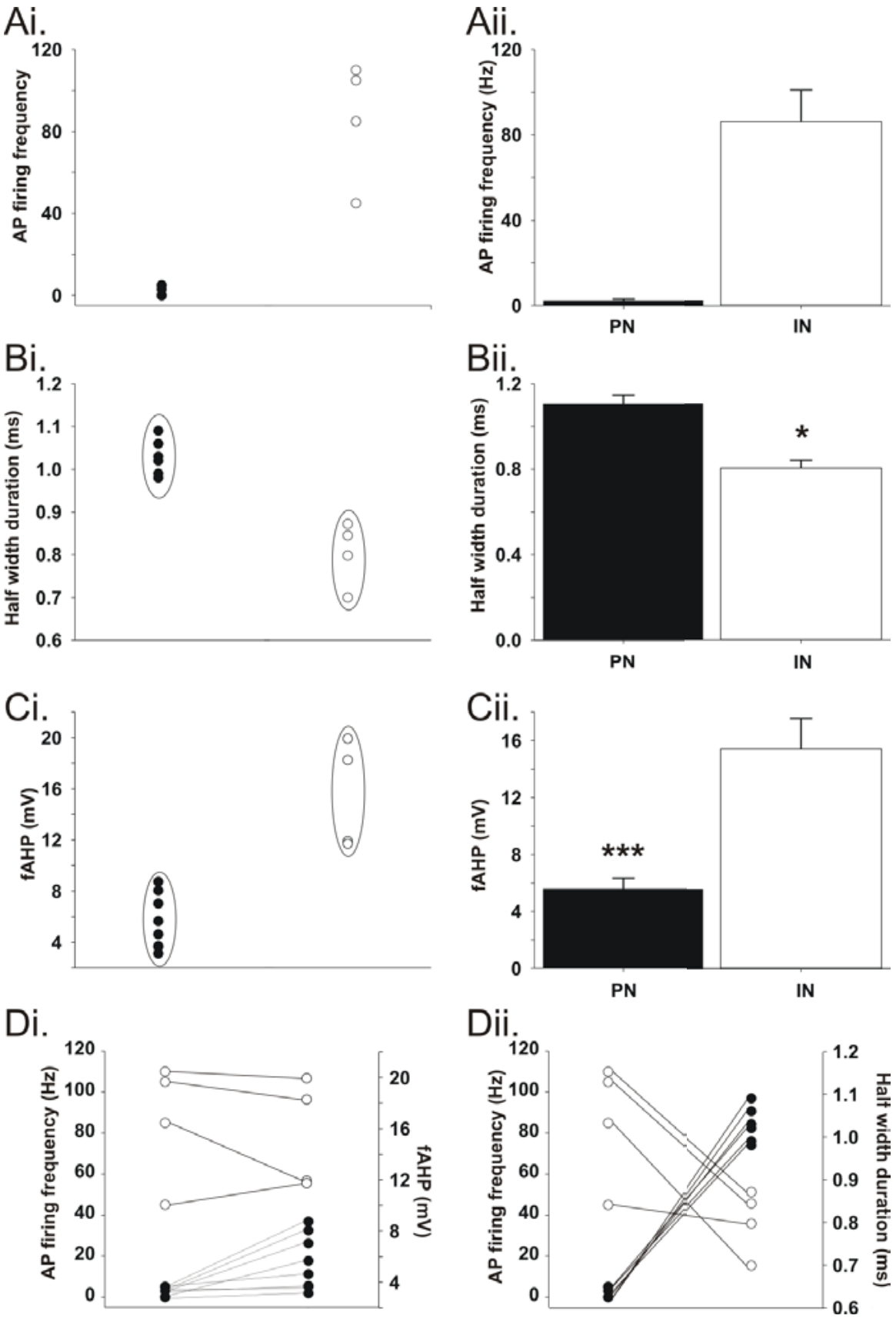
Ai.
AP firing frequency
120
80
40
0
Aii.
AP firing frequency (Hz)
120
80
40
0
PN
IN
Bi.
Half width duration (ms)
1.2
1.1
1.0
0.9
0.8
0.7
0.6
Bii.
Half width duration (ms)
1.2
0.8
0.4
0.0
*
PN
IN
Ci.
fAHP (mV)
20
16
12
8
4
Cii.
fAHP (mV)
16
12
8
4
0
***
PN
IN
Di.
AP firing frequency (Hz)
120
100
80
60
40
20
0
fAHP (mV)
20
16
12
8
4
Dii.
AP firing frequency (Hz)
120
100
80
60
40
20
0
Half width duration (ms)
1.2
1.1
1.0
0.9
0.8
0.7
0.6

Figure 4.6: Discrimination of pyramidal and interneurons. Putative interneurons displayed a high action potential frequency **(Ai.)** whilst pyramidal neurons displayed a low action potential frequency ($p<0.0001$, t-test) **(Aii.).** Putative interneurons (○) (n=4) and pyramidal neurons (●) (n=10) displayed distinct distributions for action potential half width (**Bi**) and fAHP amplitude **(Ci.)**. Action potential duration was shorter in putative interneurons **(Aii.)** ($p<0.001$, t-test), whilst the fAHP was larger in putative interneurons (**Cii**) ($p=0.004$, Mann-Whitney test). Correlation between the firing rate and fAHP amplitude **(Di.)** Correlation between the firing rate and the half width **(Dii.).** Data are mean ± S.E.M.

4.3.2 Intrinsic neuronal properties were unaltered in *Ophn-1*$^{-/y}$ CA3 pyramidal neurons

The intrinsic neuronal properties of CA3 pyramidal neurons of *Ophn-1*$^{-/y}$ and in *Ophn-1*$^{+/y}$ were delineated prior to postsynaptic currents evaluations. The rationale for the evaluation were *i)* to rule out any deficits in any of the intrinsic neuronal properties, *ii)* to assess the functionality of a wide variety of ionic channels and *iii)* to assess the excitability of *Ophn1*$^{-/y}$ neurons. The intrinsic neuronal properties included the membrane resistance (fig 4.7.) and various features of the action potentials which were shown to be unchanged in *Ophn-1*$^{-/y}$ CA3 pyramidal neurons (fig. 4.7 A. & table 4.1.). The lack of difference between *Ophn-1*$^{-/y}$ and *Ophn-1*$^{+/y}$ CA3 pyramidal neurons indicated that the currents underlying action potentials generation were not altered by the genotype. The input-output firing properties of CA3 pyramidal

neurons, which assessed the ability of the neuron to fire action potentials upon depolarising currents injected into the cell, was equally unchanged (For 0.5 nA current injection: Ophn-1$^{+/y}$: 4.75± 1.11 AP and Ophn1$^{-/y}$ 4.70 ± 0.70 AP, p=0.969 (t-test), fig. 4.7 Bi. & Bii.).

In conclusion, it is unlikely that alterations in intrinsic excitability of *Ophn1*$^{-/y}$ CA3 pyramidal neurons can explain the loss of gamma power.

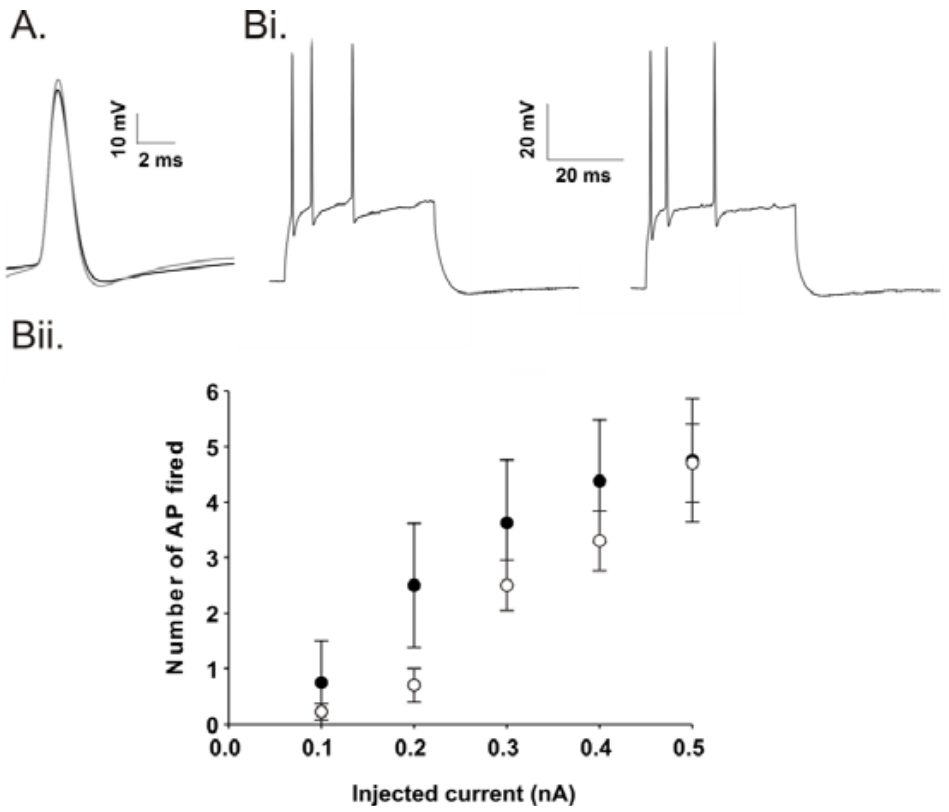

Figure 4.7: Intrinsic properties of CA3 pyramidal neurons. (A.) Overlay of a single action potentials in *Ophn-1*$^{+/y}$ and *Ophn-1*$^{-/y}$ neurons (dark and grey lines respectively) showing similar kinetics. **(Bi.)** Representative traces of action potentials firing upon 300 pA currents injected in *Ophn-1*$^{+/y}$ and *Ophn-1*$^{-/y}$ neurons (left and right panels respectively) **(Bii.)** Input-output relationship: Number of action potentials fired plotted against the injected current, *Ophn-1*$^{+/y}$ n=8 and *Ophn-1*$^{-/y}$ n=10, (ANOVA P= 0.055)

	Genotype		
	Ophn-1$^{+/y}$	***Ophn-1$^{-/y}$***	**p**
Action potential amplitude (mV)	84.5 ±2.8*(9)*	87.8 ±2.9 *(11)*	0.43
Action potential threshold (mV)	-38.8 ±1.2 *(9)*	-38.0 ±1.3 *(11)*	0.64
Half width measurement	1.19 ± 0.09 *(9)*	1.07 ± 0.05 *(11)*	0.25
Membrane resistance (MΩ)	209.2 ±20.3 *(9)*	218.8 ± 26.8 *(11)*	0.78

Table 4.1: Values for action potentials characteristics and membrane resistance. Numbers in parentheses indicate the number of individual cells

4.3.3 Excitatory postsynaptic currents of CA3 pyramidal neurons

After defining the typical characteristics of CA3 pyramidal neurons; I investigated the excitatory inputs to these neurons. These excitatory inputs originate mainly from the dentate gyrus granule cells but also from recurrent axons of CA3 pyramidal neurons. The role of the excitatory input to CA3 pyramidal neurons is important in KA-induced gamma oscillogenesis (Bartos et al., 2007). Furthermore, as the PSP was blocked by EAA blockers, the reduction of the PSP also suggested a deficit in excitatory neurotransmission. Therefore, the strength of the excitatory inputs to CA3 pyramidal neurons was evaluated through the measurement of the spontaneous excitatory postsynaptic currents.

Spontaneous excitatory postsynaptic currents

Spontaneous excitatory postsynaptic currents (sEPSCs) were recorded from voltage clamped CA3 pyramidal neurons at -75 mV using internal solution containing KMeSO4. This resulted in sEPSCs being recorded as negative deflections (fig. 4.8, see methods # 2.4.2), reflecting the activation of the ionotropic glutamatergic receptors. Figure 4.9 Ai. shows that the mean amplitude in *Ophn-1*$^{-/y}$ neurons was not significantly different to *Ophn-1*$^{+/y}$ CA3 pyramidal neurons (20.87 ±3.01 pA, n=9; 30.15 ±4.03 pA, n=8, respectively, p=0.09, fig. 4.9 Ai.). In contrast, the frequency of the sEPSCs in *Ophn-1*$^{-/y}$ neurons was lower than *Ophn-1*$^{+/y}$ CA3 pyramidal neurons (1.67 ±0.37 Hz, n=9; 6.91 ±1.50 Hz, n=8, respectively, p=0.003, fig 4.9 Bi.).

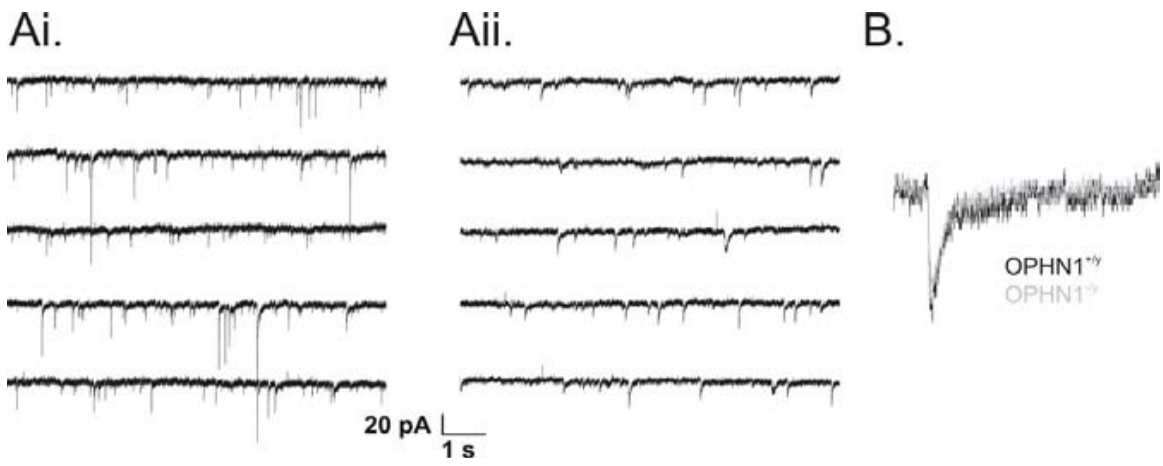

Figure 4.8: Spontaneous EPSCs were recorded from CA3 pyramidal neurons in *Ophn-1*$^{+/y}$ **(Ai.)** and *Ophn-1*$^{-/y}$ slices **(Aii.)**. **(B.)** Overlay of a single sEPSC from *Ophn-1*$^{+/y}$ (dark line) and *Ophn-1*$^{-/y}$ (grey line) CA3 pyramidal neurons

		Excitatory neurotransmission CA3		
		Ophn-1$^{+/y}$	*Ophn-1*$^{-/y}$	P (t-test)
sEPSC	10-90% rise time (ms)	4.10 ± 0.30 (6)	4.38 ± 0.9 (8)	0.71
	τ_{Decay1} (ms)	5.75 ± 0.88 (6)	5.83 ± 0.5 (8)	0.93

Table 4.2: The kinetics of excitatory postsynaptic currents were unaffected in *Ophn-1*$^{-/y}$ CA3 pyramidal neurons. 10-90% rise time and tau decay time are expressed as mean ± SEM. Numbers in parentheses denote the number of cells recorded and the p values resulted from student t-test.

Figure 4.8B. and table 4.2 demonstrated that the kinetics of the sEPSCs were unaltered in *Ophn-1*$^{-/y}$ compared to *Ophn-1*$^{+/y}$ CA3 pyramidal neurons.

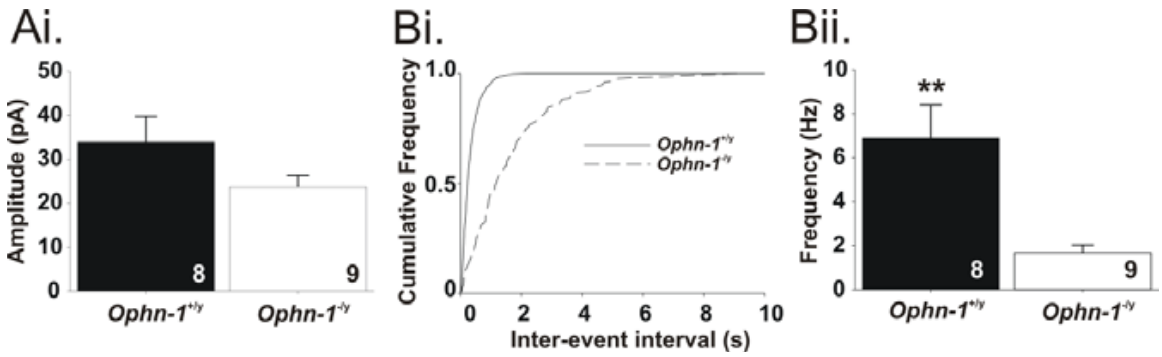

Figure 4.9: Spontaneous EPSCs of *Ophn-1*$^{-/y}$ CA3 pyramidal neurons were less frequent compared to *Ophn-1*$^{+/y}$. (Ai.) Histogram of the mean amplitude. **(Bi.)** Plot of cumulative frequency of sEPSCs showing a shift towards longer inter-event intervals in *Ophn-1*$^{-/y}$ sEPSCs CA3 pyramidal neurons. **(Bii.)** Histogram of the sEPSCs frequency (p=0.006, Man whitney rank sum test). Data are expressed as mean ± S.E.M.

In order to further investigate the mechanism underlying the loss of gamma oscillations power in *Ophn-1*$^{-/y}$ slices, I assessed inhibitory inputs to CA3 pyramidal neurons. The underlying rationale was that two studies have demonstrated that an alteration in the strength of the inhibitory inputs to pyramidal neurons modulates the power of gamma oscillations without affecting the dominant frequency (Hajos et al., 2004, Vreugdenhil et al., 2003)

4.3.4 Inhibitory postsynaptic currents of CA3 pyramidal neurons

Gamma oscillations were induced by a low concentration of KA (50 nM) which slightly depolarise neuronal populations present in the CA3 network. As a result, the pyramidal neurons synchronise their firing, owing to the inhibitory tone imposed by the perisomatic interneurons (Fisahn et al., 1998). The inhibitory inputs to the pyramidal neurons were assessed using whole-cell voltage clamp recordings of CA3 pyramidal neurons.

Characterisation of pyramidal vs interneurons was confounded by the necessary presence of Cs^+ ions in the internal ions. Blockade of K^+ currents by Cs^+ improved the space-clamp. To discriminate between pyramidal neurons and interneurons, a depolarisation step was applied shortly after the whole cell configuration was established, before appreciable amounts of Cs^+ had diffused into the cell. Moreover, to further facilitate classification of neurons, the fluorophore ALEXA 488 was included in the internal solution, which allowed the morphology of the neuron to be observed under the microscope. After confirming a neuron as a principal neuron, the

inhibitory neurotransmission was then examined. Firstly the evoked IPSCs (eIPSCs) were analysed, followed by the spontaneous IPSCs (sIPSCs) and repetitive stimulations protocols, namely paired-pulse stimulation, frequency dependent facilitation and high frequency of stimulation on eIPSCs experiments.

Evoked IPSCs: input-output relationship

Evoked inhibitory postsynaptic currents in CA3 pyramidal neurons were triggered by an electrical stimulation, using concentric stimulating electrode placed in the hilus. In *Ophn-1*$^{+/y}$ pyramidal neurons the increase of the stimulus intensity increased the amplitude of eIPSCs until a maximum plateau amplitude is reached (fig. 4.10 B.). The evoked IPSCs amplitude in *Ophn-1*$^{-/y}$ neurons was significantly smaller than *Ophn-1*$^{+/y}$ neurons (at 18 V, 845.43 ± 245.09 pA, n=8; 1746.7 ± 229.6 pA, n=7, respectively, t-test p=0.037, Fig. 4.10B). Univariate analysis of variance (ANOVA) ascertained this difference over the whole range of stimulation ($p<0.0001$). However, the mean maximal amplitude calculated from the Boltzmann fit, showed no significant differences between *Ophn-1*$^{-/y}$ and *Ophn-1*$^{+/y}$ CA3 pyramidal neurons (1361.75 ±257.01 pA, n=7; 1766.34 ±234.81 pA, n=7, p= 0.27, Statistical power= 0.081 fig. 4.10 B.). The power of statistics analysis revealed that the statistics were underpowered; therefore it may be possible that a significant deficit may have been missed. Additionally, similar comments on the spread of the stimulus to other types of interneurons present in the hilus can be made (see fig.4.1).

Figure 4.10 shows typical eIPSCs in *Ophn-1*$^{+/y}$ (black line) and in *Ophn-1*$^{-/y}$ (grey line) and the overlay of both eIPSCs normalised. The overlay of typical traces showed that the 10-90% rise time and τ decay time were unchanged as confirmed in table 4.2.

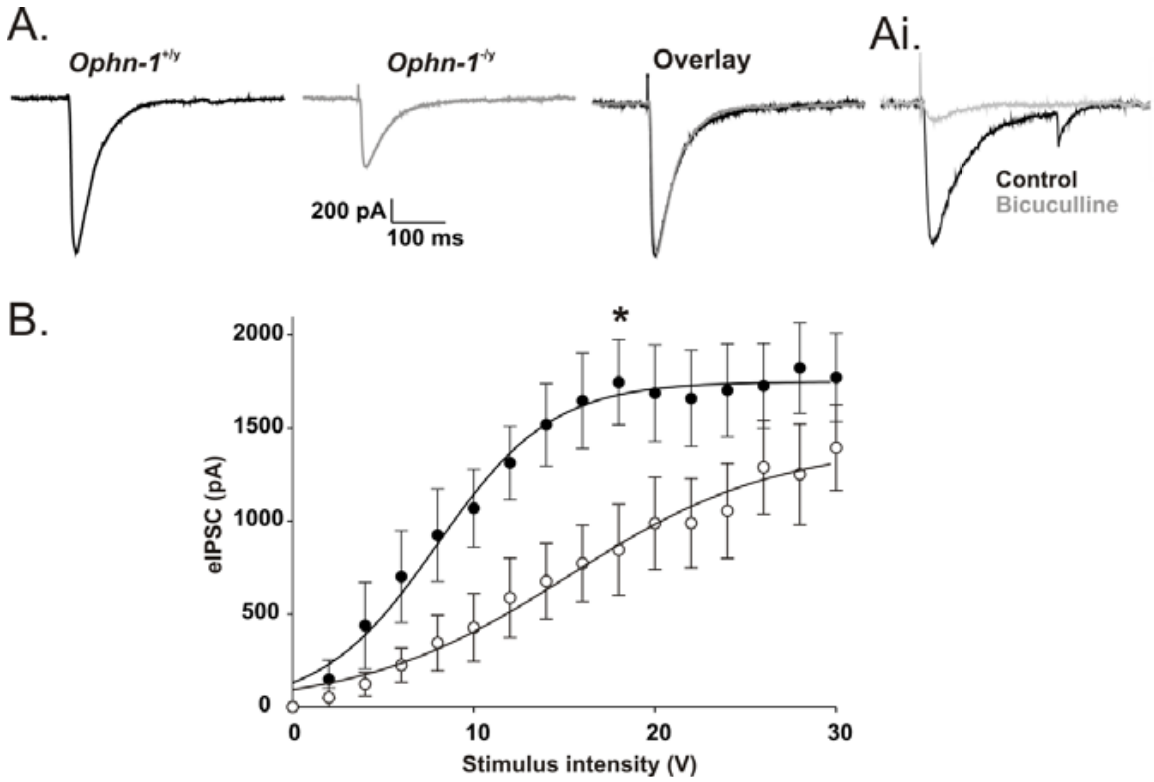

Figure 4.10: Altered eIPSCs in *Ophn-1*$^{-/y}$ CA3 pyramidal neurons. (A.) Typical eIPSCs in *Ophn-1*$^{+/y}$ (left panel) and *Ophn-1*$^{-/y}$ CA3 pyramidal neurons (middle panel); the right panel represents the overlay of eIPSCs for both genotypes. **(Ai.)** eIPSCs after application of bicuculline (10μM) **(B.)** Input-output relationship of eIPSCs fitted with a Boltzmann function in *Ophn-1*$^{+/y}$ (filled symbols, n=7) and in *Ophn-1*$^{-/y}$ (open symbols, n=7) CA3 pyramidal neurons (ANOVA $p<0.0001$). eIPSCs were recorded in presence of D-APV (25 μM) and NBQX (20 μM)

Fig 4.10Ai. shows the $GABA_A$ergic nature of the inhibitory response as revealed by the abolition of the eIPSC by bicuculline (grey line *vs.* dark line). To further

investigate the deficit in the inhibitory neurotransmission revealed by the altered input-output relationship in *Ophn-1*$^{-/y}$ CA3 pyramidal neurons, I then recorded and analysed spontaneous inhibitory neurotransmission from *Ophn-1*$^{-/y}$ and *Ophn-1*$^{+/y}$ CA3 pyramidal neurons.

Spontaneous inhibitory postsynaptic currents

The study of spontaneous IPSCs aimed to assess the inhibitory tone and the neurotransmitter release machinery of inhibitory synapses. The spontaneous release observed comprised two components: *i)* the probabilistic random fusion of synaptic vesicles and *ii)* the release of synaptic vesicles triggered by neuronal firing.

Fig 4.11 Ai. Illustrates 5 consecutive sweeps from CA3 pyramidal neurons voltage clamped at -70 mV. Spontaneous IPSCs were less frequent in *Ophn-1* $^{-/y}$ pyramidal neurons than in *Ophn-1*$^{+/y}$ (fig 4.11 Aii.) (8.78 ±0.81 Hz, n=7; 12.63 ±0.76 Hz, n=7, respectively, t-test p=0.009, statistical power = 0.774, fig. 4.12Bii). The lower frequency was confirmed by the shift towards longer interevent intervals in the cumulative frequency plot (fig 4.12 Bi). The mean amplitude of these events in *Ophn-1*$^{-/y}$ CA3 pyramidal neurons was unaffected compared to *Ophn-1*$^{+/y}$ CA3 pyramidal neurons (32.46 ±2.65 pA, n=7; 38.27 ±5.41 pA, n=7, respectively, p=0.35, fig. 4.12 Ai.). Furthermore, no differences in the kinetics of these events were observed (fig 4.11 B and table 4.3)

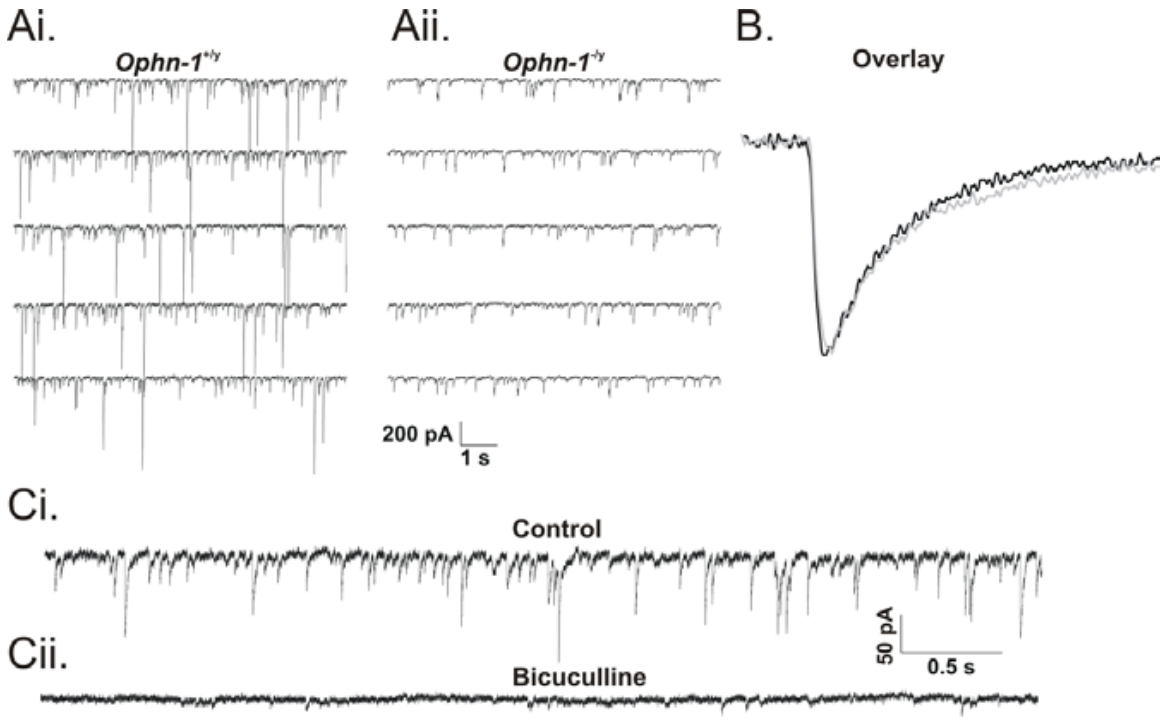

Figure 4.11: Inhibitory neurotransmission onto CA3 pyramidal neurons was reduced in *Ophn-1*$^{-/y}$ neurons. Spontaneous inhibitory postsynaptic currents (sIPSCs) recorded from *Ophn-1*$^{+/y}$ **(Ai)**, and from *Ophn-1*$^{-/y}$ CA3 pyramidal neurons **(Aii.)**. **(B.)** Overlay of eIPSCs from both genotype. Bicuculline (10 μM) abolished sIPSCs (**Cii.** *vs.* **Ci.**).

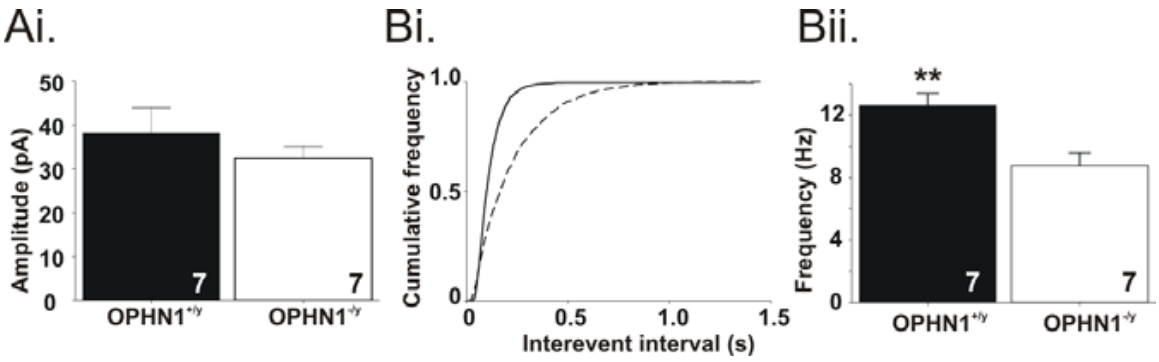

Figure 4.12: sIPSCs were of similar amplitude, but less frequent in *Ophn-1*$^{-/y}$ CA3 pyramidal neurons. (Ai.) Histogram of the mean amplitude. **(Bii.)** Plot of cumulative frequency of sIPSCs in *Ophn-1*$^{+/y}$ (full line) and *Ophn-1*$^{-/y}$ (dashed line) **(Bii.)** Histogram of the mean frequency of sIPSCs. (p=0.009) (t-test)

		Inhibitory neurotransmission CA3		
		Ophn-1$^{+/y}$	*Ophn-1*$^{-/y}$	p
eIPSC	10-90% rise time (ms)	5.52±1.05 (7)	4.63±0.36 (7)	0.44
	τ_{Decay1} (ms)	44.52±7.07 (7)	28.84±5.77 (7)	0.11
sIPSC	10-90% rise time (ms)	3.99±0.21 (7)	4.68±0.29 (5)	0.07 (power: 0.338)
	τ_{Decay} (ms)	7.58±0.53 (7)	8.70±0.65 (5)	0.21
mIPSC	10-90% rise time (ms)	4.15±0.33 (5)	4.33±0.33 (5)	0.65
	τ_{Decay} (ms)	7.98±0.90 (5)	8.37±0.61 (5)	0.72

Table 4.3: The kinetics of inhibitory currents were unaltered in *Ophn-1*$^{-/y}$ CA3 pyramidal neurons. Evoked IPSCs were best fitted by a single exponential decay. Data are expressed as mean ± S.E.M. Numbers in parentheses denote sample size.

The reduced frequency of sIPSCs in *Ophn-1*$^{-/y}$ CA3 pyramidal neurons could originate either from presynaptic or postsynaptic compartments deficits (Marinelli et al., 2003). However, evidence suggests that the deficit was probably not from a postsynaptic origin as no difference has been observed in the amplitude of sIPSCs, which is classically interpreted as a normal functionality of postsynaptic $GABA_A$

receptors. To further evaluate possible deficits in the presynaptic compartment, a study of the TTX resistant sIPSCs allowed the evaluation of the quantal content (q), which could eventually be responsible for the reduction in eIPSCs amplitude and more globally the reduction of the inhibitory neurotransmission in *Ophn-1*$^{-/y}$ CA3 pyramidal neurons

Miniature inhibitory postsynaptic currents (mIPSCs).

Superfusion of tetrodotoxin (TTX) (1 μM) abolished neuronal action potentials generation through the blockade of voltage gated sodium channel and allowed the examination of the miniatures IPSCs (mIPSCs). TTX significantly reduced the frequency of sIPSCs in *Ophn-1*$^{+/y}$ (sIPSCs 12.63 ±0.76 Hz, n=7; mIPSCs 8.03 ±0.91 Hz, n=5, p=0.003, fig 4.14.). The frequency of mIPSCs however was not significantly different between *Ophn-1*$^{-/y}$ and *Ophn-1*$^{+/y}$ CA3 pyramidal neurons (8.60 ±1.48 Hz, n=5; 8.03 ±0.91 Hz, n=5, respectively, p=0.75, fig 4.13 Cii.). Similarly, the mIPSCs amplitude was also unaffected (*Ophn-1*$^{-/y}$ 22.90 ±3.39 pA; *Ophn-1*$^{+/y}$ 27.83 ±7.01 pA, p=0.55, fig 4.13 Ci.).

To summarize, these miniatures IPSCs were not altered neither in amplitude nor in frequency by the genotype. The mean amplitude is supposed to reflect the release of a single quantum. Therefore, similar amplitude indicated that the quantal content was identical between genotypes.

Fig. 4.14 summarizes the frequencies of sIPSCs and mIPSCs in *Ophn-1*$^{+/y}$ and *Ophn-1*$^{-/y}$ CA3 pyramidal neurons.

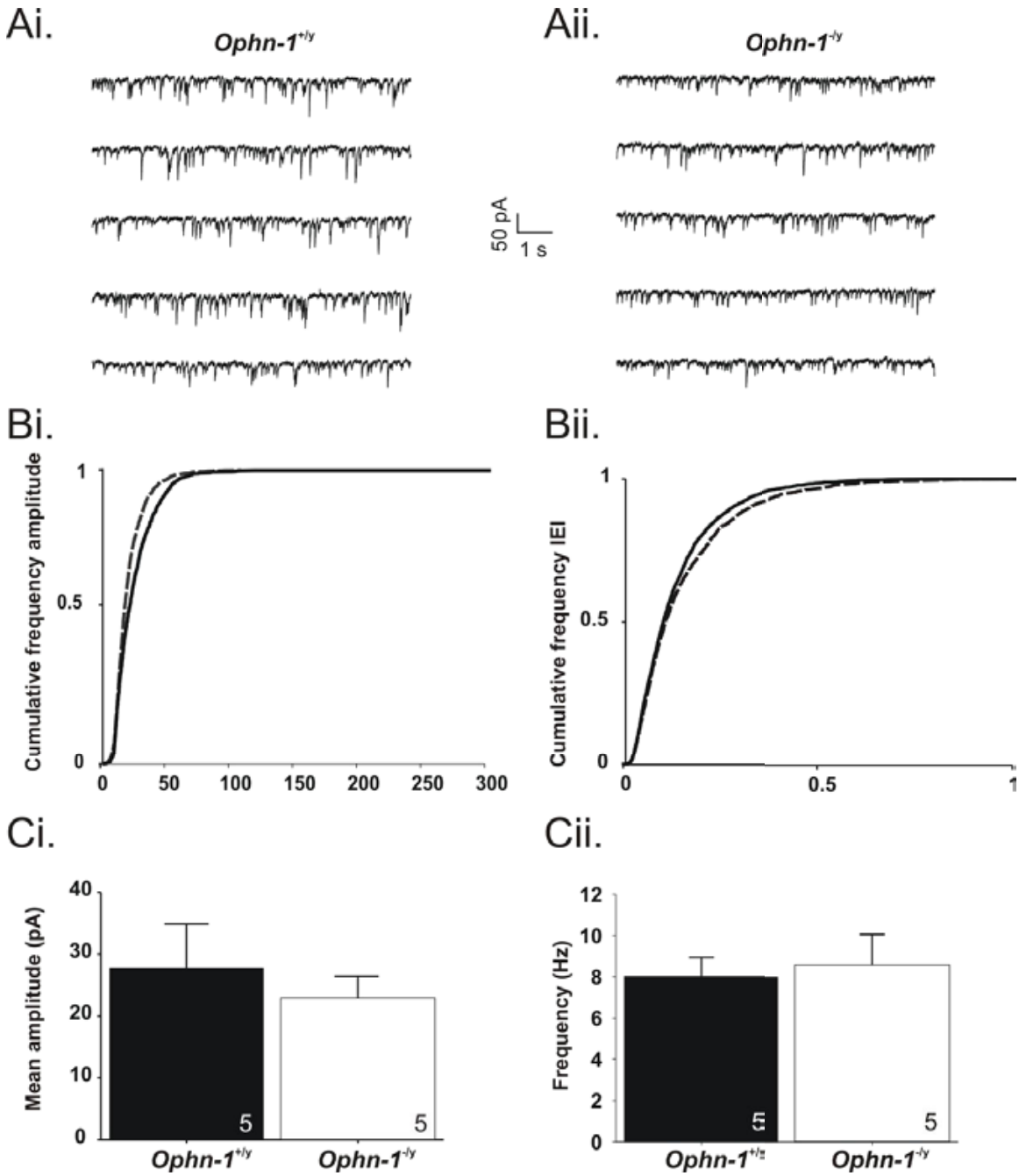

Figure 4.13: TTX resistant IPSCs were unaltered in *Ophn-1*$^{-/y}$ CA3 pyramidal neurons. Miniatures events recorded from *Ophn-1*$^{+/y}$ **(Ai.)** and from *Ophn-1*$^{-/y}$ CA3 pyramidal neurons **(Aii.)**. **(Bi.)** Cumulative frequency amplitude plot **(Bii)** Cumulative frequency inter-event intervals plot (*Ophn-1*$^{+/y}$ full line and *Ophn-1*$^{-/y}$ dotted line) **(Ci.)** Histogram of the mean amplitude p=0.55 t-test **(Cii.)** Histogram of the frequency of sIPSCs p=0.75 t-test. Embedded numbers indicate the number of repeats

These results showed that frequency of sIPSCs and mIPSCs was not significantly different (8.78 ±0.81 Hz; 8.60 ±1.48 Hz, respectively, p=0.91), indicating that oligophrenin1 protein intervene somehow in the process of action potentials-driven sIPSCs.

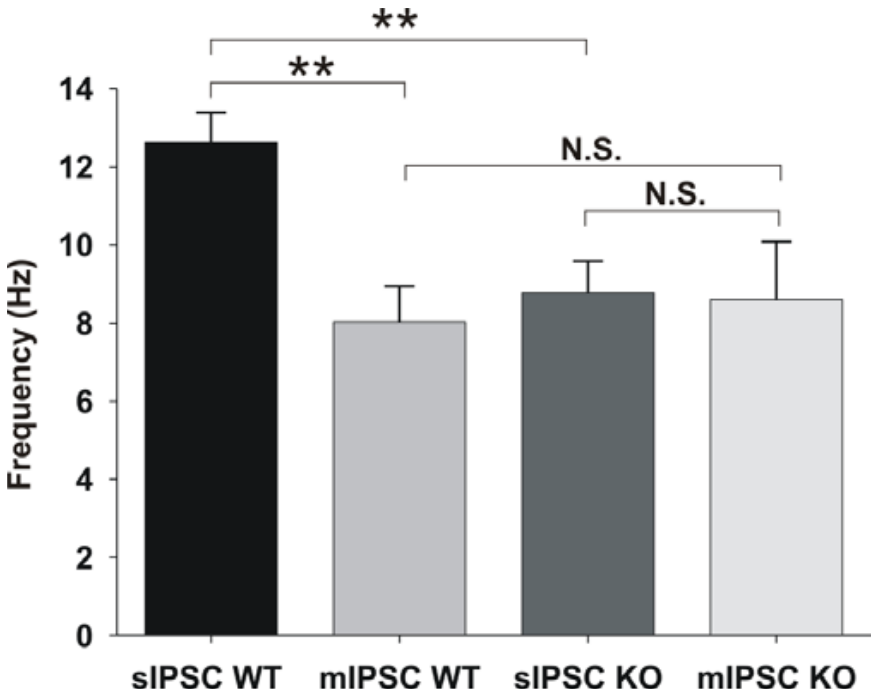

Figure 4.14: Histogram of sIPSCs and mIPSCs frequencies. N.S. means not significant. WT means *Ophn-1*$^{+/y}$ (n=7 for sIPSCs and n=5 for mIPSCs) and KO means *Ophn-1*$^{-/y}$ (n=7 for sIPSCs and n=5 for mIPSCs).

I have so far unraveled some deficits in the inhibitory neurotransmission in CA3, namely an alteration in eIPSCs in *Ophn-1*$^{-/y}$ and a reduction in the frequency of sIPSCs without change in amplitude; the latter ascertained a normal functionality of $GABA_A$ receptors. The frequency of sIPSCs and mIPSCs in *Ophn-1*$^{-/y}$ neurons were

not significantly different, possibly indicating that the deficits reside in action potentials driven sIPSCs.

Furthermore, a similar reduction in frequency of sEPSCs suggested a common deficit to inhibitory and excitatory synapses. To further investigate the presynaptic role of oligophrenin-1, I performed experiments of repetitive stimulations which mimic the firing of action potentials at various frequencies. The rationale of the following experiment was that a fast frequency of firing is necessary for higher cognitive function, which could be impaired, as it has been already suggested by a loss of gamma oscillations power in *Ophn-1*$^{-/y}$ slices.

Paired-pulse stimulation on eIPSCs

Paired pulse depression on monosynaptic $GABA_A$ergic eIPSC were evoked by two equal electrical stimuli was investigated in *Ophn-1*$^{-/y}$ CA3 pyramidal neurons. It is well known that the stimulation of synapses by a subsequent stimulus induced a synaptic depression of the response for almost all stimulus intervals. This depression is explained by the presynaptic inhibition phenomenon, which function is to modulate synaptic strength, as well as preventing excessive release of neurotransmitters. It is generated by the activation of presynaptic $GABA_B$ receptors by the spill over of GABA outside the synaptic cleft (Davies and Collingridge, 1993).

Figure 4.15 Ai. & Bi show representative eIPSCs triggered by a double stimulation of inter-pulse intervals of 20 ms and 200 ms (left and right panel respectively) in *Ophn-1*$^{+/y}$ and *Ophn-1*$^{-/y}$ CA3 pyramidal neurons. Figure 4.15 Aii. & Bii represent the digital

subtraction of the first eIPSC by an averaged waveform of the first eIPSC; this allowed the accurate determination of the amplitude of the second eIPSC. The ratio of the eIPSC2 over eIPSC1 is the measure of either the inhibition (ratio<1) or the facilitation (ratio>1). This calculated ratio was plotted in the fig 4.15 C. *Ophn-1*$^{-/y}$ CA3 pyramidal neurons displayed a significant stronger depression than in *Ophn-1*$^{+/y}$ neurons for inter-pulse intervals of 25, 200 and 500 ms. (*25 ms*: 0.63 ±0.05, n=10; 0.95 ±0.12, n=8 respectively, p=0.016; *200 ms*: 0.58 ±0.06; 0.82 ±0.08, p=0.028; *500 ms*: 0.61 ±0.07; 0.96 ±0.12, p=0.017, fig. 4.15 C.).

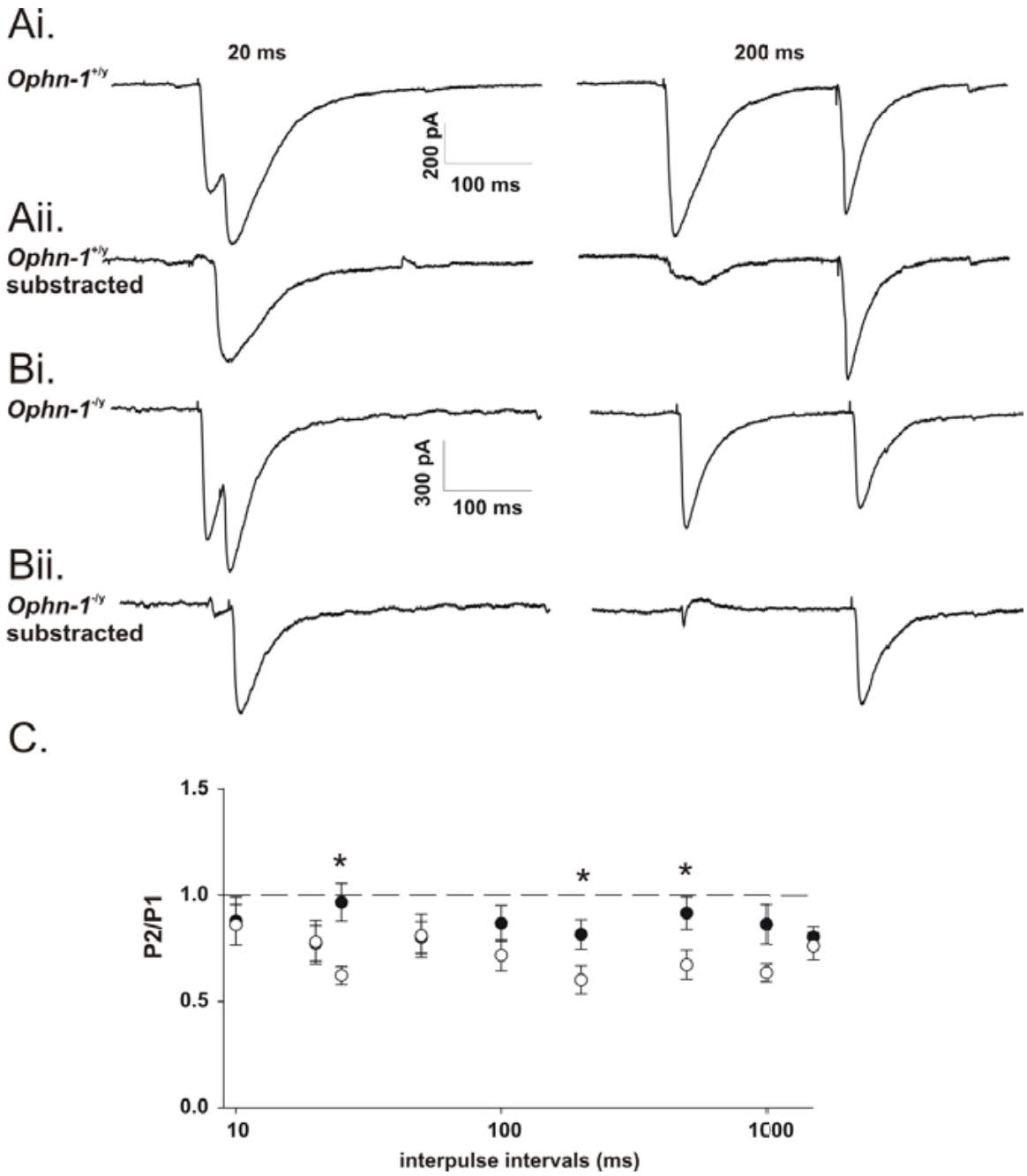

Figure 4.15: Paired-pulse depression of eIPSCs was altered in *Ophn-1*$^{-/y}$. (Ai.) Typical eIPSCs were evoked in *Ophn-1*$^{+/y}$ CA3 pyramidal neurons by paired-pulse stimulation for interpulse intervals of 20 ms (left panel) and 200 ms (right panel). **(Aii.)** Digital substraction of the first eIPSCs **(Bi.)** Typical double eIPSCs in *Ophn-1*$^{-/y}$ CA3 pyramidal neurons for IPI of 20 ms (left panel) and 200 ms (right panel). **(Bii.)** Digital substraction.**(C.)** Paired pulse ratio plotted against the log inter-pulse intervals (●) *Ophn-1*$^{+/y}$ (n=18) (○) *Ophn-1*$^{-/y}$ (n=12) (ANOVA: p=0.001 with Bonferroni correction)

Frequency dependent facilitation on eIPSCs.

The experiments of frequency dependent facilitation in response to ten stimuli were performed to further elucidate results obtained in previous paired pulse stimulation experiments. An additional rationale is that during gamma oscillations, interneurons sustain a high frequency of firing almost firing at every cycle (Bragin et al., 1995). High frequency of firing is required for cognitive functions in which gamma oscillations is involved.

This high frequency of interneuronal firing, at the origin of gamma oscillation was replicated by stimulating the inhibitory synapses at 33Hz, which is about the peak frequency of the gamma oscillations (see chapter 4). Frequency dependent facilitation protocol evaluated the presynaptic terminals to sustain repetitive stimulations and hence availability of synaptic vesicles (Powell et al, 2009, submitted)

Frequency dependent facilitation was observed in *Ophn-1*$^{+/y}$ and *Ophn-1*$^{-/y}$ CA3 pyramidal neurons for high frequency of stimulation at 100, 50 and 33 Hz (example for *Ophn-1*$^{+/y}$: ratio I_{max}/I_1: 2.24 ±0.42; 1.90 ±0.31 and 1.54 ±0.34 respectively). The high frequencies used were in physiological range of interneurons firing (Buzsaki, 2001). Neither facilitation nor depression was observed for 20 Hz (1.01 ±0.13) and a synaptic depression for 10 Hz (0.82 ±0.04) in *Ophn-1*$^{+/y}$ CA3 pyramidal neurons.

No significant difference have been observed for 10, 20, 50 and 100 Hz (50Hz, *Ophn-1*$^{-/y}$ 1.67 ±0.17; *Ophn-1*$^{+/y}$ 1.90 ±0.31, p=0.53 fig 5.16 Bi.). Interestingly,

facilitation did not occur at 33 Hz in *Ophn-1*$^{-/y}$ compared to *Ophn-1*$^{+/y}$ (ANOVA p=0.001).

The observation that only 33 Hz stimulation resulted in a significant difference between *Ophn-1*$^{+/y}$ and *Ophn-1*$^{-/y}$ is surprising as it would be expected that if Oligophrenin-1 modulates vesicle availability that 100 and 50 Hz stimulation would also be affected. The reason for this is unclear, but may reflect that the inhibitory neurons are specifically tuned to fire at 33 Hz through mutual inhibition (Jefferys et al., 1996)

This was an exciting result, as it has proved that interneurons lacking oligophrenin1 protein cannot sustain the facilitation triggered by a physiological frequency of firing (33Hz), which is necessary for normal gamma oscillations. Furthermore, a previous study by Vreugdenhil et al (2003) showed that the frequency dependent facilitation, in a mouse model in which gamma oscillations were enhanced in power, showed an enhanced facilitation at 33 Hz.

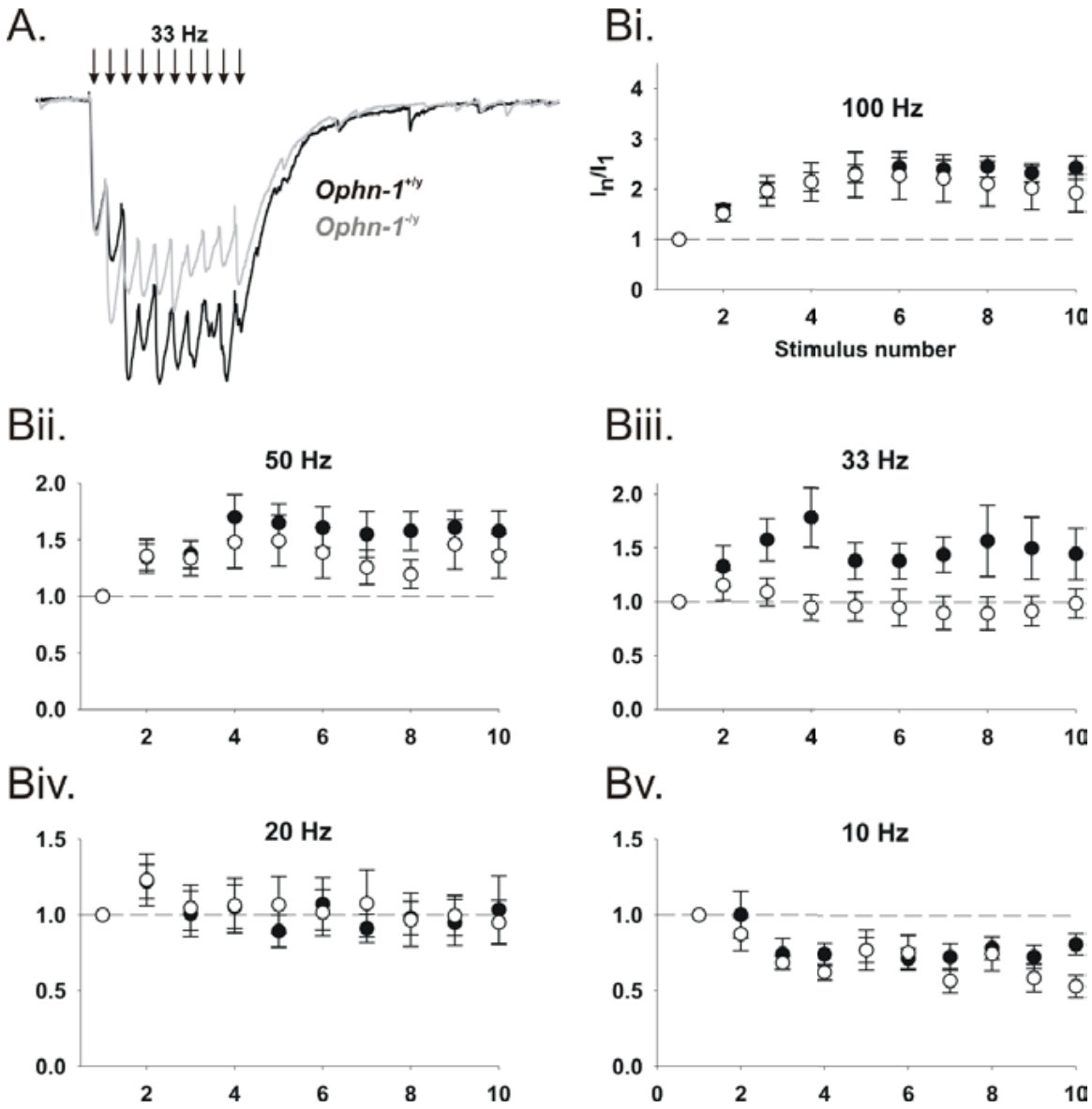

Figure 4.16: Responses to repetitive stimulation at 33Hz were reduced in *Ophn-1*$^{-/y}$ neurons. (A.) Typical eIPSCs built up in *Ophn-1*$^{+/y}$ (dark line) and in *Ophn-1*$^{-/y}$ (grey line). IPSC amplitude for every *n*th stimulus normalized to the first, for pulses trains delivered at 100Hz **(Bi.)**, 50 Hz **(Bii.)**, 33Hz **(Biii.)**, 20 Hz **(Biv.)** and 10 Hz **(Bv.)** in *Ophn-1*$^{+/y}$ (●, n = 17) and *Ophn-1*$^{-/y}$ neurons (○, n = 9).

Assessment of the readily releasable pool (RRP) size by high frequency stimulation protocol

Recent studies have suggested that vesicle endocytosis is deficient in synapses where oligophrenin-1 expression is reduced or absent (Nakano-Kobayashi et al., 2009, Khelfaoui et al., 2009). Importantly, the chemical synapses are defined morphologically by vesicle clusters in presynaptic terminalsStudies have shown that different pools of vesicles exist within the terminals, which exhibit distinct functions (Rizzoli and Betz, 2005). Among these different vesicles pool, the RRP is defined as a population vesicles filled with neurotransmitters which are directly available for release, hence their location near voltage gated calcium channels (Sudhof, 2004). This pool generally refers to the number of synaptic vesicles, which can be released in few seconds (2-3s) and which are docked in the active zone and are fusion competent through priming process. The size of the RRP is highly regulated via protein kinase C (PKC) (Stevens and Sullivan, 1998), as well as by the small GTPases protein Ral (Polzin et al., 2002). The protocol used in this study relied on high frequency of stimulation for a few seconds (2s) which decreased the amplitude of the evoked postsynaptic currents due to the depletion of the RRP. This sustained high frequency stimulation mobilize vesicles from the reserve pools and additionally the RRP is rapidly reformed by endocytosis of synaptic vesicles(Sudhof, 2004). An additional interest was that the size of the readily releasable vesicles pool is a good candidate to modulate the synaptic strength (Sudhof, 2004). As deficits in synaptic strength was already revealed by the loss of power in gamma oscillations in Ophn-1^{-}

$^{/y}$ slices (see Chapter 3). Additionally, the lack of facilitation at 33 Hz suggested altered synaptic vesicle availability.

Therefore, to further investigate this deficit in the presynaptic terminals of *Ophn-1*$^{-/y}$ CA3 pyramidal neurons, a protocol of high frequency (40 stimuli at 20Hz) of stimulation was applied to a minimum of synapses possible.(fig 4.17 A.& B.). This should deplete the RRP and consequently allow an estimation of the size of the RRP in *Ophn-1*$^{-/y}$ inhibitory synapses.

During this protocol, a decrease of IPSC amplitude was observed, which indicated a depletion of the RRP (fig 4.17 A. and B.). I then plotted the cumulative amplitude of each eIPSC, which rose during the first second and reached a plateau during the last second. I subsequently deduced the amplitude of RRP from a linear regression fit of the last 20 data points back to the y-axis. The RRP size in *Ophn-1*$^{-/y}$ neurons was significantly smaller than in *Ophn-1*$^{+/y}$ neurons (678.59 ±62.02 pA, n=4; 1466.24 ±307.74 pA, n=4, respectively, p=0.0459, statistical power= 0.56 fig 4.17 D.), resulting in fewer vesicles in the RRP in *Ophn-1*$^{-/y}$ (16 ±1 synaptic vesicles and 35 ±7 synaptic vesicles, respectively, p=0.0459, fig 4.17 E.). Despite a reduction in RRP amplitude, the amplitude of the first IPSC was not altered by the genotype (*Ophn-1*$^{-/y}$: 101.52 ± 31.80 pA, n=4; *Ophn-1*$^{+/y}$: 108.97 ±28.26 pA, n=4, fig 4.17 C.)

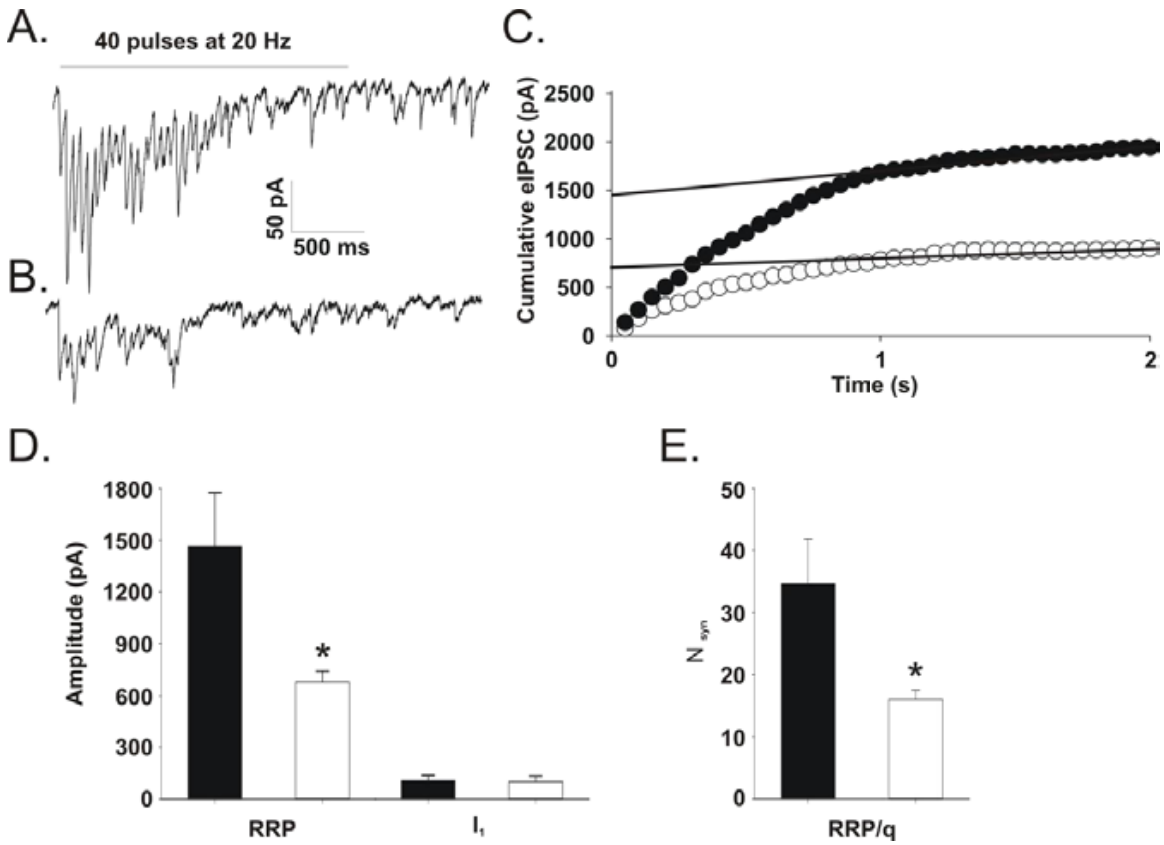

Figure 4.17: *Ophn-1*$^{-/y}$ CA3 interneurons displayed a smaller readily releasable pool size. Evoked IPSCs induced by a train of repetitive stimuli of 20Hz in an *Ophn-1*$^{+/y}$ **(A.)** and an *Ophn-1*$^{-/y}$ neuron **(B.). (C.)** Cumulative eIPSCs amplitude plot of individual *Ophn-1*$^{+/y}$ (●) and (○) *Ophn-1*$^{-/y}$ (○) neuron, the lines represent the linear regression fit of the data points between 1 and 2 s, back extrapolated to 0s in order to estimate the readily releasable pool size (RRPsyn). **(D.)** Histogram of the RRP size in *Ophn-1*$^{+/y}$ (n=4) and *Ophn-1*$^{-/y}$ (n=4) p=0.0459 and of the first eIPSC (I_1) (p>0.1) and the corresponding synaptic vesicles quantification (p=0.0459) **(E.)**

4.4 SUMMARY

Summary of deficits uncovered which explain the loss of gamma oscillations power in *Ophn-1*$^{-/y}$ slices:

i) Impairment of the excitatory and inhibitory inputs to CA3 pyramidal neurons; both of which are implicated in gamma oscillations.

ii) Reduction of the frequency of the sIPSC. A study has shown that an increase in mIPSC led to an increase in gamma oscillations power (Hajos et al., 2000)

iii) The loss of facilitation for the frequency dependent facilitation at 33 Hz for the inhibitory neurotransmission. A study has demonstrated that an increase in frequency dependent facilitation at 33Hz for the eIPSC led to an increase in power (Vreugdenhil et al., 2003)

iv) Reduction in RRP size in *Ophn-1*$^{-/y}$ inhibitory synapses in CA3 area

In conclusion, oligophrenin 1 deficient mice display reduced gamma oscillations which was explained by the inability of the inhibitory synapses to sustain neurotransmitter release required by high frequency of firing, through a reduction in readily releasable pool size in *Ophn-1*$^{-/y}$ inhibitory presynaptic terminals. I have established for the first time in *Ophn-1*$^{-/y}$ mice a clear presynaptic deficit.

Finally, these deficits observed may explain the reduction in cognitive function in affected individuals by the loss of oligophrenin1.

Chapter 5: ELECTROPHYSIOLOGICAL CHARACTERIZATION OF CA1 HIPPOCAMPAL AREA

5.1. AIM

The spine dysgenesis phenomenon has been widely observed in several X-linked mental retardations (XLMR) (Grossman et al., 2006, Kaufmann and Moser, 2000) . Purpura (1974) suggested that these morphological defects could explain the learning disabilities observed in affected individuals. It remains unclear, however, how the spine dysgenesis is related to cognitive disabilities. A previous study reduced oligophrenin1 expression using small interference RNA, and demonstrated a dysmorphy of the dendritic spines in CA1 pyramidal neurons (Govek et al., 2004) . The role of oligophrenin-1 in the maintenance of spine morphology was later confirmed in dissociated cultures of CA1 pyramidal neurons from *Ophn-1*$^{-/y}$ mice. The same study also observed a synaptic malfunction in *Ophn-1*$^{-/y}$ mice, namely a reduction in paired-pulse facilitation in CA1 area associated with some behavioural deficits (Khelfaoui et al., 2007).

In the study presented below, I propose to explore more fully the malfunction of CA1 synapses, using field potential recordings of CA1 neurons at the apical dendritic sides and the somatic area. This was enabled by the exceptional laminar arrangement of CA1 pyramidal neurons, where dendritic trees are paralleling each other. Finally I analysed excitatory and inhibitory neurotransmission, using whole cell

recording of CA1 pyramidal neurons. In these experiments, synapses were tested for spontaneous synaptic activity and as well as repetitive stimulations.

5.2 Single stimulation field potential in the CA1b area

5.2.1 Biology of evoked postsynaptic potentials in CA1 area.

Postsynaptic potentials (PSP) and population spikes (PS) were triggered by single stimulation of the Schaffer collaterals pathway. Increase of the stimulus intensity induced an increase of the slope of PSP and PS amplitude in *Ophn-1*$^{+/y}$ slices (fig.5.1).

PSP and PS were blocked by application of NBQX (20 μM) and D-APV (25 μM) (10 min. application). NBQX and D-APV are glutamatergic receptors antagonists, blocking respectively AMPA/KA receptors and NMDA receptors (fig. 5.2).

Experiments shown in figure 5.2 confirmed the glutamatergic excitatory nature of the synaptic neurotransmission at the synapse between CA3 pyramidal neurons and CA1 pyramidal neurons. (Shepherd, 2003).

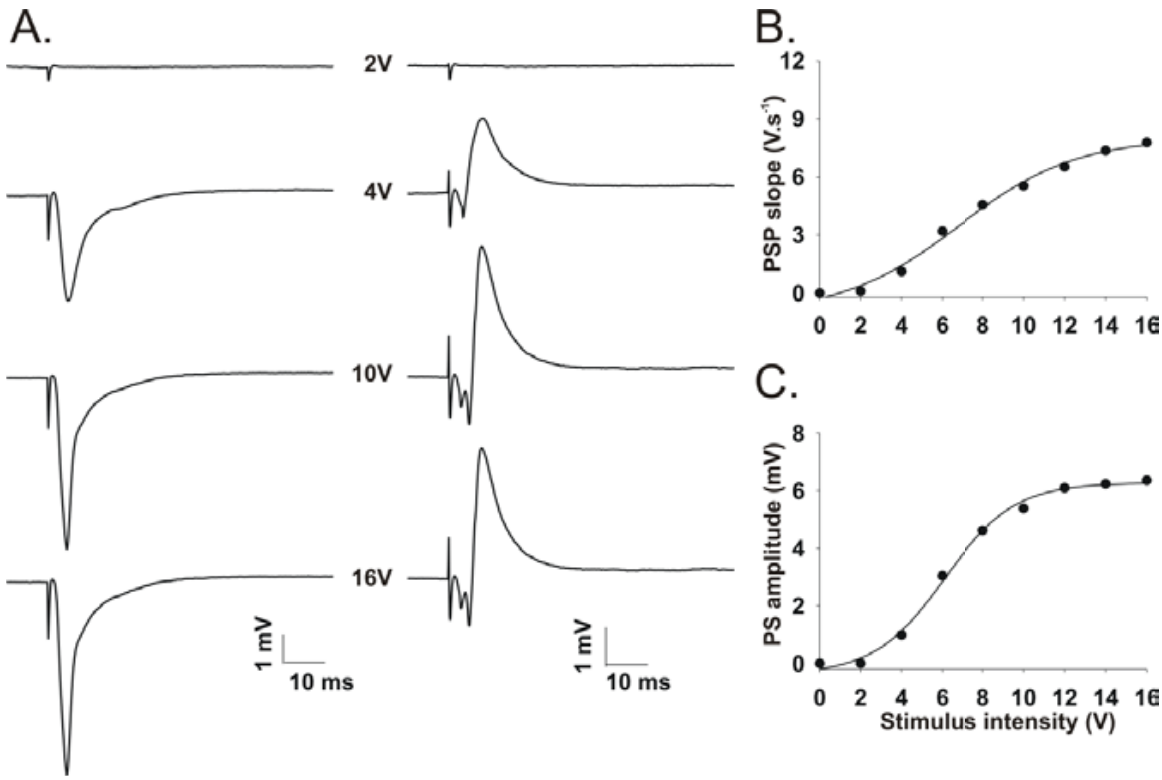

Figure 5.1: PSP and PS recorded in CA1 area *of an Ophn-1$^{+/y}$ slice.* Representative PSP and PS recorded from *s.* radiatum and *s.* pyramidale (left and right panels respectively), and evoked by various stimulus intensity (2,4,10 and 16V) **(Ai.).** The slope of the PSP and the amplitude of PS were plotted against the stimulus intensity (**B.** and **C.** respectively).

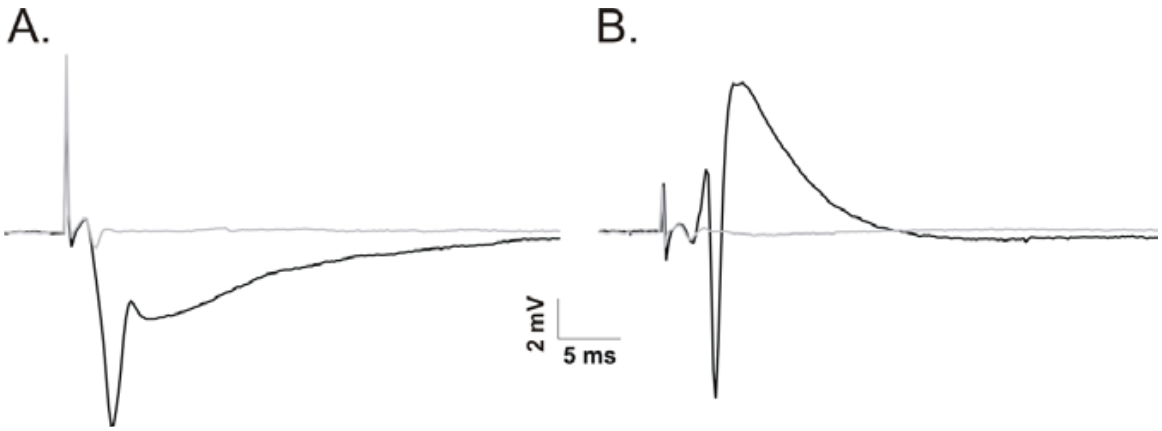

Figure 5.2: Sensitivity of the synaptic responses to NBQX and D-APV. (A.) Gray line represents the abolition of the PSP (black line). **(B.)** Grey line represents the blockade of the population spike (dark line).

5.2.2 Single evoked response in CA1 area.

The aim of this study was to investigate the synaptic transmission between CA3 and CA1 pyramidal neurons, as this has previously been suggested to be altered in *Ophn-1*$^{-/y}$ neurons(Khelfaoui et al., 2007). These neurons are connected through the Schaffer collaterals constitutive of the hippocampal trisynaptic networks (Fig.1.4 B.). The PSP were evoked by electrical stimulation of the Schaffer collaterals in which each axon connects with thousands of CA1 pyramidal cells (Ishizuka et al., 1990). This electrical stimulation induced a fast glutamatergic excitatory postsynaptic potential (EPSP) in CA1 pyramidal neurons (fig. 5.2 A.). The ability of the pyramidal neurons to elicit action potentials upon stimulation of afferent pathway was also assessed by measuring the amplitude of the population spike (PS). Electrical stimulation triggered synaptic transmission which caused cellular firing (fig. 5.3 Bi. & Bii.).

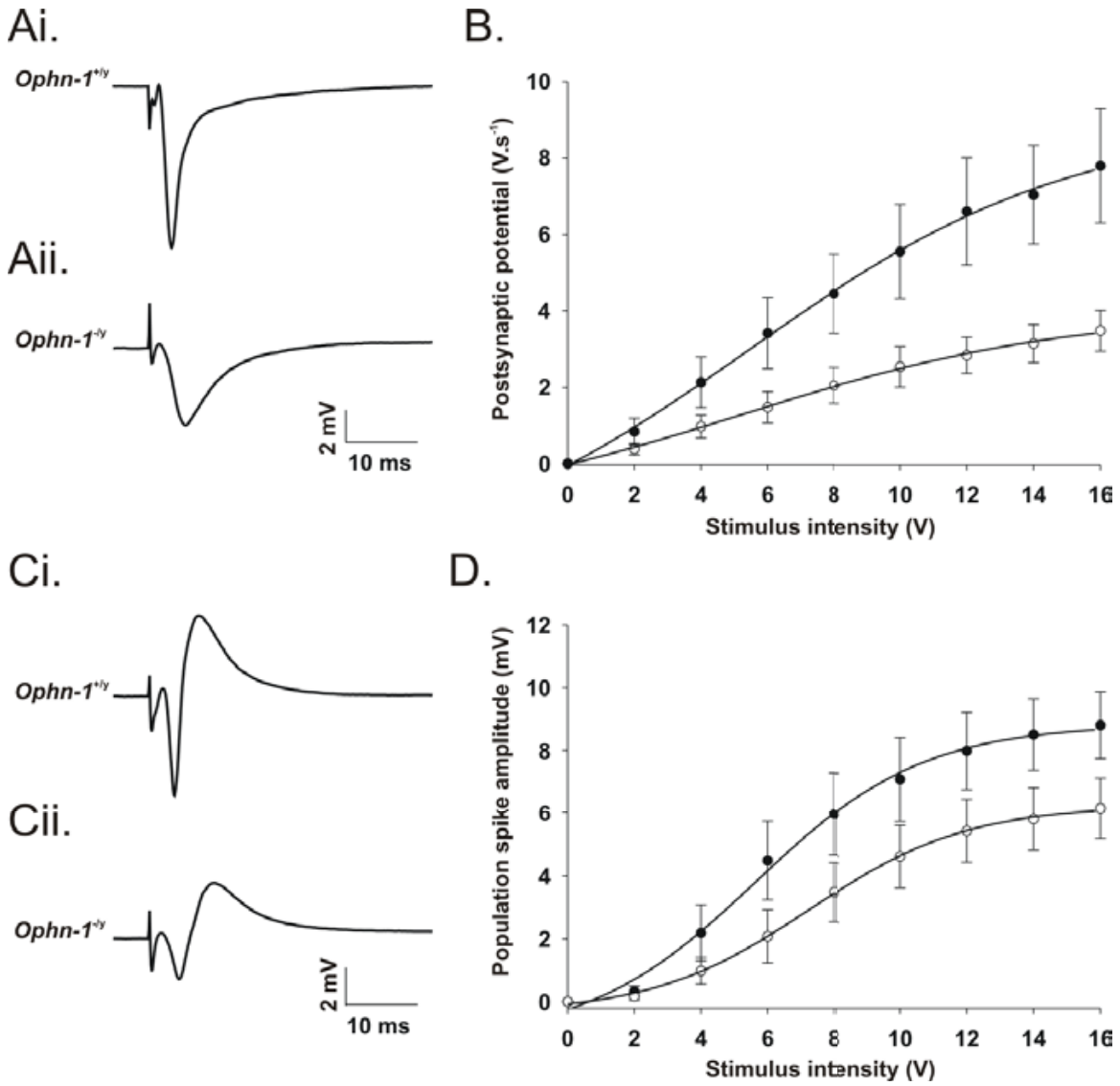

Figure 5.3: Synaptic transmission was reduced in *Ophn-1*$^{-/y}$ CA1 neurons. Representative field potentials recorded from the *s.* radiatum in *Ophn-1*$^{+/y}$ **(Ai)** and *Ophn-1*$^{-/y}$ slices **(Aii.)**. **(B.)**. The slopes of the PSP were plotted against the voltage intensity. (*Ophn-1*$^{+/y}$ (filled symbols) (n=11); *Ophn-1*$^{-/y}$ (open symbols) (n=10)) p=0.018 (maximum slope). Representative population spike recorded from *s.* pyramidale in *Ophn-1*$^{+/y}$ **(Ci.)** and *Ophn-1*$^{-/y}$ slices **(Cii.)**. **(D.)** Mean population spike amplitudes plotted vs. the stimulus intensity (*Ophn-1*$^{+/y}$ (filled symbols) (n=12); *Ophn-1*$^{-/y}$ (open symbols) (n=10)) p=0.104 (maximum amplitude). Data are mean ± SEM

The figure 5.3 Ai and Aii illustrate respectively representative PSP from *Ophn-1*$^{+/y}$ and *Ophn-1*$^{-/y}$ slices respectively. From these traces, a less steep slope can be observed in *Ophn-1*$^{-/y}$ (fig 5.3Ai.) compared to *Ophn-1*$^{+/y}$ slices (fig 5.3 Aii.). The input-output (strength of electrical stimulation / slope of PSP) relationship revealed a maximum slope of PSP in *Ophn-1*$^{-/y}$ which was significantly lower than in *Ophn-1*$^{+/y}$ slices (3.86 ±6.85 V.s^{-1}, n=10; 8.68 ±1.66 V.s^{-1}, n=11, respectively, p=0.018 (Mann-Whitney test), fig 5.3 B.)

Nonetheless, the PS maximum amplitude in *Ophn-1*$^{-/y}$ failed to be different compared PS maximum amplitude in *Ophn-1*$^{+/y}$ slices (6.43 ±0.87 mV, n=10; 8.85 ±1.07 mV, n=12, respectively, p=0.104 (t-test), power of statistics= 0.245, fig 5.3 D.). This lower maximal plateau amplitude suggested a reduced synaptic transmission in *Ophn-1*$^{-/y}$ slices.

The reduction of summated PSPs from several neurons in the vicinity of the recording microelectrode could arise from *i)* fewer connections to CA1 pyramidal neurons or *ii)* a reduced probability of release at each synapses. As the number of excitatory synaptic connection has been shown to be unaltered in *Ophn-1*$^{-/y}$ mice (Khelfaoui et al., 2007) , I analysed the latter hypothesis by investigating paired pulse stimulation paradigm.

5.3 Synaptic responses to paired-pulse stimulation were unaltered in *Ophn-1*$^{-/y}$ slices.

Paired-pulse stimulation protocol was performed to assess the functionality of the presynaptic compartment. Furthermore, *Ophn-1*$^{-/y}$ mouse is a mouse model of mental retardation, which shows learning processes deficits in behavioural tests (Khelfaoui et al., 2007). Learning is made possible only by formation of memories, which can be divided in several forms: one of them is the short term memory, in which the timeframe of action is short. Unlike long term memory, short term memory does not involve process depending on genes transcription or morphological changes of the synapse. It relies mainly on the accumulation of neurotransmitters in the synaptic cleft and enhancement of the neurotransmitters release due to the rising of the residual Ca^{2+} concentration in the presynaptic terminals (Katz and Miledi, 1968). Entry of Ca^{2+} is via the opening of voltage gated calcium channels (VGCC) by the action potentials. Paired pulse stimulation assesses how the first stimulus (termed conditioning stimulus) response affects the second stimulus response (termed test stimulus). Paired-pulse stimulation can be divided into paired-pulse facilitation and paired-pulse inhibition. Paired-pulse facilitation paradigm assessed the Ca^{2+} dynamics in the presynaptic terminals and the neurotransmitter release machinery. Whereas, paired-pulse inhibition observed for short intervals (e.g. 10 ms) implies the recruitment of feedforward inhibition system exerted by interneurons present in CA1 (10 ms is the timeframe of action of the fast inhibitory

$GABA_A$ergic neurotransmission). Hence, paired-pulse inhibition was used as a preliminary experiment to assess the inhibitory tone imposed by the GABAergic neurotransmission in CA1 area of *Ophn-1*$^{-/y}$ slices.

Finally a second rationale for this study was to replicate results already obtained in *Ophn-1*$^{-/y}$ mouse model in paired pulse stimulation with a similar protocol and approaching experimental conditions (Khelfaoui et al., 2007).

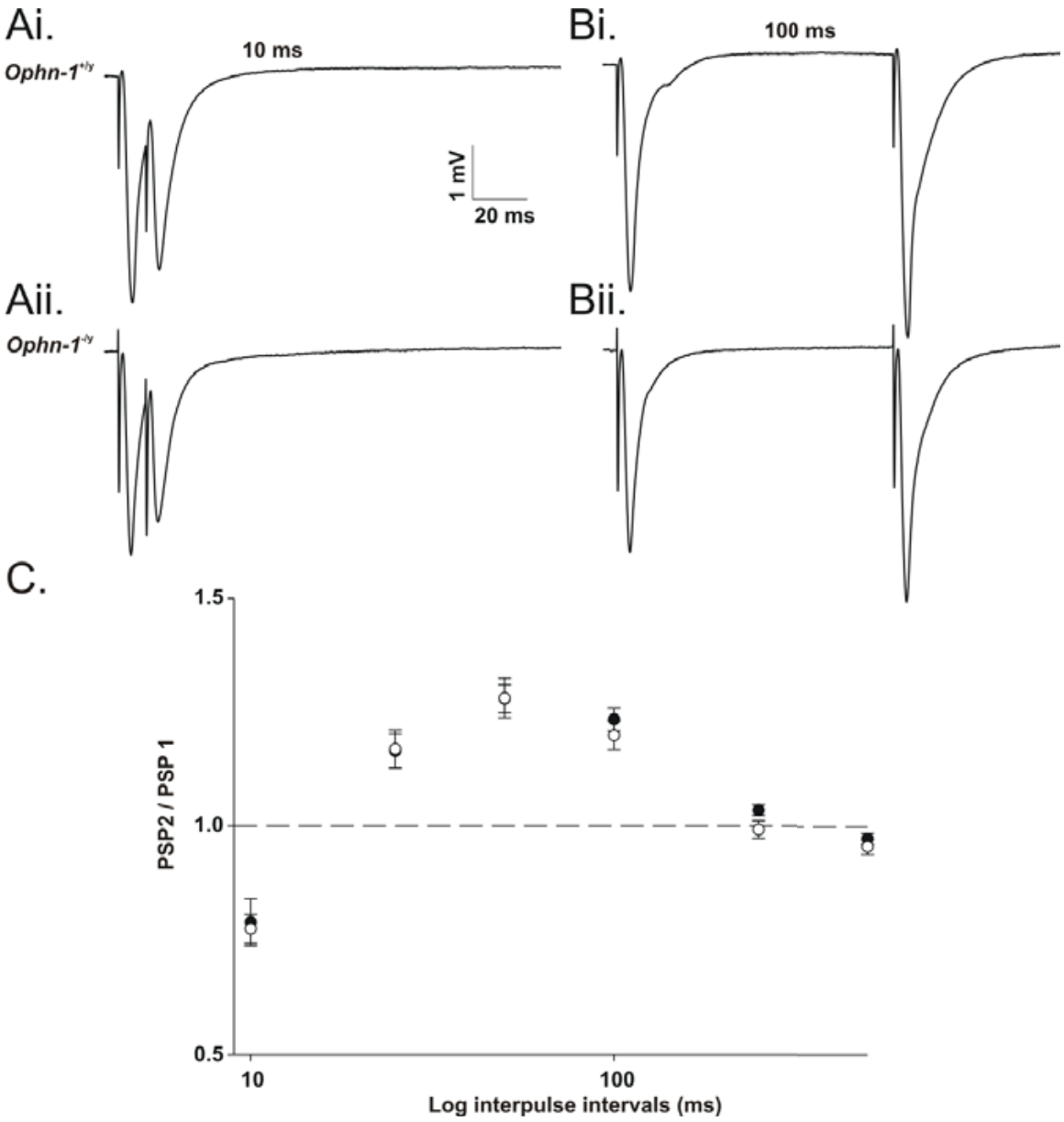

Figure 5.4: *Ophn-1*$^{-/y}$ mice displayed no difference in paired-pulse stimulation. Representative double responses obtained for an inter-pulse of 10 ms in *Ophn-1*$^{+/y}$ **(Ai.)** and *Ophn-1*$^{-/y}$ **(Aii.)**, the second response shows an inhibition, and for an inter-pulse of 100 ms in *Ophn-1*$^{+/y}$ (**Bi)** and *Ophn-1*$^{-/y}$ slices **(Bii.)** in which the second response shows a facilitation. **(C.)** Paired-pulse inhibition/facilitation. The mean of the slopes of PSP 2 over the mean of the slopes of PSP1 plotted against the log inter-pulse intervals for *Ophn-1*$^{+/y}$ (filled symbols) (n=22) and *Ophn-1*$^{-/y}$ (open symbols) (n=30) (ANOVA p>0.05).

Prior to the paired-pulse protocol, a stimulus response curve was performed to define the voltage which gives the half maximum response (V_{50}). These experiments show that the voltage necessary for an half maximal response was not different in *Ophn-1*$^{-/y}$ and *Ophn-1*$^{+/y}$ slices (7.25 ±0.92 V, n=10; 7.18 ±0.61 V, n=11, respectively, p=0.95) Then, two equal stimuli of the Schaffer collaterals, were given at various inter-pulse intervals of 10, 20, 25, 50, 100, 250 and 500 ms. (See fig.5.4 C.).

As shown in figure 5.4 C., an inhibition can be observed for an inter-pulse interval of 10 ms in *Ophn-1*$^{-/y}$ and *Ophn-1*$^{+/y}$ slices (0.77 ±0.03 and 0.79 ±0.05, respectively, p=0.81, fig. 5.4C.) due to the recurrent inhibitory loop. Facilitation was observed for inter-pulse intervals from 25 ms to 100 ms, no difference was observed in *Ophn-1*$^{-/y}$ compared to *Ophn-1*$^{+/y}$ slices (e.g. 100 ms , 1.20 ±0.03, n=30; 1.23 ±0.02, n=22, respectively, p= 0.41, fig 5.4C.). These data suggest that overall inhibition/facilitation was similar for PSP between both genotypes, which was in contrast from a previous report (Khelfaoui et al., 2007).

Figure 5.5 Ai. and Bii. represent typical PS on the CA1 somatic area in *Ophn-1*$^{+/y}$ and *Ophn-1*$^{-/y}$ slices. Double population spikes were clearly seen as an inward deflections superimposed to the PSP for inter-pulse intervals of 10 ms and 100 ms (Ai. & Aii and Bi.&Bii. respectively). For an inter-pulse interval of 10 ms a clear inhibition of the second response was observed, as opposed to 100 ms inter-pulse interval where facilitation occurred. The inhibition implied that fewer neurons are firing at the time of the second stimulation. For the inter-pulse interval of 10 ms, the inhibition in *Ophn-1*$^{-/y}$ was as strong as in *Ophn-1*$^{+/y}$ (0.30 ± 0.05, n=21; 0.61 ± 0.20, n=18 ; respectively p=0.22 fig 5.5 C.) and similarly the facilitation at inter-pulse

interval 100 ms observed was not significantly different (1.57 ± 0.13, n=21; 1.58 ± 0.16,n=18, respectively, p=0.92 , fig 5.5C.). Synaptic inhibition and facilitation were identical in both genotypes (fig. 5.5 C.).

Identical experiments has been conducted in CA1 (Khelfaoui et al., 2007), however with different results. The discrepancy between the results presented and the results of Khelfaoui et al (2007) may be due to different methods used, notably different tissue preparation. In effect, it is noteworthy that tissue preparation by Khelfaoui and colleagues, CA3 area was excised unlike in the protocol used in this study. Furthermore, the discrepancy may be explained by different intensities of the stimulus used. In the experiments presented above, an 50% maximum amplitude was used; they used a stimulus intensity evoked at least 5 mV response, they may have therefore used stronger stimulation, therefore driving the synapses more intensely, with the consequence that the *Ophn-1*$^{-/y}$ synapses are unable to cope with (see chapter 4).

As paired pulse stimulation cannot explain the observed deficits in neurotransmission, I investigated synaptic transmission input onto individual CA1 pyramidal neurons using whole cell voltage clamp techniques, which allowed excitatory and inhibitory neurotransmission to be studied in isolation.

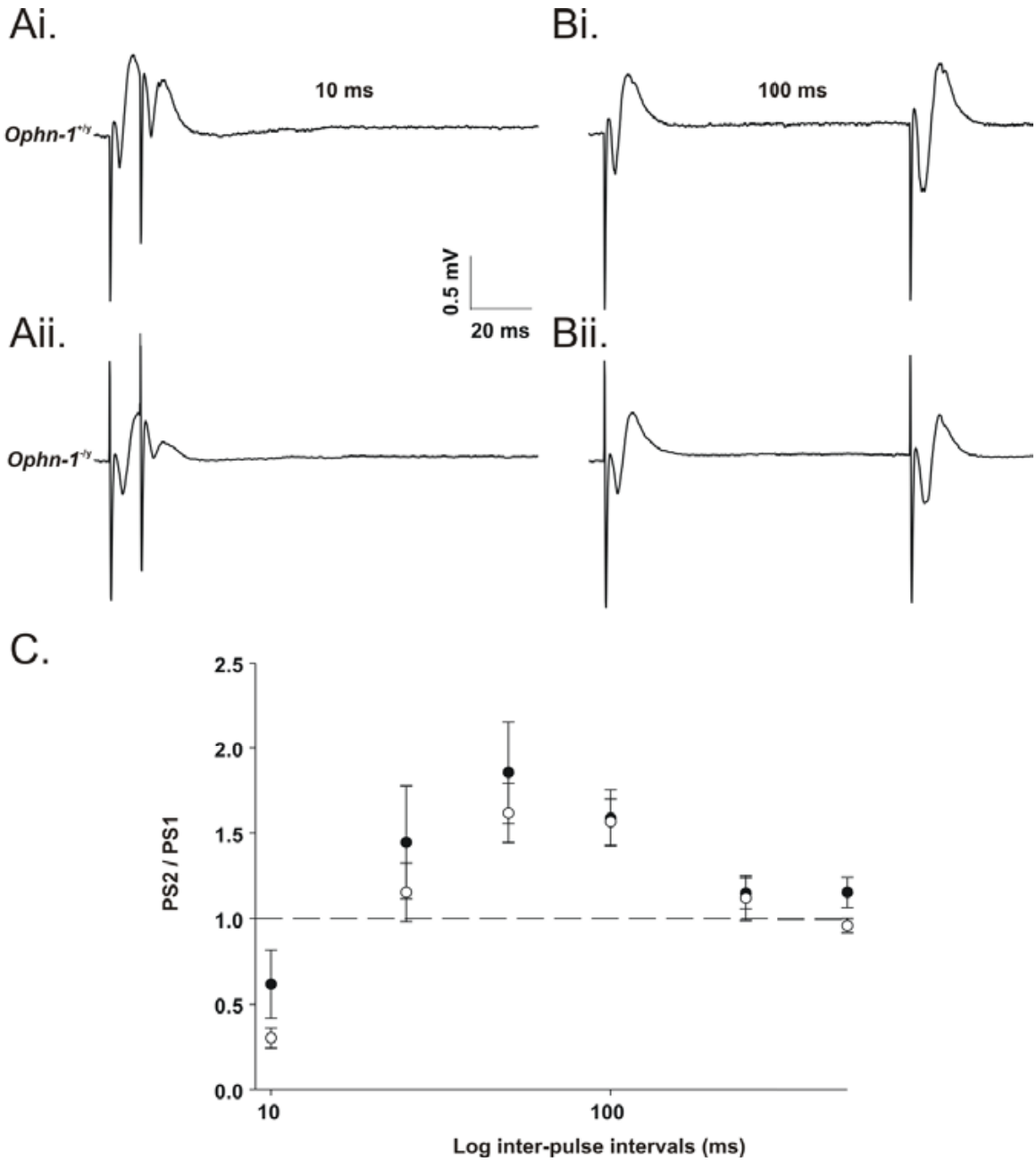

Figure 5.5: *Ophn-1*$^{-/y}$ slices displayed no difference in paired-pulse stimulation on PS. Typical responses obtained for an inter-pulse interval of 10 ms in *Ophn-1*$^{+/y}$ (**Ai.**) and *Ophn-1*$^{-/y}$ **(Aii.)** and for an inter-pulse interval of 100 ms in *Ophn-1*$^{+/y}$ (**Bii)** and *Ophn-1*$^{-/y}$ **(Bii.)**. **(C.) Paired-pulse ratio.** The mean of the population spike amplitude (PS) 2 over the mean of the population spike amplitude 1 plotted against the log inter-pulse intervals for *Ophn-1*$^{+/y}$ (filled symbols) (n= 18) and *Ophn-1*$^{-/y}$ (open symbols) (n=21)

5.4 Currents characterization of CA1 pyramidal neurons

5.4.1 CA1 Intrinsic neuronal properties

Some neurological disorders, such as epilepsy or chronic pain, exhibit changes in intrinsic neuronal properties (Beck and Yaari, 2008). The first part of this study concentrated on the investigation of the intrinsic neuronal properties of CA1 pyramidal neurons, in order to rule out any changes in the oligophrenin1 deficiency model. They included the membrane resistance evaluation, as an indication of the number of channels open on the neuronal surface. Furthermore, the properties of the action potentials were assessed, such as amplitude, threshold and half width duration (fig. 5.6 Cii.) and the input-output relationship of CA1 pyramidal neurons was also investigated (fig 5.6 Bi. & Bii.). In these experiments, the action potentials were evoked by injecting a depolarising step of currents into the cell body through the patch pipette.

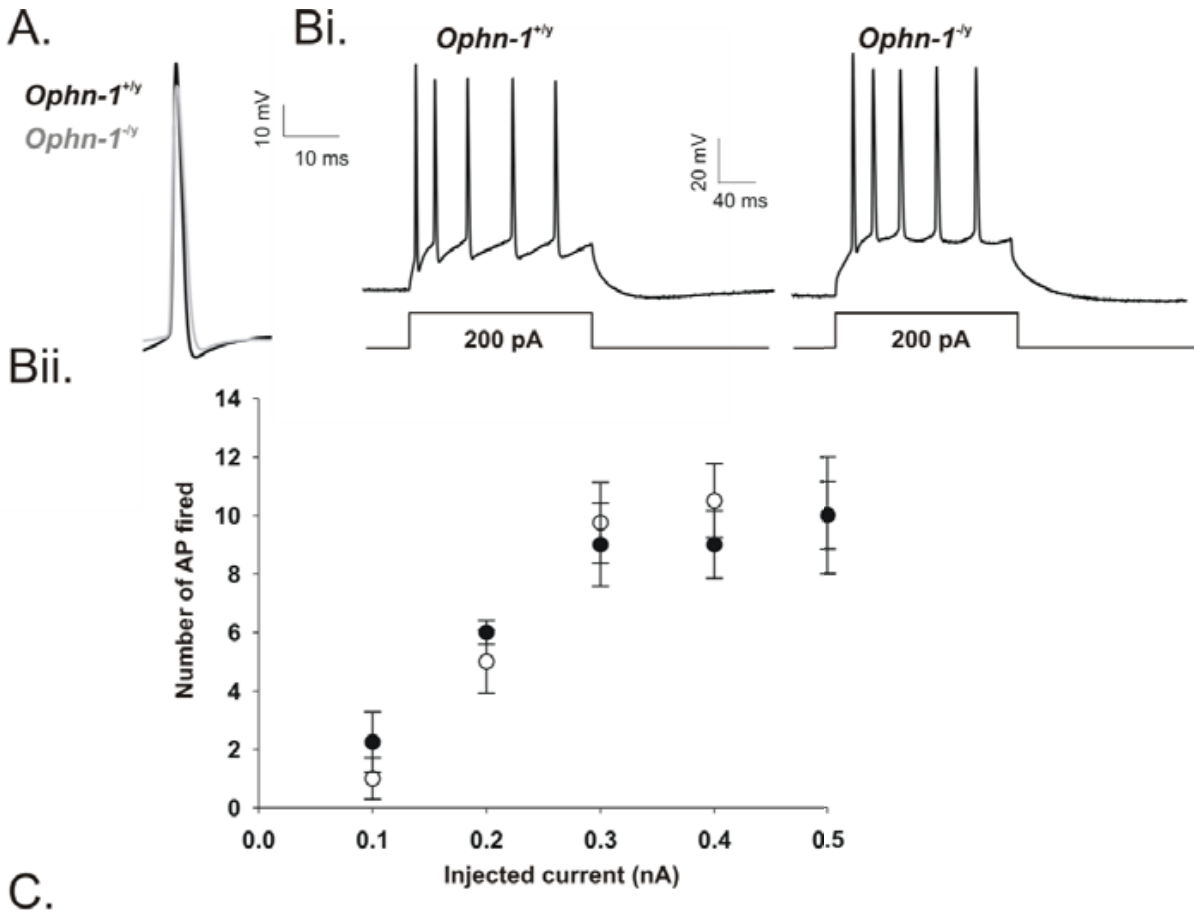

C.

Genotype	*Ophn-1* $^{+/y}$	*Ophn-1* $^{-/y}$	p
Action potential amplitude (mV)	81.9 ±3.88 *(4)*	76.97 ±3.30 *(4)*	0.37
Action potential threshold (mV)	-42.11 ±1.82 *(9)*	-45.61 ±2.60 *(4)*	0.42
Half width measurement	1.22 ±0.1 *(4)*	1.11 ±0.02 *(4)*	0.34
Membrane resistance	179.17 ±54.75 *(4)*	137.25 ±29.28 *(4)*	0.53

Figure 5.6: Intrinsic neuronal properties were unaltered in *Ophn-1*$^{-/y}$ CA1 pyramidal neurons. (A.) overlay of an *Ophn-1*$^{+/y}$ (dark line) and *Ophn-1*$^{-/y}$ (grey line) action potentials. Typical action potentials firing recorded in response to 200 pA depolarising current step (200 ms) in *Ophn-1*$^{+/y}$ (left panel) and *Ophn-1*$^{-/y}$(right panel)**(Bi). (Bii)** Number of action potentials fired (output) plotted against the amount of the depolarising current injected (input) for *Ophn-1*$^{+/y}$ (filled symbols) (n=4) and *Ophn-1*$^{-/y}$ (open symbols) (n=4).(**C.)** Values which characterized the intrinsic CA1 pyramidal neurons properties Note the number in parentheses means the number of cells analysed. Values are mean ±S.E.M.

The whole cell patch clamp technique was used to more fully understand neurotransmission at the single cell level. Initially, the intrinsic properties of CA1 neurons were tested. The ability of neurons to fire action potentials in response of a variable amount of current injected was determined and displayed no difference between *Ophn-1*$^{+/y}$ and *Ophn-1*$^{-/y}$ CA1 pyramidal neurons (e.g.: for 0.3 nA injection: 10 ± 1 action potentials, n=4; 9 ± 1 action potentials, n=4, respectively, p=0.71). Increasing the amount of current injected increased the number of action potentials fired regardless of the genotype.

Figure 5.6 C. shows similar properties of action potential features, e.g. same action potentials amplitude, threshold, half width duration. In addition, no difference was observed for the membrane resistance in *Ophn-1*$^{-/y}$ CA1 pyramidal neurons. To further characterize the activity of the membrane channels in *Ophn-1*$^{-/y}$ CA1 pyramidal neurons, the strength of the afterhyperpolarisation and the amplitude of the currents underlying them were assessed.

Afterhyperpolarisation study

The afterhyperpolarisation can be divided into three components: *i)* the fast (fAHP), *ii)* the medium (mAHP) and *iii)* the slow AHP (sAHP). These AHPs are underlined by currents, from different populations of K^+ channels activated by Ca^{2+}, termed I_C, I_{AHP} and I_{sAHP} respectively (Sah and Faber, 2002). The slow and medium afterhyperpolarisations were assessed electrophysiologically in current clamp and voltage clamp modes experiments.

The sAHP has been implicated in KA-induced gamma oscillations. It is assumed that activation of KA receptors decrease the sAHP, thus increasing neuronal excitability which in turn result in oscillogenesis (Fisahn et al., 2005, Melyan et al., 2002). It was therefore important to verify that the K^+ currents underlying it were fully functional in *Ophn-1*$^{-/y}$ CA1 pyramidal neurons.

***i)* Slow afterhyperpolarisation (sAHP) evaluation**

Figure 5.7 Ai. illustrates mAHP and s AHP evoked by 50 repetitive action potentials in current clamp mode. The arrow indicates the time of sAHP measurement, which was defined as 1s after the peak formation upon termination of the action potentials. It is important to note that the slow AHP is slow to activate (~ 500-600ms) and slow to deactivate (2-3 s). The same is true for mAHP, which are faster to activate (~60 ms) and faster to deactivate (300 ms)

Threefold deactivation time of mAHP was chosen to allow accurate sAHP measurement. The comparison of *Ophn-1*$^{-/y}$ neurons presented similar amplitude sAHP compared to *Ophn-1*$^{+/y}$ neurons, for every frequency tested (e.g. @ 20 Hz: -2.83 ±0.27 mV, n=11; -3.31 ±1.14 mV, n=4 respectively, p=0.53, fig 5.7Aii.).

Figure 5.7 Bi. represents a 300 ms depolarising step of 70 mV in voltage clamp mode, from -65 mV to + 5mV was used to elicit I_{AHP} and I_{sAHP} currents (Powell et al., 2008). As shown in figure 5.7 Bii. the I_{sAHP} was not different in *Ophn-1*$^{-/y}$ compared to *Ophn-1*$^{+/y}$ (21.57 ±4.16 pA, n=6; 31.73 ±7.17 pA, n=5 respectively, p=0.23, fig. 5.7 Bii.).

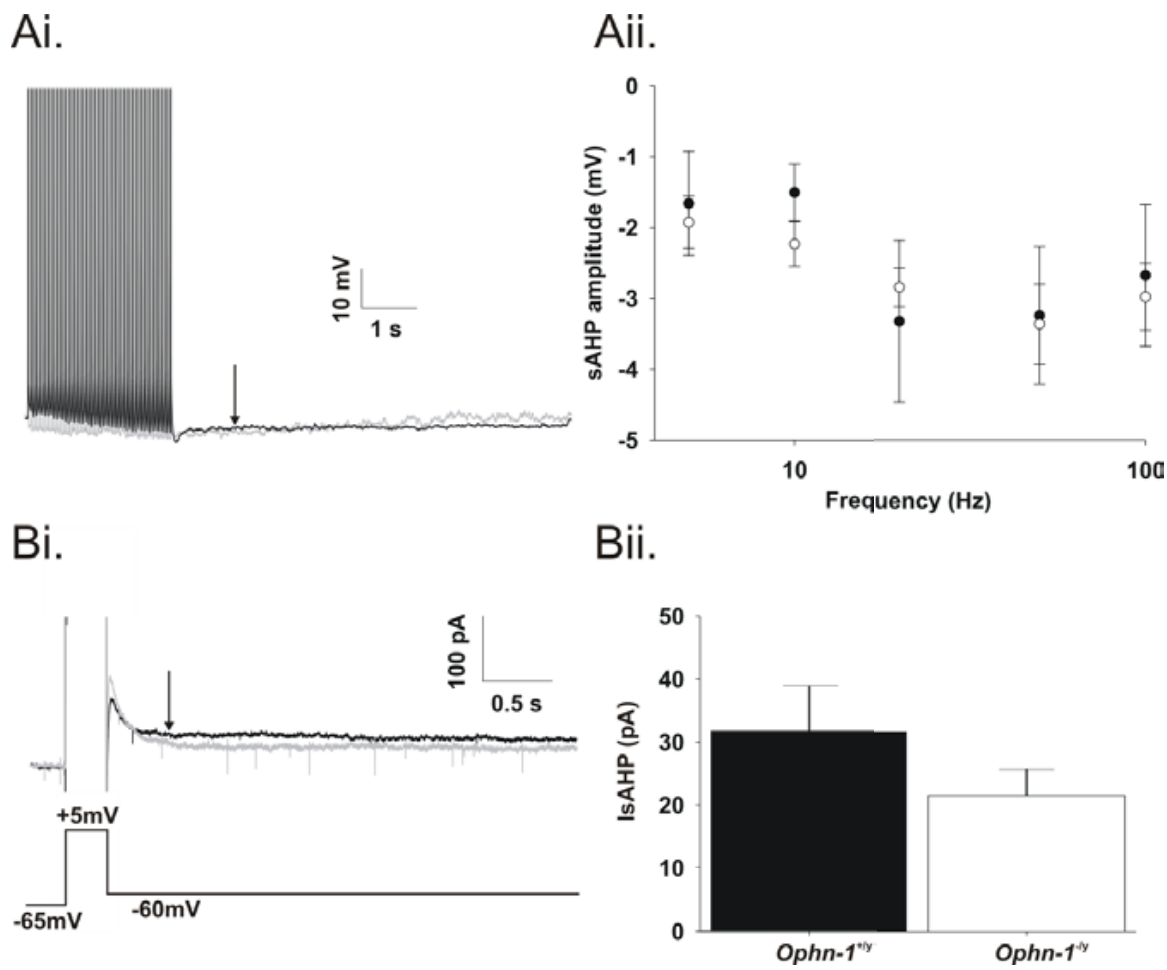

Figure 5.7: *Ophn-1*$^{-/y}$ CA1 Pyramidal neurons displayed no difference in sAHP. Representative recordings of a train of 50 action potentials at 20 Hz for *Ophn-1*$^{+/y}$ (dark line) and *Ophn-1*$^{-/y}$ (grey line) **(Ai.)**. **(Aii)** Plot of sAHP amplitude vs. train of action potentials frequencies, the sAHP amplitude was unaltered in *Ophn-1*$^{-/y}$ pyramidal neurons for every frequency tested. *Ophn-1*$^{+/y}$ (n=4); *Ophn-1*$^{-/y}$ (n=4) **(Bi.)** Voltage step of 300 ms from -65 mV to +5 mV evoked I_{sAHP}. **(Bii.)** Histogram of the amplitude of I_{sAHP} in *Ophn-1*$^{+/y}$ (n=5) and in *Ophn-1*$^{-/y}$ (n=6) (p=0.23). The power of the performed test was 0.105 < 0.8 .

Experiments suggested that the amplitude of the sAHP and the amplitude of the current I_{sAHP} were unaltered in *Ophn-1*$^{-/y}$ CA1 pyramidal neurons, although more experiments would be needed to reinforce the statistical power.

***ii)* Medium afterhyperpolarisation (mAHP) evaluation**

mAHP exhibits a faster timecourse of action and presents its maximal amplitude after the cessation of the burst of action potentials (in current clamp) or after the depolarization step (in voltage clamp). The function of mAHP is to control the repetitive firing properties of neurons. Figure 5.8 Ai illustrates a train of 50 action potentials at a frequency of 20 Hz immediately followed by a hyperpolarisation of the membrane potential induced by a K^+ ions outflow through specific channels. The amplitude of the mAHP recorded in *Ophn-1*$^{-/y}$ pyramidal neurons was unaffected as in *Ophn-1*$^{+/y}$ for every frequency tested (e.g. @ 20 Hz: -4.69 ±0.63 mV, n=10; -5 ±1.66 mV, n=4, respectively, p=0.83, fig.5.8 Aii.). Figure 5.8 Bi. shows a typical depolarization of +70 mV in voltage clamp mode which evoked I_{AHP}. The average of I_{AHP} *Ophn-1*$^{-/y}$ presented a similar amplitude as in *Ophn-1*$^{+/y}$ CA1 pyramidal neurons (117.79 ± 26.18 pA, n=6; 69.07 ± 9.33 pA, n=5 respectively; p=0.14, power of the performed test was 0.197)

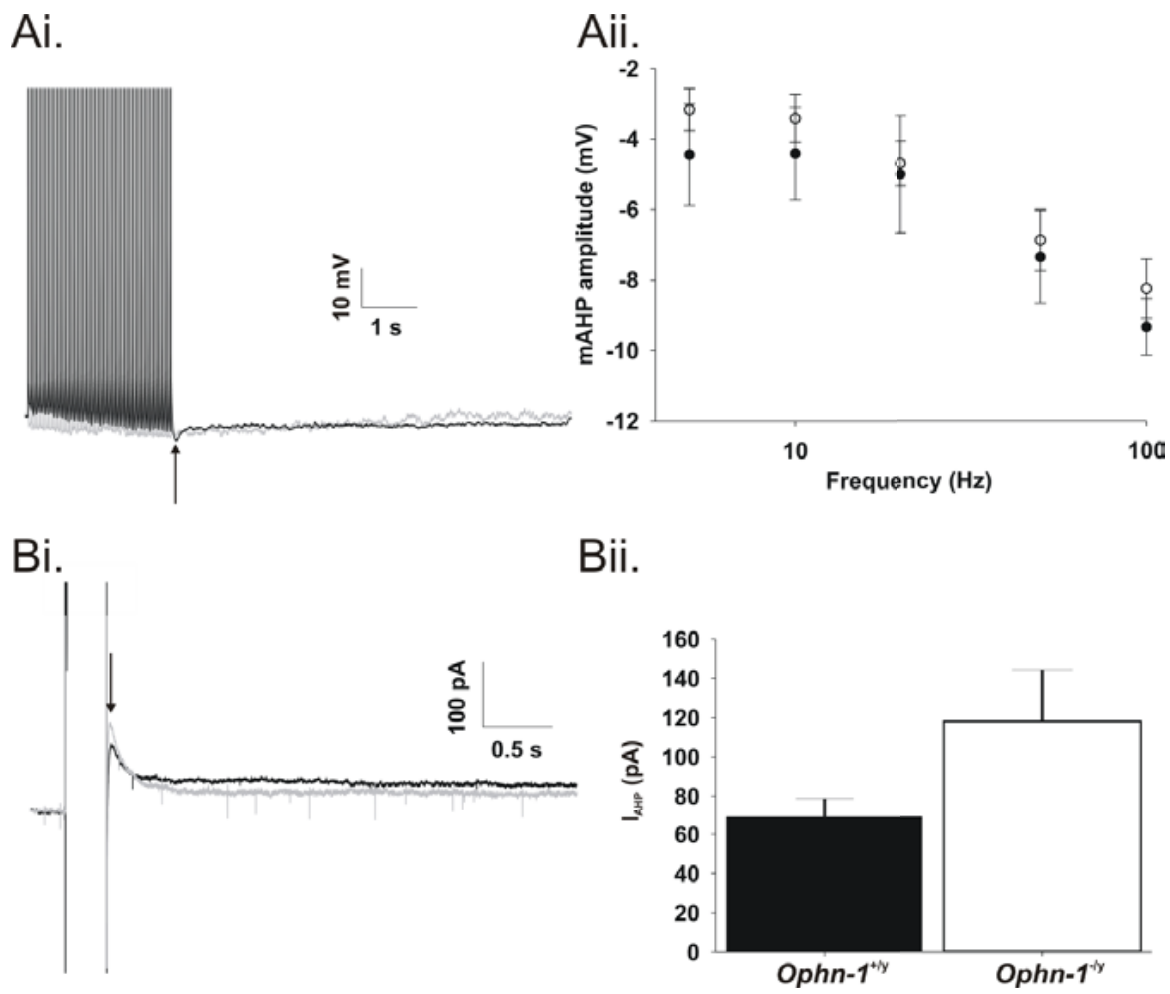

Figure 5.8: mAHP was unchanged in *Ophn-1*$^{-/y}$ CA1 pyramidal neurons. Train of 50 action potentials at 20 Hz for *Ophn-1*$^{+/y}$ (dark line) and *Ophn-1*$^{-/y}$ (grey line) **(Ai.)**. Mean amplitude of mAHP plotted against train of action potentials frequencies. (●) *Ophn-1*$^{+/y}$ (n=4); (○) *Ophn-1*$^{-/y}$ (n=4) **(Aii)**. **(Bi.)** Voltage step of 70 mV evoked I_{AHP} measured directly after the end of the depolarization (arrow). **(Bii.)** Histogram of the amplitude of I_{AHP} in *Ophn-1*$^{+/y}$ (n=5) and in *Ophn-1*$^{-/y}$ (n=6) (p=0.14).

.

The mAHP is a fast process and exhibit its maximum amplitude immediately after the end of the action potentials, unlike the sAHP which can last for several second.

The function of sAHP is to decrease the firing probability of subsequent action potentials. Slow and medium afterhyperpolarisation have been analysed in *Ophn-1*$^{-/y}$ neurons and displayed similar amplitude as well as the corresponding underlying currents, namely I_{AHP} and I_{sAHP}.

In order to investigate the reduction in PSP, which is blocked by glutamatergic antagonists, I investigated EPSCs in CA1 neurons.

5.4.2 Excitatory postsynaptic currents of CA1 pyramidal neurons.

The whole cell recordings experiments described above were performed using a K^+-based internal solution, which permitted recording of the intrinsic properties of CA1 neurons. In order to effectively study postsynaptic currents using the voltage clamp technique, K^+ was substituted with caesium (Cs^+) which blocked K^+ channels and improved the space clamp of the recorded neuron.

CA1 pyramidal neurons were voltage clamped at -75 mV (the reversal potential for $GABA_A$ergic currents) resulting in excitatory post synaptic currents (EPSCs) being recorded as negative deflections. Evoked EPSCs (eEPSCs) were generated by stimulation of the Schaffer collaterals by a concentric stimulating electrode placed in the stratum radiatum of CA1c. In addition to recording eEPSCs, spontaneous excitatory postsynaptic currents (sEPSCs) were also recorded. sEPSCs are thought to result from the synaptic activity of neurons that impinged on the dendritic tree of the cell under investigation (Sherpherd, 2003)

Stimulus response curve

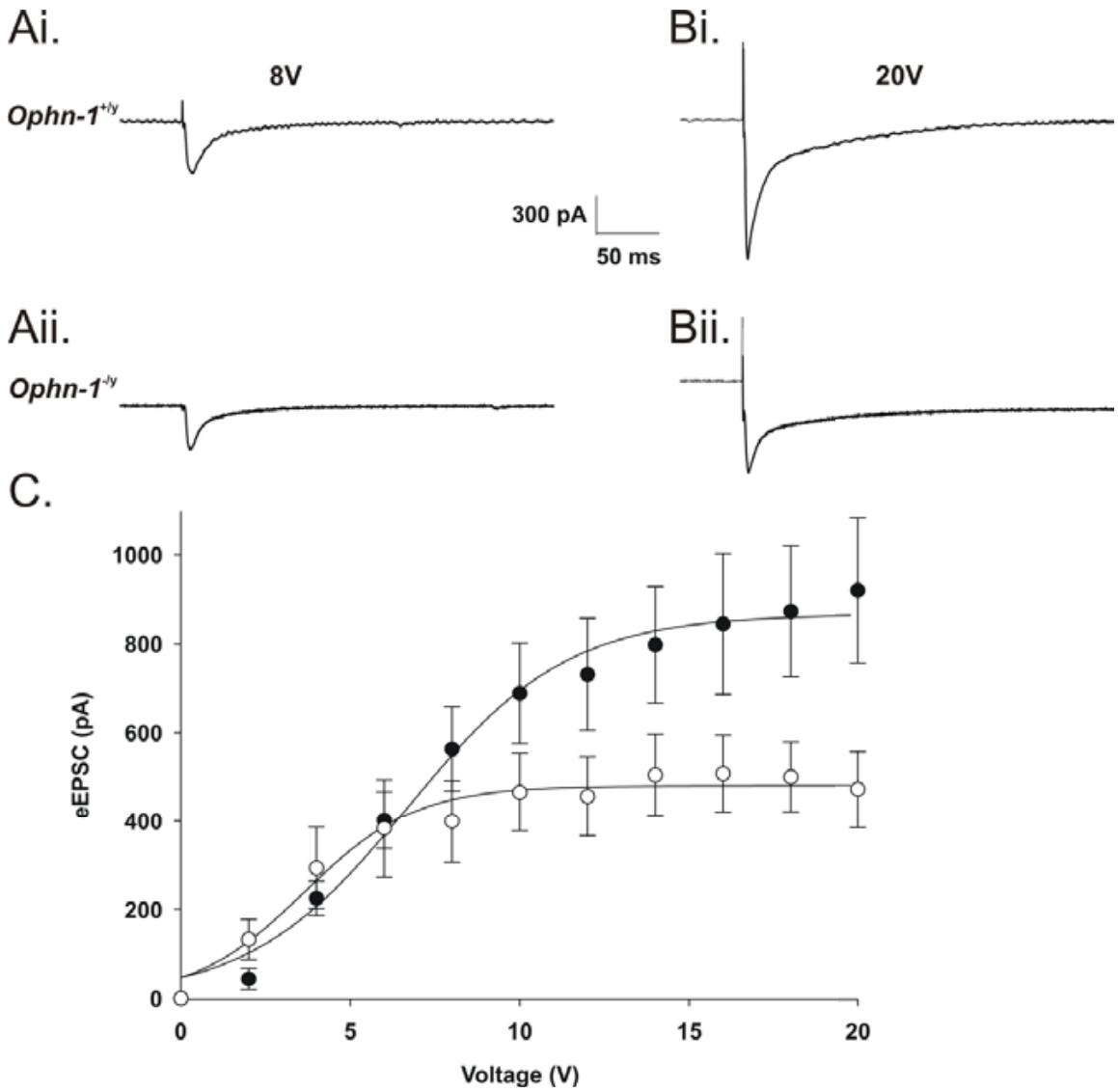

Figure 5.9: Evoked EPSCs were reduced in *Ophn-1*$^{-/y}$ CA1 pyramidal neurons. Representative eEPSCs evoked by an 8V stimulus in *Ophn-1*$^{+/y}$ **(Ai.)** and *Ophn-1*$^{-/y}$ **(Aii.)** and a 20V stimulus **(Bi.)** & **(Bii.) (C.)** Mean eEPSC amplitude plotted against the voltage intensity ((●) *Ophn-1*$^{+/y}$, n=13 and (○) *Ophn-1*$^{-/y}$, n=7), p=0.02 (Mann-Whitney test). Data points were fitted by a sigmoid (Boltzmann fit). Data are mean ± S.E.M.

With the gradual increase of the stimulus intensity, activating more presynaptic terminals, a concomitant increase of the summated eEPSCs was observed (fig. 5.9).

The maximum plateau amplitude achieved in *Ophn-1*$^{-/y}$ neurons was significantly weaker than the maximum amplitude observed in *Ophn-1*$^{+/y}$ CA1 pyramidal neurons (508 ±81 pA, n=7; 1012 ±154, n=13 respectively, p=0.03, fig. 5.9C.)

This result indicated a deficit in excitatory neurotransmission, which explained the reduction in PSP observed in field recordings. Several possible deficits could explain this result. On the presynaptic side, a decrease of the quantal content could explain this phenotype, as well as an alteration in the calcium dependence of the neurotransmitters release, a decrease in the number of release site or an alteration in vesicle dynamics. On the postsynaptic side, one could suggest an alteration in glutamatergic receptors functionality. To verify the latter, I recorded excitatory sEPSCs in *Ophn-1*$^{+/y}$ and in *Ophn-1*$^{-/y}$ CA1 pyramidal neurons.

Spontaneous excitatory postsynaptic currents.

Synaptic vesicles fusion from presynaptic terminals is thought to be random following probabilistic rules, as well as being action potentials driven.

Fig 5.10 depicts series of consecutive single sweep voltage clamped recordings illustrating small negative deflections sEPSCs in *Ophn-1*$^{+/y}$ (fig 5.10 Ai.) and *Ophn-1*$^{-/y}$ CA1 pyramidal neurons (fig. 5.10 Aii.). The application of a cocktail of glutamatergic receptors antagonists namely, NBQX (20 μM) and D-APV (25 μM) abolished sEPSCs activity, proving that the events were not contaminated by inhibitory synaptic transmission (fig 5.10 B.). The kinetics of these sEPSCs in

Ophn-1$^{-/y}$ were unaltered compared to *Ophn-1*$^{+/y}$ as predicted by the overlay of single event (fig 5.10 C & table 5.1)

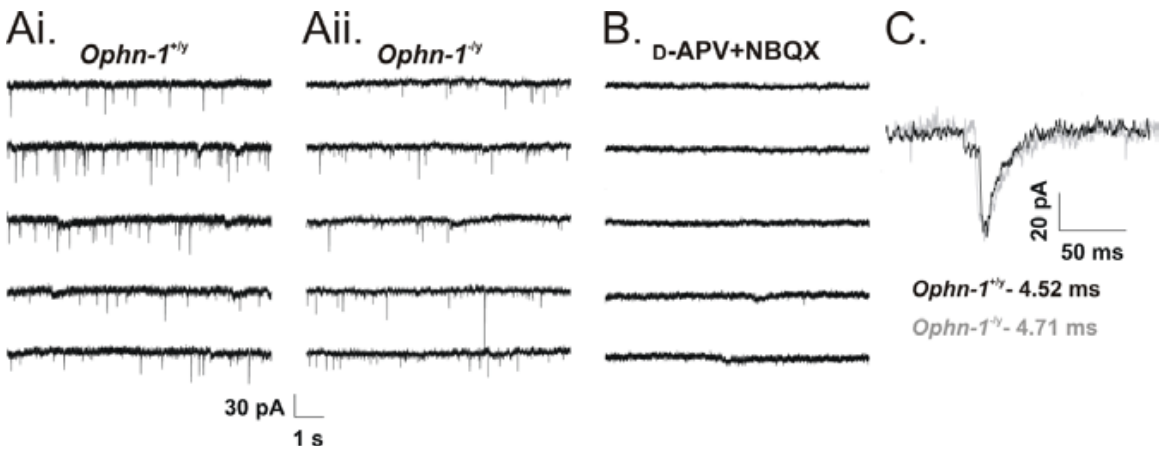

Figure 5.10: Spontaneous EPSCs recorded from CA1 pyramidal neurons. Representative raw recording traces of sEPSCs in *Ophn-1*$^{+/y}$ **(Ai.)** and in *Ophn-1*$^{-/y}$ CA1 pyramidal neurons **(Aii.)**, which were abolished by NBQX (20 μM) and D-APV (25 μM) **(B) (C.)** overlay of singles sEPSC from *Ophn-1*$^{-/y}$ (grey) and *Ophn-1*$^{+/y}$ (black) (numbers are τ decay averaged).

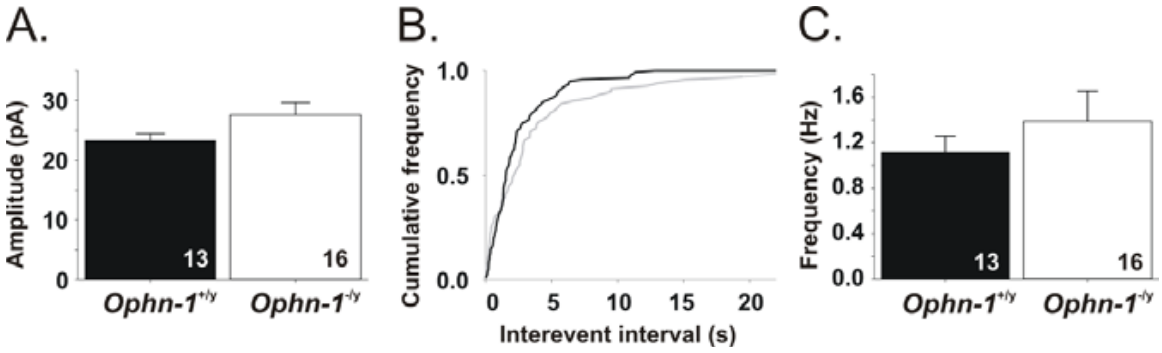

Figure 5.11: Spontaneous EPSCs showed similar amplitude and frequency by genotype. (A.) Histogram of the mean amplitude of the sEPSCs (the number represents the number of repetitions) (p=0.177) Mann-Whitney Rank Sum Test)). **(B.)** Representative cumulative frequency plot in *Ophn-1*$^{+/y}$ (dark line) and *Ophn-1*$^{-/y}$ (grey line). **(C.)** histogram of the frequency of sEPSCs, p=0.505 (Mann-Whitney Rank Sum test). Embedded numbers indicates the number of repetitions.

Analysis of sEPSCs revealed that the mean amplitude of these events in *Ophn-1*$^{-/y}$ CA1 pyramidal neurons was not significantly different compared to *Ophn-1*$^{+/y}$ CA1 pyramidal neurons (27.59 ±2.05 pA, n=16; 23.30 ±1.13 pA, n=13, respectively, (p=0.177) Mann-Whitney Rank Sum Test)), fig 5.11A.). The time between individual events was calculated and plotted as a cumulative frequency plot for each recording, in which the median inter-event intervals was extracted (fig. 5.11B.). The mean median inter-event interval in *Ophn-1*$^{-/y}$ was not significantly different from *Ophn-1*$^{+/y}$ CA1 pyramidal neurons (1347 ±273ms, n=16; 1050 ±112ms, n=13, respectively, p=0.37). For clarity matter, I have expressed the frequency of these events in Hertz (1.39 ±0.26 Hz; 1.12 ±0.14 Hz, respectively, p= 0.4, fig 5.11C.).

		Excitatory neurotransmission CA1		
		Ophn-1$^{+/y}$	*Ophn-1*$^{-/y}$	p
Evoked EPSC	10-90% rise time (ms)	2.43 ± 0.28 (13)	2.37 ± 0.14 (7)	0.88
	τ_{Decay1} (ms)	9.18 ± 1.02 (13)	11.10 ± 1.53 (7)	0.31
	τ_{Decay2} (ms)	62.90 ± 5.32 (13)	78.50 ± 15.26 (7)	0.27
Spontaneous EPSC	10-90% rise time (ms)	4.2 ± 0.32 (13)	4.71 ± 0.26 (16)	0.22
	τ_{Decay1} (ms)	4.52 ± 0.32 (13)	4.72 ± 0.26 (16)	0.63

Table 5.1: The kinetics of excitatory postsynaptic currents were unaltered in *Ophn-1*$^{-/y}$ CA1 pyramidal neurons. Evoked EPSCs were fitted by a double exponential decay. Data are expressed as mean ±S.E.M. Numbers in parentheses denote the number of cells recorded.

The experiments presented above revealed no difference in mean amplitude and kinetics of sEPSCs by genotype. Similar kinetics of sPSCs is classically interpreted as non alteration in the function of postsynaptic glutamatergic receptors. This suggested that the reduction in excitatory synaptic neurotransmission was not due to a postsynaptic deficit.

As there was no obvious postsynaptic defect in *Ophn-1*$^{-/y}$, possible presynaptic deficits were analysed with paired-pulse stimulation experiments on eEPSCs. In effect, paired-pulse facilitation is thought to rely on presynaptic phenomenon

Paired-pulse stimulation of eEPSCs

Monosynaptic glutamatergic EPSCs were evoked by double stimulations of the Schaffer collaterals/ Associational commissural pathway. The electrical stimulation intensity which evoked half maximum amplitude response (V_{50}) was used. However, the V_{50} were significantly different by genotype (4.36 ±0.52 V, n=7; 6.88 ±0.50 V, n=13 for *Ophn-1*$^{+/y}$ and *Ophn-1*$^{-/y}$ neurons respectively, p=0.005, fig 5.8C.)

Fig 5.12 Ai. and Bi illustrate typical traces of paired eEPSCs evoked by double electrical stimulation in *Ophn-1*$^{+/y}$ and *Ophn-1*$^{-/y}$ CA1 pyramidal neurons respectively, at inter-pulse intervals of 20 and 200 ms (left and right panels respectively). The ratio of the eEPSC2 over eEPSC1 estimated the inhibition (ratio<1) or the facilitation (ratio>1) and were plotted in the figure 5.12 C. Facilitation of the synaptic transmission was observed for inter-pulse intervals from 25 ms to 200 ms. (25 ms, *Ophn-1*$^{+/y}$: 1.26 ± 0.29 and *Ophn-1*$^{-/y}$: 1.18 ±0.03, p=0.101 (Mann-Whitney test); 200 ms: *Ophn-1*$^{+/y}$: 1.10 ± 0.05 and *Ophn-1*$^{-/y}$: 1.13 ±0.05, p=0.445 (Mann-Whitney test))

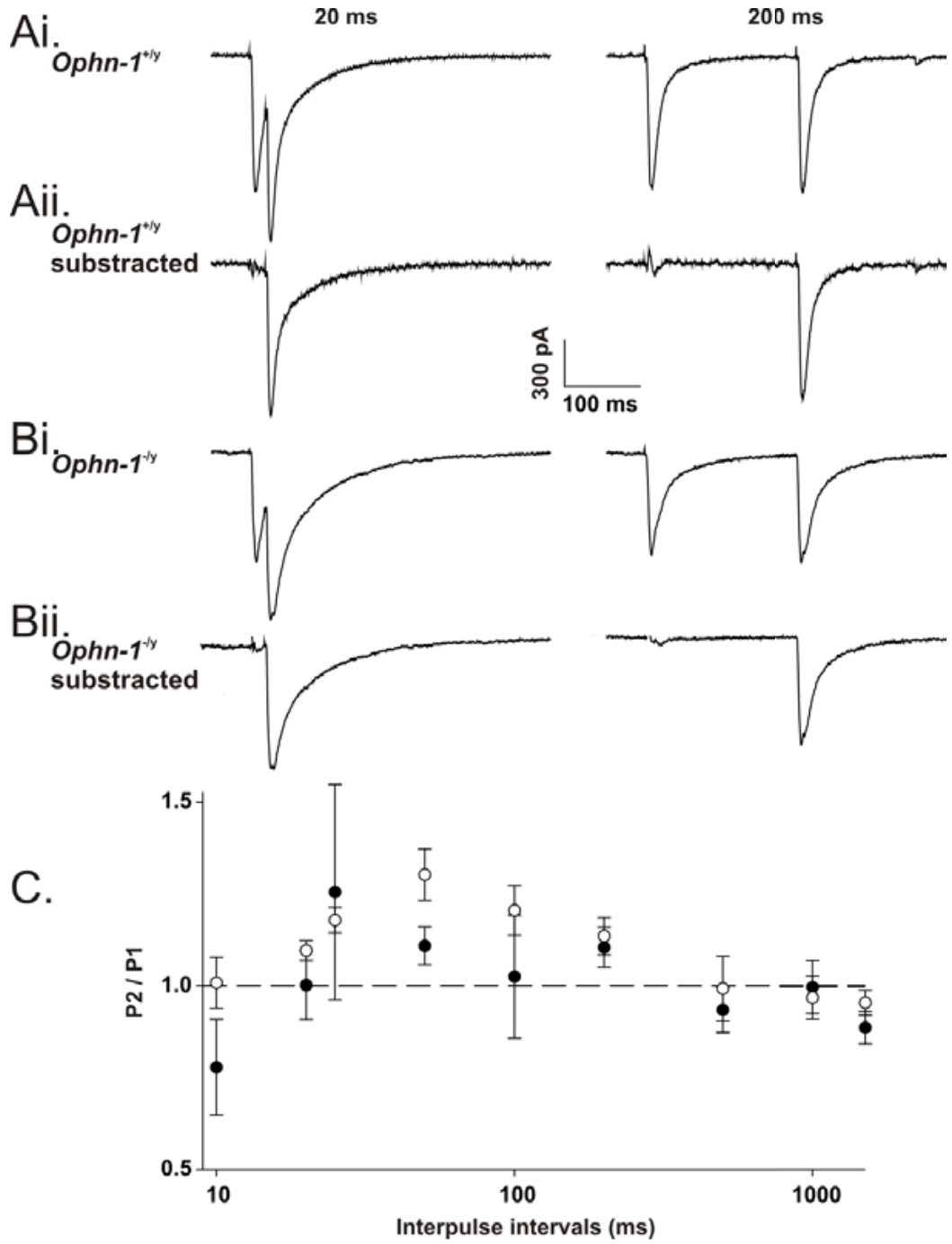

Figure 5.12: Evoked EPSCs paired-pulse stimulation was unaltered in CA1 pyramidal neurons. Representative double eEPSCs evoked by two stimulations of 20 ms (left panel) and 200 ms (right panel) inter-pulse intervals in *Ophn-1*$^{+/y}$ **(Ai.)** and *Ophn-1*$^{-/y}$ neurons **(Bi.)**. Examples of the digital subtraction of the first pulse response are shown for *Ophn-1*$^{+/y}$ **(Aii.)** and *Ophn-1*$^{-/y}$ neurons **(Bii.)**.**(C.)** Paired-pulse ratio plotted against the log of interpulse intervals. *Ophn-1*$^{+/y}$ (n=6) and *Ophn-1*$^{-/y}$ (n=7) (ANOVA p=0.091)

Frequency dependent eEPSCs facilitation

The functionality of presynaptic terminals was analysed in *Ophn-1*$^{-/y}$, by the repetitive stimulations of the Schaffer collaterals at various frequencies (from 10 Hz to 100 Hz). The frequency dependent facilitation of synapses is thought to be due to the accumulation of residual Ca^{2+} in the presynaptic terminals (Vreugdenhil et al., 2003). The facilitation of the synaptic strength was quantified by normalising every n*th* pulse amplitude eEPSCs (test pulses) over the amplitude of the first eEPSC (conditioning pulse). Figure 5.13 A. shows the eEPSCs summation in response to 10 stimulus delivered at 33 Hz in *Ophn-1*$^{+/y}$ and *Ophn-1*$^{-/y}$ (black and grey line respectively). At a frequency of 100 Hz, which is not physiological for pyramidal neurons, a maximum of facilitation at the 4th pulse was observed and was as strong in *Ophn-1*$^{-/y}$ as *Ophn-1*$^{+/y}$ CA1 pyramidal neurons (1.82 ± 0.19, n=10; 1.79 ± 0.19, n=10 respectively, p=0.91) (fig 5.13 Bi.). Similarly other frequencies tested did not reveal significant alterations in *Ophn-1*$^{-/y}$ CA1 pyramidal neurons. Nonetheless, the level of facilitation increased with the frequency, independent of the genotype.

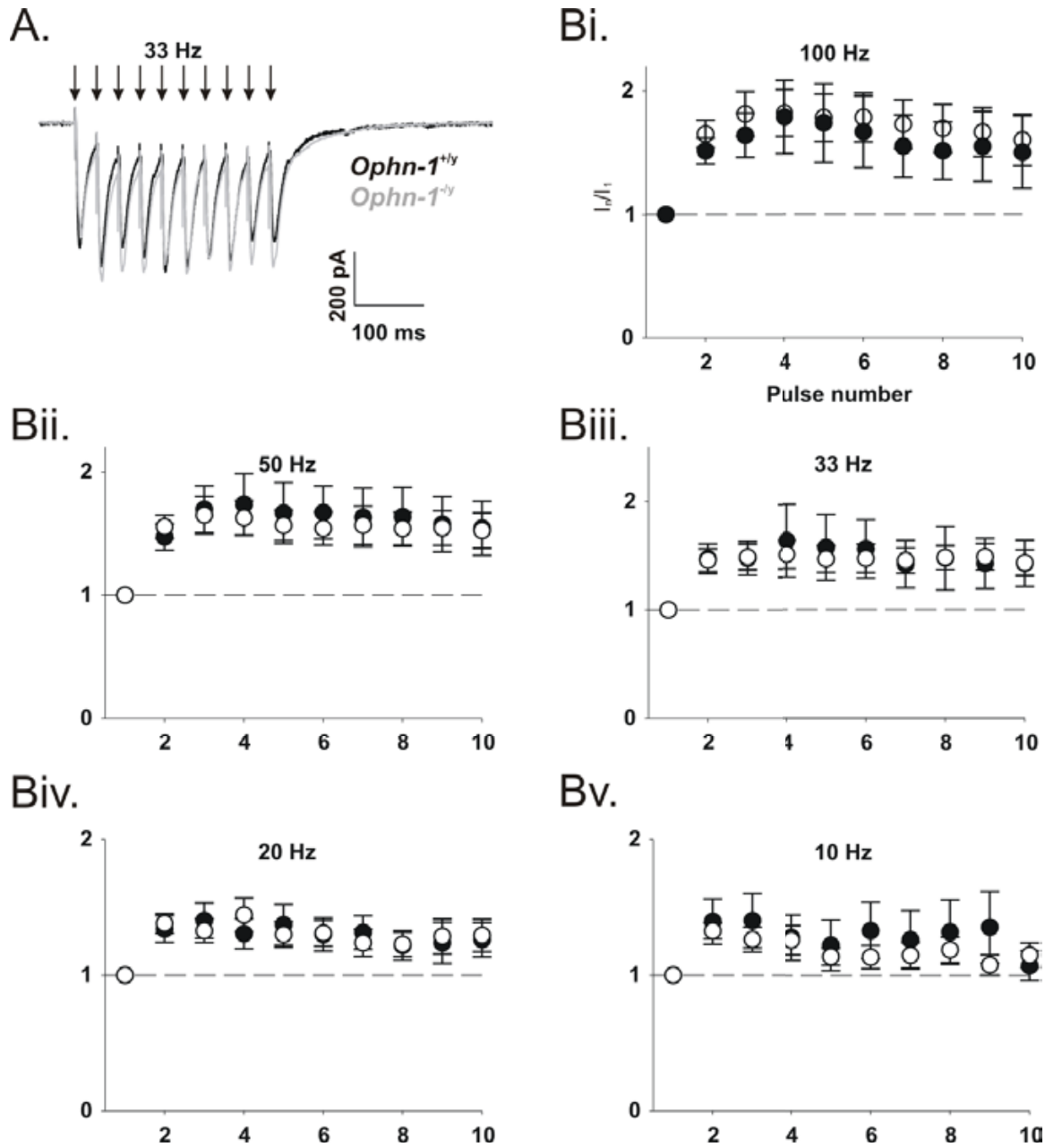

Figure 5.13: Frequency dependent facilitations of eEPSCs were unaltered in *Ophn-1*$^{-/y}$ CA1 pyramidal neurons Representative traces illustrating eEPSCs summation in response to 10 stimuli delivered at 33 Hz in *Ophn-1*$^{+/y}$ and *Ophn-1*$^{-/y}$ (black and grey lines respectively) **(A.)**. Normalisation of each eEPSC (*n*th) over the first eEPSC (conditioning pulse) for frequency of 100 Hz **(Bi.)**, 50 Hz **(Bii.)**, 33 Hz **(Biii.)**, 20 Hz **(Biv.)** and 10 Hz **(Bv.)**. *Ophn-1*$^{+/y}$ (n=10) and *Ophn-1*$^{-/y}$ (n=10)

Repetitive stimulations protocol did not revealed any differences in *Ophn-1*$^{-/y}$ slices. Therefore the reduction in PSP and eEPSCs was neither explained by postsynaptic deficits nor by presynaptic deficits.

5.4.3 Inhibitory postsynaptic currents of CA1 pyramidal neurons

Stimulus response curves

eIPSC in CA1 were evaluated through two different approaches. Firstly, a K^+-based internal solution was used, and eIPSCs were recorded as positive deflections and in isolation, from neurons voltage-clamped at 0 mV (the reversal potential for glutamatergic currents). Secondly, eIPSCs were assessed with a Cs^+-based internal solution in which cells were voltage clamped at -70mV. The stimulus response curve assessed the overall inhibitory inputs to CA1 pyramidal neurons. Fig 5.14 Ai. and Aii. show outward eIPSCs in *Ophn-1*$^{+/y}$ for a weak (4V) and a strong (16V) stimulation respectively. Fig 5.14 C is the stimulus response curve of eIPSCs which showed no difference in the maximum plateau amplitude in *Ophn-1*$^{-/y}$ compared to *Ophn-1*$^{+/y}$ CA1 pyramidal neurons (751 ±119 pA, n=7; 755 ±125 pA, n=14 respectively, p=0.98).

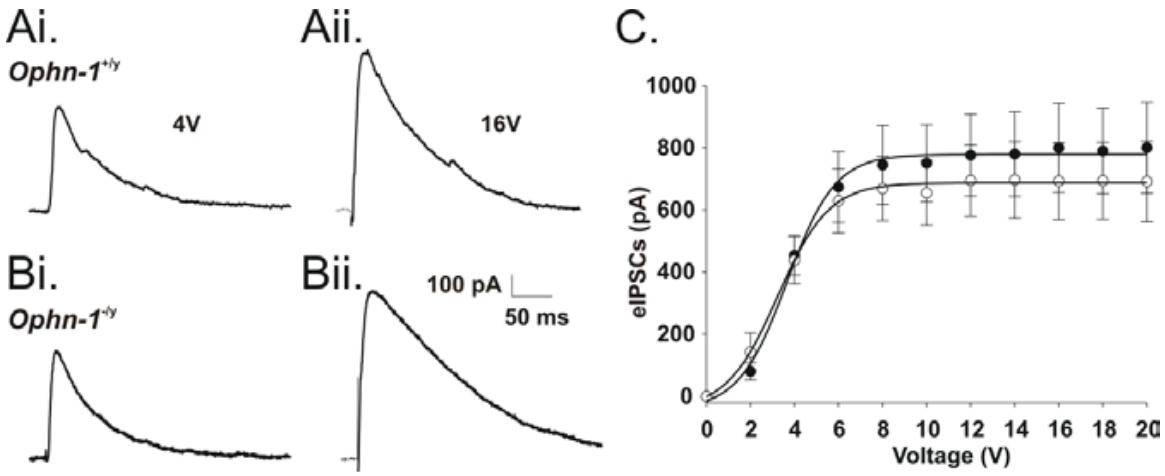

Figure 5.14: Input-output relationship of eIPSCs was unaltered in *Ophn-1*$^{-/y}$ CA1 pyramidal neurons held at 0mV. Outwards eIPSC evoked by 4V and 16 V stimuli in *Ophn-1*$^{+/y}$ (**Ai.** & **Aii.**, respectively) and in *Ophn-1*$^{-/y}$ (**Bi.** & **Bii.**, respectively) **(C.)** eIPSCs amplitude plotted against the voltage intensity stimulation. ((●) *Ophn-1*$^{+/y}$ n=14; (○) *Ophn-1*$^{-/y}$ n=7).

CA1 pyramidal neurons were voltage clamp at -70 mV with an equimolar Cl^- internal solution which displaced the reversal potential for chloride currents to 0mV. Furthermore Cs^+ was used to improve the space clamp of the patched neuron, similarly to EPSC study (see 6.4.2.). The monosynaptic eIPSC were recorded as a negative deflection with a rapid rising time and a slow decay time representative of eIPSC (fig 5.15 A., B.). Figure 5.15 C. shows the input-output plot of eIPSCs for CA1 pyramidal neurons, reaching a plateau amplitude for high intensity of stimulation. The plateau amplitude in *Ophn-1*$^{-/y}$ CA1 was in the same range of value as *Ophn-1*$^{+/y}$ (1054 ±71 pA, n=5; 918 ±114 pA, n=7 respectively, p=0.45).

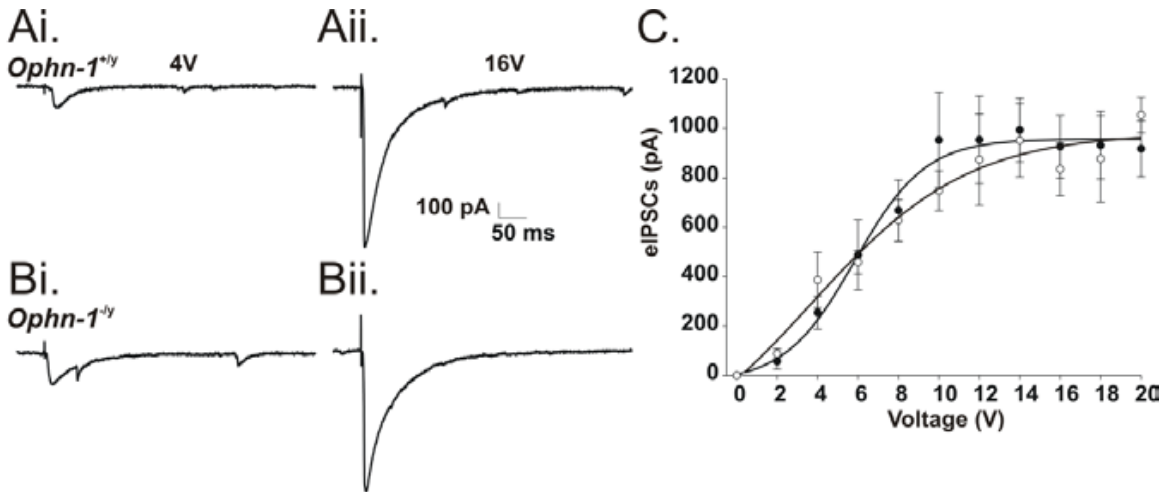

Figure 5.15: Input-output relationship of eIPSCs was unaffected in *Ophn-1*$^{-/y}$ CA1 pyramidal neurons held at -70mV. (A.) Single sweep voltage clamp recordings representing eIPSC evoked with 4V and 16V stimuli in *Ophn-1*$^{+/y}$ (**Ai.** & **Aii**. respectively) and in *Ophn-1*$^{-/y}$ CA1 pyramidal neurons (**Bi.** & **Bii.** respectively). **(C.)** eIPSC amplitude plotted against the voltage stimulus intensity ((●) *Ophn-1*$^{+/y}$ n=7; (○)*Ophn-1*$^{-/y}$ n=5).

Interestingly, the amplitudes of eIPSCs were not significantly different when recorded at 0 mV or at -70 mV with the corresponding internal solution. Independent from the solution used, the plateau amplitudes were not significantly different at 0 mV and -70 mV (*Ophn-1*$^{+/y}$: 755 ±125 pA, n=14; *Ophn-1*$^{+/y}$: 918 ± 114 pA, n=7, respectively, p=0.62). It is noteworthy that recordings at -70 mV are performed in the presence of the excitatory amino acid blockers, namely D-APV (25 μM) and NBQX (20 μM). Spontaneous postsynaptic currents resolution was enhanced with the Cs^+Cl^- based-internal solution. The reversal potential of the IPSC was predicted to be at 0 mV by the Nernst equation (E=-61 log $[Cl^-]$out/$[Cl^-]$in). This was

experimentally verified by the establishment of the current voltage curve for the eIPSCs.

Current voltage (I/V) curve

CA1 pyramidal neurons were voltage clamped and held at various membrane potential ranging from -90 mV to +30 mV. Fig 5.16 Ai. & Aii. illustrate a single sweep of voltage clamp recordings of an eIPSC at -50 mV in *Ophn-1*$^{+/y}$ and *Ophn-1*$^{-/y}$ CA1 pyramidal neurons respectively. At negative membrane potential, chloride $GABA_A$ergic currents were inwards, therefore equalling an entry of positive ions into the neurons. Conversely, at positive membrane potential inhibitory current were outwards depicted as a positive eIPSC (fig 5.16 Bi. & Bii.). Importantly, the reversal potential for the inhibitory current, during no net flow of Cl^- was observed close to 0 mV. In effect at 0 mV, the current recorded was -16.6 ± 28.4 pA ((●) *Ophn-1*$^{+/y}$ neurons, n=6) and -48.6 ± 44 pA ((○) *Ophn-1*$^{-/y}$ neurons, n=4) (fig 5.16 C.).

Fig 5.16 C. shows the current voltage curve of *Ophn-1*$^{+/y}$ and *Ophn-1*$^{-/y}$ neurons (plain line and dashed line respectively) fitted with a linear regression. The comparison of the r^2 revealed unaltered IPSC current properties in *Ophn-1*$^{-/y}$ CA1 pyramidal neurons. (r^2= 5.15 and 5.87 for *Ophn-1*$^{+/y}$ and *Ophn-1*$^{-/y}$ respectively, N.S.)

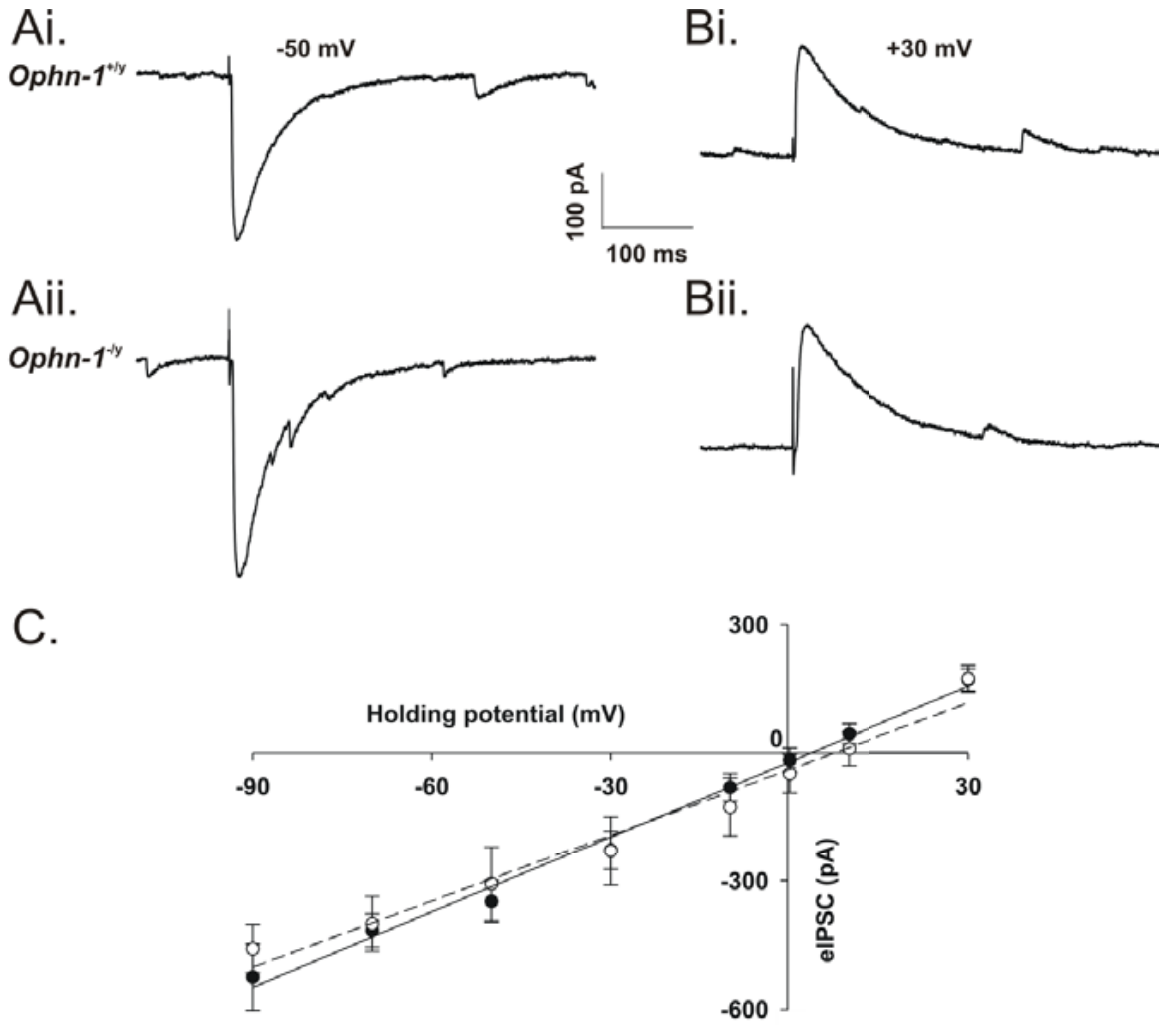

Figure 5.16: I/V relationship of eIPSCs recorded from CA1 pyramidal neurons in presence of NBQX and D-APV Inward eIPSC recorded at -50 mV **(Ai.)** and outward eIPSC at +30 mV **(Bi.)** in *Ophn-1*$^{+/y}$ and in *Ophn-1*$^{-/y}$ CA1 pyramidal neurons (Bi. & Bii. respectively) **(C.)** eIPSC amplitude plotted against the membrane potential. *Ophn-1*$^{+/y}$ (n=6) and *Ophn-1*$^{-/y}$ (n=4)

Spontaneous IPSCs in CA1 pyramidal neurons

Similarly to the EPSC, spontaneous inhibitory post synaptic currents (sIPSC) were recorded to measure their amplitude, frequency and kinetics. Figure 5.17 Ai & Aii. depict five consecutive VC recording sweeps of 9 s each sIPSCs are figured as small negative deflections which were analysed in amplitude and frequency (see Fig 5.18). Bath superfusion with bicuculline (10 μM) abolished the inhibitory neurotransmission confirming the $GABA_A$ergic nature of the spontaneous events recorded (Fig 5.17 B.).

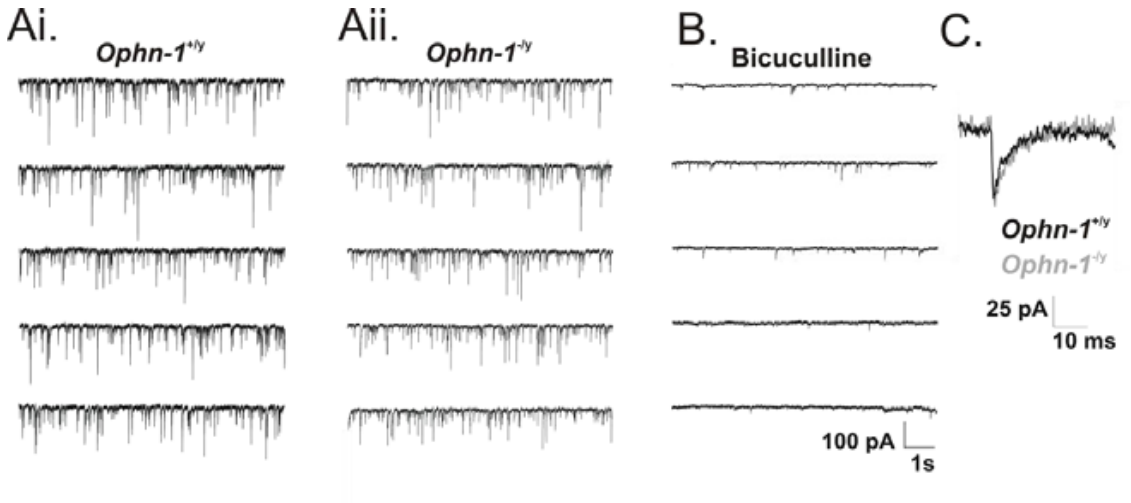

Figure 5.17: Representative spontaneous IPSCs recordings (Ai.) Consecutives single sweep voltage-clamp recordings of spontaneous IPSCs of CA1 pyramidal neurons in *Ophn-1*$^{+/y}$ and **(Ai.)** in *Ophn-1*$^{-/y}$. **(Aii.)** and in the presence of bicuculline **(B.). (C.)** Single sIPSC from *Ophn-1*$^{+/y}$ (black) and *Ophn-1*$^{-/y}$ (grey) overlaid.

The analysis of the mean spontaneous activity amplitude revealed that *Ophn-1*$^{-/y}$ sIPSCs were of the same amplitude as in *Ophn-1*$^{+/y}$ sIPSCs (45.35 ± 5.14 pA, n=10

and 38.03 ± 2.95 pA, n=10, respectively p=0.23; Fig 5.18 A.). The intervals between each event were calculated and plotted as cumulative frequency plot for each recording and median inter-event intervals were extracted from these data (fig 5.17 B.). This analysis revealed no difference in the mean median inter-event intervals by genotype (*Ophn-1*$^{-/y}$: 1343 ±273 ms, n=10; *Ophn-1*$^{+/y}$: 1050 ±112 ms, n=10, p=0.37) indicating that sIPSCs in *Ophn-1*$^{-/y}$ neurons was as frequent as in *Ophn-1*$^{+/y}$ neurons (11.67 ±0.99 Hz, n=10 and 12.34 ±1.75 Hz, n=10, respectively; p=0.72 ; Figure 5.18 C.),

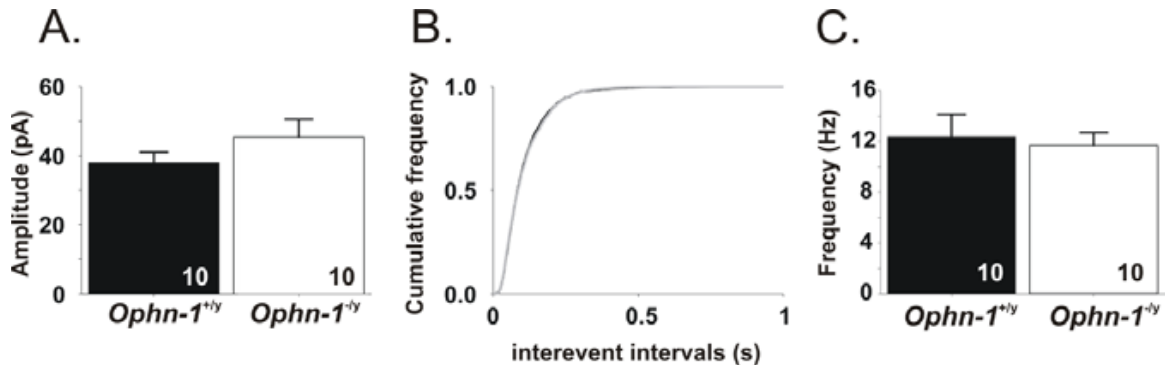

Figure 5.18: Spontaneous IPSCs mean amplitude and mean frequency were unaltered in *Ophn-1*$^{-/y}$ CA1 pyramidal neurons. (A.) Histogram of the mean amplitude of sIPSCs recorded. **(B.)** Cumulative frequency plot for a typical sIPSCs recording for *Ophn-1*$^{+/y}$ (black line) and *Ophn-1*$^{-/y}$ (grey line). **(C.)** Histogram of sIPSCs mean frequency (p=0.72). Embedded numbers indicate the number of repetitions.

		Inhibitory neurotransmission CA1		
		Ophn-1$^{+/y}$	*Ophn-1*$^{-/y}$	p
Evoked IPSC	10-90% rise time (ms)	3.41 ± 1.05 (7)	2.88 ± 0.58 (7)	0.7
	τ_{Decay1} (ms)	52.6 ± 4.2 (5)	38.5 ± 5.4	0.09 NB: power of statistic: 0.301
Spontaneous IPSC	10-90% rise time (ms)	3.30 ± 0.27 (10)	3.10 ± 0.18 (10)	0.59
	τ_{Decay1} (ms)	6.00 ± 0.96 (10)	5.11 ± 0.48 (10)	0.45

Table 5.2: The kinetics of inhibitory postsynaptic currents were unaltered in *Ophn-1*$^{-/y}$ CA1 pyramidal neurons. Evoked IPSCs and sIPSCs were fit by a single exponential decay. Data are expressed as mean ± S.E.M. Numbers in parentheses denote the number of cells recorded.

In conclusion, these experiments show that the kinetics of eIPSCs and sIPSCs were unchanged in *Ophn-1*$^{-/y}$ CA1 pyramidal neurons (table 5.2)

5.5 DISCUSSION

5.5.1 *Ophn-1*$^{-/y}$ slices displayed reduced postsynaptic potentials.

The evaluation of the synaptic transmission at the synapses between CA3 and CA1 pyramidal neurons, revealed a significant reduction of the maximum slope of PSP. However, the amplitude of PS in *Ophn-1*$^{-/y}$ compared to *Ophn-1*$^{+/y}$ slices was unaltered by the loss of oligophrenin1 protein. The PSP was blocked by glutamatergic receptors antagonists between CA3 and CA1, suggesting a deficit in glutamatergic neurotransmission. A similar reduction of PSP has been previously observed in a rat model for the foetal alcohol syndrome, which is known to be a prominent cause of mental retardation (Bellinger et al., 1999). Taken together, data suggest that a reduction in PSP may be linked to abnormal cognitive function. This reduction in synaptic efficacy could be due to less glutamatergic synapses activated upon the stimulation of the SC/AC pathway. In fact, a study of Khelfaoui et al (2007) has shown that the number of excitatory synapses was unaffected in *Ophn-1*$^{-/y}$ CA1 area (Khelfaoui et al., 2007). This suggested that the reduced PSP may not be due to fewer synapses, although this did not rule out less activation of synapses. On the presynaptic side, deficient glutamatergic release machinery, i.e. a reduction in release site or a reduced quantal content could be responsible for the reduced synaptic efficacy observed. On the postsynaptic side, a diminution in the number of ionotropic glutamatergic receptors or in their conductance, are possible reasons.

5.5.2 Paired-pulse facilitation was unaltered in *Ophn-1*$^{-/y}$ slices

Paired-pulse facilitation is thought to be an activity dependent potentiation of synaptic efficiency which is NMDA receptors independent and it is furthermore thought to be a form of short term plasticity (Bliss and Collingridge, 1993). In contrast to a previous study (Khelfaoui et al., 2007), presynaptic short term plasticity (PPF) was unaltered in *Ophn-1*$^{-/y}$ slices. This discrepancy may result from the different experimental protocols used. Several differences in the protocols used have been identified in the experimental procedures. Khelfaoui and colleagues have used a submerged recording chamber as opposed to the interface recording chamber utilized in the present study. This has been shown to have implications in the level of neuronal excitability, which is higher in a submerged recording chamber (M. Vreugdenhil, personal communication). They also used a different cutting solution, namely 189 mM glucose solution as opposed to 150 mM sucrose solution in the present study. The tissue preparation also differed; Khelfaoui et al have excised CA3, as I kept the slices intact. The age of the mice was also different; the present study used 4 to 8 weeks old mice as opposed to 2 to 3 weeks old. It is assumed that the mice are fully mature at 3 weeks old. Finally, the most striking difference in the protocol was the stimulus intensity used, which seems to be much stronger in Khelfaoui protocol. In Khelfaoui's protocol, a stimulus intensity which triggered a response of at least 5 mV was used, as opposed to a stimulus intensity chosen to evoke the half maximum amplitude used in these experiments, which was much

milder stimulus intensity. They may have driven the synapses harder, of which I have shown could entrain some deficits in *Ophn-1*$^{-/y}$ slices (see chapter 4).

The present result suggested that the kinetic of Ca^{2+} within the presynaptic terminals, i.e. the built up of residual Ca^{2+} was unaffected in *Ophn-1*$^{-/y}$ CA1 area. It also indicated a fully functional inhibitory recurrent pathway in CA1 area, as revealed by a normal fast inhibition at the inter-pulse interval of 10 ms. Also, the $GABA_B$ergic neurotransmission appeared to be unaltered, as demonstrated by the lack of effects on slow inhibition at the inter-pulse intervals 500ms.

Taken together, these results indicated that *Ophn-1*$^{-/y}$ slices displayed a reduction in synaptic efficacy, but a normal synaptic plasticity. In order to more fully investigate the reduced excitatory neurotransmission, evoked EPSC in CA1 pyramidal neurons triggered by SC/AC stimulation were studied, using whole cell recording technique.

5.5.3 *Ophn-1*$^{-/y}$ CA1 pyramidal neurons displayed a reduced eEPSC

A significant reduced maximum amplitude eEPSC has been observed in *Ophn-1*$^{-/y}$ CA1 pyramidal neurons. The reduction of the amplitude of the eEPSCs agreed with the reduction of PSP, which further confirmed that the synaptic strength at glutamatergic synapses between CA3 pyramidal neurons and CA1 pyramidal neurons was affected by the loss of oligophrenin1. These excitatory synapses originate from CA3 pyramidal neurons axons (SC) with a minor component from recurrent collaterals of neighbouring CA1 pyramidal neurons (Amaral et al., 1990). Another, with respect to the reduced PSP, possible explanation is that the number of

excitatory synapses would be reduced. However, Khelfaoui et al (2007) have quantified the number of the excitatory synapses onto CA1 pyramidal neurons, using electron microscopy analyses. In their study, excitatory synapses were identified as the appositions to a presynaptic bouton containing synaptic vesicles. They revealed a similar density of excitatory synapses in *Ophn-1*$^{-/y}$ compared to *Ophn-1*$^{+/y}$ CA1 pyramidal neurons. Therefore, a reduction in the number of excitatory synapses received by CA1 pyramidal neurons cannot account for the reduced eEPSC maximum amplitude. Another possible explanation would be a reduction in the number of pyramidal neurons. Nevertheless, Khelfaoui et al have quantified the CA1 pyramidal neurons densities, using nuclei of pyramidal neurons as reference and revealed no changes in *Ophn-1*$^{-/y}$ CA1 area. This suggested that the deficit in eEPSC/PSP was not due to fewer CA1 pyramidal neurons. It is possible to assume a deficit in the number of glutamatergic receptors or in their kinetics or in their conductance. This receptors are mainly (90%) located on the dendritic spines (Shepherd, 2003). Alteration in the number of glutamatergic receptors, their kinetics or conductance could affect the maximum amplitude of the PSP and eEPSC. To address this question, spontaneous excitatory postsynaptic currents in *Ophn-1*$^{-/y}$ CA1 pyramidal neurons were analysed.

5.5.4 Neither sEPSCs amplitude nor the frequency were affected *Ophn-1*$^{-/y}$ CA1 pyramidal neurons.

The amplitude, frequency and kinetics of spontaneous excitatory postsynaptic currents (sEPSCs) were unaffected in *Ophn-1*$^{-/y}$ CA1 neurons. A similar mean amplitude and similar kinetics of sEPSCs is typically interpreted as similar properties of glutamatergic receptors located at the postsynaptic terminals. The lack of effect on frequency indicated that the release of neurotransmitters machinery in the presynaptic terminals is fully functional in *Ophn-1*$^{-/y}$ CA1 area. To conclude, the reduced eEPSC amplitude cannot be explained by an alteration in density or kinetics of postsynaptic glutamatergic receptors in *Ophn-1*$^{-/y}$ slices.

I have shown that the deficit in excitatory neurotransmission did not originate from the postsynaptic compartments. However, future experiments should address the conductance of the ionotropic glutamatergic receptors, by performing peak scaled analysis of variance from miniatures EPSCs data. A negative result would then definitely exclude alterations of glutamatergic postsynaptic receptors.

I then addressed the possibility of a presynaptic deficit by testing the excitatory synapses to double and repetitive stimulations.

5.5.5 Paired pulse stimulation on EPSC was unchanged in *Ophn-1*$^{-/y}$ pyramidal neurons

In this experiment, two stimuli of equal intensity were applied to the SC/AC pathway at various intervals. A depression phenomenon was noticed for an interval of 10 ms where the synaptic eEPSCs was reduced in response to the latter stimulation. Nevertheless there were no differences by genotype. The depression observed was the result of the fast inhibition exerted by the interneurons through the $GABA_A$ receptors activation. For inter-pulse intervals between 20 and 200 ms, the facilitation of the latter response with respect to the former, was similarly not affected in *Ophn-1*$^{-/y}$ CA1 pyramidal neurons. The facilitation of the synaptic response is due to the built up of the residual Ca^{2+} in the presynaptic terminals, notably due to the entry of Ca^{2+} during the conditioning pulse (Katz and Miledi, 1968, Zucker and Regehr, 2002). For an inter-pulse interval of 500 ms, a depression was observed and was the result of the activation of the presynaptic $GABA_B$ receptors (Davies and Collingridge, 1993).

The lack of difference in paired-pulse stimulation on eEPSC was in accordance with the lack of effect on paired-pulse stimulation on PSP. Finally, these results suggested that the Ca^{2+} kinetics in the excitatory presynaptic terminals was fully functional in *Ophn-1*$^{-/y}$ mice (fig. 5.19). The non-alteration in Ca^{2+} kinetics could be confirmed by assessing the Ca^{2+}-dependence of the glutamatergic transmission in *Ophn-1*$^{-/y}$ neurons.

In order to investigate more fully a possible presynaptic deficit, I further submitted *Ophn-1*$^{-/y}$ synapses to a more sustained stimulation protocol, performing frequency dependent facilitation which consisted in 10 pulses applied at various frequency (Vreugdenhil et al., 2003). The aim of this experiment was to assess, more precisely the synaptic vesicles availability in *Ophn-1*$^{-/y}$ presynaptic terminals.

5.5.6 The potentiation of the eEPSC induced by frequency dependent facilitation in *Ophn-1*$^{-/y}$ CA1 pyramidal neurons was unaffected

Frequency dependent facilitation protocol induced facilitation of the eEPSCs. This facilitation is a typical presynaptic phenomenon due to its short time of action. The facilitation increased in strength with higher frequency. The data showed that no changes in the facilitation were observed in *Ophn-1*$^{-/y}$ compared to *Ophn-1*$^{-/y}$ CA1 pyramidal neurons. This result indicated that in *Ophn-1*$^{-/y}$ condition, the excitatory synapses can sustain facilitation triggered by various frequencies of stimulations. This further confirmed that the built up of Ca^{2+} in the presynaptic terminals was normal in *Ophn1*$^{-/y}$ mice and showed also that the vesicles availability was unaffected.

5.5.7 Deficits were specific to excitatory neurotransmission in CA1

I also evaluated the amplitude of evoked inhibitory postsynaptic current (eIPSC) in *Ophn-1*$^{-/y}$ CA1 pyramidal neurons. A similar deficit in the inhibitory neurotransmission

in CA1 could point at a common mechanism for excitatory and inhibitory neurotransmission. The maximal amplitudes of eIPSC were assessed in voltage-clamped CA1 pyramidal neurons, using two distinct internal solutions. For the equimolar $CsCl^-$ internal solution, as expected by the nernst equation, the reversal potential for Cl^- was experimentally confirmed at 0 mV.

The data revealed that eIPSC maximal amplitudes were unaffected in *Ophn-1*$^{-/y}$ CA1 pyramidal neurons independent of the experimental conditions used. The lack of effect on the amplitude of eIPSC indicated that the inhibitory neurotransmission exerted by the interneurons present in CA1 was not changed by the loss of oligophrenin1. It also indicated that the deficits observed are specific to the excitatory neurotransmission in CA1 area.

5.5.8 Spontaneous inhibitory postsynaptic current were unaffected in *Ophn-1*$^{-/y}$ CA1 pyramidal neurons.

The frequency, the mean amplitude and the kinetics of the sIPSCs in CA1 pyramidal neurons were not altered in *Ophn-1*$^{-/y}$. This result paralleled results obtained for sEPSCs in CA1 pyramidal neurons. The results ascertained that inhibitory interneurons in *Ophn-1*$^{-/y}$ CA1 pyramidal neurons presented a normal spontaneous activity. It also indicated that postsynaptic $GABA_A$ receptors, as well as the presynaptic release of GABA were not affected by the loss of oligophrenin1 in the CA1 area.

5.5.9 No change in intrinsic properties of neurons of *Ophn-1*$^{-/y}$ CA1 neurons

Alterations in intrinsic neuronal properties can be assumed to play a role in deficit in excitatory neurotransmission, such as e.g. faulty of ionic channels present on the surface membrane, which function is to conduct ionic currents to the soma. The intrinsic neuronal properties were analyzed in CA1 pyramidal neurons, using current clamp recording technique. The results indicated that *Ophn-1*$^{-/y}$ CA1 neurons have similar intrinsic neuronal properties as the control neurons, such as a similar membrane resistance in *Ophn-1*$^{-/y}$ compared to *Ophn-1*$^{+/y}$ CA1 pyramidal neurons. This indicated also a similar size of pyramidal neurons and a normal functionality of ionic channels at the surface membrane in CA1 pyramidal neurons from both genotypes.

Furthermore, *Ophn-1*$^{-/y}$ CA1 pyramidal neurons possessed all the channels necessary for the genesis of the action potentials, as well as the K^+ channels underlying the slow and medium afterhyperpolarisation. *Ophn-1*$^{-/y}$ pyramidal neurons displayed also an unchanged input-output relationship, meaning that the *Ophn-1*$^{-/y}$ CA1 pyramidal neurons were as prone to fire, upon depolarisation, as *Ophn-1*$^{+/y}$ CA1 pyramidal neurons.

5.5.10 Speculation and design of future experiments

The mechanism of the reduction in excitatory neurotransmission is yet to be uncovered. Several possible defects could explain this deficit, such as a defect in

quantal content on the presynaptic side. Namely a reduction in quantal content, i.e. less neurotransmitters in synaptic vesicles, is a possibility to explain the reduced PSP and the reduced eEPSCs (fig. 5.19). To prove this hypothesis, the amplitude of mEPSCs (sEPSCs TTX resistant) should be analysed and will determine the quantal content (Schneggenburger et al., 1999).

On the postsynaptic side, I demonstrated that the kinetics of the ionotropic glutamatergic receptors were unaffected. To definitely exclude a deficit in these receptors, their conductance could be assessed with analysis performed on mEPSCs, termed peak scaled analysis of variance (Traynelis et al., 1993). This analysis should then result in an estimation of the conductance of ionotropic glutamatergic receptors. A reduction in conductance of would lead to a reduction in maximal eEPSCs amplitude. However ionotropic glutamatergic receptors comprise two distinct types of glutamatergic receptors, namely AMPA/KA and NMDA.

It is possible to envisage a deficit in RRP size in excitatory synapses, as observed in inhibitory synapses in CA3 previously. Therefore a first approach should be to apply a hypertonic solution on the dendritic tree of CA1 pyramidal neurons, in order to create an osmotic shock, resulting in the depletion of the RRP, which can be then assessed (Ashton and Ushkaryov, 2005, Mozhayeva et al., 2002) . Secondly, fast stimulation protocol of single excitatory synapse will allow accurate quantification of RRP size at a single presynaptic terminal.

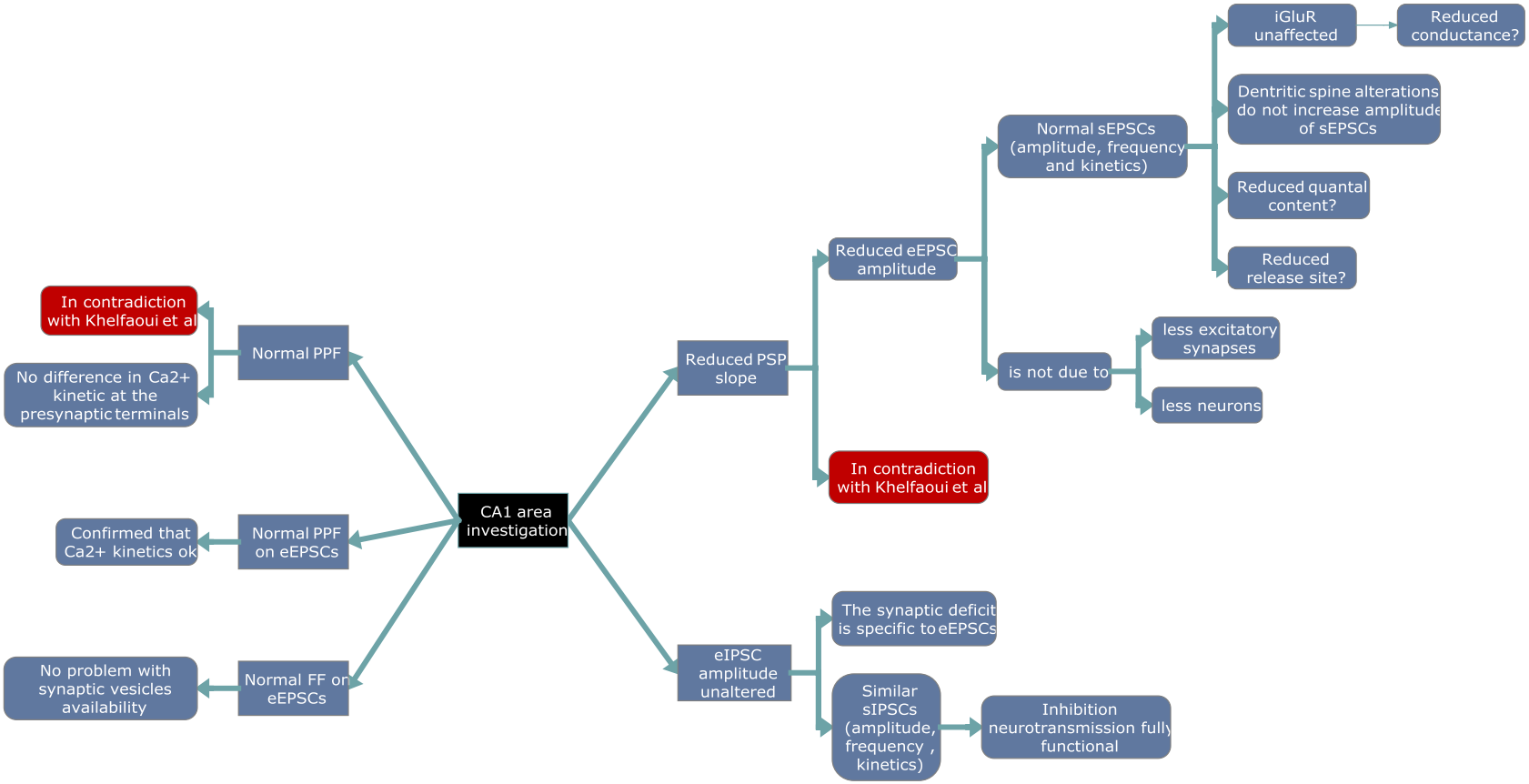

Figure 5.19: Summary of the results obtained in CA1 area.

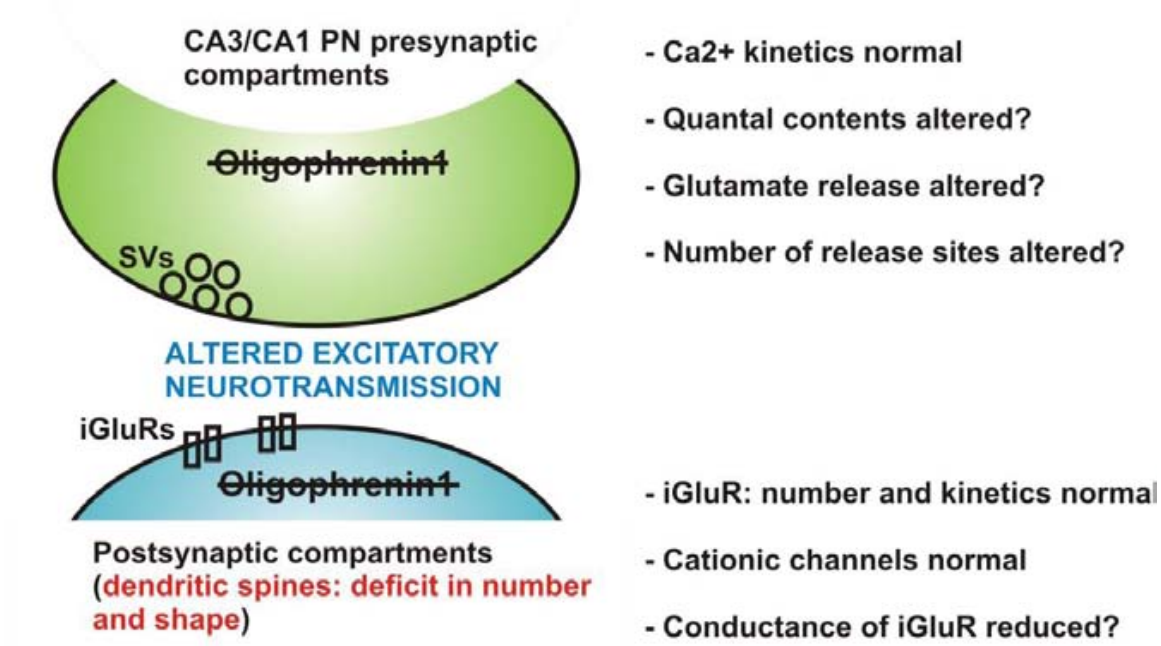

Fig 5.20: Schematic of a CA3/CA1 or CA1/CA1 pyramidal neurons synapse.

5.5.11 Conclusion on CA1

Taken together, these data presented did not suggest that the dysmorphy of dendritic spines previously observed (Govek et al., 2004;Khelfaoui et al., 2007) was responsible for the reduction in excitatory synaptic efficacy. I showed that the dysmorphy of the spines did not attenuate currents as similar mean amplitude of sEPSCs was observed. In this context it confirmed models postulating that dendritic spines are not electrical but rather a biochemical compartments (Koch and Zador, 1993).

I demonstrated that CA1 pyramidal neurons show a reduced postsynaptic potential accompanied by reduced eEPSC maximal amplitude. This study has shown that this is neither due to a change in intrinsic neuronal properties nor a change in postsynaptic glutamatergic receptor density or kinetics. Furthermore, a loss of

excitatory synapses or number CA1 pyramidal neurons cannot explain the deficit (Khelfaoui et al., 2007).

It would be tempting to think that RRP size would be altered, similar to CA3 neurons; however an unaffected sEPSCs frequency, as well as a normal paired-pulse stimulation and frequency dependent facilitation would suggest normal synaptic vesicles availability in *Ophn-1*$^{-/y}$ CA1 synapses.

The lack of difference in sEPSCs would tend to suggest that presynaptic compartments would be unaffected by the loss of oligophrenin1. It cannot be entirely excluded that the alterations in the presynaptic compartment could be too subtle or could br unapproachable to be addressed with the methods used in this study.

To conclude, presynaptic defect remains to be elucidated and postsynaptic deficit remains to be excluded.

Chapter 6: GENERAL DISCUSSION

Overview

In this thesis, the nature of the functional phenotype associated with oligophrenin1 deficiency was analysed in a mouse model. This study was performed in order to determine the biological role of oligophrenin1 and to further allow finding of pharmacological compounds which could reverse the observed deficits.

A postsynaptic role for oligophrenin1 has been previously reported (Govek et al., 2004, Khelfaoui et al., 2007). The present study now identified a new presynaptic role for oligophrenin1, which has been shown to be present in this compartment in the hippocampus (Govek et al., 2004, Khelfaoui et al., 2007), using techniques allowing changes at pre- and postsynaptic sides to be detected.

6.1 Relevance of the *Ophn-1*$^{-/y}$ mice as a model of X-linked mental retardation

In order for this mouse model to be used to investigate the pathophysiology of intellectual disabilities, it is essential that it closely mirrors the human condition. Common features of patients with oligophrenin1 mutations are lateral ventricles enlargement and cerebellar hypoplasia which is combined with medium to severe learning disabilities (Bergmann et al., 2003, Tentler et al., 1999). Khelfaoui et al

(2007) have previously shown that ventricular enlargement was observed in *Ophn-1*$^{-/y}$ mice, associated with learning impairments in the Morris water maze (MWM) task. Similar ventricular enlargements have been made in our laboratory suggesting that *Ophn-1*$^{-/y}$ mice may indeed be a suitable model to investigate the cognitive defects of people affected by XLMR, although the cerebellum hypoplasia has not been observed. Mice in this study were used between 3 and 8 weeks of age inclusive. It is known that the weaning in mouse intervened at 3 weeks old and that mouse is fertile at 6 weeks. Therefore, the mice used in this study could be defined as adolescent to young adult. It is important to note that Khelfaoui and co-workers (2007) whom had characterised the behavioural phenotype of *Ophn-1*$^{-/y}$ mice, This study presumably used adult mice but the exact age was not mentioned.

6.2 *Ophn-1*$^{-/y}$ slices displayed reduced KA-induced gamma oscillations compared to *Ophn-1*$^{+/y}$ slices

I have firstly hypothesized changes in synaptic functions in *Ophn-1*$^{-/y}$ mice based on the reduced paired-pulse facilitation in CA1 area observed by Khelfaoui et al (2007). I therefore assessed the synaptic function in *Ophn-1*$^{-/y}$ slices and observed a loss in the power of gamma oscillations in these slices. This loss of power could arise from the hypothesized changes in synaptic function and could be a potential explanation of the cognitive impairment observed in individuals affected and in *Ophn-1*$^{-/y}$ mice (Khelfaoui et al., 2007).

The rationale for studying hippocampal gamma oscillations *in vitro* in *Ophn-1*$^{-/y}$ slices was *i)* an altered cortical oscillations in human individuals affected with pathologies related to mental retardation, such as the Williams syndrome (Wittwer et al., 1996, Cantagrel et al., 2004, Grice et al., 2001) and *ii)* an altered learning in MWM for *Ophn-1*$^{-/y}$ mice compared to control mice. The MWM task is a hippocampal task related to spatial navigation (Morris, 1984, D'Hooge and De Deyn, 2001). Finally, a third rationale was that gamma oscillations were used as a tool to assess changes in strength of the synaptic activity, as some alterations in synaptic activity in *Ophn-1*$^{-/y}$ have been suspected by a previous report (Khelfaoui et al., 2007).

KA was preferred to other means to induce gamma oscillations (Carbachol application for example (Fisahn et al., 1998), due to the better analogy to *in vivo* gamma oscillations (Csicsvari et al., 2003, Buzsaki et al., 2003, Vreugdenhil and Toescu, 2005). In addition, recordings were preferably made from *s.* pyramidale (fig 6.1) owing to its larger amplitude compared to *s.* radiatum in KA-induced gamma oscillations (Vreugdenhil and Toescu, 2005) and also had the advantage to allow a more precise and consistent locus of recordings between the different slices. In the present study, 50 nM KA was chosen as the preferred method to evoke gamma oscillations as it is below the threshold of neurotoxicity for KA, which has been shown to occur at micromolar levels (Sperk, 1994)

In order to understand the implications of the following results, it is necessary to briefly summarise the proposed mechanisms of gamma oscillation genesis. Firstly, gamma oscillations are rhythmic population synaptic potentials arising from recurrent

excitatory and inhibitory currents in the CA3 neuronal network (Fisahn, 2005). A second important feature of KA-induced gamma oscillations is that synaptically- and electronically-coupled interneurons provide an inhibitory tone to CA3 pyramidal neurons which synchronizes their firing (Traub et al., 2003, Fisahn, 2005). Therefore, the interneuronal inhibitory network is thought to function as a clock (Jefferys et al., 1996). A third feature is that in KA-induced gamma oscillations the involvement of pyramidal neurons firing drives rhythmic excitatory population synaptic potentials (Bartos et al., 2007). I firstly demonstrated that *Ophn-1*$^{-/y}$ slices were able to generate gamma oscillations *in vitro*. Superfusion of KA elicited gamma oscillations which increased in amplitude over time in both *Ophn-1*$^{+/y}$ and *Ophn-1*$^{-/y}$ slices. Gamma oscillation strength was assessed by fast Fourier transformation, which allowed the determination of the power of the dominant frequency and the power of the whole gamma range frequency (20-80 Hz). A broad bandwidth ranging from 20-80 Hz was chosen to measure the power of the gamma rhythm to cancel the temperature dependence of gamma oscillations (Dickinson et al., 2003). The dominant frequency, around 30 Hz, of these gamma oscillations were unaltered by genotype and remained constant throughout the recordings. The averaged power spectrum revealed that KA-induced gamma oscillations showed oscillations over a wide frequency range, owing to a large variability in cycle length. It has been proposed that, the variation of the amplitude of field population synaptic potentials is strongly correlated to the cycle's length (Vreugdenhil and Toescu, 2005).

The mean peak power in *Ophn-1*$^{-/y}$ slices, which corresponds to the power of the dominant frequency was significantly reduced compared to *Ophn-1*$^{+/y}$ slices at each time points above 20 min. Similarly the summated power in *Ophn-1*$^{-/y}$, which assesses the power of gamma oscillations for the whole gamma range, was significantly reduced, paralleling the reduction of the mean peak power.

I have also confirmed that gamma oscillations were abolished by bicuculline application, proving its inhibition based nature, and furthermore abolished by NBQX indicating the necessity of the activation of the non-NMDA receptors, such as those that mediate fast EPSPs (Fisahn, 2005)

A preliminary conclusion can be drawn, as *Ophn-1*$^{-/y}$ slices were able to generate gamma oscillations; it is unlikely that the reduction in the power of gamma oscillations observed in *Ophn-1*$^{-/y}$ slices was a result of a defect in the basic mechanisms of the initiation of neuronal synchrony. This was further confirmed by an unaltered average gamma oscillation waveform in *Ophn-1*$^{-/y}$ slices.

The reduction in power signified that the amplitude of the gamma cycles were smaller in *Ophn-1*$^{-/y}$ than in *Ophn-1*$^{+/y}$ slices. Several precedents of similar results do exist for various pathological conditions such as Alzheimer's disease (Uhlhaas and Singer, 2006), ageing (Vreugdenhil and Toescu, 2005), hypoxia (Fano et al., 2007) and schizophrenia (Basar-Eroglu et al., 2007). Nevertheless this is, to my knowledge, the first time, that a loss of power of gamma oscillations has been observed in a mouse model of intellectual disability.

This study has demonstrated a significant reduction in the power of the gamma oscillations in *Ophn-1*$^{-/y}$ slices superfused with aCSF maintained at 30°C. However,

this reduction appeared to be less clear at a bath temperature of 32°C. An explanation might be that the increased temperature elevated the metabolic demand required for the neurons to generate and maintain persistent KA-induced gamma oscillations. If the slice is not healthy enough to cope with this energetic demand, the oscillations would just drop and collapse. As the capability of slices to generate gamma oscillations greatly varies between experiments and even throughout the day, this may mask the differences between the genotypes. An additional reason could be that at higher temperature the synaptic vesicles availability was increased, which would mask the difference between the genotypes (see section 4.3.4). Nonetheless, a significant reduction of the gamma oscillations was observed in *Ophn-1*$^{-/y}$ slices at 60 min., confirming the reduction of gamma power obtained at 30°C.

The synchronisation of KA-induced gamma oscillations was unaltered within *Ophn-1*$^{-/y}$ hippocampus.

It is also known that gamma oscillations are generated by local neuronal generator networks which can synchronize themselves over a long distance (Csicsvari et al., 2003). A study from Bottger et al (2002) demonstrated that coherence of spatially distributed gamma oscillations was a requirement for perception. Thus, it could supply the answer of the “binding problem”, correlating different features of an object (Gray et al., 1990, Jefferys et al., 1996).

In an attempt to evaluate this neuronal population synchronization, a study evaluating the coherence was performed to investigate the strength and the phase

lags of the spatial synchronisation of the oscillations throughout the whole hippocampus. The results suggested that the synchronisation of the gamma oscillations in *Ophn-1*$^{-/y}$ slices was not affected compared to *Ophn-1*$^{+/y}$ slices. This was unaffected inside local CA3 neuronal network generators and also for the synchronization of gamma oscillations from CA3 to CA1 areas. From CA3 to CA1 area, it is known that gamma oscillations are conducted via the Schaffer collaterals / associational commissural pathway, notably synapsing onto CA1 interneurons (Bragin et al., 1995).

To conclude, the unaffected synchronization within CA3c suggested that the connectivity between local generators was unaltered by the loss of oligophrenin1. Therefore, deficient connectivity within the neuronal networks cannot account for the reduced gamma oscillations power observed in *Ophn-1*$^{-/y}$ slices. Secondly, the results suggested that the learning impairments in *Ophn-1*$^{-/y}$ mice were not due to a deficient synchronization of the fast gamma rhythms within the hippocampus.

In summary, the amplitude of the gamma cycles was smaller in *Ophn-1*$^{-/y}$ slices without alteration in network connectivity. Several defects in *Ophn-1*$^{-/y}$ CA3 neuronal network could be the reason of this reduction; I have already proven that the network responsible for gamma oscillogenesis was functioning in *Ophn-1*$^{-/y}$ slices. The deficit observed was only a modulation of the power of gamma oscillations. One possible explanation could be that the lack of oligophrenin1 would induce a deficit in rhythmicity of gamma oscillations, which would lead to an overall decrease in the dominant power resulting from a greater frequency heterogeneity.

Rhythmicity of KA-induced gamma oscillations in *Ophn-1*$^{-/y}$ slices.

Contradictory results have been obtained about the rhythmicity of KA-induced gamma oscillations in *Ophn-1*$^{-/y}$ slices.Namely the auto-correlation study in *Ophn-1*$^{-/y}$ and *Ophn-1*$^{+/y}$ KA-induced gamma oscillations pointed toward a deficit in regularity. In contradiction, the event autocorrelation analysis revealed that *Ophn-1*$^{-/y}$ slices displayed a similar rhythmicity in *Ophn-1*$^{-/y}$ and *Ophn-1*$^{+/y}$ slices. Therefore, a clear conclusion was difficult to draw on these experiments. However, the event auto-correlation is a more powerful mean to assess the rhythmicity, thus it may be that the significant result obtained with the auto-correlation study was a false positive. The statistical power of this study was 0.4, which was less than the 0.8 which is generally accepted as the requirement for a robust statistical test. Therefore, as this study is underpowered, the observation of an alteration in the rhythmicity of gamma oscillations must be interpreted cautiously and requires further experiments to establish if this reduction is genuine.

Spontaneous gamma oscillations were unaltered in *Ophn-1*$^{-/y}$ slices.

Spontaneous gamma oscillations were characterised as recordings from slices where an intrinsic oscillation was observed prior to the addition of KA.. Spontaneous gamma oscillations in *Ophn-1*$^{-/y}$ slices displayed similar peak power, summated power and dominant frequency compared to *Ophn-1*$^{+/y}$ slices. The features of spontaneous gamma oscillations differ from KA-induced gamma oscillations, namely for the striking characteristic, their amplitude are smaller. Pietersen et al (2009) has shown that they display a lower peak frequency, which has not been observed in the

present study, and present a more sinusoidal waveform. Pietersen and co-workers established that spontaneous gamma oscillations are less spatially coherent and are suppressed by adenosine and cannabinoids. Finally, they concluded that different a set of interneurons are involved in their genesis than those involved in KA-induced gamma oscillations (Pietersen et al., 2009). These results suggested that the lack of oligophrenin1 had an effect only on KA-induced gamma oscillations, which would suggest that the action of oligophrenin1 was mainly required when the neuronal network needed to be driven. Paradigms of learning and memory state the requirement of a strong involvement of neuronal networks activity in order to achieve learning and memory processes (Bliss and Collingridge, 1993).

Y27632 failed to rescue the loss of power of gamma oscillations in *Ophn-1*$^{-/y}$ slices

It is known that the oligophrenin1 protein inhibits small RhoA GTPase protein, which in turn activates a protein called Rho-kinase (ROCK). Y27632 is a small molecule known to inhibit the protein ROCK, therefore switching off the RhoA/ROCK signalling pathway (Uehata et al., 1997, Ishizaki et al., 2000). In an attempt to counterbalance the loss of oligophrenin1 protein, which is known to over-activate RhoA/ROCK (Govek et al., 2004), Y27632 was used. The expected effects of Y27632 on KA-induced gamma oscillation were no change in the power of KA-induced gamma oscillations in *Ophn-1*$^{+/y}$ and an increase of the gamma power in *Ophn-1*$^{-/y}$ slices.

The data have shown an apparent reduction of the power of gamma oscillations in both *Ophn-1*$^{-/y}$ and *Ophn-1*$^{+/y}$, but this was not significant. In addition, the dominant

frequency was unaffected by the addition of Y27632. The effect of Y27632 on the KA-induced gamma oscillations in *Ophn-1*$^{-/y}$ and *Ophn-1*$^{+/y}$ slices could be due to a desynchronisation of the inhibitory neuronal network. In effect it is known that Y27632 induces an increase the frequency of sIPSCs in *Ophn-1*$^{-/y}$ granular cells in dentate gyrus (A.D. Powell, personal communication). This would lead to a somewhat desynchronisation of the firing of interneurons during gamma oscillations, impeding KA-induced gamma oscillations development.

In conclusion, the loss of the power of gamma oscillations was not rescued by the inhibition of ROCK.

6.3 Hippocampal neuronal network properties.

The functionality of the CA3 neuronal networks in *Ophn-1*$^{-/y}$ slices was further analysed by extracellular single stimulation experiments to assess the postsynaptic potentials and the resultant cellular firing assessed by the population spikes. Changes in the CA3 neuronal network could account for the reduced gamma oscillations in *Ophn-1*$^{-/y}$ slices. The nature of the synaptic transmission was mainly glutamatergic, as the majority of the postsynaptic potentials were blocked by NBQX and D-APV. This block was not complete which was unsurprising as mossy fibres terminals have been shown to contain other neurotransmitters (Romo-Parra et al., 2003). Furthermore, although I stimulated in the hilus, I cannot exclude the stimulation other synaptic pathways, such inputs from the commissural and associational fibres (Amaral et al., 1990). Concerning the population spikes, it is very

likely that I directly stimulated CA3 axons, which provides an explanation for the lack of reduction of the antidromic population spike. The evaluation of the postsynaptic potentials and population spike triggered by single stimulation of the mossy fibres pathway revealed no difference in the maximum amplitude in *Ophn-1*$^{-/y}$ compared to control slices. However, ANOVA revealed alteration in the slope of PSP and PS amplitude over the whole range of the intensity of stimulations. Nonetheless, the paired-pulse ratio of postsynaptic potentials and population spike was significantly reduced in *Ophn-1*$^{-/y}$ slices. These reduced paired-pulse facilitations can be attributed to a decrease in the neurotransmitter release owing to decrease of the probability of release at each synapses or an impairment in Ca^{2+} kinetics within the presynaptic compartments as PPF relies greatly on accumulation of residual Ca^{2+} (Katz and Miledi, 1968).

Taken together, these results demonstrated that the evoked PSP and PS were unaffected, when taking into consideration the maximum responses. However, presynaptic PPF of *Ophn-1*$^{-/y}$ synapses was altered by the lack of oligophrenin1, pointing toward a presynaptic deficit in *Ophn-1*$^{-/y}$ slices.

In order to endeavour an explanation of the loss of gamma oscillations power, I studied the excitatory and inhibitory synaptic inputs to *Ophn-1*$^{-/y}$ CA3 pyramidal neurons, using single CA3 pyramidal neurons recordings.

6.4 The excitatory and inhibitory neurotransmission in CA3 pyramidal neurons were altered in *Ophn-1*$^{-/y}$ mice.

Previous studies revealed that the strength of the inhibitory input to pyramidal neurons modulate the power of gamma oscillations without changing the dominant frequency (Hajos et al., 2000, Vreugdenhil et al., 2003). Hajos and colleagues have shown that the presynaptic suppression of the GABA release via the action of endocannabinoids, triggered a reduction in the frequency of the miniatures IPSCs. This reduction in frequency resulted in a reduction of the power of KA-induced gamma oscillations, with a similar dominant frequency. In addition, Vreugdenhil et al (2003) demonstrated that facilitated eIPSCs resulting from the lack of parvalbumin led to a threefold increase in the power of KA-induced gamma oscillations. Taken together, these studies demonstrated a key role of the inhibitory tone imposed to the pyramidal neurons in the control the power of the oscillations, without altering the dominant frequency.

eIPSCs amplitude in *Ophn-1*$^{-/y}$ CA3 pyramidal neurons

An alteration in eIPSC amplitude was observed for a mild stimulus (18V), however strong stimulation (30V) of the afferent pathway failed to evoke reduced maximum amplitude by genotype. However, statistical power analysis performed on the maximal plateau amplitude revealed that this study was underpowered. It may be that a significant reduction of eIPSC may have been missed. This idea is supported

by univariate analysis of variance (ANOVA) which revealed an overall significant alteration in eIPSC amplitude in *Ophn-1*$^{-/y}$ CA3 pyramidal neurons.

The frequency of spontaneous- EPSCs and -IPSCs was reduced in *Ophn-1*$^{-/y}$ CA3 pyramidal neurons

I assessed the inhibitory neurotransmission onto CA3 pyramidal neurons. Spontaneous inhibitory postsynaptic currents revealed a significantly reduced frequency whilst mean amplitude was unaffected. In addition, excitatory inputs to pyramidal neurons revealed a similar reduction in frequency without alteration in mean amplitude. A reduction in frequency is typically interpreted as a presynaptic deficit. These results indicated also that the deficit in *Ophn-1*$^{-/y}$ CA3 pyramidal neurons presented commonalities between the excitatory and inhibition neurotransmission.

In summary, the synaptic inputs to *Ophn-1*$^{-/y}$ CA3 pyramidal neurons were reduced.

These results were interesting as it is well established that gamma oscillations result from a synaptic interplay between CA3 pyramidal neurons and interneurons (fig. 6.1). Rhythmic EPSC and IPSC, which are phase-locked with extracellular field potentials, have been observed in CA3 pyramidal neurons during gamma oscillations(Fisahn, 2005). It is noteworthy that the rhythmic population synaptic potentials recorded on *s.* pyramidale were mainly constituted by IPSPs, resultant of IPSCs bombarding the perisomatic region of the pyramidal neurons at the gamma frequency. Concerning the kinetics of these spontaneous events, it is noteworthy that the rise time of the sIPSCs came out to be close to significance (p=0.07) and,

furthermore the statistical power came out to be underpowered (0.338< 0.8). Therefore the IPSC rise time may be slower in Ophn-1$^{-/y}$ CA3 pyramidal cells, which would eventually denote of a malfunction of $GABA_A$ receptors activation. This conclusion is rather very speculative; therefore more experiments would be needed to clarify this confounding issue. It is however noteworthy that a study in Dentate Gyrus has revealed that GABAA receptors were fully functional (Powell et al, 2009, submitted).

In conclusion, the reduction in spontaneous inhibitory postsynaptic currents weakened the inhibitory tone exerted onto CA3 pyramidal neurons. One can speculate that it would be also reduced during KA application. As a result, it can be expected a reduced in size of the rhythmic IPSPs which lead to reduced power of gamma oscillations in *Ophn1*$^{-/y}$ through less currents flowing at each cycle of the oscillations (fig. 6.1).

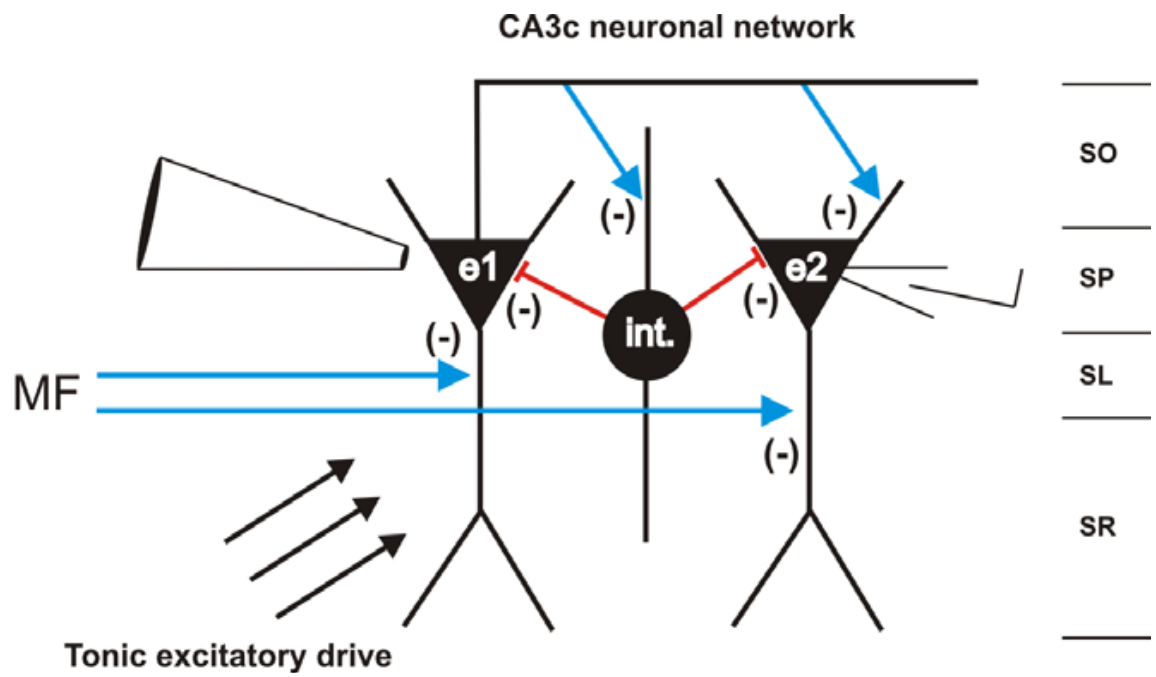

Figure 6.1: Synaptic defects observed in CA3 neuronal networks in *Ophn-1*$^{-/y}$ mice. “e1 & e2” are schematic of excitatory CA3 pyramidal neurons and “int.” display a schematic CA3 interneuron network. (-) indicate reduction of the excitatory and inhibitory synaptic inputs. The tonic excitatory drive (parallel arrows) was the consequence of KA receptor activation. The left electrode indicate the position of the extracellular electrode, as the right electrodes the patch pipette. Blue colour indicates excitatory synapses and red colour indicates inhibitory synapses. Abbr.: SO, stratum oriens; SP, stratum pyramidale, SL, stratum lucidum; SR, stratum radiatum.

The results presented above showed that the functional changes in excitatory and inhibitory inputs onto CA3 pyramidal neurons underlie the reduced power of KA-induced gamma oscillations in *Ophn-1*$^{-/y}$ slices (fig 6.1).

The quantal content was unaffected in *Ophn-1*$^{-/y}$ CA3 interneurons

In an attempt to assess the quantal content in *Ophn-1*$^{-/y}$ inhibitory synapses, slices were bathed in tetrodotoxin (TTX) which abolished action potentials generation in the neuronal network. This allowed the TTX resistant spontaneous postsynaptic current, termed miniatures IPSCs (mIPSCs) to be evaluated. No differences were found in either frequency or amplitude or kinetics of mIPSCs in *Ophn-1*$^{-/y}$ CA3 pyramidal neurons. Classically, analysis of miniatures mean amplitude yields the quantal content, suggesting that the amount of neurotransmitter contained in secretory vesicles is similar in *Ophn-1*$^{+/y}$ and *Ophn-1*$^{-/y}$ synapses.

To explain the lack of effect on mIPSCs, it might be possible that oligophrenin1 signalling pathway intervene in solely the activity-driven spontaneous release of synaptic vesicles. Sara et al (2005) showed that it was predominantly the RRP that provided activity-dependent vesicles. It is therefore assumed that only the synaptic vesicles pool responsible for spontaneous postsynaptic currents were somewhat affected by the loss of oligophrenin1, as suggested by a similar frequency of events for sIPSCs and mIPSCs in *Ophn-1*$^{-/y}$ CA3 pyramidal neurons.

Paired-pulse depression was enhanced in *Ophn-1*$^{-/y}$ CA3 pyramidal neurons

To confirm a deficit in the presynaptic compartment, I performed paired pulse stimulation experiments, which is a paradigm of transient change in synaptic strength by the action of Ca^{2+} in the presynaptic terminals.

The depression of the synaptic response is explained by the presynaptic inhibition exerted by $GABA_B$ receptors activated by spill over of GABA (Davies and

Collingridge, 1993). Ideally, these experiments should have been performed in the presence of $GABA_B$ receptors blocker (CGP55854) to alleviate the effect of the $GABA_B$-dependent neurotransmission, although the recordings were made with Cs^+ in the pipette which block the GIRK activity that drives this $GABA_B$_dependent depression. Anyway, the results revealed that the *Ophn-1*$^{-/y}$ CA3 pyramidal neurons displayed a stronger depression over the entire series of paired-pulse intervals. In other words, the paired-pulse depression of the eIPSCs was significantly enhanced in *Ophn-1*$^{-/y}$ slices. This was likely to reflect a deficit in neurotransmitter release during the test stimulus. Paired-pulse stimulation experiments rely on the accumulation of residual Ca^{2+}. Ca^{2+} which firstly enter the presynaptic terminals during the conditioning stimulus and is termed local Ca^{2+} and is located near the voltage gated calcium channels. The function of this entry of Ca^{2+} is to trigger synaptic vesicles fusion, correlated to neurotransmitter release. This deficit further pointed towards a deficit in neurotransmitter release. To investigate more fully this presynaptic deficit, I have evaluated *Ophn-1*$^{-/y}$ inhibitory synapses in response to a more sustained stimulation protocol.

Frequency dependent facilitation was reduced at 33 Hz in *Ophn-1*$^{-/y}$ CA3 pyramidal neurons

Vreugdenhil et al (2003) showed that the loss of parvalbumin induced an enhanced frequency dependent facilitation at 33Hz, associated with an increase of the power

of KA-induced gamma oscillations. They suggested that the facilitation of GABA release induced the increase of the power of KA-induced gamma oscillations. Moreover, the aim of the frequency dependent facilitation experiment was to examine the eIPSC built up which reflected the ability of *Ophn-1*$^{-/y}$ inhibitory synapses to sustain high frequency of release of GABA.

Interestingly, results demonstrated that eIPSC facilitation failed at 33 Hz, which is close to the frequency of firing of interneurons required for KA-induced gamma oscillations. Nonetheless, others frequencies of facilitation or depression were unaltered in *Ophn-1*$^{-/y}$ CA3 pyramidal neurons.

It is known that when interneurons are included in an inhibitory network, their firing frequency is tuned at 33 Hz, in other words, they may be designed to fire at this frequency, hence the lack of facilitation at this frequency only (Jefferys et al., 1996).

In conclusion, less GABA was released by *Ophn-1*$^{-/y}$ synapses for the frequency of stimulation of 33Hz. This further demonstrated a presynaptic deficit probably via an alteration in vesicles availability at the inhibitory synapses.

Taken together, these results indicated a presynaptic deficit rather than a postsynaptic deficit, in effect the decrease in frequency of spontaneous activity is typically interpreted as a presynaptic deficit. A postsynaptic deficit is very unlikely as suggested by similar postsynaptic currents amplitudes and kinetics. To further confirm the non alteration in postsynaptic receptors, peak scale analysis of variance could be undertaken to assess the conductance of $GABA_A$ receptors. However, this analysis was made difficult by the high frequency of mIPSC, in effect for peak scale

analysis of variance needed postsynaptic events to be separated in time of at least 3 times τ decay (Traynelis et al., 1993).

Furthermore, the reduction in frequency of excitatory and inhibitory postsynaptic currents are neither due to changes in intrinsic neuronal properties of *Ophn-1*$^{-/y}$ CA3 pyramidal neurons, nor to a change in input-output relationship of presynaptic neurons, i.e. Granule cells (Powell, A.D. personal communication) or CA3 pyramidal neurons via the recurrent collaterals.

To further address the question of the availability of synaptic vesicles in *Ophn-1*$^{-/y}$ presynaptic compartments, I investigated specifically the readily releasable pool (RRP) size into *Ophn-1*$^{-/y}$ interneuronal presynaptic terminals (see 6.5)

6.5 Readily releasable pool (RRP) size was reduced in *Ophn-1*$^{-/y}$ CA3 pyramidal neurons.

Release of neurotransmitters is mediated by fusion of synaptic vesicles at the active zone (fig 6.2), which is triggered by the local Ca^{2+} influx. Furthermore, synaptic vesicles trafficking is intense at the presynaptic terminal (Sudhof, 2004). The RRP is a pool of vesicles which is ready to undergo the process of fusion in the active zone upon stimulation (Schweizer and Ryan, 2006). The RRP and the reserve pool are termed the recycling pool and an equilibrium exist between these pools (fig 6.3). The RRP pool is refilled either by synaptic vesicles from the reserve pool or by recycling. However, the regulation of the size of RRP remained largely to be explored.

The RRP study was undertaken to assess any alteration in the size of the RRP *Ophn-1*$^{-/y}$ inhibitory synapse. An electrical stimulation in the middle of the hilus was used to evoke the smallest eIPSC. I hypothesized that only few synapses were investigated, with the caveat that the quantification of the RRP size in interneurons revealed that about 10 synaptic readily releasable vesicles are present in the presynaptic terminal (Kirischuk and Grantyn, 2000). A high frequency of stimulation was used in order to use the depression of eIPSC amplitude to estimate the number readily releasable vesicles, it is noteworthy that even the RRP is being depleted, vesicles replenishment occurs concomitantly. RRP is refilled in about 15 s (Kirischuk and Grantyn, 2000, Schneggenburger et al., 1999)(fig. 6.3). Interestingly, data indicated a reduction of the RRP size in *Ophn-1*$^{-/y}$ inhibitory synapses, which an estimation of a reduction of about 50% of readily releasable synaptic vesicles in *Ophn1*$^{-/y}$. As it is known that the RRP size is an important factor of the synaptic strength and plasticity (Sudhof, 2004); the reduction of the RRP size would weaken the synaptic strength of inhibitory synapses. This led consequently to the reduction in the power of gamma oscillations in *Ophn-1*$^{-/y}$ slices, with the caveat that gamma oscillations are an activity dependant modulation of synaptic strength.

The present result demonstrated a new role for the protein oligophrenin1 in the maintenance of the RRP size at the inhibitory presynaptic terminals. As oligophrenin1 is involved in regulating the actin cytoskeleton through the action of the small Rho GTPase proteins, it is likely that I shed in light a new mechanism of

synaptic vesicles trafficking. With the caveat, that the small GTPase protein Ral has been already implicated in synaptic vesicles transport (Polzin et al., 2002).

Interestingly, a study by Powell, A.D. (personal communication) has demonstrated similar reduction in RRP size together with impairment in vesicles recycling in *Ophn-1*$^{-/y}$ dentate gyrus area.

This is in agreement with a new presynaptic role of oligophrenin1 in synaptic vesicles transport.

In addition, it is now acknowledged that the retrieval of synaptic vesicles in hippocampal synapses is mainly achieved through clathrin-mediated endocytosis (CME) (Granseth et al., 2006). Interestingly, Khelfaoui and colleagues have demonstrated an impairment in clathrin mediated endocytosis (Khelfaoui et al., 2009). They firstly showed that oligophrenin1 interact with proteins involved in CME such amphiphysin, endophilin and CIN85. They therefore speculated that oligophrenin1 would play a role in CME. The mechanism would be as follow: oligophrenin1 would be recruited and decrease RhoA/ROCK signalling pathway, this would release the inhibitory action of ROCK on endocytosis mediated by clathrin.

In agreement with this hypothesis, they have shown that the reduction of endocytosis in *Ophn-1*$^{-/y}$ has been rescued by Y27632. RhoA/ROCK signalling pathway has already be shown to be involved in receptor endocytosis, namely an increase of ROCK activity led to reduction in CME (Kaneko et al., 2005). Therefore, oligophrenin1 could belong to the set of proteins necessary for CME.

One can assume that if the recycling of vesicles is impaired in *Ophn-1*$^{-/y}$ inhibitory synapses; this would be the cause of the smaller RRP size, through an impaired replenishment of the RRP.

In addition, oligophrenin1 could also interact with other signalling pathway such as with the myosin light chain kinase (MLCK) signalling pathway, as inhibition of MLCK has been shown to reduced vesicles mobility (Ryan, 1999) and alter the RRP size (Srinivasan et al., 2008) (fig. 6.3). Another downstream effector of ROCK could be Lin-11, Isl-1 and Mec-3 Kinase (LIMK) (+ Cofilin), in effect it is known that LIMK by phosphorylating the cofilin inhibit its actin depolymerising activity (Ding et al., 2008). Both MLCK and LIMK signalling contribute to actin cytoskeleton reorganisation (fig.6.3).

Future immunohistochemistry experiments with a GFP-tagged synaptobrevin2, which is a marker of synaptic vesicles, in *Ophn-1*$^{-/y}$ cultured CA3 interneurons could be undertaken to confirm the reduction of the RRP size in *Ophn-1*$^{-/y}$ mice. Finally, the determination RRP size using the application of a hyperosmotic solution will yield an estimation of the RRP size (Simsek-Duran and Lonart, 2008). Finally, to assess the RRP at a single synapse, microstimulation could be performed, this would confirm or infirm the role of oligophrenin1 in synaptic vesicles transport.

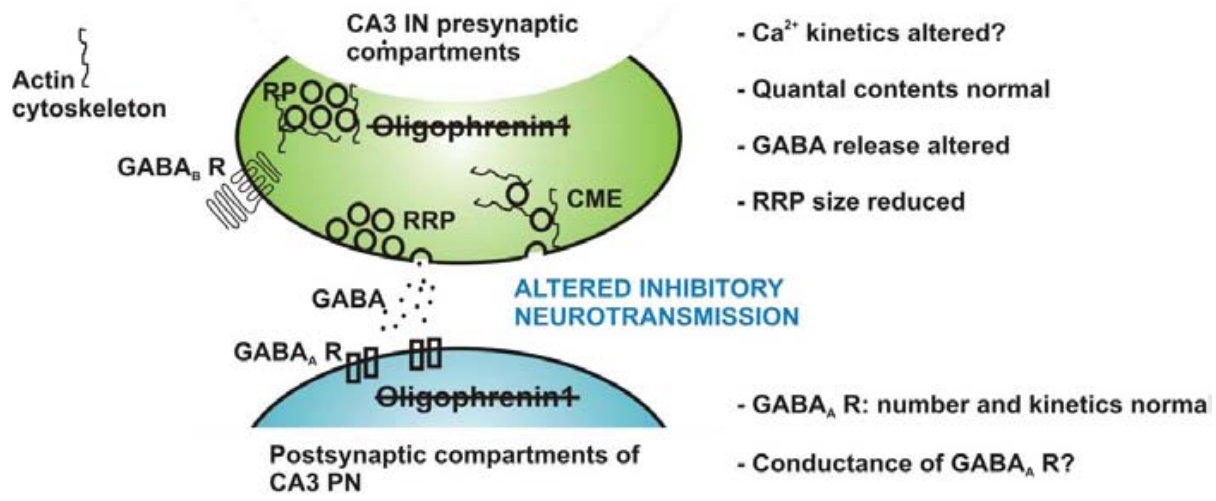

Figure 6.2: Schematic of a GABAergic synapses. Recapitulation of the results obtained on IPSC in *Ophn-1*$^{-/y}$ CA3 pyramidal neurons.

6.6 Putative mechanism of action of oligophrenin1

The aim of the project was to establish the phenotype of a mouse model deficient for oligophrenin1 protein. This study suggested possible deficient mechanisms leading to cognitive deficit in mice and possibly in individuals affected. It is important to note that during normal neuronal development and functioning, oligophrenin1 was previously reported to inhibit RhoA /ROCK in order to maintain the dendritic spine length (Govek et al., 2004). Alternatively, the reduction of the power in Ophn-1$^{-/y}$ mouse could result from various different mechanisms as the one described in this study, namely, recent finding delineate the crucial role of a secreted protein S100B by astrocytes, which is a calcium binding protein, and its implication in the modulation of KA-induced gamma oscillations power in vivo (Sakatani et al., 2008).

The present study demonstrated a reduction in the power gamma oscillations in *Ophn-1*$^{-/y}$ slices which suggested an impairment of the hippocampal function. This impairment in hippocampal function could underlie the impairment of the higher cognitive function in *Ophn-1*$^{-/y}$ mice, such as the altered MWM behaviour in *Ophn-1*$^{-/y}$ mice (Khelfaoui et al., 2007).

The investigation of the inhibitory and excitatory neurotransmission in CA3 area provided a compelling mechanistic explanation for the reduced power of the gamma oscillations in *Ophn-1*$^{-/y}$ slices (fig. 6.1)

I have shown a reduction in frequency of sIPSCs in *Ophn-1*$^{-/y}$ CA3 pyramidal neurons. This reduction in frequency demonstrated a clear presynaptic deficit. In addition, I have demonstrated a reduction in frequency of sEPSCs to a similar extent, suggesting a common mechanism to excitatory and inhibitory synapses. Then, altered paired-pulse depression as well as a reduction of frequency dependent facilitation at 33 Hz further confirmed a presynaptic deficit most likely related to deficit in synaptic vesicles availability. This has been confirmed by a clear reduction in the RRP size at inhibitory synapses in *Ophn-1*$^{-/y}$.

Thus, I have provided compelling evidences that oligophrenin1 is involved in neurotransmission *Ophn-1*$^{-/y}$ mice. The trafficking/handling of synaptic vesicles in nerve terminals would be somewhat impaired in *Ophn-1*$^{-/y}$ mice.

A. Powell demonstrated the implication of ROCK. However, the next effectors remained to be established, it could either MLCK or LIMK (and cofilin) (fig. 6.3).

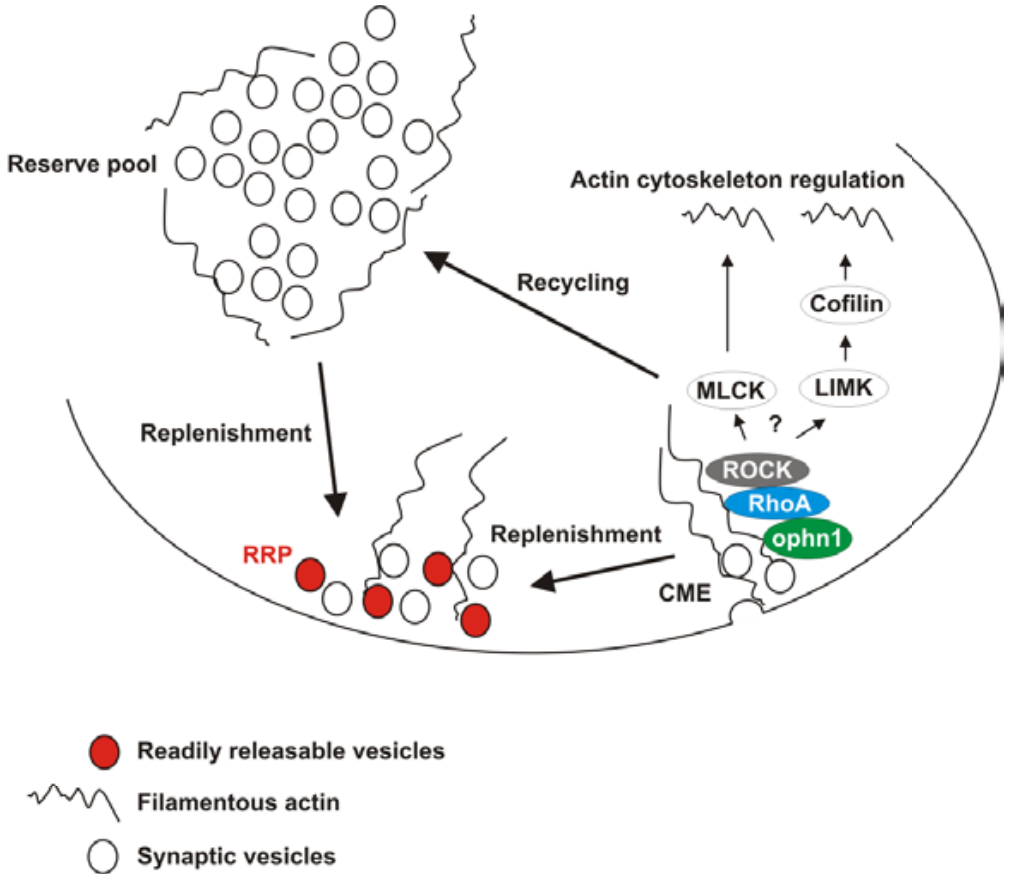

Figure 6.3: Schematic of a presynaptic terminal

6.7 Differences observed between CA3 and CA1 hippocampal areas.

i) Field recordings.

Several differences and discrepancies have been unravelled between CA3 and CA1 areas in extracellular recordings. The results are summarized in the figure 6.4. The evoked postsynaptic potentials have been shown to be reduced at the synapses

between CA3 and CA1 neurons, but not at the synapses between granule cells and CA3 neurons. This apparent discrepancy could be explained by different neuronal populations involved.

In addition, CA1 area showed reduced evoked postsynaptic potentials and normal paired-pulse facilitation, in contrast with results from Khelfaoui and colleagues (2007) which showed a normal evoked postsynaptic potential associated with a reduction in paired-pulse facilitation. Reasons for this discrepancy have been already discussed in the section 5.5.2.

Another possible explanation for the discrepancy between CA3 and CA1 areas would be that two GAP proteins, namely rich 1 and rich 2, which present a similar pattern of expression functional domains in the hippocampus as oligophrenin1. These proteins could overtake the function of oligophrenin1 in *Ophn-1*$^{-/y}$ CA1 area.

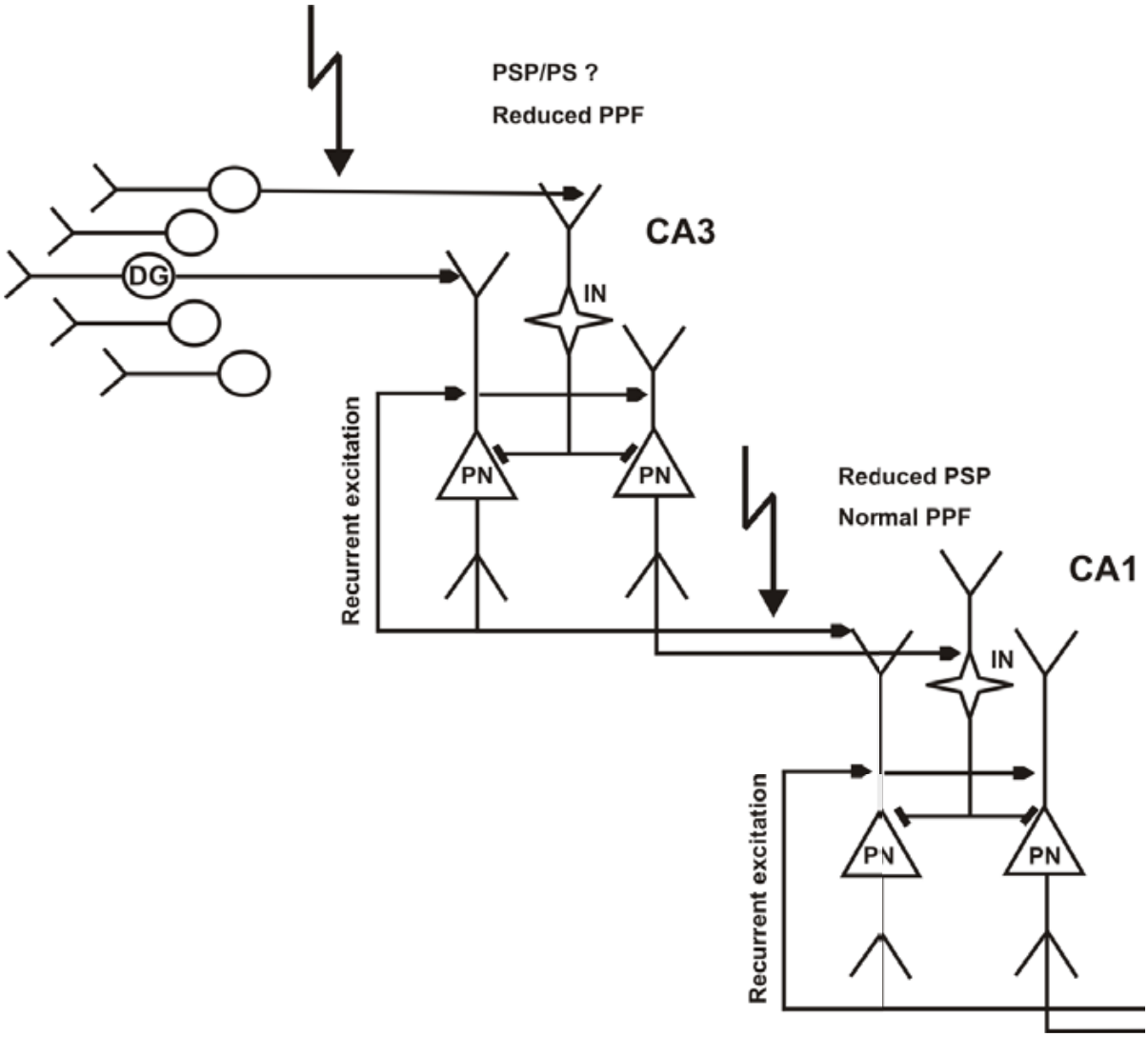

Figure 6.4: Schematic representation of the hippocampal neuronal circuitry. Arrows indicate the respective loci of stimulations for CA3 and CA1 area. Abbreviations: PN: pyramidal neuron; interneurons: interneurons, DG: dentate gyrus; CA3 : cornus ammonis 3 ; CA1 : cornus ammonis 1

ii) Excitatory and inhibitory postsynaptic currents

Differences in spontaneous postsynaptic currents have been observed, namely a reduction in frequency in CA3 pyramidal neurons as opposed to unaffected spontaneous postsynaptic currents have been observed in CA1.

For sIPSCs, this can be explained by different interneurons subtypes in CA3 and CA1 areas (Buzsaki, 2001). Concerning sEPSCs, differences in excitatory terminals could explain the opposite result. Similarly to field potentials, one may assume a redundancy in the function of oligophrenin1 by Rich1 or Rich2 in CA1 area.

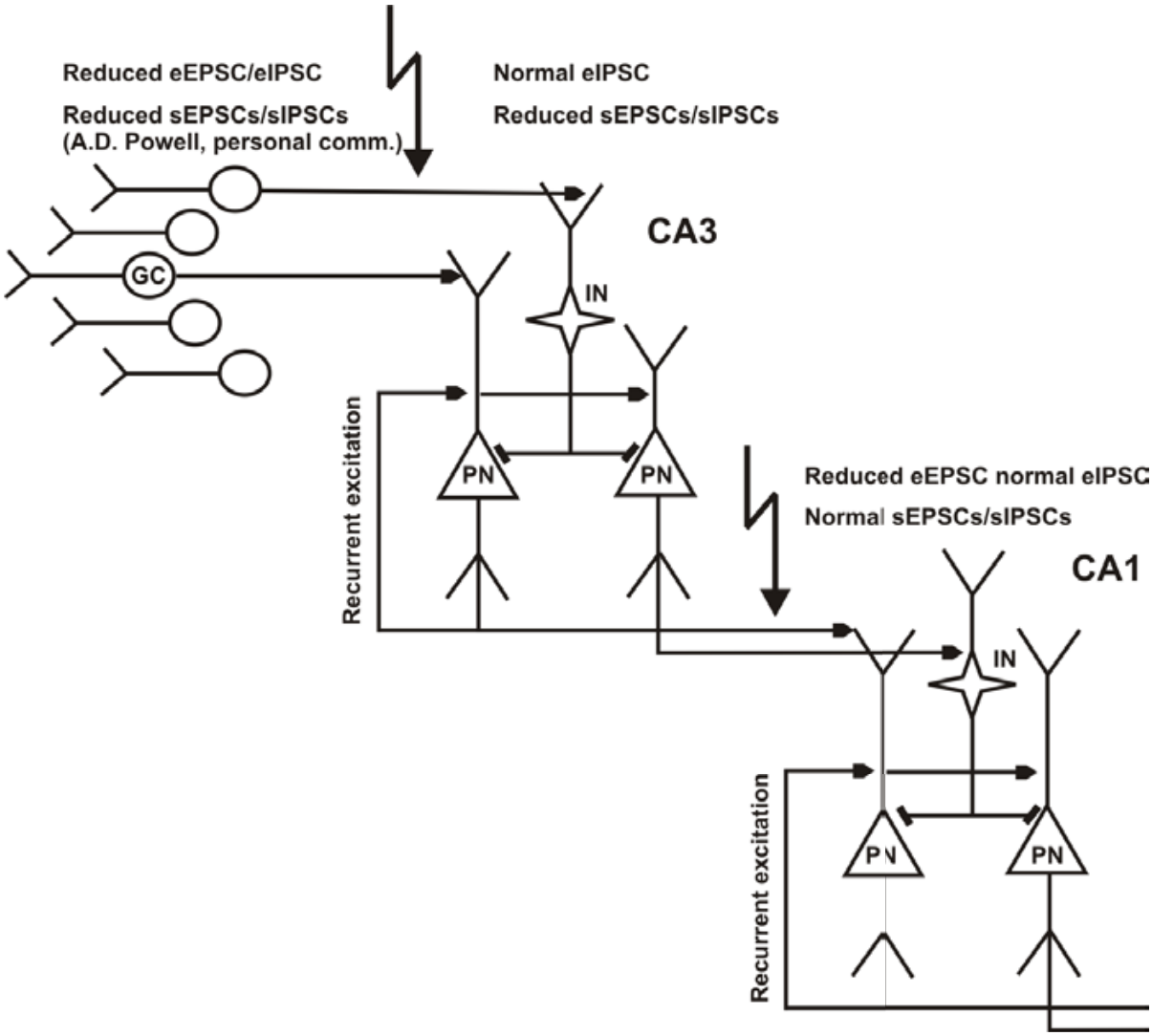

Figure 6.5: Schematic representation of different neuronal populations of the hippocampal pathways.

6.8 Conclusion

I provided compelling evidence that the loss of oligophrenin1 protein led to impaired synaptic transmission, especially impaired repetitive neurotransmission at 33 Hz, which resulted in a reduction of the power of gamma oscillations in *Ophn-1*$^{-/y}$ mice. This reduction is a potential explanation of the cognitive impairment.

In conclusion, the elucidation of the role of oligophrenin1 provided new insights into mechanisms of brain function.

AGHAJANIAN, G. K. & RASMUSSEN, K. (1989) Intracellular studies in the facial nucleus illustrating a simple new method for obtaining viable motoneurons in adult rat brain slices. *Synapse,* 3**,** 331-8.

ALLEN, K. M., GLEESON, J. G., BAGRODIA, S., PARTINGTON, M. W., MACMILLAN, J. C., CERIONE, R. A., MULLEY, J. C. & WALSH, C. A. (1998) PAK3 mutation in nonsyndromic X-linked mental retardation. *Nat.Genet.,* 20**,** 25-30.

AMARAL, D. G., ISHIZUKA, N. & CLAIBORNE, B. (1990) Neurons, numbers and the hippocampal network. *Prog.Brain Res.,* 83**,** 1-11.

ANDERSEN, P., MORRIS, R., AMARAL, D., BLISS, T. & O'KEEFE, J. *The Hippocampus Book* (Oxford Univ. Press, New York, 2007).

ASHTON, A. C. & USHKARYOV, Y. A. (2005) Properties of synaptic vesicle pools in mature central nerve terminals. *J Biol Chem,* 280**,** 37278-88.

AXMACHER, N., MORMANN, F., FERNANDEZ, G., ELGER, C. E. & FELL, J. (2006) Memory formation by neuronal synchronization. *Brain Res.Rev.,* 52**,** 170-182.

BARTOS, M., VIDA, I. & JONAS, P. (2007) Synaptic mechanisms of synchronized gamma oscillations in inhibitory interneuron networks. *Nat Rev Neurosci,* 8**,** 45-56.

BASAR-EROGLU, C., BRAND, A., HILDEBRANDT, H., KAROLINA KEDZIOR, K., MATHES, B. & SCHMIEDT, C. (2007) Working memory related gamma oscillations in schizophrenia patients. *Int J Psychophysiol,* 64**,** 39-45.

BECK, H. & YAARI, Y. (2008) Plasticity of intrinsic neuronal properties in CNS disorders. *Nat Rev Neurosci,* 9**,** 357-69.

BEDESCHI, M. F., NOVELLI, A., BERNARDINI, L., PARAZZINI, C., BIANCHI, V., TORRES, B., NATACCI, F., GIUFFRIDA, M. G., FICARAZZI, P., DALLAPICCOLA, B. & LALATTA, F. (2008) Association of syndromic mental retardation with an Xq12q13.1 duplication encompassing the oligophrenin 1 gene. *Am J Med Genet A,* 146A**,** 1718-24.

BELLINGER, F. P., BEDI, K. S., WILSON, P. & WILCE, P. A. (1999) Ethanol exposure during the third trimester equivalent results in long-lasting decreased synaptic efficacy but not plasticity in the CA1 region of the rat hippocampus. *Synapse,* 31**,** 51-8.

BEN-ARI, Y. & COSSART, R. (2000) Kainate, a double agent that generates seizures: two decades of progress. *Trends Neurosci.,* 23**,** 580-587.

BERGMANN, C., ZERRES, K., SENDEREK, J., RUDNIK-SCHONEBORN, S., EGGERMANN, T., HAUSLER, M., MULL, M. & RAMAEKERS, V. T. (2003) Oligophrenin 1 (OPHN1) gene mutation causes syndromic X-linked mental retardation with epilepsy, rostral ventricular enlargement and cerebellar hypoplasia. *Brain,* 126**,** 1537-1544.

BIENVENU, T., DER-SARKISSIAN, H., BILLUART, P., TISSOT, M., DES PORTES, V., BRULS, T., CHABROLLE, J. P., CHAUVEAU, P., CHERRY, M., KAHN, A., COHEN, D., BELDJORD, C., CHELLY, J. & CHERIF, D. (1997) Mapping

of the X-breakpoint involved in a balanced X;12 translocation in a female with mild mental retardation. *Eur J Hum Genet,* 5**,** 105-9.

BILLUART, P., BIENVENU, T., RONCE, N., DES, P. V., VINET, M. C., ZEMNI, R., ROEST, C. H., CARRIE, A., FAUCHEREAU, F., CHERRY, M., BRIAULT, S., HAMEL, B., FRYNS, J. P., BELDJORD, C., KAHN, A., MORAINE, C. & CHELLY, J. (1998) Oligophrenin-1 encodes a rhoGAP protein involved in X-linked mental retardation. *Nature,* 392**,** 923-926.

BLISS, T. V. & COLLINGRIDGE, G. L. (1993) A synaptic model of memory: long-term potentiation in the hippocampus. *Nature,* 361**,** 31-9.

BODA, B., ALBERI, S., NIKONENKO, I., NODE-LANGLOIS, R., JOURDAIN, P., MOOSMAYER, M., PARISI-JOURDAIN, L. & MULLER, D. (2004) The mental retardation protein PAK3 contributes to synapse formation and plasticity in hippocampus. *J.Neurosci.,* 24**,** 10816-10825.

BOTTGER, D., HERRMANN, C. S. & VON CRAMON, D. Y. (2002) Amplitude differences of evoked alpha and gamma oscillations in two different age groups. *Int J Psychophysiol,* 45**,** 245-51.

BRAGIN, A., JANDO, G., NADASDY, Z., HETKE, J., WISE, K. & BUZSAKI, G. (1995) Gamma (40-100 Hz) oscillation in the hippocampus of the behaving rat. *J.Neurosci.,* 15**,** 47-60.

BUZSAKI, G. (2001a) Electrical wiring of the oscillating brain. *Neuron.,* 31**,** 342-344.

BUZSAKI, G. (2001b) Hippocampal GABAergic interneurons: a physiological perspective. *Neurochem Res,* 26**,** 899-905.

BUZSAKI, G., BUHL, D. L., HARRIS, K. D., CSICSVARI, J., CZEH, B. & MOROZOV, A. (2003) Hippocampal network patterns of activity in the mouse. *Neuroscience,* 116**,** 201-11.

BUZSAKI, G (2006) “Rhythms of the brain”, Oxford university press.

CANTAGREL, V., LOSSI, A. M., BOULANGER, S., DEPETRIS, D., MATTEI, M. G., GECZ, J., SCHWARTZ, C. E., VAN, M. L. & VILLARD, L. (2004) Disruption of a new X linked gene highly expressed in brain in a family with two mentally retarded males. *J.Med.Genet.,* 41**,** 736-742.

CHABROL, B., GIRARD, N., N'GUYEN, K., GERARD, A., CARLIER, M., VILLARD, L. & PHILIP, N. (2005) Delineation of the clinical phenotype associated with OPHN1 mutations based on the clinical and neuropsychological evaluation of three families. *Am.J.Med.Genet.A.,* 138**,** 314-317.

CHAHROUR, M. & ZOGHBI, H. Y. (2007) The story of Rett syndrome: from clinic to neurobiology. *Neuron,* 56**,** 422-37.

CHELLY, J. (2000) MRX review. *Am.J.Med.Genet.,* 94**,** 364-366.

CHELLY, J. & MANDEL, J. L. (2001) Monogenic causes of X-linked mental retardation. *Nat.Rev.Genet.,* 2**,** 669-680.

COSSART, R., ESCLAPEZ, M., HIRSCH, J. C., BERNARD, C. & BEN-ARI, Y. (1998) GluR5 kainate receptor activation in interneurons increases tonic inhibition of pyramidal cells. *Nat.Neurosci.,* 1**,** 470-478.

COSSART, R., TYZIO, R., DINOCOURT, C., ESCLAPEZ, M., HIRSCH, J. C., BEN-ARI, Y. & BERNARD, C. (2001) Presynaptic kainate receptors that enhance

the release of GABA on CA1 hippocampal interneurons. *Neuron,* 29**,** 497-508.

CSICSVARI, J., JAMIESON, B., WISE, K. D. & BUZSAKI, G. (2003) Mechanisms of gamma oscillations in the hippocampus of the behaving rat. *Neuron.,* 37**,** 311-322.

D'ADAMO, P., MENEGON, A., LO, N. C., GRASSO, M., GULISANO, M., TAMANINI, F., BIENVENU, T., GEDEON, A. K., OOSTRA, B., WU, S. K., TANDON, A., VALTORTA, F., BALCH, W. E., CHELLY, J. & TONIOLO, D. (1998) Mutations in GDI1 are responsible for X-linked non-specific mental retardation. *Nat.Genet.,* 19**,** 134-139.

D'HOOGE, R. & DE DEYN, P. P. (2001) Applications of the Morris water maze in the study of learning and memory. *Brain Res Brain Res Rev,* 36**,** 60-90.

DAN, Y. & POO, M. M. (2006) Spike timing-dependent plasticity: from synapse to perception. *Physiol Rev.,* 86**,** 1033-1048.

DAVIES, C. H. & COLLINGRIDGE, G. L. (1993) The physiological regulation of synaptic inhibition by GABAB autoreceptors in rat hippocampus. *J Physiol,* 472**,** 245-65.

DES PORTES, V., BODDAERT, N., SACCO, S., BRIAULT, S., MAINCENT, K., BAHI, N., GOMOT, M., RONCE, N., BURSZTYN, J., ADAMSBAUM, C., ZILBOVICIUS, M., CHELLY, J. & MORAINE, C. (2004) Specific clinical and brain MRI features in mentally retarded patients with mutations in the Oligophrenin-1 gene. *Am.J.Med.Genet.A,* 124**,** 364-371.

DICKINSON, R., AWAIZ, S., WHITTINGTON, M. A., LIEB, W. R. & FRANKS, N. P. (2003) The effects of general anaesthetics on carbachol-evoked gamma oscillations in the rat hippocampus in vitro. *Neuropharmacology,* 44**,** 864-872.

DING, Y., MILOSAVLJEVIC, T. & ALAHARI, S. K. (2008) Nischarin inhibits LIM kinase to regulate cofilin phosphorylation and cell invasion. *Mol Cell Biol,* 28**,** 3742-56.

ENDRIS, V., WOGATZKY, B., LEIMER, U., BARTSCH, D., ZATYKA, M., LATIF, F., MAHER, E. R., TARIVERDIAN, G., KIRSCH, S., KARCH, D. & RAPPOLD, G. A. (2002) The novel Rho-GTPase activating gene MEGAP/ srGAP3 has a putative role in severe mental retardation. *Proc.Natl.Acad.Sci.U.S.A.,* 99**,** 11754-11759.

ENGEL, A. K., FRIES, P. & SINGER, W. (2001) Dynamic predictions: oscillations and synchrony in top-down processing. *Nat.Rev.Neurosci.,* 2**,** 704-716.

ETIENNE-MANNEVILLE, S. & HALL, A. (2002) Rho GTPases in cell biology. *Nature,* 420**,** 629-635.

FANO, S., BEHRENS, C. J. & HEINEMANN, U. (2007) Hypoxia suppresses kainate-induced gamma-oscillations in rat hippocampal slices. *Neuroreport,* 18**,** 1827-31.

FAUCHEREAU, F., HERBRAND, U., CHAFEY, P., EBERTH, A., KOULAKOFF, A., VINET, M. C., AHMADIAN, M. R., CHELLY, J. & BILLUART, P. (2003) The RhoGAP activity of OPHN1, a new F-actin-binding protein, is negatively controlled by its amino-terminal domain. *Mol.Cell Neurosci.,* 23**,** 574-586.

FAULKNER, H. J., TRAUB, R. D. & WHITTINGTON, M. A. (1998) Disruption of synchronous gamma oscillations in the rat hippocampal slice: a common mechanism of anaesthetic drug action. *Br.J.Pharmacol.,* 125**,** 483-492.

FISAHN, A. (2005) Kainate receptors and rhythmic activity in neuronal networks: hippocampal gamma oscillations as a tool. *J.Physiol.,* 562**,** 65-72.

FISAHN, A., CONTRACTOR, A., TRAUB, R. D., BUHL, E. H., HEINEMANN, S. F. & MCBAIN, C. J. (2004) Distinct roles for the kainate receptor subunits GluR5 and GluR6 in kainate-induced hippocampal gamma oscillations. *J.Neurosci.,* 24**,** 9658-9668.

FISAHN, A., HEINEMANN, S. F. & MCBAIN, C. J. (2005) The kainate receptor subunit GluR6 mediates metabotropic regulation of the slow and medium AHP currents in mouse hippocampal neurones. *J.Physiol.,* 562**,** 199-203.

FISAHN, A., PIKE, F. G., BUHL, E. H. & PAULSEN, O. (1998) Cholinergic induction of network oscillations at 40 Hz in the hippocampus in vitro. *Nature,* 394**,** 186-189.

GAMBLIN, S. J. & SMERDON, S. J. (1998) GTPase-activating proteins and their complexes. *Curr.Opin.Struct.Biol.,* 8**,** 195-201.

GASMAN, S., CHASSEROT-GOLAZ, S., BADER, M. F. & VITALE, N. (2003) Regulation of exocytosis in adrenal chromaffin cells: focus on ARF and Rho GTPases. *Cell Signal.,* 15**,** 893-899.

GOVEK, E. E., NEWEY, S. E., AKERMAN, C. J., CROSS, J. R., VAN, D. V. & VAN, A. L. (2004) The X-linked mental retardation protein oligophrenin-1 is required for dendritic spine morphogenesis. *Nat.Neurosci.,* 7**,** 364-372.

GOVEK, E. E., NEWEY, S. E. & VAN, A. L. (2005) The role of the Rho GTPases in neuronal development. *Genes Dev.,* 19**,** 1-49.

GRANSETH, B., ODERMATT, B., ROYLE, S. J. & LAGNADO, L. (2006) Clathrin-mediated endocytosis is the dominant mechanism of vesicle retrieval at hippocampal synapses. *Neuron,* 51**,** 773-86.

GRAY, C. M., ENGEL, A. K., KONIG, P. & SINGER, W. (1990) Stimulus-Dependent Neuronal Oscillations in Cat Visual Cortex: Receptive Field Properties and Feature Dependence. *Eur.J.Neurosci.,* 2**,** 607-619.

GRAY, C. M., KONIG, P., ENGEL, A. K. & SINGER, W. (1989) Oscillatory responses in cat visual cortex exhibit inter-columnar synchronization which reflects global stimulus properties. *Nature,* 338**,** 334-337.

GRAY, C. M. & SINGER, W. (1989) Stimulus-specific neuronal oscillations in orientation columns of cat visual cortex. *Proc.Natl.Acad.Sci.U.S.A,* 86**,** 1698-1702.

GRICE, S. J., SPRATLING, M. W., KARMILOFF-SMITH, A., HALIT, H., CSIBRA, G., DE, H. M. & JOHNSON, M. H. (2001) Disordered visual processing and oscillatory brain activity in autism and Williams syndrome. *Neuroreport.,* 12**,** 2697-2700.

GROSSMAN, A. W., ALDRIDGE, G. M., WEILER, I. J. & GREENOUGH, W. T. (2006a) Local protein synthesis and spine morphogenesis: Fragile X syndrome and beyond. *J.Neurosci.,* 26**,** 7151-7155.

GROSSMAN, A. W., ELISSEOU, N. M., MCKINNEY, B. C. & GREENOUGH, W. T. (2006b) Hippocampal pyramidal cells in adult Fmr1 knockout mice exhibit an immature-appearing profile of dendritic spines. *Brain Res.,* 1084**,** 158-164.

GRUBER, T., MULLER, M. M. & KEIL, A. (2002) Modulation of induced gamma band responses in a perceptual learning task in the human EEG. *J.Cogn Neurosci.,* 14**,** 732-744.

GULLEDGE, A. T. & KAWAGUCHI, Y. (2007) Phasic cholinergic signaling in the hippocampus: functional homology with the neocortex? *Hippocampus,* 17**,** 327-32.

HABERNY, K. A., PAULE, M. G., SCALLET, A. C., SISTARE, F. D., LESTER, D. S., HANIG, J. P. & SLIKKER, W., JR. (2002) Ontogeny of the N-methyl-D-aspartate (NMDA) receptor system and susceptibility to neurotoxicity. *Toxicol Sci,* 68**,** 9-17.

HAJOS, N., KATONA, I., NAIEM, S. S., MACKIE, K., LEDENT, C., MODY, I. & FREUND, T. F. (2000) Cannabinoids inhibit hippocampal GABAergic transmission and network oscillations. *Eur J Neurosci,* 12**,** 3239-49.

HAJOS, N., PALHALMI, J., MANN, E. O., NEMETH, B., PAULSEN, O. & FREUND, T. F. (2004) Spike timing of distinct types of GABAergic interneuron during hippocampal gamma oscillations in vitro. *J.Neurosci.,* 24**,** 9127-9137.

HALL, A. (1998) Rho GTPases and the actin cytoskeleton. *Science,* 279**,** 509-514.

HEDGES, L. V. & NOWELL, A. (1995) Sex differences in mental test scores, variability, and numbers of high-scoring individuals. *Science.,* 269**,** 41-45.

HORMUZDI, S. G., PAIS, I., LEBEAU, F. E., TOWERS, S. K., ROZOV, A., BUHL, E. H., WHITTINGTON, M. A. & MONYER, H. (2001) Impaired electrical signaling disrupts gamma frequency oscillations in connexin 36-deficient mice. *Neuron.,* 31**,** 487-495.

HUCHZERMEYER, C., ALBUS, K., GABRIEL, H. J., OTAHAL, J., TAUBENBERGER, N., HEINEMANN, U., KOVACS, R. & KANN, O. (2008) Gamma oscillations and spontaneous network activity in the hippocampus are highly sensitive to decreases in pO2 and concomitant changes in mitochondrial redox state. *J Neurosci,* 28**,** 1153-62.

HUTTENLOCHER, P. R. (1970) Dendritic development and mental defect. *Neurology.,* 20**,** 381.

ISHIZAKI, T., UEHATA, M., TAMECHIKA, I., KEEL, J., NONOMURA, K., MAEKAWA, M. & NARUMIYA, S. (2000) Pharmacological properties of Y-27632, a specific inhibitor of rho-associated kinases. *Mol Pharmacol,* 57**,** 976-83.

ISHIZUKA, N., WEBER, J. & AMARAL, D. G. (1990) Organization of intrahippocampal projections originating from CA3 pyramidal cells in the rat. *J Comp Neurol,* 295**,** 580-623.

JAFFE, A. B. & HALL, A. (2005) Rho GTPases: biochemistry and biology. *Annu.Rev.Cell Dev.Biol.,* 21:247-69.**,** 247-269.

JEFFERYS, J. G., TRAUB, R. D. & WHITTINGTON, M. A. (1996) Neuronal networks for induced '40 Hz' rhythms. *Trends Neurosci.,* 19**,** 202-208.

JENSEN, O., KAISER, J. & LACHAUX, J. P. (2007) Human gamma-frequency oscillations associated with attention and memory. *Trends Neurosci.*

JENSEN, O. & LISMAN, J. E. (2005) Hippocampal sequence-encoding driven by a cortical multi-item working memory buffer. *Trends Neurosci.,* 28**,** 67-72.

JOHNSTON, D., and WU, S. 1995 Foundations of Cellular Neurophysiology. Cambridge, Massachussetts; MIT

KANEKO, T., MAEDA, A., TAKEFUJI, M., AOYAMA, H., NAKAYAMA, M., KAWABATA, S., KAWANO, Y., IWAMATSU, A., AMANO, M. & KAIBUCHI, K. (2005) Rho mediates endocytosis of epidermal growth factor receptor through phosphorylation of endophilin A1 by Rho-kinase. *Genes Cells,* 10**,** 973-87.

KATZ, B. & MILEDI, R. (1968) The role of calcium in neuromuscular facilitation. *J Physiol,* 195**,** 481-92.

KAUFMANN, W. E. & MOSER, H. W. (2000) Dendritic anomalies in disorders associated with mental retardation. *Cereb.Cortex,* 10**,** 981-991.

KHELFAOUI, M., ALICE, P., POWELL, A. D., VALNEGRI, P., CHEONG, K. W., BLANDIN, Y., PASSAFARO, M., JEFFERYS, J. G., CHELLY, J. & BILLUART, P. (2009) Inhibition of RhoA pathway rescues the endocytosis defects in Oligophrenin1 mouse model of mental retardation. *Hum Mol Genet*.

KHELFAOUI, M., DENIS, C., VAN, G. E., DE, B. F., SCHMITT, A., HOUBRON, C., MORICE, E., GIROS, B., RAMAKERS, G., FAGNI, L., CHELLY, J., NOSTEN-BERTRAND, M. & BILLUART, P. (2007) Loss of X-linked mental retardation gene oligophrenin1 in mice impairs spatial memory and leads to ventricular enlargement and dendritic spine immaturity. *J.Neurosci.,* 27**,** 9439-9450.

KIRISCHUK, S. & GRANTYN, R. (2000) A readily releasable pool of single inhibitory boutons in culture. *Neuroreport,* 11**,** 3709-13.

KOCH, C. & ZADOR, A. (1993) The function of dendritic spines: devices subserving biochemical rather than electrical compartmentalization. *J.Neurosci.,* 13**,** 413-422.

LI, F. & HIGGS, H. N. (2003) The mouse Formin mDia1 is a potent actin nucleation factor regulated by autoinhibition. *Curr Biol,* 13**,** 1335-40.

LISMAN, J. E. (1999) Relating hippocampal circuitry to function: recall of memory sequences by reciprocal dentate-CA3 interactions. *Neuron.,* 22**,** 233-242.

LJUBIMOVA, J. Y., KHAZENZON, N. M., CHEN, Z., NEYMAN, Y. I., TURNER, L., RIEDINGER, M. S. & BLACK, K. L. (2001) Gene expression abnormalities in human glial tumors identified by gene array. *Int.J.Oncol.,* 18**,** 287-295.

LUO, L. (2000) Rho GTPases in neuronal morphogenesis. *Nat.Rev.Neurosci.,* 1**,** 173-180.

LUTZ, A., GREISCHAR, L. L., RAWLINGS, N. B., RICARD, M. & DAVIDSON, R. J. (2004) Long-term meditators self-induce high-amplitude gamma synchrony during mental practice. *Proc Natl Acad Sci U S A,* 101**,** 16369-73.

MADRIGAL, I., RODRIGUEZ-REVENGA, L., BADENAS, C., SANCHEZ, A. & MILA, M. (2008) Deletion of the OPHN1 gene detected by aCGH. *J Intellect Disabil Res,* 52**,** 190-4.

MAEKAWA, M., ISHIZAKI, T., BOKU, S., WATANABE, N., FUJITA, A., IWAMATSU, A., OBINATA, T., OHASHI, K., MIZUNO, K. & NARUMIYA, S. (1999) Signaling from Rho to the actin cytoskeleton through protein kinases ROCK and LIM-kinase. *Science,* 285**,** 895-898.

MANN, E. O., SUCKLING, J. M., HAJOS, N., GREENFIELD, S. A. & PAULSEN, O. (2005) Perisomatic feedback inhibition underlies cholinergically induced fast network oscillations in the rat hippocampus in vitro. *Neuron.,* 45**,** 105-117.

MANZONI, O. & BOCKAERT, J. (1995) Metabotropic glutamate receptors inhibiting excitatory synapses in the CA1 area of rat hippocampus. *Eur J Neurosci,* 7**,** 2518-23.

MARINELLI, S., DI MARZO, V., BERRETTA, N., MATIAS, I., MACCARRONE, M., BERNARDI, G. & MERCURI, N. B. (2003) Presynaptic facilitation of glutamatergic synapses to dopaminergic neurons of the rat substantia nigra by endogenous stimulation of vanilloid receptors. *J Neurosci,* 23**,** 3136-44.

MATILLA, A., ROBERSON, E. D., BANFI, S., MORALES, J., ARMSTRONG, D. L., BURRIGHT, E. N., ORR, H. T., SWEATT, J. D., ZOGHBI, H. Y. & MATZUK, M. M. (1998) Mice lacking ataxin-1 display learning deficits and decreased hippocampal paired-pulse facilitation. *J Neurosci,* 18**,** 5508-16.

MCBAIN, C. J. & FISAHN, A. (2001) Interneurons unbound. *Nat.Rev.Neurosci.,* 2**,** 11-23.

MCLAREN, J. & BRYSON, S. E. (1987) Hemispheric asymmetries in the perception of emotional and neutral faces. *Cortex,* 23**,** 645-54.

MELYAN, Z., WHEAL, H. V. & LANCASTER, B. (2002) Metabotropic-mediated kainate receptor regulation of IsAHP and excitability in pyramidal cells. *Neuron.,* 34**,** 107-114.

MENG, Y., ZHANG, Y., TREGOUBOV, V., JANUS, C., CRUZ, L., JACKSON, M., LU, W. Y., MACDONALD, J. F., WANG, J. Y., FALLS, D. L. & JIA, Z. (2002) Abnormal spine morphology and enhanced LTP in LIMK-1 knockout mice. *Neuron,* 35**,** 121-133.

MENTEN, B., BUYSSE, K., VERMEULEN, S., MEERSSCHAUT, V., VANDESOMPELE, J., NG, B. L., CARTER, N. P., MORTIER, G. R. & SPELEMAN, F. (2007) Report of a female patient with mental retardation and tall stature due to a chromosomal rearrangement disrupting the OPHN1 gene on Xq12. *Eur.J.Med.Genet.,* .

MONTGOMERY, S. M. & BUZSAKI, G. (2007) Gamma oscillations dynamically couple hippocampal CA3 and CA1 regions during memory task performance. *Proc Natl Acad Sci U S A,* 104**,** 14495-500.

MORRIS, R. (1984) Developments of a water-maze procedure for studying spatial learning in the rat. *J Neurosci Methods,* 11**,** 47-60.

MOZHAYEVA, M. G., SARA, Y., LIU, X. & KAVALALI, E. T. (2002) Development of vesicle pools during maturation of hippocampal synapses. *J Neurosci,* 22**,** 654-65.

NAKANO-KOBAYASHI, A., KASRI, N. N., NEWEY, S. E. & VAN AELST, L. (2009) The Rho-Linked Mental Retardation Protein OPHN1 Controls Synaptic Vesicle Endocytosis via Endophilin A1. *Curr Biol*.

NAKAYAMA, A. Y., HARMS, M. B. & LUO, L. (2000) Small GTPases Rac and Rho in the maintenance of dendritic spines and branches in hippocampal pyramidal neurons. *J.Neurosci.,* 20**,** 5329-5338.

NARUMIYA, S. & YASUDA, S. (2006) Rho GTPases in animal cell mitosis. *Curr.Opin.Cell Biol.,* 18**,** 199-205.

NEWEY, S. E., VELAMOOR, V., GOVEK, E. E. & VAN, A. L. (2005) Rho GTPases, dendritic structure, and mental retardation. *J.Neurobiol.,* 64**,** 58-74.

O'DONNELL, W. T. & WARREN, S. T. (2002) A decade of molecular studies of fragile X syndrome. *Annu.Rev.Neurosci.,* 25**,** 315-338.

PETER, B. J., KENT, H. M., MILLS, I. G., VALLIS, Y., BUTLER, P. J., EVANS, P. R. & MCMAHON, H. T. (2004) BAR domains as sensors of membrane curvature: the amphiphysin BAR structure. *Science,* 303**,** 495-499.

PHILIP, N., CHABROL, B., LOSSI, A. M., CARDOSO, C., GUERRINI, R., DOBYNS, W. B., RAYBAUD, C. & VILLARD, L. (2003) Mutations in the oligophrenin-1 gene (OPHN1) cause X linked congenital cerebellar hypoplasia. *J.Med.Genet.,* 40**,** 441-446.

PIETERSEN, A. N., PATEL, N., JEFFERYS, J. G. & VREUGDENHIL, M. (2009) Comparison between spontaneous and kainate-induced gamma oscillations in the mouse hippocampus in vitro. *Eur J Neurosci*.

PITT, D., WERNER, P. & RAINE, C. S. (2000) Glutamate excitotoxicity in a model of multiple sclerosis. *Nat Med,* 6**,** 67-70.

POLZIN, A., SHIPITSIN, M., GOI, T., FEIG, L. A. & TURNER, T. J. (2002) Ral-GTPase influences the regulation of the readily releasable pool of synaptic vesicles. *Mol Cell Biol,* 22**,** 1714-22.

PURPURA, D. P. (1974) Dendritic spine "dysgenesis" and mental retardation. *Science.,* %20;186**,** 1126-1128.

PURPURA, D. P. (1979) Pathobiology of cortical neurons in metabolic and unclassified amentias. *Res.Publ.Assoc.Res.Nerv.Ment.Dis.,* 57:43-68.**,** 43-68.

RAMAKERS, G. J. (2002) Rho proteins, mental retardation and the cellular basis of cognition. *Trends Neurosci.,* 25**,** 191-199.

RAYMOND, F. L. (2006) X linked mental retardation: a clinical guide. *J.Med.Genet.,* 43**,** 193-200.

RENIERI, A., PESCUCCI, C., LONGO, I., ARIANI, F., MARI, F. & MELONI, I. (2005) Non-syndromic X-linked mental retardation: from a molecular to a clinical point of view. *J.Cell Physiol.,* 204**,** 8-20.

RIVA, D. & GIORGI, C. (2000) The cerebellum contributes to higher functions during development: evidence from a series of children surgically treated for posterior fossa tumours. *Brain,* 123 (Pt 5)**,** 1051-61.

RIZZOLI, S. O. & BETZ, W. J. (2005) Synaptic vesicle pools. *Nat.Rev.Neurosci.,* 6**,** 57-69.

ROMO-PARRA, H., VIVAR, C., MAQUEDA, J., MORALES, M. A. & GUTIERREZ, R. (2003) Activity-dependent induction of multitransmitter signaling onto pyramidal cells and interneurons of hippocampal area CA3. *J Neurophysiol,* 89**,** 3155-67.

ROPERS, H. H. & HAMEL, B. C. (2005) X-linked mental retardation. *Nat.Rev.Genet.,* 6**,** 46-57.

ROSS, M. T., GRAFHAM, D. V., COFFEY, A. J., SCHERER, S., MCLAY, K., MUZNY, D., PLATZER, M., HOWELL, G. R., BURROWS, C., BIRD, C. P., FRANKISH, A., LOVELL, F. L., HOWE, K. L., ASHURST, J. L., FULTON, R. S., SUDBRAK, R., WEN, G., JONES, M. C., HURLES, M. E., ANDREWS, T. D., SCOTT, C. E., SEARLE, S., RAMSER, J., WHITTAKER, A., DEADMAN, R., CARTER, N. P., HUNT, S. E., CHEN, R., CREE, A., GUNARATNE, P., HAVLAK, P., HODGSON, A., METZKER, M. L., RICHARDS, S., SCOTT, G., STEFFEN, D., SODERGREN, E., WHEELER, D. A., WORLEY, K. C., AINSCOUGH, R., AMBROSE, K. D., NSARI-LARI, M. A., ARADHYA, S., ASHWELL, R. I., BABBAGE, A. K., BAGGULEY, C. L., BALLABIO, A., BANERJEE, R., BARKER, G. E., BARLOW, K. F., BARRETT, I. P., BATES, K. N., BEARE, D. M., BEASLEY, H., BEASLEY, O., BECK, A., BETHEL, G., BLECHSCHMIDT, K., BRADY, N., BRAY-ALLEN, S., BRIDGEMAN, A. M., BROWN, A. J., BROWN, M. J., BONNIN, D., BRUFORD, E. A., BUHAY, C., BURCH, P., BURFORD, D., BURGESS, J., BURRILL, W., BURTON, J., BYE, J. M., CARDER, C., CARREL, L., CHAKO, J., CHAPMAN, J. C., CHAVEZ, D., CHEN, E., CHEN, G., CHEN, Y., CHEN, Z., CHINAULT, C., CICCODICOLA, A., CLARK, S. Y., CLARKE, G., CLEE, C. M., CLEGG, S., CLERC-BLANKENBURG, K., CLIFFORD, K., COBLEY, V., COLE, C. G., CONQUER, J. S., CORBY, N., CONNOR, R. E., DAVID, R., DAVIES, J., DAVIS, C., DAVIS, J., DELGADO, O., DESHAZO, D., et al. (2005) The DNA sequence of the human X chromosome. *Nature.,* 434**,** 325-337.

RYAN, T. A. (1999) Inhibitors of myosin light chain kinase block synaptic vesicle pool mobilization during action potential firing. *J Neurosci,* 19**,** 1317-23.

SAH, P. & FABER, E. S. (2002) Channels underlying neuronal calcium-activated potassium currents. *Prog.Neurobiol.,* 66**,** 345-353.

SAKATANI, S., SETO-OHSHIMA, A., SHINOHARA, Y., YAMAMOTO, Y., YAMAMOTO, H., ITOHARA, S. & HIRASE, H. (2008) Neural-activity-dependent release of S100B from astrocytes enhances kainate-induced gamma oscillations in vivo. *J Neurosci,* 28**,** 10928-36.

SALA, C., FUTAI, K., YAMAMOTO, K., WORLEY, P. F., HAYASHI, Y. & SHENG, M. (2003) Inhibition of dendritic spine morphogenesis and synaptic transmission by activity-inducible protein Homer1a. *J.Neurosci.,* 23**,** 6327-6337.

SARA, Y., VIRMANI, T., DEAK, F., LIU, X. & KAVALALI, E. T. (2005) An isolated pool of vesicles recycles at rest and drives spontaneous neurotransmission. *Neuron,* 45**,** 563-73.

SCHMITZ, A. A., GOVEK, E. E., BOTTNER, B. & VAN, A. L. (2000) Rho GTPases: signaling, migration, and invasion. *Exp.Cell Res.,* 261**,** 1-12.

SCHMITZ, D., SCHUCHMANN, S., FISAHN, A., DRAGUHN, A., BUHL, E. H., PETRASCH-PARWEZ, E., DERMIETZEL, R., HEINEMANN, U. & TRAUB, R. D. (2001) Axo-axonal coupling. a novel mechanism for ultrafast neuronal communication. *Neuron.,* 31**,** 831-840.

SCHNEGGENBURGER, R., MEYER, A. C. & NEHER, E. (1999) Released fraction and total size of a pool of immediately available transmitter quanta at a calyx synapse. *Neuron,* 23**,** 399-409.

SCHULZ, P. E., COOK, E. P. & JOHNSTON, D. (1994) Changes in paired-pulse facilitation suggest presynaptic involvement in long-term potentiation. *J Neurosci,* 14**,** 5325-37.

SCHWEIZER, F. E. & RYAN, T. A. (2006) The synaptic vesicle: cycle of exocytosis and endocytosis. *Curr Opin Neurobiol,* 16**,** 298-304.

SEDERBERG, P. B., KAHANA, M. J., HOWARD, M. W., DONNER, E. J. & MADSEN, J. R. (2003) Theta and gamma oscillations during encoding predict subsequent recall. *J.Neurosci.,* 23**,** 10809-10814.

SEGAL, M. (1995) Dendritic spines for neuroprotection: a hypothesis. *Trends Neurosci.,* 18**,** 468-471.

SHEPHERD, G. M. & GREER, C. A. (2003) The Synaptic Organization of the Brain, ed. Shepherd, G. M. (Oxford Univ. Press, New York, 5th edition)

SIMSEK-DURAN, F. & LONART, G. (2008) The role of RIM1alpha in BDNF-enhanced glutamate release. *Neuropharmacology,* 55**,** 27-34.

SPERK, G. (1994) Kainic acid seizures in the rat. *Prog Neurobiol,* 42**,** 1-32.

SRINIVASAN, G., KIM, J. H. & VON GERSDORFF, H. (2008) The pool of fast releasing vesicles is augmented by myosin light chain kinase inhibition at the calyx of Held synapse. *J Neurophysiol,* 99**,** 1810-24.

STEVENS, C. F. & SULLIVAN, J. M. (1998) Regulation of the readily releasable vesicle pool by protein kinase C. *Neuron,* 21**,** 885-93.

SUDHOF, T. C. (2004) The synaptic vesicle cycle. *Annu.Rev.Neurosci.,* 27**,** 509-547.

SYMONS, M. & SETTLEMAN, J. (2000) Rho family GTPases: more than simple switches. *Trends Cell Biol.,* 10**,** 415-419.

TALLON-BAUDRY, C. & BERTRAND, O. (1999) Oscillatory gamma activity in humans and its role in object representation. *Trends Cogn Sci.,* 3**,** 151-162.

TASHIRO, A., MINDEN, A. & YUSTE, R. (2000) Regulation of dendritic spine morphology by the rho family of small GTPases: antagonistic roles of Rac and Rho. *Cereb.Cortex.,* 10**,** 927-938.

TENTLER, D., GUSTAVSSON, P., LEISTI, J., SCHUELER, M., CHELLY, J., TIMONEN, E., ANNEREN, G., WILLARD, H. F. & DAHL, N. (1999) Deletion including the oligophrenin-1 gene associated with enlarged cerebral ventricles, cerebellar hypoplasia, seizures and ataxia. *Eur.J.Hum.Genet.,* 7**,** 541-548.

TRAUB, R. D., CUNNINGHAM, M. O., GLOVELI, T., LEBEAU, F. E., BIBBIG, A., BUHL, E. H. & WHITTINGTON, M. A. (2003a) GABA-enhanced collective behavior in neuronal axons underlies persistent gamma-frequency oscillations. *Proc.Natl.Acad.Sci.U.S.A,* 100**,** 11047-11052.

TRAUB, R. D., JEFFERYS, J. G. & WHITTINGTON, M. A. (1997) Simulation of gamma rhythms in networks of interneurons and pyramidal cells. *J.Comput.Neurosci.,* 4**,** 141-150.

TRAUB, R. D., PAIS, I., BIBBIG, A., LEBEAU, F. E., BUHL, E. H., HORMUZDI, S. G., MONYER, H. & WHITTINGTON, M. A. (2003b) Contrasting roles of axonal (pyramidal cell) and dendritic (interneuron) electrical coupling in the generation of neuronal network oscillations. *Proc.Natl.Acad.Sci.U.S.A.,* 100**,** 1370-1374.

TRAYNELIS, S. F., SILVER, R. A. & CULL-CANDY, S. G. (1993) Estimated conductance of glutamate receptor channels activated during EPSCs at the cerebellar mossy fiber-granule cell synapse. *Neuron,* 11**,** 279-89.

UEHATA, M., ISHIZAKI, T., SATOH, H., ONO, T., KAWAHARA, T., MORISHITA, T., TAMAKAWA, H., YAMAGAMI, K., INUI, J., MAEKAWA, M. & NARUMIYA, S. (1997) Calcium sensitization of smooth muscle mediated by a Rho-associated protein kinase in hypertension. *Nature,* 389**,** 990-4.

UHLHAAS, P. J. & SINGER, W. (2006) Neural synchrony in brain disorders: relevance for cognitive dysfunctions and pathophysiology. *Neuron.,* 52**,** 155-168.

VENTER, J. C., ADAMS, M. D., MYERS, E. W., LI, P. W., MURAL, R. J., SUTTON, G. G., SMITH, H. O., YANDELL, M., EVANS, C. A., HOLT, R. A., GOCAYNE, J. D., AMANATIDES, P., BALLEW, R. M., HUSON, D. H., WORTMAN, J. R., ZHANG, Q., KODIRA, C. D., ZHENG, X. H., CHEN, L., SKUPSKI, M., SUBRAMANIAN, G., THOMAS, P. D., ZHANG, J., GABOR MIKLOS, G. L., NELSON, C., BRODER, S., CLARK, A. G., NADEAU, J., MCKUSICK, V. A., ZINDER, N., LEVINE, A. J., ROBERTS, R. J., SIMON, M., SLAYMAN, C., HUNKAPILLER, M., BOLANOS, R., DELCHER, A., DEW, I., FASULO, D., FLANIGAN, M., FLOREA, L., HALPERN, A., HANNENHALLI, S., KRAVITZ, S., LEVY, S., MOBARRY, C., REINERT, K., REMINGTON, K., BU-THREIDEH, J., BEASLEY, E., BIDDICK, K., BONAZZI, V., BRANDON, R., CARGILL, M., CHANDRAMOULISWARAN, I., CHARLAB, R., CHATURVEDI, K., DENG, Z., DI, F. V., DUNN, P., EILBECK, K., EVANGELISTA, C., GABRIELIAN, A. E., GAN, W., GE, W., GONG, F., GU, Z., GUAN, P., HEIMAN, T. J., HIGGINS, M. E., JI, R. R., KE, Z., KETCHUM, K. A., LAI, Z., LEI, Y., LI, Z., LI, J., LIANG, Y., LIN, X., LU, F., MERKULOV, G. V., MILSHINA, N., MOORE, H. M., NAIK, A. K., NARAYAN, V. A., NEELAM, B., NUSSKERN, D., RUSCH, D. B., SALZBERG, S., SHAO, W., SHUE, B., SUN, J., WANG, Z., WANG, A., WANG, X., WANG, J., WEI, M., WIDES, R., XIAO, C., YAN, C., et al. (2001) The sequence of the human genome. *Science.,* 291**,** 1304-1351.

VERKERK, A. J., PIERETTI, M., SUTCLIFFE, J. S., FU, Y. H., KUHL, D. P., PIZZUTI, A., REINER, O., RICHARDS, S., VICTORIA, M. F. & ZHANG, F. P. (1991) Identification of a gene (FMR-1) containing a CGG repeat coincident with a breakpoint cluster region exhibiting length variation in fragile X syndrome. *Cell,* 65**,** 905-914.

VIDA, I., BARTOS, M. & JONAS, P. (2006) Shunting inhibition improves robustness of gamma oscillations in hippocampal interneuron networks by homogenizing firing rates. *Neuron.,* 49**,** 107-117.

VIGNES, M. & COLLINGRIDGE, G. L. (1997) The synaptic activation of kainate receptors. *Nature.,* 388**,** 179-182.

VREUGDENHIL, M., JEFFERYS, J. G., CELIO, M. R. & SCHWALLER, B. (2003) Parvalbumin-deficiency facilitates repetitive IPSCs and gamma oscillations in the hippocampus. *J.Neurophysiol.,* 89**,** 1414-1422.

VREUGDENHIL, M. & TOESCU, E. C. (2005) Age-dependent reduction of gamma oscillations in the mouse hippocampus in vitro. *Neuroscience.,* 132**,** 1151-1157.

WHITTINGTON, M. A., TRAUB, R. D. & JEFFERYS, J. G. (1995) Synchronized oscillations in interneuron networks driven by metabotropic glutamate receptor activation. *Nature.,* 373**,** 612-615.

WITTWER, B., KIRCHEISEN, R., LEUTELT, J., ORTH, U. & GAL, A. (1996) New X-linked mental retardation syndrome with the gene mapped tentatively in Xp22.3. *Am.J.Med.Genet.,* 64**,** 42-49.

XIAO, J., NEYLON, C. B., HUNNE, B. & FURNESS, J. B. (2003) Oligophrenin-1, a Rho GTPase-activating protein (RhoGAP) involved in X-linked mental retardation, is expressed in the enteric nervous system. *Anat.Rec.A Discov.Mol.Cell Evol.Biol.,* 273**,** 671-676.

YOSHINO, M., SAWADA, S., YAMAMOTO, C. & KAMIYA, H. (1996) A metabotropic glutamate receptor agonist DCG-IV suppresses synaptic transmission at mossy fiber pathway of the guinea pig hippocampus. *Neurosci Lett,* 207**,** 70-2.

YUSTE, R. & BONHOEFFER, T. (2004) Genesis of dendritic spines: insights from ultrastructural and imaging studies. *Nat.Rev.Neurosci.,* 5**,** 24-34.

ZANNI, G., SAILLOUR, Y., NAGARA, M., BILLUART, P., CASTELNAU, L., MORAINE, C., FAIVRE, L., BERTINI, E., DURR, A., GUICHET, A., RODRIGUEZ, D., DES, P. V., BELDJORD, C. & CHELLY, J. (2005) Oligophrenin 1 mutations frequently cause X-linked mental retardation with cerebellar hypoplasia. *Neurology,* 65**,** 1364-1369.

ZECHNER, U., WILDA, M., KEHRER-SAWATZKI, H., VOGEL, W., FUNDELE, R. & HAMEISTER, H. (2001) A high density of X-linked genes for general cognitive ability: a run-away process shaping human evolution? *Trends Genet.,* 17**,** 697-701.

ZUCKER, R. S. & REGEHR, W. G. (2002) Short-term synaptic plasticity. *Annu Rev Physiol,* 64**,** 355-405.